Universidad Complutense de Madrid

Facultad de Óptica, Optometría y Visión

Doctoral Thesis

Presbyopia Corrections: Optical, Perceptual and Adaptational Implications

Correcciones para la Presbicia:

Implicaciones Ópticas, Perceptuales y Adaptativas

by

Aiswaryah Radhakrishnan

for the degree of

Doctor of Philosophy

under the combined supervision of

Carlos Dorronsoro Diaz

Susana Marcos Celestino

Instituto de Optica Daza de Valdes, Madrid, 2016

To my Parents

"It is not the strongest of the species that survives, nor the most intelligent that survives. It is the one that is most adaptable to change"

-Charles Darwin

Contents

Acknowledgements

I express my sincere gratitude to my Supervisor, *Prof. Susana Marcos* for her professional guidance and her incisive insights. Her dedication, vast knowledge and unsurpassed enthusiasm has been a great source of inspiration. Above all, I thank her for giving me the opportunity to work in this multidisciplinary research group. It has been an incredible experience that helped me grow both as a researcher and as a person.

I am very thankful to my co-supervisor *Dr. Carlos Dorronsoro* for his support in both research work and otherwise. I very much appreciate the informal discussions and constructive criticisms (that kept me going during "on and off times") and being able to count on you in times of need. The repeated instructions on the 'matiz'es of sophisticated Spanish words have not gone unnoticed.

My acknowledgements to OpAL-Marie Curie ITN funding that supported my first three years of stay in Madrid, and the travels to the annual meetings and conferences. Thanks to Instituto de Optica, CSIC for providing a productive environment and Gerencia (IO) for their assistance in these four years.

Thanks to *Prof. Michael Webster* from University of Nevada, Reno and *Prof. Eli Peli* from Schepens Eye Research Institute, Massacheusets, for putting a spin to our point of view. Thanks for the taking time out for providing encouraging suggestions, your critical thinking definitely enriched the thesis. Thanks to *Prof. Peter Unsbo and Prof. Linda Lundstrom* for the long discussions during my two short stays at the BiOX lab, KTH, Sweden and a special thanks to *Abinaya Priya* for hosting me during both the visits. I am glad to have collaborated with the group on a topic of common interest, and I am gladder that I got to enjoy both a winter and summer in Stockholm. I sincerely thank *Prof. Pablo Artal* for allowing me to visit the optics laboratory at Universidad de Murcia, to see successful implementation of SLM in various optical systems.

I am indebted to the then and now members of the Adaptive Optics team. A special thanks *Lucie Sawides*, for introducing me to the AO system, for many hours of patient teaching in the lab and for the Matlab programs that helped to kick-start the measurements. Her attention to detail is impressive and intimidating. Thanks *Maria Viñas*, for the technical discussions and, more importantly, for the survival tips. I also thank *Pablo de Gracia*, for the hours spent with the SimVis. Thanks to the duo *Dani C and*

Dani P. Between the two of you, there is nothing that could not be resolved in the lab and your professional expertise was indispensable. I also thank *Jose-Ramon* for his role in miniaturizing the SimVis and for the beautiful 3D images.

My heartfelt thanks to all the members of VIOBIO. *Alberto* and *Lucie*, thanks for taking care of me during my first days in Madrid, it is because of you I survived the first few home-sick weeks. I will forever remember the first experience of night life in Lavapies, strolling in El Rastro, the manifestations and the several evenings you both spent with me to find an apartment. Thanks a lot!! I am also thankful to *Sergio Barbero* for sharing his vast knowledge, be it on the "osos de Madrid" or the Helmholtz's treatise. Thanks for referring me to La Prospe and organizing the "easy" hiking excursions.

A special mention about my extranjero contemporaries Nandor, Stephanie and Andres. *Nandor*, I have enjoyed every moment of your company during coffee-lunch breaks, Spanish classes and during the skiing/IOSA trips, your humor was a delightful diversion. *Stephanie*, thanks for putting up with me in the office during these four years listening to my odd ravings of various things. It had been such a pleasant experience being with you at 301 and during all the OpAL and non-OpAL travels. *Andres*, you could always be counted on whenever I needed little translations, tips on trying new cuisines and traveling to new cities, and not to forget the never ending conversations on homologations. Thanks to you three, for taking our friendship outside of CSIC.

I am much grateful to *Enrique Bustos* for guiding me through the several paper works that I had to do. You were always so dependable, whether on matters of ARVO registrations, homologations, NIE extensions or just for a positive word. Thanks are due to *Pablo Perez*. Your optimistic attitude is infectious, *Jorge* and *Judith* for their good-natured banter and *Miriam* for helping me with the oddities. Thanks to *Edu* and *James*, for the vague philosophical discussions on time travel or for simple questions on Black hole or for all those jokes I hardly understand. It provided a much needed form of escape from my routine. I also thank my *Tupper buddies*. The impromptu classes helped (I hope) improve my deficits with Spanish grammar.

I am thankful to the IOSA student chapter members. The monthly meetings, invariable last minute preparations for the week of science, travels to the islands and MUNCYT were fun and challenging. A special thanks to *Mario* for his special dose of "chistes"

during (IO)SA sponsored events. Thanks to all those members of IO-CSIC who spoke encouraging words in the 'ascensor' trips or in the cafeteria.

I sincerely thank all the principal investigators of OpAL for being the first time audience of our project results, polishing it with thoughtful comments and inquisitive suggestions. I would like to thank my fellow ESRs and ERs of OpAL for sitting through patiently during the annual meetings, asking questions, providing suggestions or just being politely attentive. The group photos will speak volumes of how the International assortment blended so well for the same goals, scientific or not.

I am very thankful to *Baskar Theagarajan*, being there in times of need either by bank transfers or by skype calls. Thank you for organizing the Copenhagen and Kalmar trip and for lodging me in your apartment, you were a wonderful company in all the trips we had. I am much thankful to *Karthikeyan Baskaran* for sensitizing me about this fellowship and this specific opportunity. I immensely enjoyed your company in Barcelona and Orlando. Girish, my first Matlab instructor…Thanks for your patience in introducing the complex language of programing.

It would be unfair if I do not mention many people who formed my comfort zone here in Madrid. *Sudha* and *Lakshmi*, no words can explain the joy and peace I enjoyed in your company. Sevilla, Leon, Toledo, Flamenco, Prado, Zoo…the memories linger. *Toney*, I cannot thank you enough for the equal doses of support and fun. Thanks for introducing me to skiing, for the insider info on latest mallu movies, innumerable shopping trips, and regular visits to "La Mordida" and for the early morning "chaya". *Gnaneshwari, Raghu* and *Vyas*, thanks for opening the doors of your homes and kitchens for my foodie whims and couch for my overnight stays. Thanks to Escuela La Prospe, for teaching Spanish, the seasonal excursions, the doses of feminism and for fiestas de la comida internacional. Many thanks to my Spanish teachers *Patricia* and *Juan Manuel*, you both are excellent teachers and wonderful human beings.

I express my thanks to my Alma Mater Elite School of Optometry and Medical Research Foundation, for equipping me with skills that doesn't come with the curriculum. My heartfelt thanks *Dr. Srinivasa Varadharajan*, *Prof. Seshasayee* and *Dr. Prema Padmanabhan* for their continual encouragement and blessings. A very special thanks to my friends from my previous lab *Ammu, Anshi, Kabi, Madhu, Priyanka, Sharu and Sid*, who despite being in different time zones now, are still in contact and give the "home-touch" every now and then. Thank you guys, for giving me one more thing to look forward to, when I eventually return.

Thanks to all the subjects for their time and diligence, during the never ending measurement sessions.

Finally, my sincerest thanks to my parents and my husband. *Amma* and *acha*-my first teachers. Thanks for imparting in me, this enthusiasm and the flair for adventure. Thanks for standing on my side when needed, for supporting my decisions, for the unconditional love and thanks for all those virtues that I cannot justifiably describe. Amma, thanks for sitting through the rehearsals of every single talk, going through every presentation, each manuscript and this thesis. You were an indispensable source of strength. *Vinu*, thanks for being a pillar of support, for your understanding, for the long Skype hours and for accepting me as I am. Thanks also to my extended family who gave the moral support in times of need and just the right amount of push.

Thank you all!! Muchas gracias a todos!!!

Aishu

Abstract

Purpose

Presbyopia is the physiological inability of the crystalline lens to accommodate for objects at near distance. While accommodative lenses are the ideal solutions for presbyopia, current optical solutions rely on providing an acceptable quality of vision at near and far distances. Optimization of the optical solutions rely on better understanding of how the visual system copes with the visual quality produced by the various optical solutions. The aim of this thesis is to study optical, visual and perceptual performance of different presbyopic corrections such as alternating vision, monovision and simultaneous vision, and to study the effect of adaptation on perceptual performances.

Methods

We measured and corrected ocular aberrations using custom developed adaptive optics setup, used images blurred by real aberrations of different orientation and/or magnitude and measured the internal code for blur in eyes with long term differences in blur magnitude or orientation using a classification-image like technique. We later used numerically convolved images of different far/near energy and different near additions to study the short term adaptation to pure simultaneous vision using single stimulus detection and scoring tasks. We developed, first, an on-bench and then a hand-held simultaneous vision simulator to optically simulate pure or segmented simultaneous vision corrections. Psychophysical methods were employed to study the change in visual acuity and perceptual quality for different zones of radial or angular patterns, for different orientations of an angular pattern and for different simultaneous vision solutions with two and three different far/near energy ratios. We performed simulations to predict perceptual performance from the ocular aberrations of the subjects.

Results

In subjects with different blur magnitude/orientation between eyes, we found a unique internal code for blur for both eyes. It correlated with the blur magnitude and orientation of the eye with better optical quality. Positive neural PSF was oriented significantly different from negative neural PSF. We found that simultaneous vison produced maximal perceptual degradation at around low additions (0.50 D) and the change in blur perception was correlated to the far/near ratio and amount of near addition in the adapting image. We also found that angularly segmented bifocal patterns were preferred over radially segmented patterns and two segments were preferred over multiple segments. In addition, subjects preferred different orientations (mostly along horizontal axis) of the angular bifocal pattern, and that was closely predicted by the ocular aberrations. Also, comparing the bifocal and trifocal simultaneous vision corrections, a trifocal simultaneous correction, that was dominant at far was preferred by most subjects on an average. Monovision corrections provided better perceptual quality.

Conclusions

We found that a cyclopean locus for perception and adaptation, in subjects with different blur magnitude between eyes, influenced by the eyes with better optical quality. We also demonstrated that mechanism of adaptation to simultaneous vision is similar to that of blur adaptation, influenced mostly by retinal image contrast. We also demonstrated systematic changes in visual and perceptual performance influenced by multifocal design and testing distance. The large intersubject variability was associated, though not completely explained by the optics of the eye. Our results confirm that the existing optical solutions should be chosen based on the subjective needs and the ocular optics would be an ideal starting point to customize optical solutions of presbyopia for optimal performance.

Resumen

Objetivo

La presbicia es la incapacidad del cristalino para enfocar objetos cercanos. Mientras que las lentes acomodativas son una buena solución para la presbicia, las soluciones más actuales se basan en una corrección aceptable de la visión cercana y lejana simultáneamente. La optimización de estas soluciones pasa por comprender cómo reacciona el sistema a las diferentes correcciones ópticas. El objetivo de esta tesis es el estudio óptico, visual y perceptual de diferentes correcciones a la presbicia como la visión alternante, la mono visión y la visión simultánea, y el estudio del efecto de la adaptación desde el punto de vista perceptual.

Métodos

Se han medido y corregido las aberraciones oculares mediante un sistema de óptica adaptativa de construcción propia y se han usado imágenes desenfocadas con aberraciones reales con diferentes magnitudes y/u orientaciones para medir el código interno de emborronamiento en los ojos para los diferentes desenfoques y orientaciones mediante métodos de clasificación de imágenes. Posteriormente se han usado imágenes convolucionadas numéricamente con diferentes proporciones en las energías del enfoque cercano o lejano y con diferentes adiciones para estudiar la adaptación a corto plazo en la visión simultánea pura a través de la detección y valoración de estímulos individuales. Se ha desarrollado primero un dispositivo de simulación de visión simultánea pura o segmentada montado en un banco óptico y después se ha hecho portátil y compacto. Para medir los cambios en agudeza visual y perceptual para diferentes patrones radiales o angulares con diferentes orientaciones y ratios de energía cerca/lejos se han empleado métodos psicofísicos. Se han hecho simulaciones numéricas para predecir los resultados perceptuales a través de sus aberraciones ópticas.

Resultados

En sujetos con diferentes magnitudes u orientaciones de desenfoque entre ambos ojos se han encontrado un código único de emborronamiento para ambos ojos. Está relacionados con la magnitud del desenfoque y la orientación en el ojo con mejor calidad óptica. También hemos encontrado que la visión simultánea produce una degradación perceptual máxima en adiciones bajas (0.50 D) y que el cambio en la percepción del desenfoque está relacionado con el ratio de energía lejos/cerca y la cantidad de adición cercana en la imagen de adaptación. Así mismo, hemos visto que se prefieren los patrones segmentados angularmente en oposición a los patrones segmentados radialmente y los patrones de dos segmentos se prefieren sobre los segmentos múltiples. Dependiendo de los sujetos se preferían unas orientaciones u otras en el patrón angular bifocal, fácilmente predecibles mediante el conocimiento de las aberraciones. Finalmente, comparando la corrección de visión simultánea bifocal y trifocal, la corrección preferida por la mayoría de los sujetos fue la trifocal con más energía en el foco lejano. Además, correcciones monovision tenía mejor calidad perceptual.

Conclusiones

Hemos encontrado que el locus ciclópeo para percepción y adaptación en sujetos con diferente desenfoque entre ojos está influenciado por el ojo con mejor calidad óptica. También hemos demostrado que los mecanismos de adaptación a la visión simultánea y el de adaptación al desenfoque, asociado al contraste en retina, son similares. Finalmente, descubrimos sistematicidad en los cambios en la sensación visual y perceptual influidos por el diseño bifocal y la distancia del estímulo. La variabilidad intersujetos se puede relacionar parcialmente a las características ópticas de cada ojo. Nuestros resultados confirman que las soluciones ópticas existentes deben escogerse basándose en las necesidades del sujeto. Así mismo, se observa que las características ópticas de cada ojo son un punto inicial necesario a la hora de personalizar soluciones personales a la presbicia.

Key Words

human eye, optics, crystyalline lens, accommodation, **presbyopia**, alternating vision, contact lens, intraocular lens, **simultaneous vision**, segmented bifocals, extended DoF, **monovision**, physiological optics, ocular aberrations, **interocular blur difference**, optical simulation, visual optics, **retinal image quality**, metrics of image quality, **point spread function**, modulation transfer function, RMS contrast, **strehl ratio**, visual strehl, visual psychophysics, visual acuity, blur detection, spatial vision, perception, **blur adaptation**, contrast adaptation, parafoveal blur, simultaneous blur, **cyclopean locus**, orientation preference, **neural PSF**, internal code for blur, visual performance, pattern preference, ophthalmic instrumentation, **Hartmann-Shack**, aberration measurement, **adaptive optics**, aberration correction, **vision simulator**

List of Abbreviations

AO: Adaptive Optics

CL: Contact Lens

D: Diopters

DL: Diffraction Limited

HOA: Higher Order Aberrations

IOL: Intraocular Lens

MF: Multifocal

MTF: Modultaion Transfer Fucntion

OD: Oculus Dexter (Right Eye)

OS: Oculus Sinister (Left Eye)

OTF: Optical Transfer Function

PBF: Perceived Best Focus

PD: Pure Defocus

PSF: Point Spread Function

RMS: Root Mean Square

SimVis: Simultaneous Vision Simulator

SR: Strehl Ratio

SV: Simultaneous Vision

VSOTF: Visual OTF

Chapter ONE

Introduction

The goal of this doctoral thesis is to study the optical, perceptual and adaptational implications to newer solutions of Presbyopia, in specific the simultaneous bifocal and multifocal corrections. In this chapter we introduce the main background and key concepts regarding the approach followed in the thesis. The complexities of the visual system; factors affecting retinal image quality and perception; basic concepts of aberration measurement and correction; and, metrics of optical quality are introduced briefly. A comprehensive review of blur adaptation followed by a brief overview on newer presbyopic corrections, concepts pertaining to simultaneous vision corrections and their impact on visual performance are elaborated.

1.1 Motivation

Restoration of near vision in a presbyope is challenging. Despite the availability of conventional optical solutions such as alternating vision, monovision and simultaneous vision corrections are becoming increasingly used solutions to restore near vision in presbyopic patients (Kohnen, 2008, Charman, 2014b, a). Alternating vision is usually provided in the form of spectacles, with distinct portions for far, near (and intermediate) corrections and the wearer has clear vision at one distance only (Charman, 2014a). In monovision one eye is corrected for far vision and the other eye is corrected for near vision, using contact lenses or surgical means (LASIK or IOLs). Though this provides a presbyope with clear vision, for a large field, it induces problems on binocular vision (Garland, 1987, Evans, 2007). Simultaneous vision is provided by multifocal optical contact lenses or IOLs, using different parts of the pupil of the same eye for corrections at far and near distances. These multifocal solutions produce at the retina superimposed blurred and sharp image refracted by the different refracting components (Charman, 2014b). While, these corrections augment near vision better than a monofocal correction at distance, it comes at the expense of a degradation of the distance visual performance (Leyland and Zinicola, 2003, Montes-Mico and Alio, 2003, Cillino et al., 2008, Cochener et al., 2011). It is speculated that the brain counteracts this complex blur by the suppression of either distance or near image, eventually adapting to the other. However, not all subjects can adapt to this complex blur, as indicated by the explantation rate with multifocal IOLs (Bellucci, 2005, Kamiya et al., 2014, van der Mooren et al., 2015). A better understanding of the optical properties of these corrections and how they influence the visual perception and adaptation will help in designing better optical solutions for presbyopia, which provides an optical visual and perceptual quality at all distances.

1.2 The Human Visual System

Functionally, the human visual system consists of two parts: the eye and (part of) the brain. It is probably the classic example of the optimization of performance with evolution. It is the most complex and robust image processing system working with a balanced combination of optical, biological and psychological processes. The rapid and accurate processing of the 3D environment creates a perceptual veridicality.

The physiology of seeing (Crescitelli, 1960) is a complex process with the transformation of a scene from the external world to a certain perception happening in various stages: Focusing of the light from the scene by the eye's optics; initial sampling by the photoreceptors transducing light into voltage and electrochemical signals, sampling by the retinal ganglion cells, after being processed by the horizontal, bipolar, and amacrine cells (Rea et al., 2005); ending with formation of perceptual representation at the visual cortex. How exactly the highly ambiguous pattern of light that is detected at the retina is transformed into visual consciousness remains one of the greatest unsolved problems of science. Subsequent sections in this chapters describes these processes in justifiable detail.

1.2.1 The Human Eye: Overview

Charles Darwin accurately described the adaptability and the sophistication of the eye as in his "*Origin of Species by means of Natural selection*" as *"To suppose that the eye with all its inimitable contrivances for adjusting the focus to different distances, for admitting different amounts of light, and for the correction of spherical and chromatic aberration, could have been formed by natural selection, seems, I freely confess, absurd in the highest degree"*. The path of the light entering the eye is modulated by various optical components (the tear film-cornea and crystalline lens) before impinging on the retina. Figure 1.1 shows the anatomical cross section of the eye. The outermost collagenous layer of the eye is called sclera. Underneath sclera is the choroid, which is the vascular pigmented layer, and continues anteriorly as the ciliary body and the iris. The choroid is responsible for absorbing most of the scattered light within the eye. The innermost nervous layer that lines the back of the eye is called the retina. The two major refracting components: The cornea and the crystalline lens, act as compound lenses with an approximate refraction of 60 D and are aligned at their optical axes (Atchison and Smith, 2000). In addition, the diameter of the pupil (a diaphragm controlled by the iris) is constantly modulated in response to the luminance, controlling the effect of diffraction or aberrations in the retinal image. The retina is conveniently positioned at the back focal length of this compound lens system (the axial length of the eye, 22.22 mm) which further transmits the information (Smith and Atchison, 1997) to the brain. The shape of the retina, also compensates for the chromatic errors and field distortions in refraction (Rynders et al., 1998).

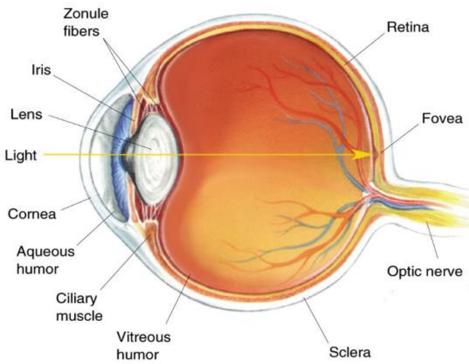

Figure 1.1: Sagittal section of the Human eye

Cornea

Cornea is a multilayered meniscus lens with a central thickness of 520 µm and a peripheral thickness of about 650 µm and has a transmissibility of 97%. The cornea is a mildly prolate structure with an asphericity of -0.15. The radius of curvature of the anterior surface is about 8 mm and that of the posterior surface is about 6.5 mm; and the diameter is about 11 mm (Barbero, 2006, Navarro, 2009). In general, the cornea is considered a homogeneous medium with an accepted refractive index 1.376. The tear-film and the anterior cornea constitute for about 80% (48 D) of the total refractive power of the eye. The posterior surface contributes about -6 D to the total refractive power of the eye. The average corneal astigmatism is 0.45 D along the vertical axis (Atchison and Smith, 2000, Navarro, 2009).

The human cornea is comprised of five morphologically distinct layers: Epithelium, Bowman's membrane, Stroma, Descemet's membrane and Endothelium (Barbero, 2006). Functionally, there are two limiting membranes: epithelium and endothelium, and the stroma. Epithelium is a tight multi cellular layer interdigitating with the tear film forming a smooth anterior surface. The stroma comprises about 90% of corneal volume and primarily contains oriented collagen fibers interspersed in an intercellular matrix of less denser material. The ability of cornea to perform as a refractive element is possible due to the critical organization of the stromal collagen fibrils and maintenance of dehydration by the monocellular endothelium.

Crystalline Lens and Accommodation

The human crystalline lens is a transparent, biconvex lens with aspheric surfaces situated between the iris and the vitreous. Typically, the crystalline lens is described as an onion-like structure that has densely packed concentric fibers in an elastic capsule. Radially arranged bundles of zonular fibers connect the lens equator to the ciliary body. The equatorial diameter of the lens is 10 mm and the antero-posterior thickness in an unaccommodated state is about 4 mm. The average anterior radius of curvature is 10 mm and the radius of curvature of the posterior surface is -6 mm. The capsular epithelium regenerates lens fibers throughout life forming the denser nucleus at the center and the relatively loosely packed cortex. The crystalline lens has a Gradient Refractive INdex (GRIN) with the refractive index gradually increasing from 1.38 in the cortex to 1.41 in the nucleus (Campbell, 1984, de Castro et al., 2010). It contributes about 16 D to the total power of the eye.

The crystalline lens has a unique ability to change its shape and size with change in the object vergence. This process of increasing optical power of the lens is called accommodation. The most accepted theory of accommodation was proposed by Helmholtz (Hartridge, 1925). During accommodation, the contraction of the ciliary muscle reduces zonular tension around the lens equator, resulting in the relaxation of the lens capsule. This in turn results in increase in anterior curvature of the lens and an increase in central thickness. In fact, the change in the lens curvature is accompanied by convergence of the two eyes and constriction of the pupil (miosis) comprising the classic *near triad* or *the accommodative reflex* (Myers and Stark, 1990). The ability to accommodate declines with age (Glasser and Campbell, 1998) and results in Presbyopia (see later).

The Neurosensory Retina

The retina is a nervous tissue situated posteriorly approximately at the focal length of the optical components of the eye. Its thickness varies between 0.1 mm from the ora serrata to 0.5 mm near the optic disc. The light focused by the eye's optical system is converted to electrical impulses to be transmitted to the cortical center by a process called photochemical transduction (Rea et al., 2005). Fovea centralis is the most sensitive part of the retina, which is situated as a depression at the center of macula, which is located slightly temporal to the optic axis of the eye. The optic disc is located at the center of the retina and the optic nerve emerges from here transmitting information to the brain. This region of the retina is not light sensitive and is called the blind spot.

A radial section of a portion of the retina (Fig. 1.2) reveals organization of the different retinal layers. The neural retina consists of three main groups of neurons (Oyster, 1999): the photoreceptors, the bipolar cells and the ganglion cells. The rods and cones together comprise the photoreceptors and are responsible for scotopic and photopic vision respectively; and are adjacent to the retinal pigment epithelium. The bipolar cells are the first order neurons connecting the photoreceptors to the ganglion cells. The ganglion cells lie innermost in the retina closest to the lens and front of the eye and are relay neurons.

Light must, therefore, travel through the thickness of the retina before striking and activating the rods and cones. Subsequently, the absorption of photons by the visual pigment of the photoreceptors is translated into first a biochemical message and then an electrical message that can stimulate all the succeeding neurons of the retina. The retinal message concerning the photonic input and some preliminary organization of the visual image into several forms of sensation are transmitted to the brain from the spiking discharge pattern of the ganglion cells (Atchison and Smith, 2000, Rea et al., 2005). The organization of the photoreceptors and the neurons vary from center to periphery resulting in sensory and functional differences between the central and peripheral retina (Oyster, 1999). Finally, only about 10% of information that reaches the eye is transmitted to the visual cortex for processing.

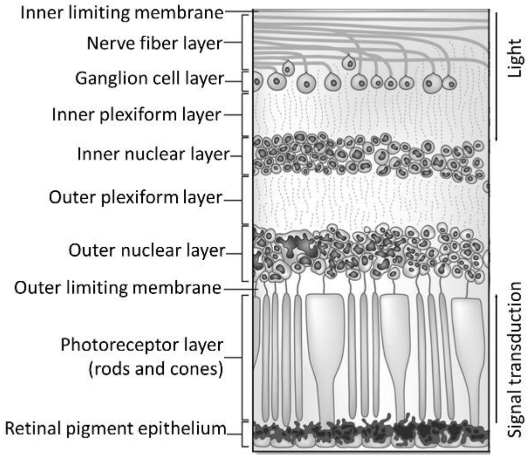

Figure 1.2: Section of retina showing different layers involved in phototransduction (Adapted from: (Maghzi et al., 2013)

1.2.2 Retinal Image Quality

The incongruencies between the optical components of the eye is well known and render the retinal image far from perfect. The retinal image quality is quite dynamic. Intrinsic factors like accommodation, pupil size and quality of the tear film; and extrinsic factors like luminance in the scene can augment or deteriorate the retinal image quality (Artal and Navarro, 1994, Thibos et al., 2002b). Imbalances between the optical distances and the focal length of the optical components; or the minute misalignment of the optical components could result in lower or higher order ocular aberrations.

Ocular aberrations

von Helmholtz (1881) first reported the presence of monochromatic aberrations in the human eyes in his Treatise on Physiological Optics as "*The monochromatic aberrations in the optical system of the eye are not, like the spherical aberration of glass lenses, symmetrical about an axis. They are much more unsymmetrical and of a kind that is not permissible in a well-constructed optical instrument*". The presence of monochromatic aberrations blurs the retinal image, resulting in reduced image contrast at different spatial frequencies thereby reducing the resolving power of the eye. The lower order aberrations, defocus and astigmatism, are the most prominent of the ocular aberrations (Thibos et al., 2002b). Myopic or hyperopic defocus and astigmatism are generally of larger magnitude and can be treated by providing refractive corrections as spectacles, contact lenses or refractive surgeries. The higher order aberrations like coma or spherical aberrations, in the absence of the lower order aberrations, are responsible for the light spread in the retina. Recent research indicates that the higher order aberrations introduced by the cornea are compensated to a certain extent by the internal optics of the eye (Artal et al., 2001, Smith et al., 2001). Also, recent studies show that the ocular aberrations interact with each other resulting in a favorable retinal image quality, including partial compensation of chromatic aberration (Applegate et al., 2003, McLellan et al., 2006). Statistically significant differences in the ocular aberrations between eyes and between ethnic groups are noted (Porter et al., 2001, Thibos et al., 2002b). Some studies also report interocular mirror symmetry, especially along the vertical meridians in the aberrations (Marcos and Burns, 2000).

Measurement of Ocular aberrations

Several techniques have been developed in the recent past to measure the aberrations of the human eye (Howland and Howland, 1976, Howland and Howland, 1977). The working principle of most of the aberrometers is to measure the local derivative (slope) of the wave aberration by measuring the deviation of the emergent wavefront (outgoing aberrometry) or the image of the standard beam at the retina (ingoing aberrometry). In this thesis, we have used a custom developed Shack-Hartmann wavefront sensor (SH), which is an outgoing aberrometer.

The ***Double-pass method*** (Marcos, 2003) is another method in which a series of images of a point source at the retina is recorded. This technique provides relevant information on the eye's optical quality. In ***Laser Ray Tracing (LRT)*** technique (Marcos, 2003) the pupil is sampled sequentially by scanning a laser beam across it. Aberrations are computed as angular deviations between the centroids of each aerial image captured using a CCD camera in the conjugate plane (Marcos, 2003).

In ***Shack-Hartmann*** aberrometry (Marcos, 2003) narrow beam of light is focused onto the retina. Reflected wave from various parts of the pupil is then sampled by an array of lenslets (Fig. 1.3) that focuses the emergent light onto a CCD camera. Figure 1.3 shows an image of the spots from a perfect system and from an aberrated eye. The wavefront can be reconstructed by comparing the emergent wavefront from a reference sphere.

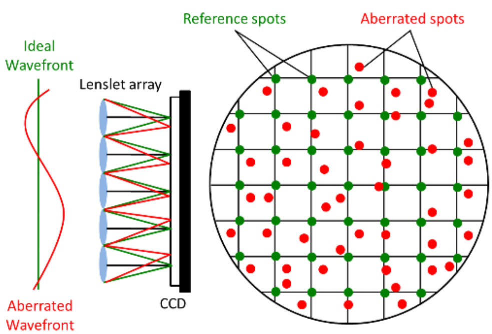

Figure 1.3 Shack-Hartmann aberrometry: Illustration of sampling by the lenslet array of an ideal and aberrated wavefronts

Availability of rapid and compact aberrometers, in the last decades has enabled not only researchers, but also the clinicians to measure accurately the corneal and ocular aberrations following refractive surgery or contact lens fitting. In the recent years methods to compensate for these aberrations have also been developed, which enable better visualization of the retina. This technique, called Adaptive Optics has been increasingly used in vision science not only for correction of aberrations, but also for inducing newer aberrations and studying the changes in perception (See later).

Representation of monochromatic aberrations

Ocular aberrations can be represented as wave aberrations. The imagery of a perfect optical system of finite focus is a sphere. A wavefront map is two or three dimensional representation of the deviation of the ocular wavefront from the reference sphere (Fig. 1.4) in the pupil plane. Numerous mathematical methods are available for representing wavefront aberrations (Born and Wolf, 1999). In Taylor's polynomials the aberrations are represented as Cartesian co-ordinates and in Seidel's polynomials geometric aberrations of centered optical system are represented in polar coordinates.

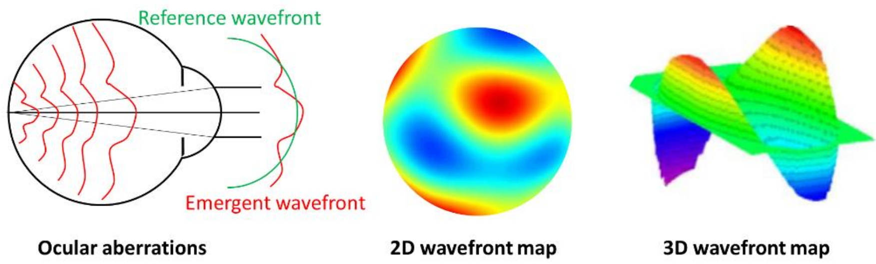

Figure 1.4: Representation of ocular wavefront aberrations from reference sphere (Adapted from Marcos, 2005)

Any three-dimensional surface which is bordered by a circular curve can be represented by a weighted sum of polynomials called the Zernike polynomials (Thibos et al., 2002a), which is the most commonly used mathematical representation. The aberrations are represented as polar co-ordinates specified by a radial order n and a frequency number m which corresponds to the highest exponent of the radial variable ρ and the coefficient of the angular variable θ respectively. It is given by the formula

$$W(\rho,\theta) = \sum_{n,\,m} C_n^m Z_n^m(x,y) \qquad \text{(Eq 1.1)}$$

The Zernike polynomials are most suitable for circular pupils and vary with pupil size (Schwiegerling, 2002). Zernike polynomials are orthonormal for a unit circle and hence subsequent addition of higher orders does not influence the values of lower orders. The 2-D wavefront maps of the Zernike polynomials up to the sixth order are given in figure 1.5A. The second order terms correspond to the defocus and astigmatism.

Metrics of Retinal Image Quality

Several retinal image quality metrics are proposed from Fourier computations of the wavefront aberrations (Goodman, 1996). These can be broadly classified in to pupil plane based metrics and image plane based metrics. We will discuss the retinal image quality metrics used in the thesis.

The most commonly used global retinal image quality metric is ***the Root Mean Square (RMS)*** of the wavefront error (Born and Wolf, 1999). It is a pupil plane metric, but it does not provide information on the shape of the wavefront. It is simply the square of sum of the Zernike coefficients:

$$RMS = \sqrt{\sum_{n,m} {C_n^m}^2} \qquad \text{(Eq 1.2)}$$

The image plane metrics can be subdivided as metrics based on the point spread function or metrics based on the optical transfer function.

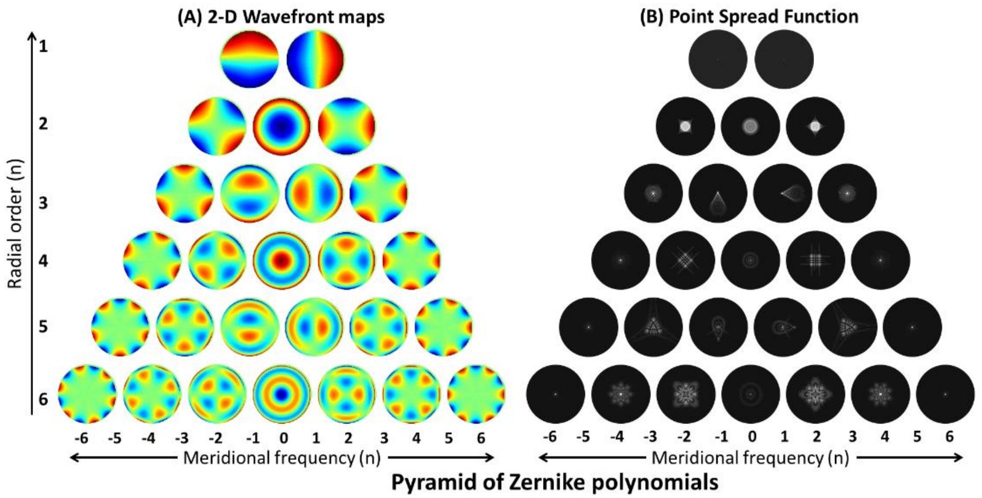

Figure 1.5: Zernike polynomials (A) 2 D wavefront maps (B) Point Spread Functions. Computed using Fourier transformation for 0.5 microns and 5 mm pupil size

Point Spread Function (PSF) is the spread of an ideal point as measured in the spatial domain of the image, calculated as the squared magnitude of the inverse Fourier transform of the pupil function (Born and Wolf, 1999, Bass et al., 2010) .

$$PSF(x,y) = K\left| FT\left[A(x,y)\exp\left(i\frac{2\pi}{\lambda}W(x,y) \right) \right]_{fx=\frac{x}{z},fy=\frac{y}{z}} \right|^2 \quad \text{(Eq 1.3)}$$

$$= K\left| FT\left[P(x,y) \right]_{fx=\frac{x}{z},fy=\frac{y}{z}} \right|^2$$

where, K is a constant, P(x, y) is the pupil function, A(x, y) is an apodization function (when the waveguide nature of cones is considered) and W(x, y) is the wave aberration. The pupil function, P(x, y) is zero outside the pupil. FT is the Fourier Transform operator, z is the distance from the pupil to the image (eye length). The PSFs for the corresponding Zernike coefficients in the Zernike Pyramid is given in Figure 1.5B. In a perfect optical system, the PSF is limited by Fraunhofer's diffraction.

Modulation Transfer Function (MTF) is a representation of the decrease in image contrast as a function of spatial frequencies (Fig. 1.6A). It is calculated as the modulus of the ***Optical Transfer Function (OTF)*** obtained by Fourier transforming the PSF. The phase of the OTF, gives the ***Phase Transfer Function (PTF)***, significantly influences the image quality metric in presence of asymmetrical aberrations such as astigmatism and coma (Applegate et al., 2003, Marsack et al., 2004).

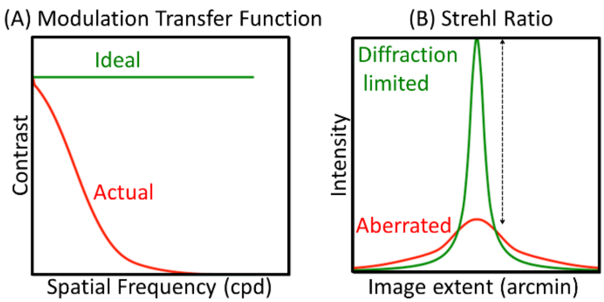

Figure 1.6: Retinal Image Quality Metrics (A): Modulation transfer function of an ideal optical system and an aberrated system (B) Illustration of Strehl ratio as the peak intensity ratio of diffraction limited PSF and PSF of aberrated eye

Strehl Ratio (SR) is a scalar metric (Bass et al., 2010) calculated as the maximum value of PSF of the aberrated eye to the maximum value of the PSF in a diffraction limited eye (Fig. 1.6B). Thus the SR can range between 0 and 1. Similar to RMS, this is a global metric and provides no information on the shape of the wavefront. It can also be computed as the volume under the OTF. Recently, Iskander (2006) proposed ***Visual OTF (VSOTF)*** an image quality metric that closely represents visual quality. VSOTF is computed by calculating the volume under the OTF obtained by multiplying inverse of population-average Contrast Sensitivity Function (CSF) with the actual OTF.

However, in addition to wave aberration (including diffraction) various factors such as scatter and chromatic aberration affect retinal image quality. These factors reduce the predictability of these retinal image quality metrics for perceptual performances (Thibos et al., 1991, Cheng et al., 2004).

1.2.3 The Visual Cortex

The visual cortex is located at the occipital lobe of the human brain. The pioneering work that has led us to the current understanding of the locus of vision in the occipital cortex was conducted by the physiologist Hermann Munk in 1878 (Finger, 1994). His experiments of "Psychic Blindness" in dogs opened a whole new arena in Neuroscience for vision. The path taken by the light leaving the retina can be seen in figure 1.7A. The electrical signals pass through the optic nerve, following a path that crosses at the optic chiasma. The crossed signals reach the primary visual cortex (V1, or striate cortex) as optic radiations after crossing the lateral geniculate nucleus. Over 20 extra-striate cortical regions (Greenlee and Tse, 2008) have been identified (V2, V3, V4 and V5/MT). The visual area constitutes about a quarter of the cortex and foveal neurons occupy majority of the primary visual cortex (Fig. 1.7B). At the visual cortex the signals are processed in V1 and communicated via multiple pathways to numerous visually responsive cortical areas.

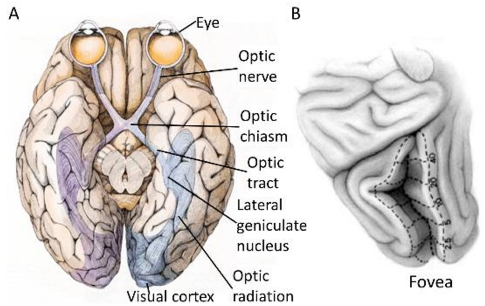

Figure 1.7: Visual Cortex (A) Visual pathway (Hubel, 1988) (B) Representation of fovea in the left visual cortex (Greenlee and Tse, 2008)

Visual system is a complex cascade of feedforward, feedback and parallel processing signals (Grill-Spector and Malach, 2004). The primary visual cortex/V1 is the predominant region of pattern vision. Cortical area V2 has larger receptive fields and are responsible for illusory contours. The cortical area V4 has even larger receptors and alters recognition due to attention and enhances foveal representation. The foveal magnification factor is highest at V4 (Greenlee and Tse, 2008). The inferotemporal cortex neurons are highly active in processing irregular shapes. This region is also affected by familiarity, and the neurons respond stronger to familiar patterns (Gregory, 1997). These neurons respond regardless of object rotation and dimension. Receptive fields of the visual cortex are also known to be tuned for orientation and spatial detection (Webster and De Valois, 1985, Ringach et al., 1997).

Recent research has added ample information on how and where each component of a visual perception such as luminance, edges, textures, colors, motion etc. are processed. Yet we are far from understanding how perception of the real world's complex scene occurs.

Spatial Vision and Visual Perception

Psychophysically, perception is the ability of the visual system to interpret the information present in the visual scene. The three major concepts that help in understanding the visual perception are perceptual organization, perceptual segregation and perceptual construction (De Valois and De Valois, 1988, Gregory, 1997).

Perceptual organization is simply structuring the information. Also known as Gestaltism, this concept explains basic visual concepts such as apparent movements and illusory contours. Perceptual organization is found to be crucial especially in discrimination tasks.

Perceptual segregation is the concept of separating the foreground from background. Various factors such as symmetry, contour, orientation, familiarity and size influence construction of foreground (or the object). It is however debated whether the segregation happens before or after the actual perception.

Perceptual construction is a result of interaction between the neural bottom-up and top-down processes. The main principle of construction is totality which accounts for the global perception of a complex scene.

In addition to the above mentioned processes, a number of factors including previous experience, intelligence and cognitive capabilities influence visual perception to various extents, which could account for the discrepancy between the stimuli and response, in other words the objective and subjective visual quality.

Factors affecting Vision

Visual resolution of an image in a controlled environment is mediated by three main factors: Anatomical, Optical and Neural (Campbell and Green, 1965). Spatial phase errors are introduced by ocular aberrations. Correcting ocular aberrations might result in superior retinal image quality, however, this might not be translated to improved visual performance due to limitations imposed by the anatomical and neural factors. ***Contrast Sensitivity Function (CSF)*** is the representation of contrast sensitivity as a function of spatial frequency and shows that human eyes have a peak sensitivity around mid-spatial frequencies. The difference between the MTF and the CSF (Fig. 1.8) accounts largely for the neural processing and is referred as ***Neural transfer Function***.

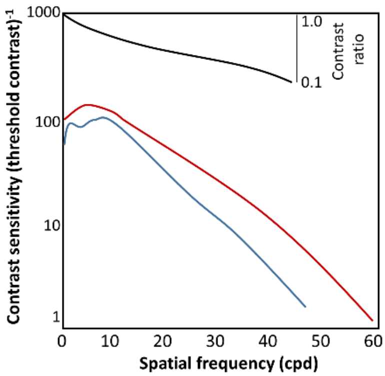

Figure 1.8: Modulation transfer function of the eye (in black), measured retinal contrast sensitivity function (in red) and subjective contrast sensitivity function (in blue). (Adapted from Campbell and Green, 1965)

The sampling of the image by the retinal mosaic forms an important limitation to the resolving power of the eye at fovea (Thibos, 1998, Thibos, 2012). The basis of sampling theory comes from the assumption of Helmholtz who proposed that, as shown in figure 1.9A, for visual resolution it requires at least one unstimulated neuron between two relatively stimulated neurons (De Valois and De Valois, 1988).

The photoreceptors at the fovea are densely packed and have one to one connection with the ganglions. According to Nyquists theorem, the photoreceptor packing density needed to resolve a signal is twice the maximum frequency content in the stimulus, called the *Nyquists frequency* (De Valois and De Valois, 1988). Any improvement in the optics leads to abnormal sampling by the photoreceptors resulting in aliasing (Fig. 1.9B). In fact the optics of the eye acts as a low-pass spatial filter to avoid aliasing in the fovea. The luminance information sampled by photoreceptors are integrated resulting in spatial summation. Foveal vision is also optimized by the Stiles-Crawford phenomenon. The cones act as a waveguide transmitting light that are parallel to their orientation and scattering the rest.

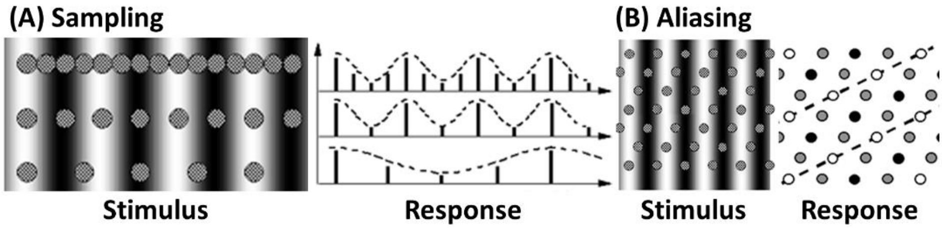

Figure 1.9: Sampling theory: (A) Oversampling (Top row), optimal sampling (middle row) and undersampling (bottom row) of the receptors of the same spatial frequency and the corresponding responses (B) Undersampling resulting in aliasing and misrepresentation orientation (Thibos, 2012)

The visual system can function over a large range of luminance levels, and different rates of change in luminance. The periodic sampling of the image happens spatially as well as over time (Cornsweet, 1970, Schwartz, 2004). The visual system usually averages any given information over a period of time. Intermittent stimuli are perceived as separate if the rate of presentation is less than a period of time. A slow rate of presentation produces a sensation of flicker, which ceases beyond the *critical flicker frequency (CFF)*. The factors affecting this critical flicker frequency are temporal summation and temporal resolution. For a stimulus to be perceived it should be presented for a certain period of time called the critical duration (Fig. 1.10A), and stimulus detection depends on temporal summation (Fig. 1.10B). In addition, for two flashes to be perceived separate, they must be presented with an interval of critical duration (Fig. 1.10C). The average CFF for foveal scotopic vision is about 60-75Hz.

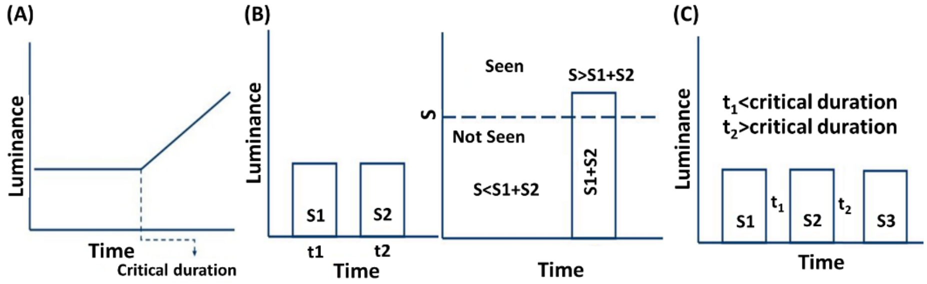

Figure 1.10: Temporal visual processing (A) Bloch's law for critical duration (B) Temporal summation (C) Temporal resolution (Adapted from Schwartz, 2004)

While these factors form the first step in visual perception, actual form vision is influenced by factors like contrast, contour, attention and familiarity. Contrasts and contour could be attributed as extrinsic factors associated with the stimulus. While familiarity alone is insufficient to provide perceptual advantage, it is an important subjective factor affecting visual perception (Cornsweet, 1970, Schwartz, 2004).

At peripheral retina, resolution and perception are not just accounted for by the density of cones and rules of sampling. The receptive field size is larger and that in combination with a reduced representation of neurons in the V1 results in a poorer visual resolution in the periphery, but for the same reason, the peripheral retina outperforms fovea in motion detection (Grill-Spector and Malach, 2004).

Psychophysics and Vision

The term psychophysics was first introduced by Fechner (Ehrenstein and Ehrenstein, 1999), with the goal of using a scientific method to study the relationship between physical and phenomenal facts. Psychophysical methods are frequently used in various aspects of vision science like, visual acuity measurements, quantifying contrast sensitivity, color vision testing, blur judgments etc., involve perceptual tasks resulting in measurement of absolute or relative threshold. Conventionally, the threshold is defined as the point in the frequency-of-seeing curve (Fig. 1.11A) where the stimulus is seen at least 50% of the times. Absolute threshold is the minimum amount of energy that a stimulus should possess to produce visual sensation and the amount of energy required to produce Just-Noticeable-Difference (JND) in visual perception is called as differential threshold (Geischeider, 1997, Ehrenstein and Ehrenstein, 1999).

The perceptual tasks can be broadly grouped to detection, identification, and discrimination and scaling (Pelli and Farell, 1995, Phipps et al., 2001). Target detection tasks require the perception of just presence or absence of the stimuli (e.g. Visual acuity measurement with Tumbling E and Landolt's C). Visual acuity measurements with Snellen or ETDRS charts could be examples of identification or recognition tasks. Discrimination depends on the differential threshold, where the task of the subject is to identify one stimuli from other. Color vision testing with FM100 method involves discrimination of different hues of the same color. Scaling or matching tasks are usually used in contrast sensitivity measurements. The observer scales the contrast of a given stimulus until it is seen or not seen.

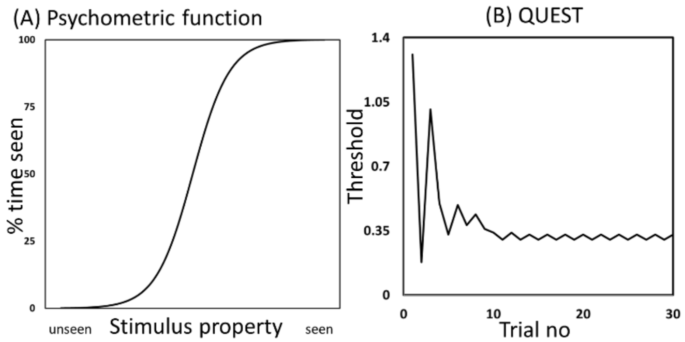

Figure 1.11 Psychophysical methods (A) Psychometry function: The Frequency-of-Seeing curve (B) Threshold estimation by QUEST

While the task itself is subjective, there are various methods by which the stimulus properties can be changed to obtain the threshold. ***Method of adjustments*** is the simplest and quickest way to determine absolute and differential thresholds. Usually the subject is allowed to adjust the stimulus intensity until it is just visible/becomes just noticeably different from a standard stimulus. Though this method is quite rapid, the results could be highly variable and requires a large number of repetitive trials. ***Method of constant stimuli*** usually starts with a set of stimuli values that are determined by adjustment, presented in quasi random order. The subject's response is recorded for each trial. ***Method of limits*** is another method where the stimulus intensity is increased or decreased from non-seeing to seeing or seeing to non-seeing area. The subject's response for each of the ascending or descending trials is noted and the threshold is obtained (Pelli and Farell, 1995, Geischeider, 1997).

Adaptive testing procedures based on the method of limits have also been proposed (Phipps et al., 2001). The stimulus value is changed according to the subject's response, resulting in lesser number of trials required to arrive at the threshold (Fig. 1.11B). The most commonly used adaptive testing methods are Parameter Estimation by Sequential Testing **(PEST)** and Quick Estimation by Sequential Testing **(QUEST)**. These psychometric procedures assume that the underlying psychometric function is sigmoid in nature and modifies the likelihood probability density function of threshold estimation according to the subject's response (Watson and Pelli, 1983).

Most of these are discrimination tasks and require large number of trials. They differ from the adjustment method by limiting the number of alternative responses that the observer is allowed. In this thesis, we have used two and eight alternative forced choice methods. In a two alternative forced choice the subject is sequentially presented two stimuli and is forced to choose whether the better focused image is presented first or second. In such a case, there is a 50% chance of guessing the corerct response (0.5 guess rate) and hence the threshold is set at the midpoint above this guess rate (75%).

Choosing a right psychophysical paradigm and the perceptual task depends very much on the threshold measured. In this study we have used several psychophysical methods, which will be described in detail in subsequent chapters corresponding to the methods and the specific experiments.

Stimulus Manipulation for Psychophysics

Earlier studies on visual optics used Gabor stimulus or Optotypes to study effect of blur on visual acuity and contrast sensitivity. Fourier methods to describe optical quality of the eye was introduced by Flamant (Arnulf et al., 1951), where a Slit Target was convolved with the Line Spread Function of the eye and later, light distribution was studied by Westheimer and Campbell (1962). However visual stimulus contains a plethora of information in addition to the restricted spatial frequencies tested by these methods.

Natural images or complex noise stimuli were introduced in visual psychophysics by early researchers. Webster and colleagues sharpened or blurred the natural images by modifying the slope of the amplitude spectrum as shown in figure 1.12 (Webster et al., 2002, Elliott et al., 2011). This approach was adopted by many researchers to understand perception and contrast adaptation in the central and peripheral vision.

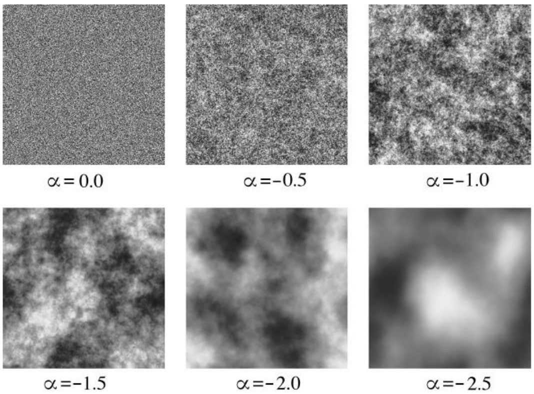

Figure 1.12: Manipulation of image by altering the slope of amplitude spectrum (Elliott et al., 2011)

A more naturalistic representation of the retinal image quality can be obtained by convolving the image with the PSF of the eye (Fig. 1.13) for specific pupil size, viewing angle and wavelength. Initially this method was employed by researchers to simulate the retinal image quality from the measured aberrations (Artal, 1990). Later, Thibos and Bradley (1995) studied the effect of spatial filtering and sampling on neural processing by mathematically manipulating the images. Ever since various vision scientists have used images manipulated with the measured ocular aberrations or simple defocus and astigmatism to study visual functions like visual acuity, or blur judgements.

Images convolved with ocular aberrations were used to study the effect of aberrations on visual acuity (Applegate et al., 2003) and to study the effect of manipulated aberrations on visual perception and adaptation (Sawides et al., 2011a, Sawides et al., 2011b). Similar techniques have also been employed to study the effect of defocus and astigmatism on visual acuity and perception (Sawides et al., 2010, Ohlendorf et al., 2011b, a, Vinas et al., 2012). Peli and Lang (2001) and de Gracia et al. (2013a) simulated image quality through multifocal lens and attempts have been made by researchers recently to simulate multifocality by image manipulation (Radhakrishnan et al., 2014).

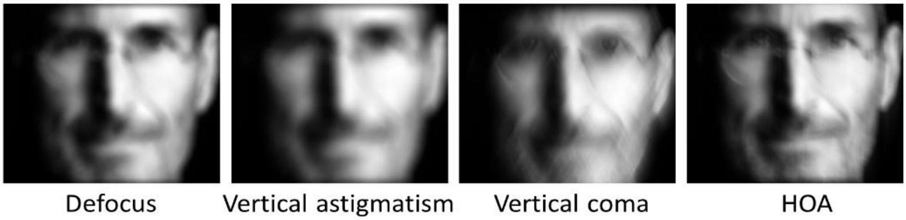

Figure 1.13: Blurring of image with 0.5 microns of defocus, astigmatism, coma and higher order aberrations of a normal eye

Though some studies show that differences exist between actual and simulated measurements, such manipulations allow better control of stimulus properties, especially when presented through an adaptive optics setup.

Adaptive Optics for Vision Science: Visual benefits and Stimulus Manipulation

The concept of Adaptive Optics (AO) for vision was adopted from astronomy where they were used to obtain theoretically best optical resolution. The principal components of an adaptive optics system are a wavefront sensor, for wavefront measurement; and a deformable mirror that runs either in closed or open loop to correct aberrations (Porter et al., 2005).

In the earlier sections we saw a brief account of various wavefront sensors. There are two basic types of phase modulators or deformable mirrors: Segmented and continuous (Fig. 1.14). These mirrors alter the phase profile of the incident wave by altering its surface. The efficiency of correction is indicated by stroke width which depends on the number of actuators available for correction. AO was first used in vision science by Dreher et al., (1989) using a deformable mirror to correct astigmatism during Scanning Laser Ophthalmoscopy to obtain better retinal images in tomographic measurements. The advent of wavefront sensors for ocular aberration measurements by Liang et al., (1994), led to tremendous leap in the use of AO in retinal imaging. Figure 1.14 shows a basic adaptive optics setup used for vision science. Roorda et al., (Roorda and Williams, 2002, Roorda, 2010) developed one of the first confocal scanning laser ophthalmoscopes for retinal imaging. This enabled imaging the photoreceptors with better resolution as seen from figure 1.15.

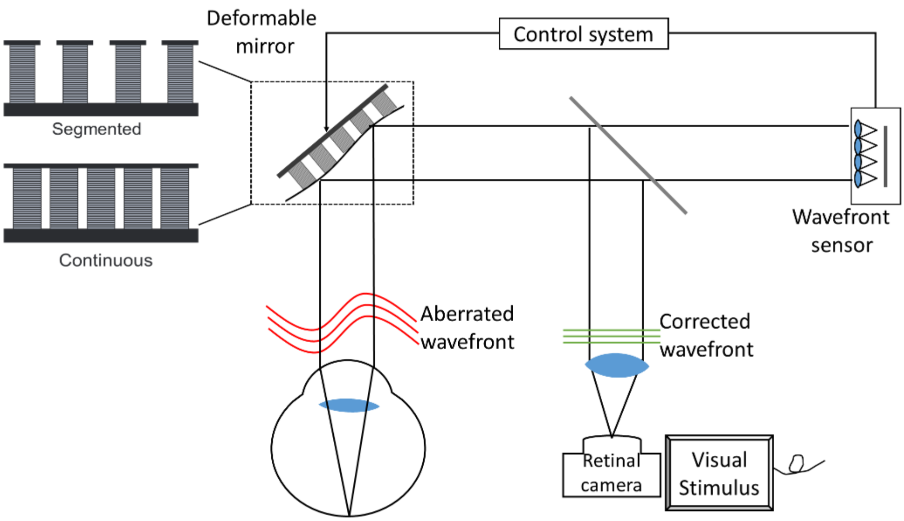

Figure 1.14: Adaptive optics for vision science

A number of modifications were later implemented by several researchers towards improving the image quality by expanding to broader spectrums of wavelength or compensating for the fixational eye movements (Burns et al., 2007).

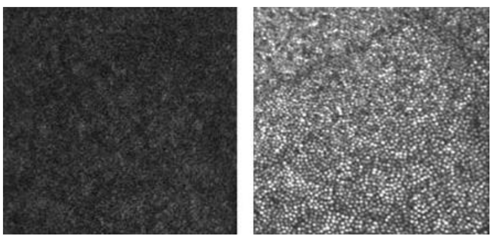

Figure 1.15: Photoreceptor mosaic imaged with SLO without AO (left) and with AO (right) (Roorda and Williams, 2002)

Later AO imaging was combined with optical coherence tomography which provided quantum leap in the 3D measurements of the retina (Liang et al., 1997, Miller et al., 2011). These developments have enabled researchers to investigate optical properties of retinal neurons (photoreceptors as waveguides, reflectance by the limiting membranes) and provide structural correlates of functional aspects of vision like, color vision (Roorda, 2011).

Several researchers then attempted to use AO to study the visual benefits of correcting aberrations. Logean et al. (2008) reported that PSF measured with AO was at least 6-9 times narrower than PSF measured without AO. The improvement in optical quality also resulted in an improvement is visual performance.

Visual acuity improved over different luminances and a visual benefit of 1.2 – 1.6 times was observed with aberration correction (Fig. 1.16A) over different spatial frequencies by Yoon and Williams (2002). Similar improvements in visual acuity were later reported by several researchers. Marcos et al. (2008), measured visual acuity under AO correction for two different contrast polarities and 7 different luminance conditions. As seen from figure 1.16B, there was an improvement in visual acuity across all luminances with aberration correction.

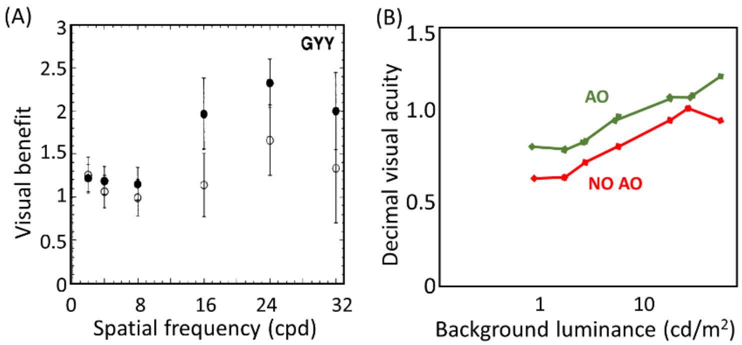

Figure 1.16: Visual benefit (A) and Improvement in visual acuity (B) with adaptive optics correction (Yoon and Williams, 2002, Marcos et al., 2008)

Atchison and Guo (2010) studied the effect of ocular aberrations on blur threshold by modulating only lower order and/or higher order aberration magnitudes using adaptive optics. It was reported that subjective tolerance to oriented blur was better compared to radial blur. They also reported that complete correction of aberrations worsen spatial visual performance. Later, a psychophysical channel was coupled with adaptive optics to simulate visual experiences pertaining to newer refractive corrections. Artal et al., used adaptive optics system to induce aberrations other than the eye's own aberrations and found that maximum visual performance was obtained with the eye's own aberrations and not with zero-aberration at retina (Fig. 1.17A). They also studied subjective image quality by altering aberrations (Artal et al., 2004, Artal, 2014).

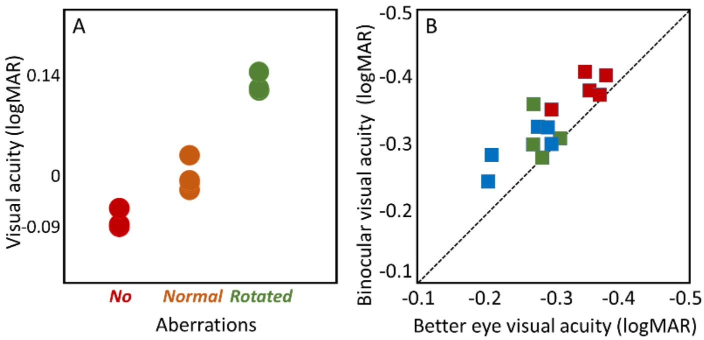

Figure 1.17: Improvement in visual acuity with aberration correction (Sabesan et al., 2012, Artal, 2014)

Sawides and colleagues used adaptive optics extensively to correct aberrations, and presented numerically manipulated images through AO to study blur perception and adaptation (Marcos et al., 2008, Sawides et al., 2011a, Sawides et al., 2011b). They also studied accommodative responses with aberration correction and reported that accommodative lag increases with induction of coma and spherical aberrations and decreases when the aberrations are corrections (Gambra et al., 2009). Sabesan et al. (2012) measured binocular visual performance on correcting higher order aberrations. They reported that aberration correction improves binocular summation, in addition to improving visual acuity (Fig. 1.17B).

Over time, adaptive optics has evolved as an ideal tool to study the facets of neural adaptation by controlled manipulation of the retinal image and finds wide applications in studies of multifocality, binocular vision and polychromatic vision.

1.3 Neural Adaptation

The visual environment is a dynamic one constantly changing in time and space. There are also changes within an observer due to aging, treatments or diseases. The term adaptation refers to the process through which the visual system continually adjusts to these changes (Elliott et al., 2007). Visual neural adaptation is important to attain perceptual constancy in vision which is a key aspect for perceptual interaction with the extrinsic world and is important for normal development of visual cues (Georgeson and Sullivan, 1975).

Clifford and colleagues (2007) described visual adaptation as "*the processes by which the visual system alters its operating processes in response to changes in the environment*". Both visual perception and adaptation are affected by sensory history. This dependence varies over a wide range of time scales (Webster, 2011). Short term neural adaptational effects arise from sensory experience anywhere between few milliseconds to few minutes. Unlike long term adaptation, the after-effects of short term adaptation usually does not last longer. It is believed that the short term adaptation is a necessary precursor to long term adaptation.

Cufflin et al. (2007) reported an increase in blur sensitivity and discrimination after adaptation, associated with an expansion of the depth of focus. Various factors including color, stimuli type, spatial extent of the stimuli and the depth planes, affect blur adaptation. In this section we will review briefly, the literature that aids in understanding of neural adaptation to the context of this thesis.

1.3.1 Color Vision

A classic example of short term adaptation to color is demonstrated by McCollough effect (Webster et al., 2006, Webster, 2011). As can be seen from figure 1.18, adaptation to one color produces an after-effect of the complementary color. Visual scenes vary widely in color and the same environment could appear differently in a different lighting condition or season. Development of cataract can also cause changes in the image spectra. The question then is, does the perception of color change in these cases? While it is true that there could be different adaptation states for the same subject, the perception depends on a common state of adaptation that is developed over periods of long exposures.

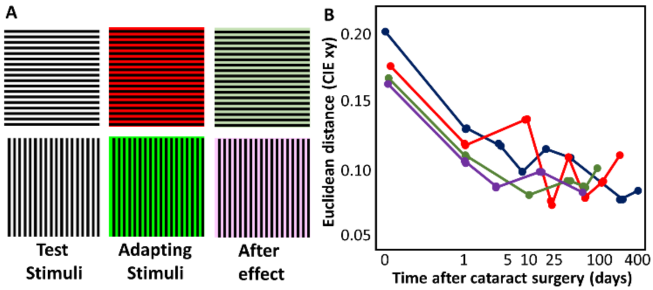

Figure 1.18: Color constancy (A) McCollough effect (Adapted from McCollough and Webster, 2011) (B) Renormalization of color perception in different subjects following cataract surgery (color constancy (Delahunt et al., 2004)

Werner and Schefrin (1993) measured the achromatic locus in normal subjects and reported that this does not change with age. In another study (Delahunt et al., 2004), the achromatic point was measured longitudinally in subjects post cataract surgery. The achromatic point shifted towards blue and renormalized after about 12 weeks post-surgery (Fig. 1.18B). One of the strongest and most demonstrable property of perceptual constancy is color constancy. It is also interesting to note that mechanisms of color adaptation begins at the retinal level and hence can occur independently for each eye (Webster et al., 2006, Webster, 2011). While spatial vision and color vision are different in many respects, color vision provides the basis of understanding the mechanisms of neural adaptation to spatial functions like contrast and blur.

1.3.2 Contrast Adaptation

Psychophysical studies show that adaptation to a high contrast image reduces the apparent contrast in the test image (Blakemore and Campbell, 1969a, Blakemore et al., 1970). Adapting short term to a high contrast grating of similar orientation will render previously visible region of a low contrast gratings invisible for a short period of time (Fig. 1.19 A,B). While adapting to grating that are orthogonally oriented does not induce any such effects (Fig. 1.19C). In addition to demonstrating reduction in apparent contrast, this experiment also describes two other features of contrast adaptation: selectivity to orientation and spatial frequency (Blakemore and Campbell, 1969b).

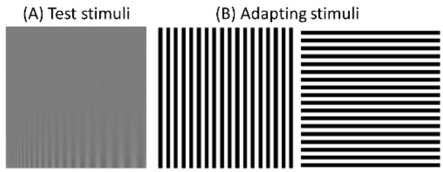

Figure 1.19: Reduction in apparent contrast

De Valois et al. (1982) measured CSF using sinusoidal gratings, pre- and post-adaptation to specific spatial frequencies. He reported that a band-limited loss in sensitivity was noted around the adapting frequencies (Fig. 1.20A). Similar results were previously described by Campbell and Green (1965). It has been observed by various researchers that CSF, unlike the MTF is not a linear processing channel and in fact has multiple channels with peaks around specific spatial frequencies (Fig. 1.20B) which explains for the frequency tuning during adaptation (Blakemore and Campbell, 1969b).

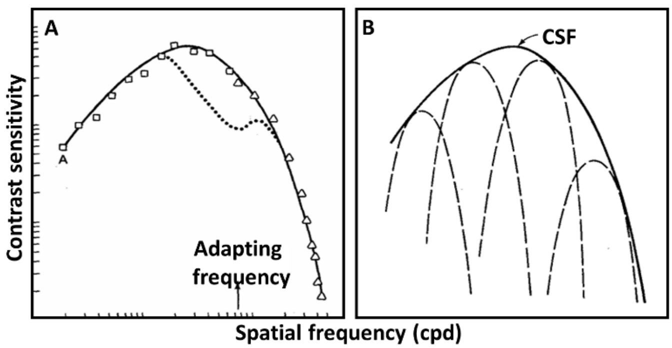

Figure 1.20: Spatial frequency tuning in contrast adaptation (Adapted from Campbell and Green, 1965, Blakemore and Campbell, 1969b)

Studies using fMRI and EKG show adaptation-induced-plasticity in the V1 in both short term and long term in cats' cortex. It was shown that after long term adaptation to unpreferred orientation, the preference in orientation actually shifts to the adapting orientation (Dragoi et al., 2000). It has been therefore determined that the locus of contrast adaptation is in V1, although some researchers favor a first level adaptation at the retinal level (Diether and Schaeffel, 1999, Diedrich and Schaeffel, 2009).

1.3.3 Blur adaptation

The retinal image quality is constantly exposed to optical blur due to various factors, including presence of refractive error (or residual refractive error), microfluctuations in accommodation, change in depth of focus with change in pupil size etc. In addition to modulating the defocus thresholds, this optical blur also plays a significant role in emmetropization (Schaeffel and Howland, 1991, Ohlendorf and Schaeffel, 2009). We will limit our discussions to the effect of defocus, astigmatism and higher order aberrations on those pertaining to visual functions and perception.

Changes in Contrast Sensitivity

The mechanism of contrast adaptation to defocus is very similar to that of adaptation to lower spatial frequencies. Various studies report a large reduction in contrast from low to mid spatial frequencies after adaptation to defocus. In addition systematic differences in adaptation was noted between various refractive error groups. Radhakrishnan et al., (2004) reported that myopes showed larger reduction in contrast sensitivity when adapted to hyperopic defocus compared to myopic defocus (Fig. 1.21A), suggesting an optimization due to preadaptation. Georgeson and Sullivan (1975) showed that, in astigmatic subjects, orientation selective contrast sensitivity was found. This was closely associated with astigmatic axis. Also, sensitivity at lower contrasts improved when the orientation of gratings matched with that of the orientation of the astigmatism.

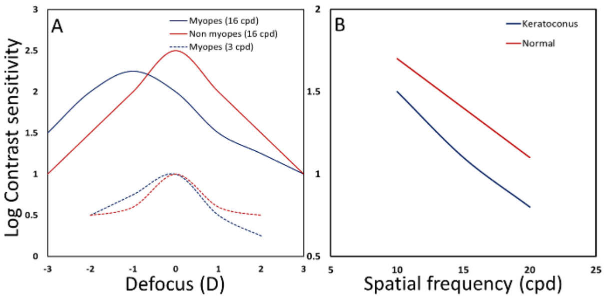

Figure 1.21: (A) Change in contrast sensitivity with defocus (Adapted from Radhakrishnan et al., 2004) (B) Contrast sensitivity with aberration correction (Adapted from Rouger et al., 2010)

Charman and Jennings (1976) calculated the effect of spherical aberration on the contrast and showed that it improves at intermediate spatial frequencies in the presence of spherical aberration and negative defocus from positive defocus. Similar effects of spherical aberration have also been demonstrated in myopic subjects, suggesting an adaptation to the aberration. Studies on keratoconic eyes by Rouger et al.,(2010) showed that contrast sensitivity decreased in these eyes after correction of higher order aberrations (Fig. 1.21B), as opposed to the improvement noted in normal eyes. These results indicate that the eyes were tuned to the contrast degradation imposed by the higher order aberrations.

Changes in Visual Acuity

A large number of clinical and experimental studies on changes in visual acuity with refractive error is available. In two independent studies by Mon-Williams and Rosenfield, myopic subjects showed marginal increase in visual acuity following adaptation to a period of no-spectacle wear. Mon-Williams et al. (1998) optically induced 1 D of myopia in normal subjects and measured visual acuity before and following adaptation. As seen from figure 1.22A, most subjects showed improvement in visual acuity following adaptation with no apparent change in refraction, indicating that the improvement is a result of neural adaptation to the optical defocus.

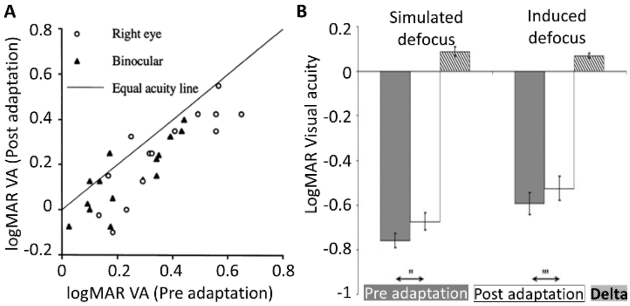

Figure 1.22: Change in visual acuity after adaptation to (A) defocus (Mon-Williams et al., 1998) and (B) astigmatism (Ohlendorf et al., 2011b)

Similar results were later reported by Poulere and colleagues (2013). Ohlendorf and colleagues measured visual acuity after adaptation to simulated or optical astigmatism in non-astigmatic subjects. The subjects watched a video blurred with optical astigmatism or simulated astigmatism during adaptation. A significant increase in visual acuity was found (Fig. 1.22B) when the orientation of astigmatic axis in adapting and testing stimuli were at 0°. There was no adaptation effect noted when the astigmatism was orthogonal in the adapting and test image.

Pesudovs (2005) first showed that visual acuity improved by 0.02 logMAR following few weeks of adaptation post refractive surgery, this was attributed as adaptation to the blur produced by LASIK introduced higher order aberrations. Artal and colleagues (Artal et al., 2001, Artal et al., 2004) induced reversed aberration patterns and measured visual acuity in these subjects. They reported that 25 minutes after adaptation visual acuity improved up to 70% of the initial levels. Also, an improvement in visual acuity was reported by de Gracia and colleagues (2011) under combined astigmatism and coma, in those subjects with uncorrected astigmatism. Similar to contrast sensitivity measurements, correcting the higher order aberrations resulted in decrease in visual acuity in eyes with keratoconus (Rouger et al., 2010).

Changes in Perceived Best Focus

Perceived Best Focus (PBF) is the image blur that produces neither a sensation of blur, nor a sensation of sharpness. This is a quantification of the subjective perceptual quality, irrespective of the kind and type of blur used in the measurement.

Webster and colleagues reported that previously normal appearing images appear to be blurred following a short period (few seconds) of exposure to sharpened image and after exposure to a blurred image, subsequent normal images appeared sharper (Webster et al., 2002, Elliott et al., 2011). Images were blurred or sharpened by altering the amplitude spectra of the image. They reported that the effect persisted for different kinds of images (Fig. 1.23A). They reported that these shifts are not just "repulsion effects" to sharpened or blurred images, but rather renormalization due to adaptation.

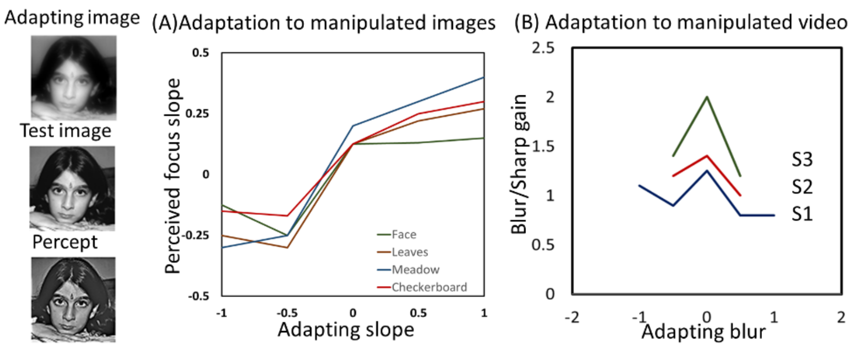

Figure 1.23: Change in perception with adaptation (Adapted from Webster et al., 2002, Haun and Peli, 2013)

Haun and Peli (2013) studied blur adaptation with sharpened and blurred videos and reported that the after-effects of adaptation are strongest for sharpened videos with sharp adaptation and blurred videos for blur adaptation (Fig. 1.23B). These results further support the invariance demonstrated in blur adaptation by previous studies using static images.

Webster et al., (Webster et al., 2001) measured blur adaptation by using images as shown in figure 1.24. Even if the physical blur in the center image was the same in both images, subjects consistently reported that the center image flanked with sharp images appeared more blurred compared to the one flanked with blurred images. Some contact lens designs for myopia and presbyopia correction might produce such retinal images across different retinal eccentricities and it is important to understand the adaptational issues in these cases, to provide better visual outcomes.

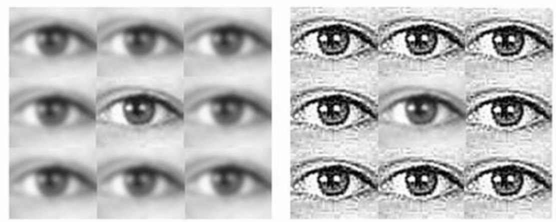

Figure 1.24: Effect of surround blur on blur perception ((Webster et al., 2001)

Sawides and colleagues (2010) measured changes in adaptation to images blurred with second order astigmatic blur. They reported that adapting to horizontal blur resulted in perception of an isotropic image to be vertically oriented and vice versa (Fig. 1.25A). Changes in perceptual judgments were measured by Vinas et al.,.(2012) after astigmatism correction. They reported that uncorrected astigmats are adapted to the orientation of the astigmatism and that the perceived neutral point significantly shifts even with brief periods of astigmatic correction, and that it stabilized over longer periods (Fig. 1.25B).

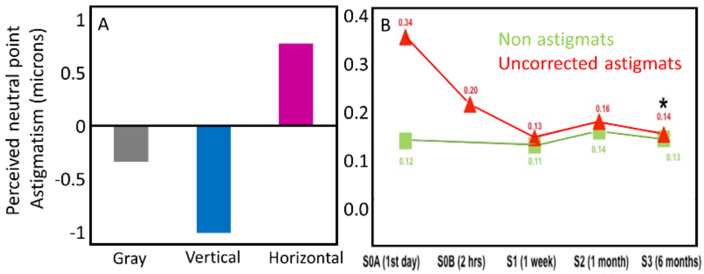

Figure 1.25: Change in blur perception with adaptation to (A) induced astigmatism (Sawides et al., 2010) and (B) corrected astigmatism (Vinas et al., 2012)

Neural adaptation to higher order aberrations has been studied under three facets: Adaptation to natural aberratiosn, corrected aberrations and induced aberrations.

Perceived best focus was measured as the Strehl Ratio that produces neutral percept, in normal subjects by Sawides et al. (2011b). The test images were blurred by PSFs measured from 128 subjects and the blur ranged from Strehl Ratio 0.08 to 0.73. They reported that the magnitude of blur reported as best perceived correlated significantly with the blur produced by their own higher order aberrations (Fig. 1.26A).

They further studied changes in the perceived best focus after adaptation to scaled factors of the subjects' own aberrations (Sawides et al., 2011a). It was found that the least change in the perceived best focus was noted for a factor of 1, with adaptation to image blur factor >1 producing blur adaptation effect and adapting to factor <1 producing a sharp adaptation effect (Fig. 1.26B). Similarly, as seen from figure 1.26C, adaptation to images blurred with aberrations of other subjects produced larger changes in perceived best focus compared to adaptation to the own aberrations.

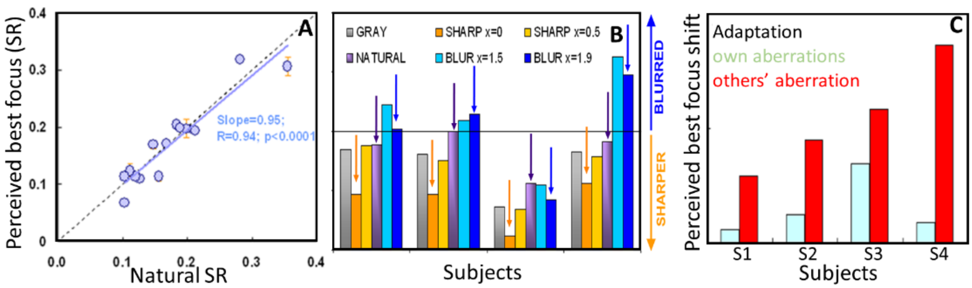

Figure 1.26: Adaptation to eye's own aberration magnitude

Artal et al. (2004) studied perceptual performance using a matching task. Subjects viewed a stimulus through an adaptive optics system that recreated the natural aberrations or their reversed patterns. As seen in figure 1.27A, they reported that about 20% increase in blur was required to produce a matching when the aberrations were reversed as compared to the natural orientation. This was concurrent with the decrease in visual acuity noted in the same subjects with rotated aberrations.

Sawides and colleagues (2013) also studied preference to orientation of aberrations using images convolved with PSFs. Subjects viewed, through an adaptive optics system, pairs of images that had similar blur magnitude, but different blur orientation. Subjects performed pattern preference task, selecting the image that appeared better focused of the two. They reported that the orientation of the PSF better perceived correlated with that of the orientation of the PSF of the eye (Fig.

1.27B) than that of the PSFs that were perceived blurred. These results indicate that subjects are indeed adapted to the orientation of the blur imposed by the higher order aberration.

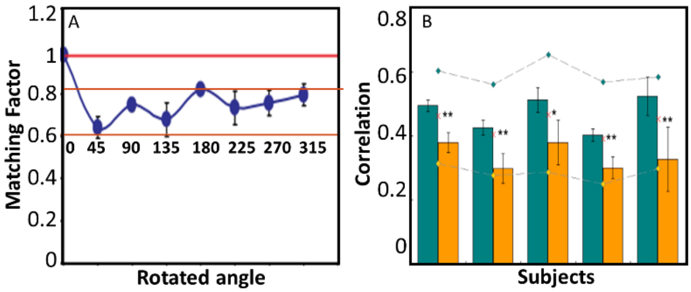

Figure 1.27: Adaptation to eye's own aberration orientation

1.3.4 Perceptual learning vs Adaptation

One of the hallmark features of any biological system is adaptability. Learning is an important aspect of this adaptability. Perceptual learning is the phenomenon where training or practice in a specific perceptual task results in improvement in that particular perceptual performance (Gibson, 1963). This is also a key factor that distinguishes perceptual learning from adaptation. Perceptual learning operates in a very specific manner, which depends on stimulus and task, whereas adaptation is thought to reflect a recalibration of the visual system to handle a change in the visual world. While it is true that specificity of adaptation is undeniable, it is not task dependent. In perceptual learning what is learned is highly specific to the stimulus, the task, trained retinal location, spatial frequency, orientation, texture, etc.,.

One of the earliest studies, by Fiorentini and Berardi (1980), on perceptual learning in the discrimination of gratings of different forms, showed that the learning was specific to both orientation and tuning. This was later reported in long term learning of a texture discrimination task. The authors further reported that, the learning was specific to the eye trained and there was little interocular transfer of learning to the contralateral eye. Poggio and colleagues (1992) studied perceptual learning in hyper-acuity tasks and reported that though the learning was specific for the visual field, this could happen in relative faster time scales (within an hour of training).

Contradicting reports by McGovern suggest that the sensory improvements derived from learning form memory and can in fact transfer between tasks (McGovern et al., 2012). McGovern in addition suggested, that although perceptual learning and adaptation are separate entities, the boundary between these two are becoming increasingly blurred, indicating the possibility of interaction between learning and adaptation. Yehezkel et al. (2010) attempted to study the effect of learning on adaptation. They reported on repeated measurements, the bias introduced by blur is reduced owing to perceptual learning. They suggested that with long experience, adaptation is transferred to memory that is engaged or disengaged when blur is applied or removed, resulting in lack of after-effects.

Studying adaptation is of interest for two distinct reasons: First, as a coping mechanism of the visual system to short-term changes in the sensory environment and second, as a tool for studying general issues of plasticity. Visual corrections for refractive errors in the form of optical (spectacles, contact lenses) or surgical (intra-ocular lenses) means introduce both short term and long term changes in visual perception. Presbyopia, with evolving newer designs and corrections being introduced in the later part of life, forms an interesting allegory.

1.4 Presbyopia

Functionally, presbyopia is the inability to see near objects. In a young eye with no refractive error, the accommodative virtue of the crystalline lens enables one to see clearly at all distances. This ability to accommodate declines steadily with age; from 14 D during infancy to 1.5 D at 60 years of age (Charman, 2008). This age-related physiological inadequacy in accommodation is called presbyopia (Fig. 1.28). The most contributing factor for this decrease in amplitude of accommodation is the sclerosis of the lens, associated with stiffening of lens capsule and decreased efficiency of the ciliary muscles with age.

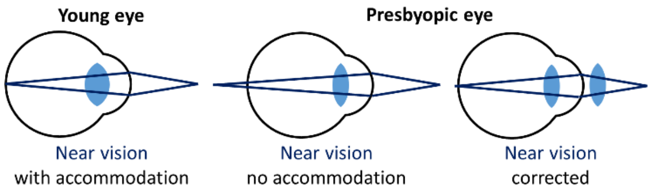

Figure 1.28: Near vision in a presbyopic eye with and without near addition

The onset of presbyopia itself cannot be determined by the residual amplitude of accommodation, for it mainly depends on the onset of symptoms. For most, the symptoms start at around 40 years, when the amplitude of accommodation decreases to 6 D (Charman, 2008). This will be accompanied by either inability to focus at closer distance, or inability to read fine prints at closer distance or inability sustain reading for a long periods of time. Though it can be safely assumed that presbyopia onsets in 100% of subjects over 45 years of age, it still depends patient's preferred working distance, the nature of the close work and the length of time for which it is done.

As outlined in figure 1.29, various treatment modalities have been in practice or being developed for improving vision at near for presbyopes. In the subsequent sections will review the solutions for presbyopia, with a special emphasis to its visual and functional implications.

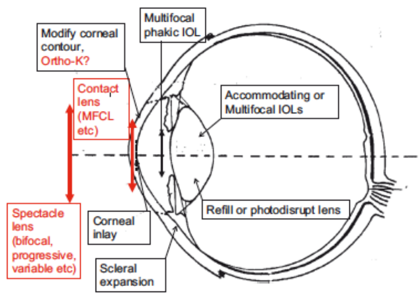

Figure 1.29: Presbyopia correction modalities (Charman, 2014a)

1.4.1 Conventional treatments for Presbyopia

The basic treatment for presbyopia is simply by providing the additional positive power by means of a convex lens, correctly called as the near addition. The amount of near addition depends on the patients' age and the working distance and demands. This is however only a partial solution because, the near addition, invariably renders the far vision blurred. The current treatment options for presbyopia can be classified into three categories: Alternating vision, Monovision and Simultaneous vision. Each of the techniques have pros and cons and can be provided by optical and/or surgical means.

Alternating vision

This is by far the most common correction and has been in existence since its invention by Benjamin Franklin in the late 1700s. The near correction can be provided as a single vision 'reading spectacles' or bifocals or Progressive Addition Lenses. In bifocal lenses, a portion of the lens is used for far correction and another portion for near correction. While this might provide clear vision at the two distances of correction, the intermediate vision is compromised (especially for advanced presbyopes). Progressive lenses practically provide clear vision from infinity to near, yet the regions of useful vision are small and need longer adaptation periods. In alternating vision corrections, the entire pupil is utilized for either distance or near correction (Charman, 2014a). The wearer makes a compensatory eye movement associated with near vergence to utilize the near or intermediate (in progressives) regions of correction.

Even though this is a convenient method of correction, limitation of useful area for which clear vision for distance/near could be obtained, image jump in bifocal certain designs and peripheral distortions introduced by the progressive addition lenses introduce significant functional handicap in the wearers. However, this kind of correction does not present much challenge for blur adaptation.

Monovision

Monovision, as the name suggest is a monocular correction for distance and for near in each eye. Originally in monovision, the dominant eye is corrected for distance with a residual myopia and the non-dominant eye is corrected for near, with the depth of focus augmenting for the acceptable level of acuity (Fig. 1.30A). By this way the refractive states between eyes are not left too disparate and the binocularity is not compromised much (Charman, 2014b). However, newer schools of thoughts support correcting the dominant eye completely for distance (Evans, 2007), resulting in clear vision in one eye for far and in the other eye for near.

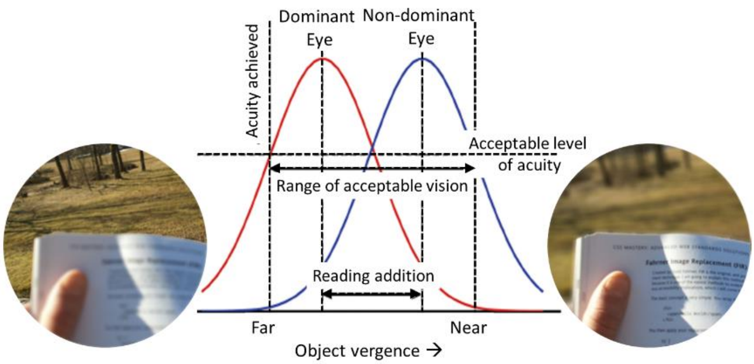

Figure 1.30: Monovision correction (Charman, 2014b)

Monovision corrections can be provided by spectacles, or contact lenses or by refractive surgeries. Binocular rivalry introduced by these corrections cause both loss in stereoacuity and decrease in functional vision. Johannsdottir and Stelmach (2001) report that for subjects using an addition of +2.5 D, the functions of binocularity is comparable to those with normal vision under normal lighting conditions. However, this drops drastically at low luminance. Handa et al.,(2005) have shown that binocular summation occurs only in eyes displaying strong ocular dominance(conventionally tested with sighting dominance tests) and suggested ocular dominance to be an important factor in monovision correction success. However, another study by Lopes-Ferreira et al. (2013) shows poor agreement in ocular dominance tests using sighting and sensory dominance tests.

Another school of thoughts assume that the brain chooses the sharper image at the specific distance suppressing the blurred image from the contralateral eye. Collins and Goode (1994) studied subjective and objective characteristics of adaptation to monovision and suggested that it depends of a subject's ability to adapt to the induced anisometropia. In a study by Kompaniez et al. (2013), after-effects were measured in both eyes of normal subjects by adapting them to a blurred or sharp image in either eyes. They reported that, irrespective of the eye that was adapted, the after-effects were dominated by the eye adapted to sharp image (Fig. 1.31). These studies provide cursory understanding of blur interaction and transfer of adaptation between eyes. However, at large a little is understood on how the brain compensates for interocular blur differences.

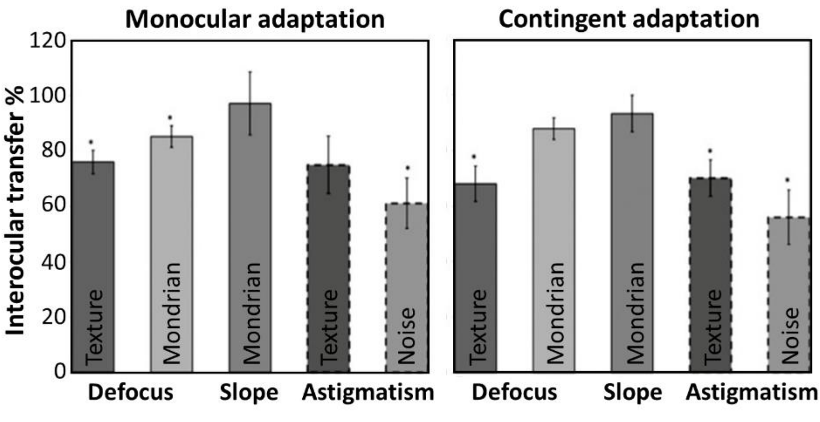

Figure 1.31: Interocular transfer of blur adaptation (Kompaniez et al., 2013)

Simultaneous vision corrections for Presbyopia

A large range of diffractive or refractive contact lenses and intraocular lenses are available for presbyopia correction (Fig. 1.32A). These increasingly popular solution for presbyopia are based on simultaneous-image principle (Charman, 2014a). In these corrections, parts of the pupil are used for distance vision correction and parts of the pupil are used for near vision correction. This results in light from different distances, being focused by different zones of the lens, at the same point in the retina. Though the intended multifocality is achieved, this results in a complex image degradation on the retina at any distance, where a sharp image (at the desired plane of focus) is superimposed with a blurred background (from other planes). This is illustrated in figure 1.32B.

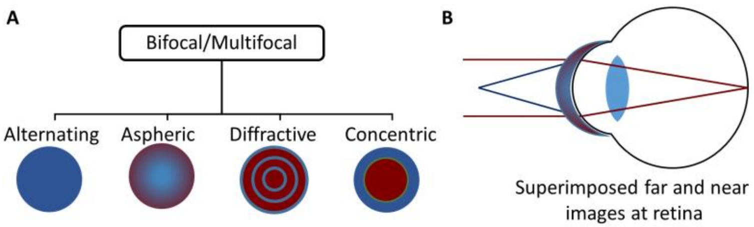

Figure 1.32: (A) Different simultaneous vision corrections (Adapted fromCharman, 2014b) (B) Image formed by Simultaneous vision correction

The visual performance with the bifocal or multifocal (MF) lenses are often measured as the extent to which the depth of focus is enhanced. There are also several reports on loss of contrast at medium and high spatial frequencies. Several researchers have discussed the impact of different designs of multifocal lenses on retinal image quality.

Simpson (1992) measured the MTF through diffractive MF lens and report that for both the focal planes, the MTF was reduced compared to a monofocal lens. Navarro et al. (1993) measured the retinal image modulation in subjects implanted with MF-IOL and reported that it was 2.5 times lesser than that obtained for young emmetropic subjects (Fig. 1.33A).

Studies show a trade-off in uncorrected distance visual acuity resulted in a gain in the uncorrected near visual acuity, in eyes implanted with MF-IOLs (Montes-Mico and Alio, 2003). The effect of near addition on distance visual acuity was studied by de Gracia and colleagues (2013b) by optical simulation of pure simultaneous vision using a simultaneous vision simulator. As can be seen from figure 1.33B, the change in visual acuity (high and low contrast) with near addition was non monotonous, with largest decrease in acuity occurring for intermediate additions (+1.5 to +2D) and this corresponded to the measured and simulated decrease in image contrast.

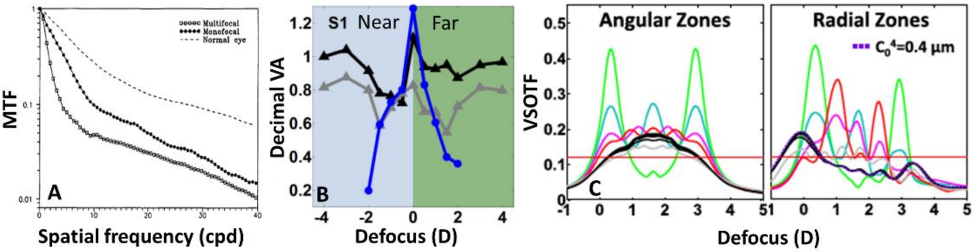

Figure 1.33: Optical and Visual performance with Simultaneous vision (Navarro et al., 1993, de Gracia et al., 2013a, de Gracia et al., 2013b)

Differences in optical and visual performance with different designs of MF lenses have also been studied. Ocular aberrations measurements in eyes MF-IOLS show higher values of coma and/or spherical aberration compared to normal eyes. However, some of these aberrations are attributed to tilt and decentration of the intraocular lenses introduced during the surgery. Numerical simulations by de Gracia et al., (2013a) showed that the optical performances of MF lenses with an angular designs was better than a radial profile (Fig. 1.33C). They also reported that, the maximum optical quality and the MF benefit varied with the number of multifocal zones.

Simultaneous vision correction have obvious limitations with centration of the lens with the pupil and smaller pupil size associated with senility. The limits of acceptable degradation in visual performance and understanding neural adaptation are additional challenges with simultaneous vision corrections.

1.4.2 Alternative solutions for Presbyopia

Optical solutions that provide full correction for presbyopia are being developed over years. Variable power lenses, have been tried unsuccessfully in the past. These are convex and concave lenses mounted with a variable distance between them. Light sword lens with varying power along the orientation of the semi diameter, which provides superior optical performance, are also being developed (Petelczyc et al., 2011). However, these lenses can be considered as a variation of alternating vision corrections.

Accommodating IOLs and lens refilling provide the most promising solution and are still being researched (Charman, 2014b). Various authors report that in patients implanted with accommodating IOLs, the near visual acuity improves without compromising the distance visual acuity.

Recently, Polat and colleagues (2012) trained presbyopes in near visual tasks. They reported that with perceptual learning near vision aspects like visual acuity and reading speed could be improved. Yet again, the extent of plasticity of the visual system in this arena is to be explored.

It is estimated that an adult will spend roughly about half their lives as presbyopes and this has serious socio-economic implications. There is extensive research aiming at providing a presbyope with an optical correction that is as good as the physiological lens. A systematic approach to understanding how the visual system interacts with existing solutions, will provide insights towards improving the current optical designs.

1.5 Open questions

The large number of optical solutions available for presbyopia correction has made the task of choosing the 'optimal' solution for an individual very difficult. A better understanding of their optical, visual and adaptational implications will aid in customizing the existing optical solutions towards improved performance. The studies included as part of these thesis aim to address the following questions:

1. How does the brain compensate for the blur differences introduced between eyes? Can long term adaptation to monovision be explained by differences in blur magnitude and orientation between eyes imposed by higher order aberrations?
2. How does subjects adapt to simultaneous vision corrections? What is the role of far/near energy distribution and the near addition in neural adaptation to simultaneous vision? In particular can image quality metrics be used to predict adaptation to simultaneous vision? Are there differences in neural adaptation to numerically and optically simulated simultaneous images?
3. Are there systematic differences in subjective preferences to angular and radial multifocal patterns? Are there differences in preferences to different orientations of angular patterns? Are there interactions between ocular higher order aberrations and a bifocal pattern? DWhat factors determine subjective preferences of a particular multifocal pattern?

1.6 Hypothesis and Goals

The thesis addresses the following hypotheses:

- In subjects with interocular optical quality differences, the visual system is calibrated to the magnitude and orientation of blur imposed by the eye with better optical quality and that it plays a role in adaptation to monovision.
- The visual system recalibrates to the form and strength of blur imposed by bifocality, following similar mechanisms to those of adaptation to defocus.
- Ocular aberrations play a primary role in perception and adaptation to bifocal correction.

The specific goals of this thesis are

- To study differences in blur adaptation between eyes.
- To study the influence of far/near energy ratio in bifocal corrections on visual performance and neural adaptation.
- To investigate the response of the visual system to increasing blur in the simultaneous vision correction.
- To understand the extent of involvement of ocular aberrations in adaptation to pure and segmented bifocal vision corrections.
- To develop and validate hand-held simultaneous vision simulator for clinical use.

1.7 Structure of thesis

This chapter **(chapter 1)** presents motivation of the thesis and the relevant background literature.

Chapter 2 provides an overview of the psychophysical methods and a description of the setups, used throughout this thesis. In particular, it includes descriptions of the Adaptive Optics system, modified Simultaneous Vision Simulator to simulate bifocal corrections and the portable hand-held simultaneous vision simulator.

In **chapter 3**, we studied the interocular differences in adaptation to differences in blur magnitude imposed by ocular higher order aberrations. Aberrations were measured and corrected using the adaptive optics system. Convolved images were used to measure Perceived Best Focus and its changes after adaptation to scaled versions of interocular aberrations.

In **chapter 4**, we measured the neural PSF in subjects with different PSF orientations between eyes, with same or different blur magnitudes. Images blurred by different PSFs with different orientations and a similar blur level was used. Pattern preference method with a reverse correlation technique was employed to obtain the internal code for blur.

In **chapter 5**, we evaluated the effects of Pure Simultaneous vision on visual perception and neural adaptation using an adaptive optics system. Perceptual scoring tasks and Perceived Best Focus were measured before and after adaptation to numerically-convolved simultaneous images of different far/near energy ratios and for different near additions.

C**hapter 6**, presents the subjective preferences to different angular and radial patterns of bifocal corrections, generated using Spatial Light Modulators incorporated in the Simultaneous Vision setup. We also present results of customized optical simulations of these subjective preferences.

In **chapter 7**, we report the results on orientation preference to a commercial segmented bifocal correction, simulated optically using the modified simultaneous vision simulator. We also present an ideal observer model based on ocular aberrations to simulate the preferences.

In **chapter 8,** we studied changes in Perceived Best Focus after adaptation to a pure simultaneous vision, optically induced using simultaneous vision simulator for three different energy ratios between far and near.

Chapter 9, presents visual performance results assessed using monocular hand-held prototype of simultaneous vision simulator to study visual performance and perceptual preference to bifocal and trifocal corrections. The multifocal corrections were simulated using temporal multiplexing technique using a tunable lens.

In **chapter 10**, the results of binocular visual performance and perceptual quality with different presbyopic corrections are presented. We optically induced monofocal, simultaneous vision, monovision and modified monovision corrections using a binocular, open-field visual simulator based on temporal multiplexing.

Finally, the last chapter **(Conclusions)** summarizes the major findings of this work, and their implications.

Chapter TWO

Methods

In this chapter, the optical setups and psychophysical methods used in various experiments are described. In particular, we briefly describe the custom-developed adaptive optics setup, coupled with a psychophysical channel to perform subjective tasks under aberration correction/induction. The steps involved in everyday calibration of the setup are also described.

We also describe the modifications carried out for generating bifocal patterns, in the simultaneous vision simulator by the author of this thesis in collaboration with Pablo de Gracia, Carlos Dorronsoro, Daniel Pascual and Susana Marcos. Validation and calibration of the setup for defocus and pupil pattern induction is presented. The development and validation of the monocular/ binocular portable Simultaneous Vision Simulator in collaboration with Daniel Pascual, Carlos Dorronsoro and Susana Marcos is described in detail.

General psychophysical measurement protocols applicable to all the studies is described. The psychophysical protocols were developed in collaboration with Lucie Sawides, Carlos Dorronsoro and Susana Marcos. The details pertaining to a specific study is described in the respective chapters.

2.1 Adaptive Optics

The VioBio lab adaptive optics system is used for performing psychophysical measurements under aberration correction and manipulation. The various stages of development of the system is described in several literatures from the laboratory (Marcos et al., 2008, Gambra et al., 2009, Gambra et al., 2010).

2.1.1 Setup

Figure 2.1 shows the principal components and different channels in the adaptive optics (AO) system custom developed in the VioBio Lab. Figure 2.1A shows the pupil and retinal planes. The elements highlighted in red show the pupil planes which are centered and conjugated with the Shack-Hartmann wavefront sensor and membrane deformable mirror. A pinhole (x1 magnification factor with subject's pupil) at the first pupil plane ensured accurate pupil diameter to be set for both aberration and psychophysical measurements. The elements highlighted in blue represent the retinal plane and another pinhole placed at the first retinal plane enabled elimination of undesired reflections from cornea and allowed verification of retinal image projection for psychophysical measurement. As seen from figure 2.1B, the AO system comprises the Illumination channel (green path), the aberration measurement and correction channel (red path), the psychophysical channel (blue path) and the pupil monitoring channel (in orange).

The illumination channel

The illumination channel mainly consists of the Super-Luminescent-Diode coupled with an optical fiber (Superlum, Ireland) emitting a collimated beam of about 1 mm at 827 nm. For measurement in human eyes, the current limit is set to 90 mA which provides an irradiance of 8 μW on the cornea, which is well within the maximum permissible exposure set by ANSI standards (Delori et al., 2007). To avoid corneal reflectance, the beam enters the cornea about 1 mm nasal and inferior to the pupil center.

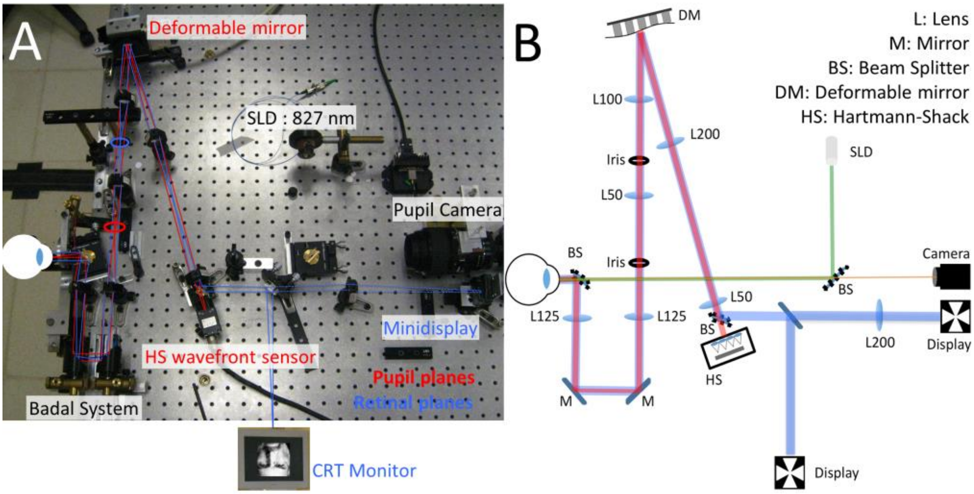

Figure 2.1: (A) Photograph of the Adaptive Optics setup with highlighting of principle components and the retinal (in blue) and pupil planes (in red) (B) Schematic diagram of the VioBio lab Adaptive optics setup showing the four principle channels

The measurement channel

The collimated beam of light from the SLD entering the eye is reflected by the retina and passes through the Badal system, the electromagnetic membrane deformable mirror and then is focused on to the Shack-Hartmann wavefront sensor.

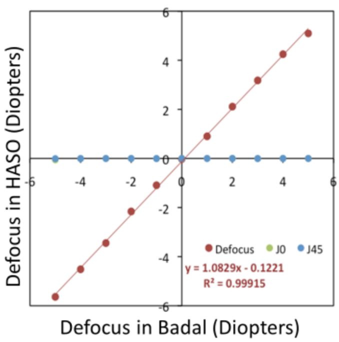

Figure 2.2: Linear change in defocus in HASO with induction of defocus in Badal. No change in astigmatism

The Badal system is a system of a pair of plane mirrors and plano- convex lenses of focal length 125 mm, mounted on a motorized platform, with the pupil of the eye placed at the focal length of the first lens. The system compensates for positive and negative spherical refractive errors of the subjects when the distance between the lenses and the mirrors are increased or decreased; 1 mm displacement introduces 0.125 D change in focus. The change in the sphero-cylindrical focus measured at Shack-Hartmann wavefront sensor, with defocus induced using the Badal system can be seen in figure 2.2.

The Shack-Hartmann wavefront sensor has a matrix of 32x32 microlenses of aperture diameter 160 microns, with a CDD camera at the focal length of the lenslets (HASO 32 OEM, Imagine Eyes, France). The effective diameter of the wavefront sensor is 3.65 mm and for a 7 mm pupil, there are 1024 equidistant spots sampled by the microlens array for a flat incident wavefront (Fig. 2.3A). This reference array serves to set the origin of coordinates for each subapertures on the focal plane. For an aberrated wavefront, the deviation of the local tilt at each subapertutre will determine the centroid position of each spot focal plane (Fig. 2.3B). A computer software is used to calculate the x and y centroid positions of each spot and the wave aberrations are reconstructed.

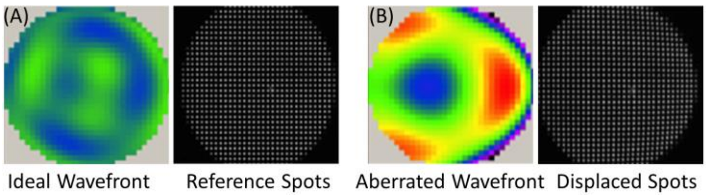

Figure 2.3: Sampling by the Shack-Harmann lenslets of (A) Ideal and (B) Aberrated wavefront

The magnetic deformable mirror is a high quality reflecting membrane (>98% for 830 nm wavelength) with 52 actuators (MIRAO 52, Imagine Eyes, France), comprised of magnet and coil, assembled in an aluminum housing (Fig. 2.4A). An electromagnetic field is created by applying voltage to the coils which can push or pull the magnets allowing a local change in the mirror shape providing a maximum stroke width of 50 microns. The interactuator distance is 2 mm and the effective diameter of the mirror is about 15 mm. In our setup, the incident beam from the eye is reflected at an angle of 15 degrees to the HASO. The voltage applied to each actuator can be visualized as a matrix (Fig. 2.4B).

The pupil plane is conjugated with the HASO with a x0.5 magnification factor and the deformable mirror is conjugated to the pupil plane with a x2 magnification factor by a pair of relay lenses of focal lengths 200 mm and 50 mm. In an artificial eye, the RMS was reduced by over 97% and in human eyes the correction efficiency was about 89%. The fluctuations in RMS measured with MIRAO over 3 hours was less than 0.3% described in a study by Fernandez et al. (2006).

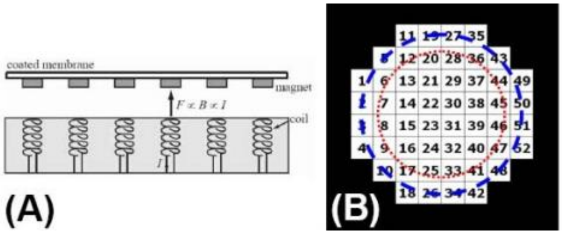

Figure 2.4: Schematic of MMDM and the matrix of actuators

An interactive software was custom-developed in Visual C++ (Microsoft Inc)., using Software Development Kit from Imagine eyes. The software allowed simultaneous control of Badal system, parameters of HASO for aberration measurement, matrices of MIRAO for aberration correction in close loop or aberration induction and pupil monitoring. This has been described extensively in previous studies from our laboratory (Marcos et al., 2008, Gambra et al., 2009, Gambra et al., 2010) and discussed briefly in section 2.1.3 in this thesis.

The psychophysical channels

The AO system has two psychophysical channels: A minidisplay (LE400, LiteEye Systems, France) and a CRT monitor (Mitsubhishi Inc.,.) incorporated beyond the wavefront sensor allowing image manipulation for psychophysical tasks under controlled optical aberrations. A flip-mounted mirror is used for selecting either of the channels.

The minidisplay is 12 x 9 mm OLED display projected at optical infinity of the eye with an achromatic lens of 200 mm focal length and subtends 2.5 degrees on the retina. The SVGA has a resolution of 800 x 600 pixels and maximum luminance of

100 cd/m^2 measured using ColorCal (Cambridge Research Systems, UK). In this thesis, the minidisplay was used to project a Maltese cross for selection of subjective best focus, prior to aberration measurements and for fixation during measurement and correction of the subjects' aberrations.

The CRT monitor is 40 x 30 cm in dimension with a resolution of 1024 x 768 pixels at 100 Hz. The monitor was placed 2.60 meters from the retinal plane. A 480 pixel image subtended 1.98 degrees at the retina. This channel was introduced in the system by means of a flip-mount mirror placed just beyond the wavefront sensor. The monitor was calibrated to present gray-scale images with linear luminance and had effective luminance of 100 cd/m^2 calibrated using a ColorCal (Cambridge Research Systems, UK). The monitor was controlled using a ViSaGe platform (Cambridge Research Systems, UK) for both stimulus presentation and gamma correction. Gamma correction was performed using the 64 tones and 64 readings with a linear fitting and validated with methods described by Brainard (1997) and Pelli and Farell (1995) using PsychToolbox in Matlab.

The pupil monitoring channel

A CCD camera (TELI, Toshiba) with an objective is placed collinear to the optical axis of the imaging system using a beam splitter and is conjugate to the artificial pupil. The subject's pupil is illuminated using infrared LED rings and the pupil centration is achieved using a mechanical stage with respect to the camera's center. The camera also allows for continuous pupil monitoring during aberration measurement/correction and psychophysical measurements.

The measurement and pupil monitoring channels were controlled using C++ software in one computer and the Visage psychophysical platform and CRT monitor were controlled using Matlab (Mathworks Inc.) in another computer. The computers were synchronized using the User Datagram Protocol for a rapid presentation of visual stimuli under controlled conditions. However, in this thesis, the synchronization was done manually.

2.1.2 Calibration

A CCD camera was used in conjugacy with different pupil planes to ensure centration and alignment of the optical components of the system. A graduated paper was used to measure magnification introduced at the HASO, MIRAO and by the Badals. These calibration procedures have been described in the doctoral thesis by Sawides and is illustrated schematically figure 2.5.

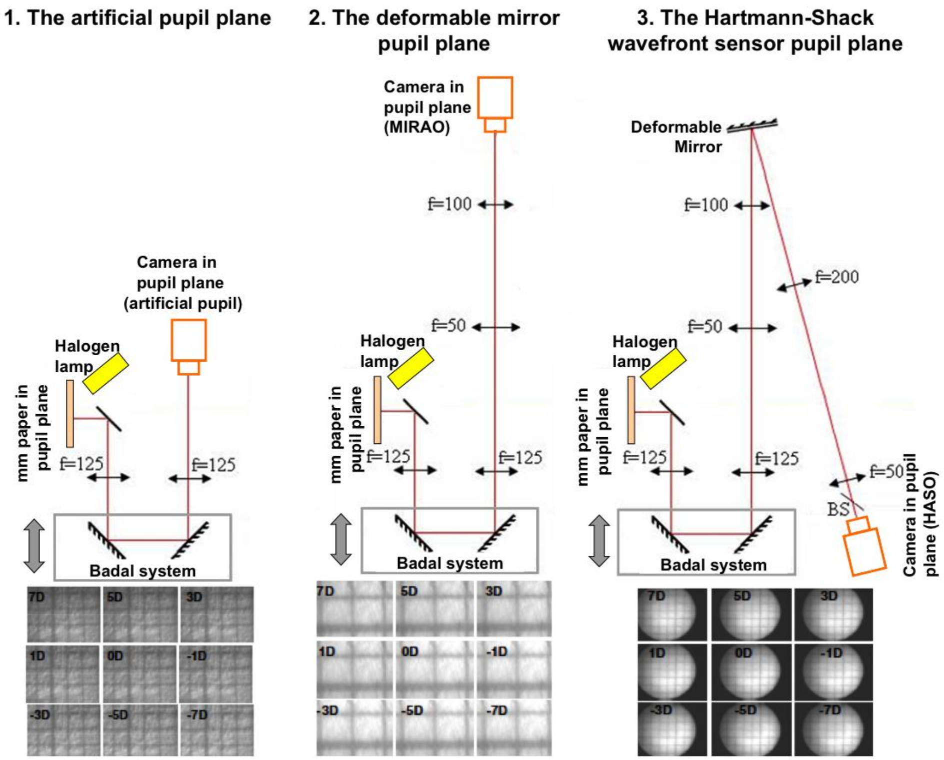

Figure 2.5: Alignment and calibration of AO (Adapted from Sawides, 2013)

In this section we describe the four major steps involved in every day calibration of the measurement and closed-loop correction of wave aberrations. An achromatic doublet with 35 mm focal length combined with a rotating diffuser (at the focal length of the lens) was used at the pupil plane as an artificial eye. The current limit of SLD was set to 60 mA for daily calibration purposes and the artificial eye centered using the pupil monitoring camera. The daily calibration is done with the commercial software CASAO.

Local Slopes Acquisition

The wavefront aberrations are calculated from the local slope acquired from the images obtained with the 32 x 32 microlens matrix of the Shack-Hartmann sensor. According to the phase reconstruction mode chosen, the system calculates automatically the calculable subaperture and largest pupil diameter for every acquisition. The slope estimates are described as vectors (Fig. 2.6) whose amplitudes correspond to the amplitude of slope and the direction of the vector corresponds to the angle of largest slope and the center of the grid corresponds to the center of the microlens array. The slope of the adjacent subapertures are interpolated to obtain the wavefront aberrations.

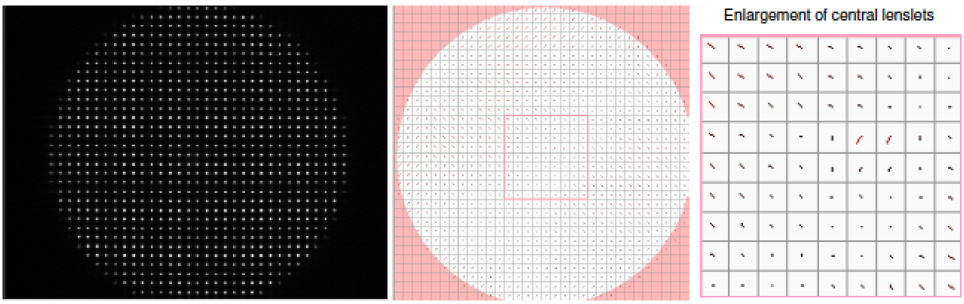

Figure 2.6: Hartmann-Shack sensor spots (left) and the corresponding local slopes in the subapertures (middle and right)

Interaction Matrix Acquisition

The surface deformation produced when a unit voltage is applied to one actuator of the deformable mirror is called the actuator's influence function. The matrix containing the influence function of each actuator is called the Interaction matrix (Fig. 2.7). It is obtained by applying ±0.2V to each actuator and recording its effect on the membrane.

Figure 2.7: Interaction matrix

Command Matrix Construction

The command matrix is the pseudo-inverse matrix of the Interaction Matrix. It accounts for the voltage that should be applied to each actuator to generate different patterns of aberrations. A modal reconstruction algorithm with 48 modes is used for reconstruction of Zernike polynomials up to 7th order.

Closed-Loop Correction

A closed loop correction consists of acquisition of local slopes, calculation of voltage required for the actuator to change the slope, reacquisition of residual slope and recalculation of the voltage required for N number of iterations until a desired wavefront is produced. A large number of iterations results in slower measurements and lower number of iterations results in poorer correction. Also, the stability of this correction is influenced by the gain, larger gain results in better but unstable correction and lower gains result in highly stable but poorer corrections.

For measurements in this thesis we typically used an integration time of 45 – 55 ms, a gain of 0.3 - 0.5 and 15 - 25 iterations. As mentioned before and as can be seen from figure 2.8, these parameters provided rapid and good aberration correction (97%). The close-loop was calculated for a pupil size of 7 mm and 5 mm (used in psychophysical measurements) and stored as 'Flat mirror' state. In addition to the calibration of the adaptive optics setup, the centration of the psychophysical channels are evaluated by assessing the symmetry in alignment of the Maltese cross displayed in both displays at the retinal plane. The magnification at the pupil plane is also assessed using a graduated paper and verifying the displayed diameter to the actual diameter set in the paper.

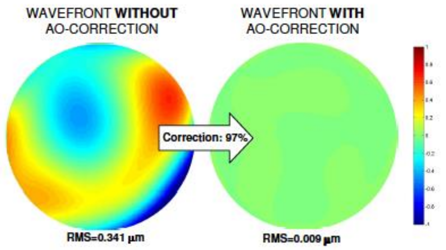

Figure 2.8: Closed-Loop correction showing wavefront aberration pre and post AO correction

2.1.3 *Ocular aberration measurements in Humans subjects*

For the measurement of ocular aberrations in human subjects, the custom developed adaptive optics software is used. This software consists of several modules (Fig. 2.9) for simultaneous control of Badal channel during aberration measurement, correction and induction, and pupil monitoring. The subject's descriptive information can be entered and the Zernike coefficients for the measured pupil diameter is automatically saved.

Subjective best focus with Badal

The first step after aligning the subject in the adaptive optics setup is to obtain the best spherical refraction compensation. Subjective best focus measurement was measured by asking the subject to adjust the Badal from a myopic defocus (corresponding to their refractive error) with a keyboard until the high contrast Maltese cross on the minidisplay appears clear for the first time. The process is repeated three times and the average spherical error is set as 0 for aberrations measurement and correction. The deformable mirror is set in the flat mirror state during this measurement.

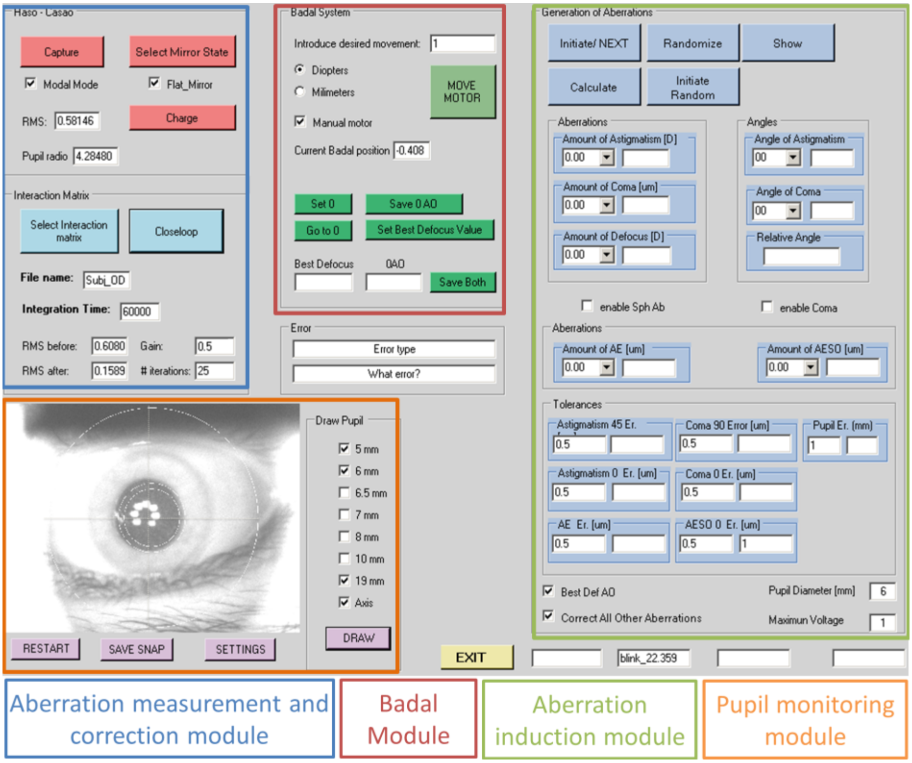

2.9: Configuration of custom developed AO software

Measurement and correction of aberrations

After obtaining the subjective best focus, the alignment of the pupil is re-monitored and the aberrations of the subject's eye are measured using the flat mirror state. During each measurement 20 readings of the Zernike coefficients are obtained. The diameter of pupil is set with the artificial pupil. Three reliable measurements are performed for each subject. A measurement is unreliable if the measured pupil diameter is smaller than the intended pupil diameter, or if the measurement happens with more than 3 'blinks'. A blink occurs when the reflectance from the retina is low as a result of tear disturbance, improper fixation or actual blinking by the subject, resulting in slope measurements from which the Zernike coefficients cannot be computed.

Following aberration measurement, a closed-loop correction is performed with 0.5 gain and 25 iterations. The closed loop correction was considered ideal when the residual aberration is less than 0.2 microns. The residual aberrations are measured with this mirror state and the close-loop is repeated if necessary. This closed loop correction is stored as a new mirror state and used for further measurements. The whole process of aberration measurement, correction and reassessment takes less than 10 seconds.

In this thesis, the psychophysical measurements were performed under static closed-loop correction to avoid longer exposure of the laser spot. A psychophysical experiment lasted anywhere between 1 – 7 hours and during this time, the AO correction and the fixation are monitored at continual intervals. The closed loop correction is repeated if and when necessary.

2.2 Simultaneous Vision Simulator

Multifocal solutions for presbyopia correction introduce large phase shifts between different zones refracting for far and near distances. A deformable mirror, while is very useful in simulating smooth changes in an optical surface, is little useful to introduce the large discontinuities. A simultaneous vision simulator was first developed in our lab to assess visual performance with pure simultaneous vision (de Gracia et al., 2013). This was achieved by using a beam splitter to send the stimuli through two independent Badal channels and recombining the images at the pupil plane (Dorronsoro and Marcos, 2009).

To optically simulate refractive multifocal lenses (angular or radial designs with different far-near energy ratios) we modified, during this thesis, the simultaneous vision simulator incorporating a spatial light modulator (LC2002, Holoeye Inc.,.) and improved the extent of test stimuli that could be presented through the system for psychophysical tasks. In this section we will describe the setup, calibration and general measurement with the Modified Simultaneous Vision simulator (SimVis).

2.2.1 Setup

A schematic representation of the modified simultaneous vision simulator (SimVis) is shown in figure 2.10A highlighting the pupil and retinal planes of interest corresponding to each Badal channel. An artificial pupil was introduced with a pinhole (x1 magnification factor with subject's pupil) at the first pupil plane after the Badal channels. The modified SimVis comprises of three main paths: The bifocal channel (Badal 1+2, SLM), the psychophysical channel (DLP) and the pupil monitoring channel. The pupil plane is conjugated with the SLM with a x0.5 magnification factor and the psychophysical is conjugated to the pupil with a x2 magnification factor by a pair of relay lenses of focal lengths 200 mm and 100 mm. A stop placed in front of the SLM at the focus of the conjugate lens helps in eliminating the diffractive orders introduced by the SLM. An on-bench view of the modified SimVis is shown in figure 2.10B.

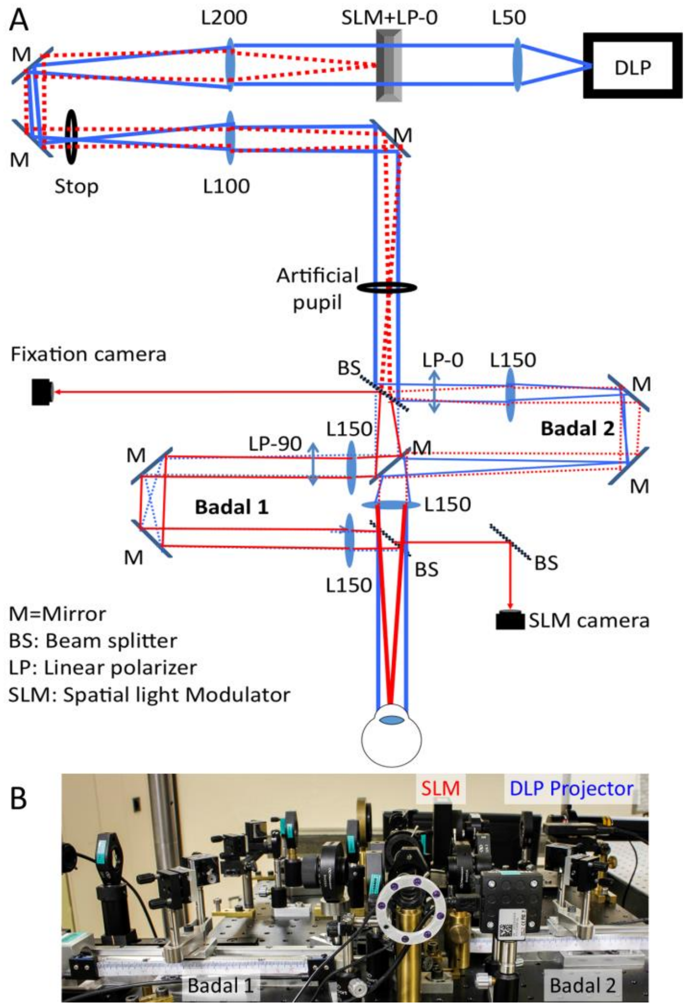

Figure 2.10: (A) Schematic diagram of the modified SimVis showing the retinal planes (in blue) and pupil planes (in red) for Badal channels 1 and 2. It also shows the principal components of the system (DLP, SLM and Badal systems) (B)Photograph of the modified SimVis setup highlighting the principle components

The bifocal channel

The bifocal channel comprises of a transmissive spatial light modulator, which is used to introduce phase profiles corresponding to any lens design; and the Double Badal channels introduce the disparity in foci between far and near distances. Both the channels are collinear along the optical axis.

The Spatial Light Modulator (SLM) is a liquid crystal microdisplay with a resolution of 800 x 600 pixels, a fill factor of 85%, a pixel pitch of 32 microns and a transmissibility of 90%. The property of modulation of the amplitude and phase of light by the device is widely applied in optical processing, digital holography and adaptive optics (Efron, 1995). We used a transmissive SLM to introduce phase shift by displaying black and white phase patterns on the SLM using a computer interface. Light from the psychophysical channel passes through a linear polarizer and is incident on the SLM with the phase patterns. The polarizing angle of the transmitted light passing through the black portion (reversed phase) is changed by 90 degrees and that passing through the white portion remains unchanged (Davis et al., 2000). This concept of spatial multiplexing is depicted in figure 2.11. A CCD camera placed in the conjugate pupil plane enables real-time visualization of the pattern presented at the SLM.

Figure 2.11: Spatial multiplexing with a transmissive SLM

The double Badal channel is used to introduce defocus without changing the magnification. Both the channels have a pair of achromatic doublets of 150 mm focal length and a set of mirrors. A 1 D change in refraction is brought about by moving the mirrors about 11 mm and both the Badals have a defocus range of -6 D to +10 D. However, as could be seen from figure 2.10 the design of the system is asymmetric, with the foci being in between the mirrors in Badal 1, at the second mirror in Badal 2. Typically, Badal 2 is used for correcting the refraction at far and Badal 1 is used to correct refraction at near, by introducing positive defocus.

The transmitted beam from the SLM is split using a 50/50 optical beam splitter. Two linear polarizers, with polarizing angle parallel to and orthogonal to the first linear polarizer, is placed in the path of the beam entering the far and near channels respectively. These allow the light transmitted from white portion to enter the far channel and that transmitted from the black portion to enter the near channel. These two beams are recombined by another 50/50 optical beam splitter placed at the first pupil plane in front of the eye. The steps involved in alignment of the Badals are described under the calibration section.

The psychophysical channel

The stimuli for psychophysical measurement is presented using a DLP projector (Texas Instruments) at 640 x 480 pixels at 60 Hz. The condensing lens of the projector was removed the DMD array was collimated using an achromatic doublet of 50 mm focal length. The maximum luminance of the projector was 160 cd/m^2 and the effective luminance at the retinal plane was 39 cd/m^2. A 130 x 130 pixel image subtended 2 degrees at the subject's retina. Owing to the limitations introduced by the SLM, the maximum extent of retinal image that could be tested without overlapping of the diffractive orders was about 3 degrees. An NDF filter was used during gamma correction and luminance measurements. The gamma correction was performed manually using the PsychCal function of the Psychtoolbox-3 following methods described by Brainard (1997) and Pelli and Farell (1995).

The pupil monitoring channel

The CCD camera (Thorlabs Inc) is conjugated, using an optical beam splitter, with the pupil plane with x0.5 magnification. An infrared LED ring is used to illuminate subject's pupil for centration and monitoring fixation during measurements. Centration of the subject is achieved using a mechanical stage that can be moved in the x-y-z axes.

The DLP projector, the SLM and the Badal motors were connected to a computer and synchronized using custom developed routines in Matlab using Psychtoolbox (Brainard, 1997). The CCD cameras were controlled in another computer using the commercial software obtained from the developer (Thorlabs Inc).

2.2.2 *Calibration*

During reconstruction phase of the modified SimVis an image of a collimated source was obtained with a CCD camera at the conjugate planes of the SLM, DLP and the Badal to ensure centration and alignment of each of the optical components in the x-y-z axes. In addition, the collinearity of the two Badal channels were assessed for different dioptric positions of each Badal channel using a camera placed at the exit pupil location. These are described in detail in this section.

Validation of the Badals

For simulating an ideal simultaneous correction, the Badal channels must be aligned coaxially and should not produce magnification while a change in the defocus is induced in either of the channels. A CCD camera with an objective was placed at the ocular position to obtain the retinal image plane and the image of a high contrast stimuli projected through the Badals were captured. The images of the object from only the far and near channels (at 0 D), from both Badal channels at 0 D, both Badal channels at ±3 D, one Badal in focus and the other at ±3 and vice versa were obtained. As can be seen from figure 2.12, neither displacement nor magnification was observed, for the different positions of the Badal channels.

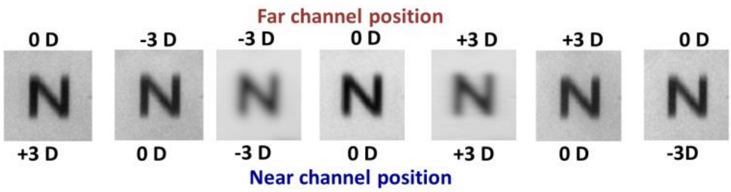

Figure 2.12: Validation of Badal channels. High contrast target images through different defocus positions of each Badal channel

Characterization and Validation of the SLM

The performance of the SLM depends very much on the proper characterization of the transmission properties of the SLM. We validated the transmission properties given by the manufacturer using a setup as shown in figure 2.13A. A collimated linearly polarized source of known intensity is incident on an SLM with a white image on the display. The preset gamma correction controls in the developer software was set to 0. The gamma curve was obtained by measuring input versus transmission intensities using PsychCal of PsychToolbox, described by Brainard (1997) and Pelli and Farell (1995). The SLM had a transmission of 88.4% and the gamma curve was linear.

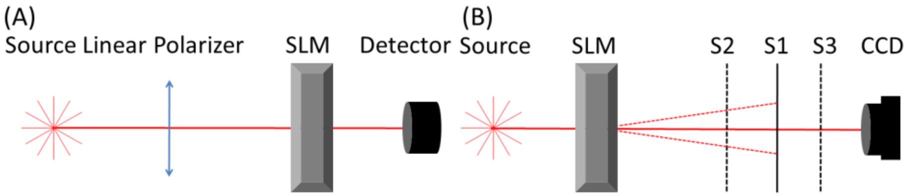

Figure 2.13: Setup for calibration of SLM (A) Transmission and Gamma correction (B) Pixel pitch

The pixel pitch was validated by methods described by Banyal and Prasad (2005) as shown in figure 2.13B. The diffraction pattern formed by the SLM of a collimated source is imaged at three image planes. Pixel pitch is calculated from the displacement of the secondary maxima, that is, the change in position of the second diffractive order when moving the SLM. In our system, we found a pitch pixel of 31 microns and 33 microns in the x and y axes respectively.

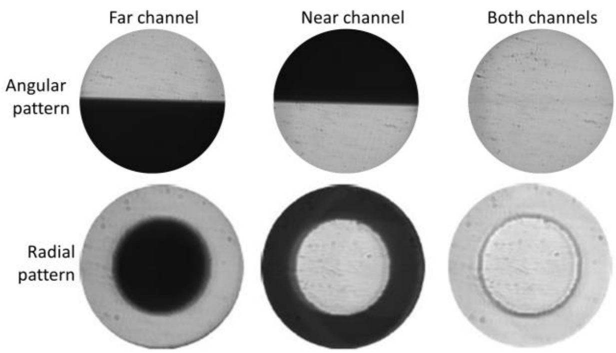

Figure 2.14: Phase pattern introduced at the SLM imaged at the pupil plane through independent Badal channels (Both Badals at 0 D).

The SLM was conjugated with the artificial pupil plane with a magnification of x0.5. The magnification and alignment of the pupil patterns through each Badal channel was validated by placing a CCD camera at the pupil plane. Black and white phase patterns projected by the SLM was imaged through either and both the Badal channels. Figure 2.14 shows examples of pupil pattern obtained from each channel. Everyday calibration involved verifying the alignment and superposition of both the Badal channels at retinal and pupil planes at different positions of each Badal channels.

2.2.3 *Measurement in Human subjects*

In this thesis, the simultaneous vision simulator was used to study neural adaptation to simultaneous bifocal vision, visual performance and perception with different patterns of angular and radial designs. Similar to adaptive optics measurements, the subject is first aligned to the optical axis of the system using the optomechanical stage and monitoring fixation through the CCD camera. The eyes were cyclopleged and subjective best focus measurement was performed by asking the subject to adjust the Far channel Badal with a keyboard until the high contrast Maltese cross presented through the projector appears sharp. This measurement is repeated three times.

For simulating a far vision condition, the far channel is placed at best focus and the near channel is placed at best focus + 3 D. On the other hand, for simulating near vision, the near channel is placed at best focus and the far channel is placed at best focus - 3 D. An intermediate vision is evaluated by placing both the Badals at 1.5 D out of focus, with the near channel having focus in front of the retina and the far channel behind the retina. The psychophysical measurements were performed in these configurations of Badal with the pupillary distribution being introduced in the SLM simultaneously with the test image at DLP. Maintenance of cycloplegia and fixation monitoring were done periodically throughout the duration of measurements.

2.3 Miniaturized Simultaneous Vision Simulator

We developed and validated a see through hand-held simultaneous vision simulator using an optomechanical tunable lens (Optotune Inc.,.). We later developed a binocular setup of similar working principles. The tunable lens was programmed by Daniel Pascual and the design was evolved in collaboration with Jose-Ramon Alonso (Dorronsoro et al., 2013).

2.3.1 Setup

Figure 2.15A shows the schematic of the miniaturized SimVis. The principal component of the system is a tunable lens (EL-10-30-C, Optotune Inc), which is a combination of polymer membrane with optical fluid that changes its curvature when a voltage is applied (Fig. 2.15B). Combined with an offset lens, the tunable lens has a refraction range of -1.5 D to +10 D with an effective aperture of 10 mm. The tunable lens with an artificial pupil is placed conjugate to the exit pupil plane of the eye using a pair of achromatic doublets of 75 mm focal length. Image reinversion is achieved by using 4 mirrors that act as roof prism. The system has a magnification of x1 and a field of about 14 degrees (Fig. 2.15C).

Multifocality is achieved by temporal multiplexing of the tunable lens to different refractive states. In our system, the transition of refraction states occur at 60 KHz. The visual system integrates these images over time and perceives it as a static simultaneous image. The energy dedicated to a specific distance is determined by the amount of time the lens remains in that state. Thus, by modifying the time and the refraction states, bifocal and trifocal pure simultaneous images of different far/near energy ratios can be optically simulated. The tunable lens is controlled for generating refractive states by custom routines written in Visual C. Refractive errors in the eye could be compensated by the tunable lens.

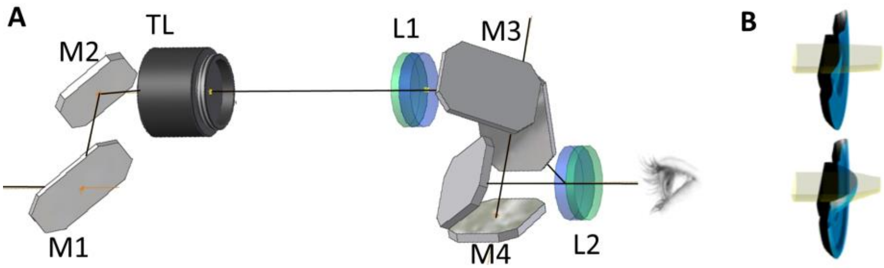

Figure 2.15: (A) Schematic of SimVis mini (B) Working principle of Tunable lens

Figure 2.16A shows the miniaturized Simultaneous Vision Simulator. The binocular system (SimVis Bino) consists of two identical channels with optical design similar to the monocular system, with the exception of image inversion being achieved by a roof-pechan prism placed in front of the tunable lens. The tunable lens in both the channels are synchronized to perform with a desired state at the same time. The laboratory prototype of SimVis Bino is shown in figure 2.16B. The interpupillary distance and convergence can be changed by moving the channels lateral to the optical axis and by rotating the channels along the optical axes.

Figure 2.16: Simultaneous vision simulators based on temporal multiplexing (A) See-through portable monocular SimVis Mini (B) Binocular, open-field vision simulator

2.3.2 *Calibration*

The important step in calibration of miniaturized SimVis in addition to identification of the retinal and pupil planes, is the validation of the tunable lens. The retinal and pupil planes were first identified by ray tracing with optical design software (Zemax Inc.,.). The distance between the lenses, position of the tunable lens and the position of the eye (the pupil and retinal planes) were checked and adjusted by imaging a collimated source through the lens system using a CCD camera with an objective focused at infinity. Magnification was checked by placing an artificial pupil and the CCD camera at the exit pupil planes as described in the previous sections.

Characterization of the Tunable Lens

The voltage-diopter reciprocity of the tunable lens was characterized using a setup as seen in figure 2.17A. The image of an ETDRS chart placed at distance of 3 m was imaged by the tunable lens on to a CCD camera. The CCD camera with an objective focused at infinity was placed in conjugate focus with the tunable lens using a Badal system. Defocus was introduced in the setup with the Badals and the change in voltage required to compensate for the introduced defocus is noted, these measurements were repeated over time. As can be seen from figure 2.17B, the voltage and defocus induced had an almost linear correspondence. A change in voltage of 0.5 V corresponded approximately to 1 D change in the defocus. Aberrations measured using laser ray tracing showed that coma-like aberrations (RMS 0.32microns, PD 7mm) were introduced for a defocus value over 6 D. Figure 2.20C shows the measured change in voltage over time for various multifocal configurations. Further optical calibrations of the lens is described in Chapter 9.

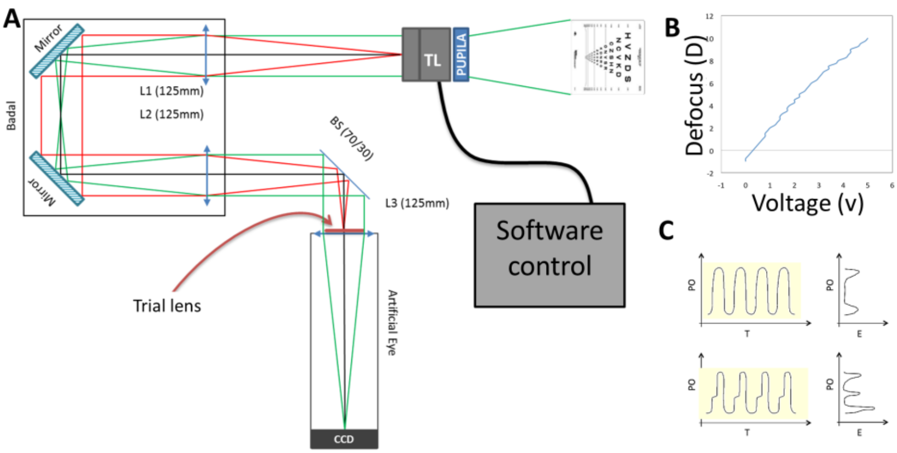

Figure 2.17: Validation of Tunable lens (A) Setup (B) Defocus-Voltage reciprocity (C) Change in voltage for multifocal configuration

2.2.3 *Measurement protocols*

We performed visual acuity, visual performance and perceptual preference measurements for various multifocal profiles. Cyclopleged subjects were asked to see through the system to a visual scene that comprised a mix of natural images and high contrast targets at far, intermediate and near distances. The optimal correction at each distance was first obtained by modified subjective refraction techniques. The defocus in the tunable lens is changed until the subject sees sharp at that distance. Further visual tests are performed with these refraction states. In case of SimVis Bino, a cross hair is placed at the entrance pupil plane and the subject is asked to move the two channels until crosshairs overlap. The subjective responses are documented manually by the examiner.

2.4 Psychophysical measurements

The quantitative assessment of subjective response to a stimulus depends on the stimulus properties and the subjective task. In this section we briefly describe the various parameters like the task involved, stimulus used in different experiments of the thesis.

2.4.1 Visual stimuli

In the measurements involving judgment of blur and its changes with adaptation (Perceived Best Focus and Perceptual score, described later), natural images (two different face images) of varying blur type and magnitude were used. The same image is used both as testing and adapting images. All the images had a 1/f profile (calculated as described by (Elliott et al., 2011) and as seen from figure 2.18 and had comparable slopes (especially at the mid spatial frequencies). We also measured decimal visual acuity by generating high contrast white on black E letter presented in eight orientations of varying size. In two experiments a commercial software (Fast Acuity XL) was used to measure logMAR acuity displayed in a high resolution retina display tablet (Apple Inc).

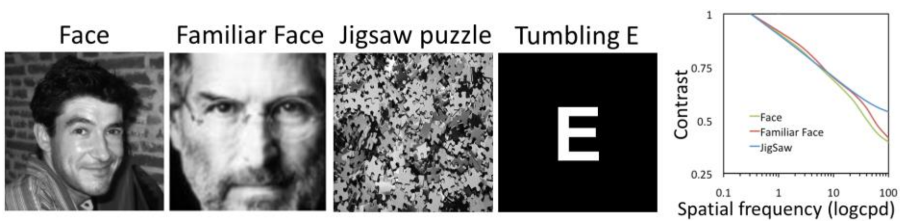

Figure 2.18: Test stimuli (Left) and 1/f pattern for the natural images used in the thesis (right)

For measurements done using the adaptive optics system, the blur in the stimulus was manipulated computationally by convolving the image with series of PSFs, which was then presented through AO corrected optics (Fig. 2.19A). Depending on the objective of the experiment and the outcome measured, the blur in the image was varied by introducing only defocus, or defocus and sharp image or different Zernike coefficients of varying blur magnitude and/or orientations. The bifocal blur magnitude/orientations in the SimVis (Fig 2.19B) and miniaturized SimVis mini was introduced optically.

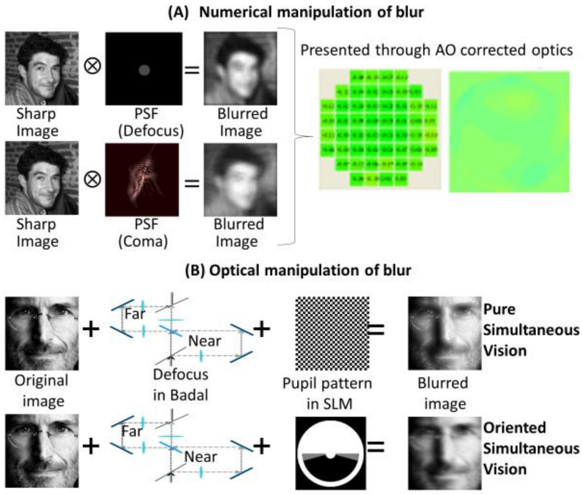

Figure 2.19: Manipulation of blur in stimuli (A) Numerical convolution (B) Optical induction

2.4.2 *Subjective tasks and psychophysical paradigms*

Several psychophysical paradigms and subjective tasks, specific to the measured outcome were implemented in this thesis. In this section we will see brief overviews of the methods which will be later elaborated in the respective chapters.

Perceived Best Focus

Perceived Best Focus (PBF) is defined as the amount of blur in the test image that is perceived neutral by the subject (Sawides et al., 2011). In other words, this is the threshold of blur detection. For measuring natural PBF the subject is adapted to a equiluminant gray background for 15 s. Then a random image, from a series of images (usually 150 to 250 images, called the test series) with varying blur values, is presented for 500 ms. The subject performs a single stimulus blur detection task i.e., the subject responds as to whether the presented image is blurred or sharp. Depending on the subjective response the blur level in the next test image is modulated in a modified staircase using a QUEST paradigm (Watson and Pelli, 1983, Phipps et al., 2001). A reversal is obtained when the subject responds from blur to sharp or vice versa. A typical run consists of 40 trials or 16 reversals. The PBF is calculated as the average blur level corresponding to the last 10 reversals. The procedure is summarized in figure 2.20.

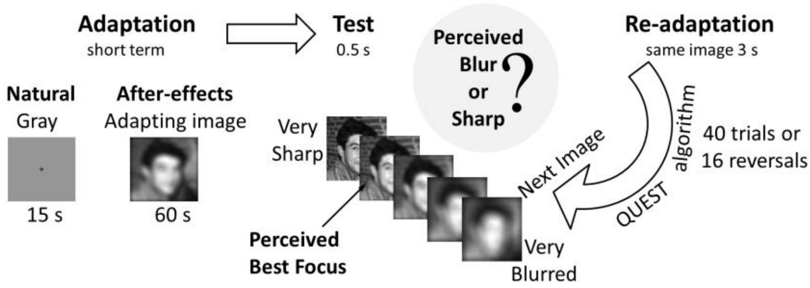

Figure 2.20: Perceived Best Focus measurement

For measuring after-effects, an adapting image is presented for 60 s prior to presentation of the test image and the PBF is measured as described before. The adapting image is jittered spatially in the x-y axes to prevent adaptation to local features in the adapting image. The difference in the PBF between gray adaptation and image adaptation represents the after-effect of adaptation.

Perceptual score

Perceptual score is a technique of category scaling which involves judgment of single stimulus. This is a rapid method to study the perceived similarity between different test categories or subjects. Every image in a test series is presented for 500 ms in random order to the subject. For each presentation the subject ranks the image from very blurred to very sharp. The measurement is repeated ten times, the ranks are then assigned a score, and the average score per image is calculated. Similar to PBF measurements, the subjects are adapted to a gray field or the adapting image and the change in the score between the two conditions is calculated as the after-effect of adaptation.

Weighted Preference

For measuring a preference, we used a classification inspired method (Ahumada, 2002, Eckstein and Ahumada, 2002). The subject is presented with a pair of images successively and the task of the subject is a 2-AFC task with 3 levels of choice. Each image is presented for 1.5 s with interposition of a gray screen for 500 ms. The subject's task was to choose the better focused image of the pair and to indicate the confidence of selection on a 3-level scale. A score is assigned to the level of confidence: very confidant 10, less confident 5 and not confident 1. Images that were chosen were assigned positive scores and the other image in the pair is assigned a negative score. The weighted score is derived from the sum of these repeated measurements. The analysis and interpretation of these weights differed between different experiments and are discussed specifically in the respective chapters.

Visual Acuity

Visual acuity was measured using an 8-AFC procedure with high contrast white tumbling E letters on a black background. The width of each stroke and the gap between the strokes in the letter was 1/5th of the total size of the letter. A letter of random orientation and a specific size (usually large) is presented for 500 ms. The subject responds with a keyboard the orientation of the presented letter (left, up-left, up, up-right, right, down-right, down, down-left). The size of the next letter is varied using a QUEST algorithm. The size of the letter is increased if the displayed orientation is identified correctly or is increased if the orientation is not identified correctly. A typical run consists of 50 trials or 20 reversals.

For all the measurements in AO and SimVis, the stimulus presentation and response acquisition were programmed using PsychToolbox in Matlab. The presentation of stimuli were accompanied with an auditory feedback. In some of the experiments, the stimulus presentation was facilitated with a ViSaGe platform and in some experiments the stimulus presentation was done using a screen function. Similarly, the responses from the subjects were obtained using ViSaGe response box or a simple keyboard. In all the measurements, the parameters of measurement, including subject's response was automatically saved in an Excel format (Microsoft Inc).

2.5 Measurement protocols

This section describes the general protocols followed with human subjects who participated in the study. A total of 72 subjects participated in different experiments described in this thesis. All were normal subjects with refractive errors/presbyopia and no ocular diseases with age range of 21 to 62 years. The refractive error ranged between +1 D to -5.50 D with less than 1 D astigmatism.

Ethics Statement

All the subjects were provided with an information sheet (in Spanish), describing various procedures involved in the study (Annex A). The procedures were reviewed and approved by Institutional Bioethical Committees of the Consejo Superior de Investigaciones Científicas and met the tenets of the Declaration of Helsinki. The subjects provided were fully informed, understood and signed an informed consent before enrolment in the study.

Refractive error measurements

Sphero-cylindrical refractive errors were objectively measured using an autorefractor (AR 597, Humphrey Zeiss Inc.) prior to the experiments. Those with an astigmatism of > 1 D were excluded from further measurements. The spherical error provided an initial setting for subjective best focus measurement with Badal.

Obtaining dental impression

For precise centration and alignement of the subjects' eye to the optical system, a dental impression was obtained using nontoxic moldable chemical on a mountable metal support. This impression was mounted on to the mechanical stage for the alignment.

Pharmacological pupil dilation

Three experiments (Chapter 3-5) were performed with natural pupils and rest of the studies (Chapter 6-9) were performed with mydriasis and cycloplegia introduced using 3 drops of 1% tropicamide instilled at intervals of 5 minutes and 30 minutes prior to beginning of other measurements (Hofmeister et al., 2005). All the subjects had underwent prior clinical assessment to test for adverse effects to mydriasis.

Psychophysical Task

A demonstration of the psychophysical task was given to the subjects when indicated. All the measurements were performed with periodic breaks and the subjects could also take breaks when required.

Chapter THREE

Neural adaptation to interocular differences in blur magnitude

Long-term differences in blur magnitude can be introduced by monovision corrections. Studying how the visual system copes with inherent differences in higher order blur magnitude will provide insight to mechanisms of adaptation to these corrections.

This chapter is based on the paper by Radhakrishnan, et al., "A cyclopean neural mechanism compensating for optical differences between the eyes" Current Biology, 2015. The co-authors of the study are Lucie Sawides, Carlos Dorronsoro, Michael Webster and Susana Marcos.

The author of this thesis designed and performed the measurements, and analyzed the data in collaboration with the co-authors. This work was presented in parts at the Association for Research in Vision and Ophthalmology (ARVO) annual meeting, May 2014 in Orlando, Florida, USA, and at the Visual and Physiological Optics conference, Wroclaw, Poland as an oral contribution.

3.1 Introduction

The visual system includes many imperfections and limitations, yet these often pass unnoticed in perception, because of mechanisms that compensate for sensitivity losses and distortions in visual coding. The neural processes that 'discount' the image blur (resulting from optical aberrations) from our perceptual experience have been explored in a number of studies, yet the nature of these processes remains poorly understood. We specifically asked how the perception of blur is calibrated for an individual, when the optics differs between the two eyes. At short timescales, vision adjusts to blur through adaptation (Webster, 2011). For example, brief exposure to blurred images shifts the physical blur level that appears in focus (Webster et al., 2002, Vera-Diaz et al., 2010), and can lead to improvements in acuity (Mon-Williams et al., 1998) or result in renormalization of perceived focus for the level of blur (Elliott et al., 2011). Recent studies probing a single eye suggest that vision is also calibrated over very long timescales closely to the amount of blur produced by their own optics, and also is weakly tied to the specific pattern of their higher-order aberrations (Artal et al., 2004, Sawides et al., 2011a, Sawides et al., 2011b, Sawides et al., 2013).

It remains unknown whether these compensatory processes operate to calibrate spatial vision for each eye independently or whether they instead depend on a single binocular site, and how information from the two eyes might be combined at this site. Although optical quality between the two eyes is normally similar (Porter et al., 2001, Kim et al., 2007), differences in magnitude and pattern of higher-order aberrations are in fact common (Marcos and Burns, 2000). Moreover, interocular blur differences can exist due to differences in refractive power (anisometropia) and are also introduced in some clinical treatments such as monovision correction for presbyopia. Short-term blur adaptation shows strong interocular transfer (Kompaniez et al., 2013), implicating a cortical locus for the sensitivity changes at stages in the visual pathway where information from the two eyes has begun to converge. However, it is unknown what binocular interactions occur over the very long timescales at which observers are chronically exposed to their own interocular differences in blur.

We probed how the neural coding for visual blur is calibrated over both long and short timescales, by comparing judgments of perceived focus and how they change with adaptation, to the actual levels of retinal image blur within the left and right eyes.

3.2 Methods

Judgments of image focus (Perceived Best Focus) and how these change with adaptation were assessed using images computationally degraded with differing amounts of optical blur measured from real eyes. Figure 3.1A,B shows the general experimental procedure. All measurements were performed monocularly in both eyes of normal subjects with undilated pupils.

3.2.1 Apparatus

The ocular aberrations were measured and corrected using the VioBio Adaptive Optics system (Marcos et al., 2008, Sawides et al., 2010). Defocus was compensated with a Badal optometer, residual astigmatism and aberrations were measured using a Shack Hartmann wavefront sensor and were corrected using a deformable mirror and monitored periodically during psychophysical measurements. The subjects viewed the visual stimuli presented through the AO system, on a CRT monitor connected to a psychophysical platform (ViSaGe, Cambridge Research System, UK). The stimulus presentation was programmed in using PsychToolbox in Matlab (Brainard, 1997).

The wavefront maps and PSFs corresponding to the measured Zernike coefficients was calculated for a 5 mm pupil diameter using Fourier techniques (Goodman, 1996). From the PSFs, Strehl Ratio (SR) was calculated for each subject. The level of defocus was chosen to maximize optical quality (Liang and Williams, 1997, Born and Wolf, 1999, Porter et al., 2001, Goodman, 2004). The average SR prior to and following adaptive optics correction was 0.149±0.096 and 0.55±0.12 respectively, and was periodically monitored during the psychophysical measurements. Repeated measurements in our subjects resulted in an average variability of 6% SR (SD 6%). Thus difference of >30% SR between eyes was considered a meaningful difference in optical bur magnitude between eyes (>5 times the variability of the measurement).

3.2.2 Subjects

Aberrations and focus judgments were obtained for twelve young subjects (age range: 22 to 42 years) with spherical error ranging from +1.00 D to -5.50 D and astigmatism <1 D. Five of the twelve subjects had prior experience in performing psychophysical experiments. Subjects S1 and S5 (myopia >4 D) performed the experiments with contact lenses. Sighting dominance was tested in subjects using the Miles test (Roth et al., 2002). Subjects S1-S5 participated in both Experiment 1 and Experiment 2.

3.2.3 Experiment 1: Perceived Best Focus measurements

The experiment allowed blur levels (as indexed by Strehl Ratio) to be varied over a wide range that appeared either "too blurry" or "too sharp" to the observer. A psychophysical task was used to estimate the boundary between these percepts, at which the image appeared to have the "Perceived Best Focus".

Stimuli

Test stimuli were generated by convolving a face image (480 x 480 pixels) with the optical blur (Zernike coefficients) measured in 128 eyes assuming a 5 mm pupil diameter. The amount of simulated blur varied from a SR of 0.75 (very sharp) to 0.008 (very blurred). The images subtended 1.98 degree at the retina.

Procedure

Perceived Best Focus was measured as the amount of SR that was perceived as neither blurred nor sharp. The subject first adapted to a gray screen for 30 s and then a test image with a random blur magnitude (SR) was presented for 500 ms. According to their subjective criterion for a optimally focused image, the subject performed a single stimulus blur detection task (Ehrenstein and Ehrenstein, 1999).

Depending on the response, the blur in the next image was chosen by a QUEST algorithm (Pelli and Farell, 1995, Brainard, 1997, Phipps et al., 2001). Thus a series of test images interspersed with a gray screen was presented until the test converged (usually in 40 or less trials). PBF was the level of blur corresponding to the average of the last 10 stimulus values that oscillated around the boundary with a standard deviation less than 0.02 SR. The measurements were done in one eye first (three repetitions), followed by the other eye, chosen randomly. Overall the session lasted for approximately 1 hour per subject.

3.2.4 Experiment 2: Measurement of after-effects

For the 5 subjects (S1-S5) that had the strongest differences in blur between their eyes, we assessed how adaptation to blur in either eye affected their focus judgments (Fig. 3.1B).

Stimuli

For each subject, a series of test images was created from their own PSF (Zernike coefficients) by varying only the magnitude of blur by scaling it by a factor from 0 to 3 times the original PSF in steps of 0.01, yielding 301 different levels. For three subjects (S1, S2, S5) their two eyes differed only in the magnitude but not the shape of the PSF, and thus the series were generated from the PSF of their better eye. For the other two subjects the PSFs had slightly different orientations, and thus the series was based on the average PSF between eyes. A face image was then convolved with each of these scaled PSF's to generate the image series, which ranged from no blur (Strehl Ratio of 1) to 3 times the blur of their better eye (S1,S2, S5) or their average blur (S3, S4).

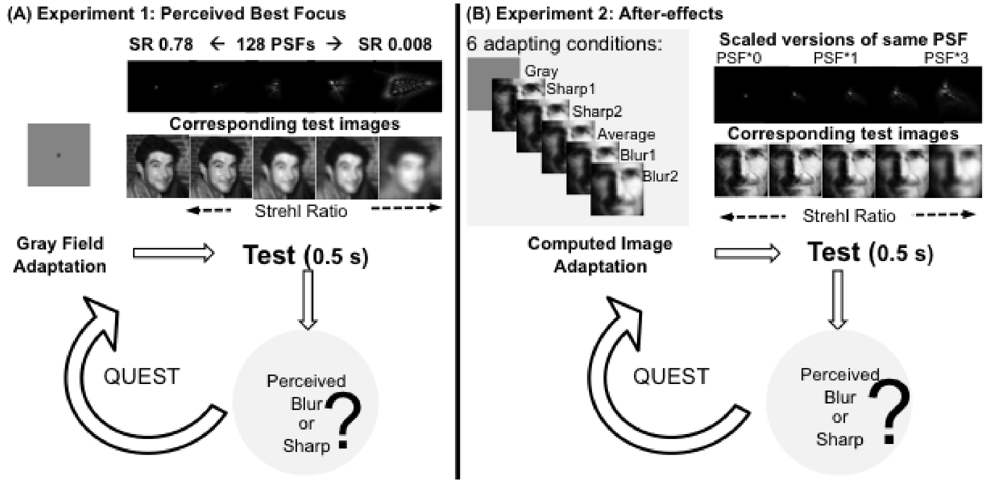

Figure 3.1: (A) Experiment 1: Perceived-Best-Focus measurement under neutral gray field adaptation (B) Experiment 2: After-effects measurement after adaptation to different levels of image blur

Observers, judged the blur level that appeared neither too blurred nor too sharp, after adapting to the gray field and to adapting images that had different degrees of blur. Five adapting images that varied linearly in SR steps were chosen to bracket the magnitude of blur between eyes: an image with blur level corresponding to each eye, the intermediate blur level based on averaging the two eyes, and extreme levels that were either sharper than the better eye or blurrier than the worse eye.

Procedure

The same psychophysical task was used as in Experiment 1. Subjects initially adapted to an adapting image with given blur level for 60 s jittered spatially over time. Each subsequent test image presentation was preceded by a 3 s period of re-adaptation, until the QUEST algorithm converged. Both the adapting conditions and the eye measured (left or right) were randomized. The gray adaptation condition was repeated three times to establish the baseline, and measurements following a given adapting condition were performed once. A complete session lasted approximately 2 hours.

3.2.5 Data Analysis

Non-parametric mean comparisons and correlations were performed for the Perceived Best Focus measurements (Experiment 1) and non-parametric analysis of variance was done to study the changes with adaptation (Experiment 2).

3.3 Results

3.3.1 Ocular aberration profile

The wavefront aberration maps, RMS wavefront error, Point Spread Function and the corresponding Strehl Ratios for each subject are given in figure 3.2. Subjects S1-S5 had similar orientation and different blur magnitude, S6, S7 had similar orientation and magnitude, S8, S9 had different orientation and similar magnitude and S10, S11 had different orientation and magnitude and S12 had mirror symmetric PSFs between eyes.

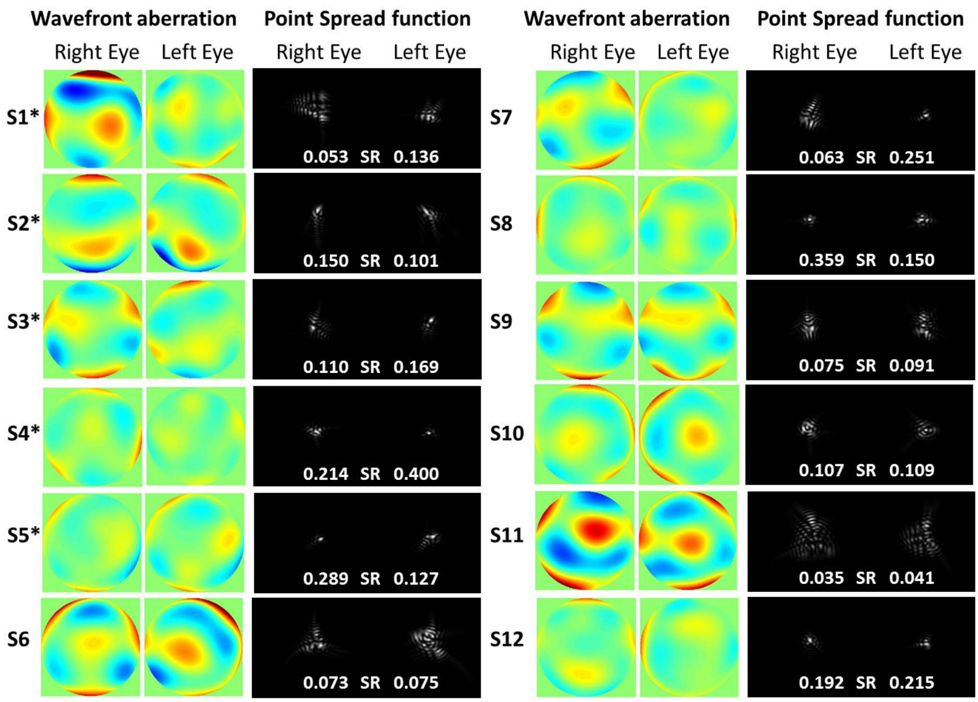

Figure 3.2: Aberration profile of subjects. Wavefront aberration maps, Point Spread functions (PSFs) for both eyes of all subjects. In the PSF panel, symbols + indicate the eye with sighting dominance and * indicate the eye with better optical quality. S1-S5 participated in Experiment 1 and 2

The average blur magnitude in the right eye was 0.143±0.099 SR and in the left eye was 0.156±0.096 SR. The average interocular differences in SR was 0.080±0.080 and corresponded to a 26% difference in optical quality between eyes of the subjects. There was a weak correlation (r=0.441, p=0.052) between the right and left eye blur magnitude (Fig. 3.3A). In most subjects (10 of 12), the eye with better optical quality was also the eye with sighting dominance.

3.3.2 Perceived Best Focus

Despite the differences in optical quality between the eyes, the judgments of image focus were very similar, when viewing the images through either eye. The amount of physical blur that observers perceived as "in focus" (neither blurred nor sharp) was 0.197±0.095 SR in the better eye and 0.191±0.094 SR in the worse eye, and the difference between eyes was not significant (SR 0.01±0.007, p=0.547). There was also a strong correlation (r=0.984, p<0.0001) between the right and left eye focus judgments (Fig. 3.3B).

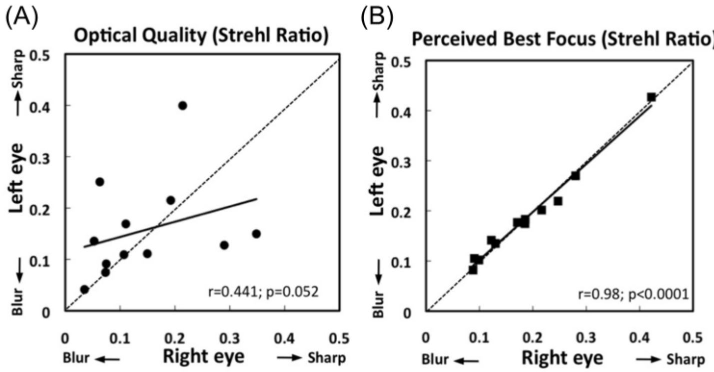

Figure 3.3: (A) Correlation in Optical quality between eyes (r=0.441, p=0.052) and (B) Correlation of right eye PBF and left eye PBF (r =0.984, p<0.0001)

3.3.3 Perceived Best Focus Vs Optical quality

Figure 3.4A compares the blur level that observers chose as best focused with the level of retinal image blur in each of their eyes. As suggested above, the percepts of image focus were very similar despite interocular differences in retinal image blur. Moreover, the focus judgments covaried with the observer's own optical quality. For example, Figure 3.4B shows a close correspondence between optical quality (x axis) and the perceptual quality (y axis) in terms of the eye with motor dominance (larger symbols) and the fellow eye. As noted before, in most subjects this dominance also corresponded to the eye with better optical quality.

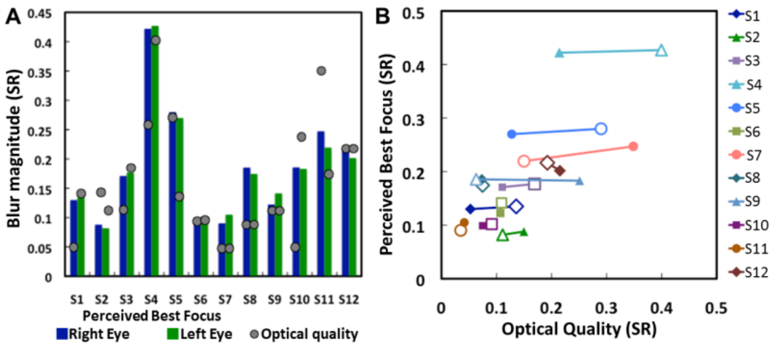

Figure 3.4: Perceived quality vs Optical quality A. Perceived-Best-Focus (bars) and Optical Image Quality (stars) in both eyes of all subjects. B. Perceptual Image Quality vs. Optical Image Quality. Same color and symbol shape represent both eyes of the same subject (linked by a segment). Large, Open symbols denote the motor dominant eye for each subject.

The subjective neutral focus points align more closely with the blur level of the better eye. This was quantified as the absolute difference between the focus settings and the blur level in each eye or the average of the two eyes (Fig. 3.5).

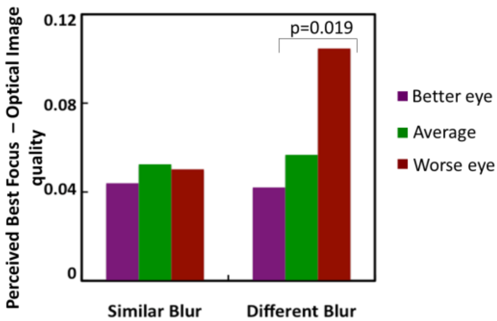

Figure 3.5: Comparison of Perceived-Best-Focus with different Ocular Image Quality. The bars represent difference between the Perceived-Best-Focus and optical quality of the better eye, the average and the worse eye, averaged across subjects with similar and different blur between eyes.

In subjects with different blur magnitudes between their eyes (S1-S7), the Perceived-Best-Focus was much closer to the blur level dictated by the better eye quality (0.042+0.04) than the worse eye (0.104+0.058), a difference which was significant (p=0.019).

3.3.4 Perceived Best Focus and its shift following adaptation

The effects of adaptation on judgments of focus are shown in figure 3.6. Despite large differences between subjects in PBF (SR 0.094 to 0.412), for each subject the pattern of after-effects was very similar between their eyes with a difference of 0.002±0.002 SR averaged across subjects and adapting conditions. Moreover, despite the differences in the test images in experiment 1 and 2, the judgments on the gray background remained very similar in both measurements. This indicates that subjects are primarily sensitive to the overall magnitude of blur as measured by SR irrespective of the specific pattern of blur.

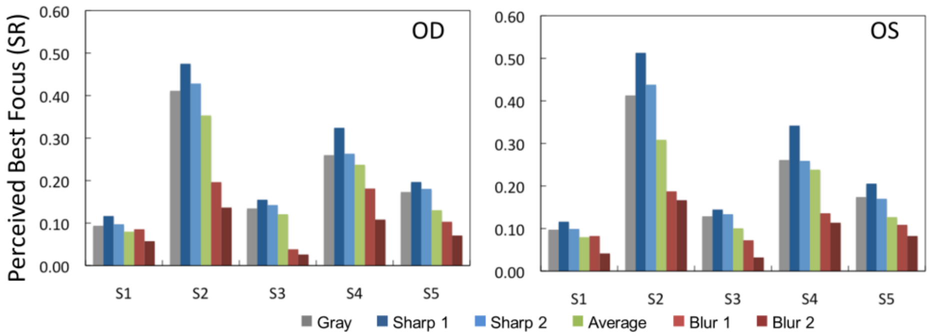

Figure 3.6: Best-Perceived Focus following adaptation to a gray field and different amounts of blur. Adapting conditions were: Gray; Sharp 1: Strehl Ratio of better eye+Average Strehl Ratio between eyes; Sharp 2: Strehl Ratio of better eye; Average Strehl Ratio between eyes; Blur 1: Strehl Ratio of worse; Blur 2: Average Strehl Ratio between eyes - Strehl ratio of worse eye. Left panel shows results for right eyes; right panel for left eyes.

The natural adaptation settings were strongly affected by adaptation to images with different blur levels. Figure 3.7 shows the after-effects following adaptation for all subjects and averaged across subjects. The sharpest adapting images (i.e. less blurred than the better eye) caused the blur level that was rated best focused under gray adaptation to appear too blurred. Subjects thus chose a less blurred image to compensate for this bias. Alternatively, adaptation to the most blurred image (more blurred than the poorer eye image quality) induced the opposite after-effect. These after-effects are consistent with previous measurements of blur after-effects (Webster et al., 2002).

Probing the blur level that did not produce an after-effect, and how this depended on the adapting eye, we found, for either eyes, the blur level at which the after-effect was nulled corresponded closely to the better eye, while exposure to the worse eye's blur or the average blur of the two eyes caused the previous subjective focus level to appear too sharp. A non-parametric ANOVA further revealed that there was no difference in the magnitude of the effects between the right and left eye (p=0.819). Thus both the focus judgments and how they were biased by the adaptation were completely determined by the better eye, and were consistent with a neural calibration matched to the optical quality of the less aberrated eye.

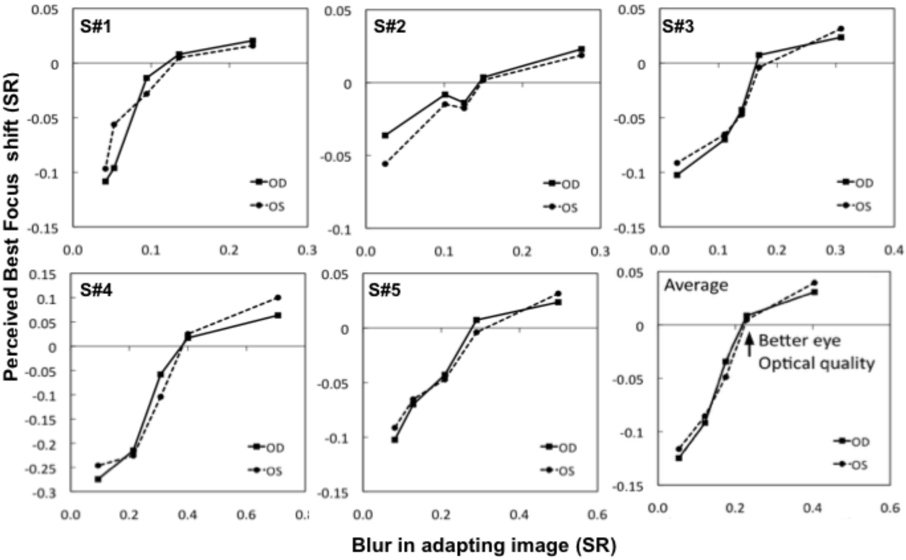

Figure 3.7: Shift of Perceived-Best-Focus following adaptation to different amounts of blur. Adapting images levels are those described in Figure 3.6. Panel A-E show data for subjects S1-S5, and Panel F shows average data. Solid lines and squares are data for right eyes; dashed lines and circles are data for left eyes. No after-effects occur for an adapting image blurred with the aberrations of the better eye, when either eye is tested.

3.4 Discussion

Visual blur is a fundamental dimension of spatial sensitivity and image quality (Watson and Ahumada, 2011), and is a feature of the world that the visual system is correcting for constantly by accommodation. The stimulus that appears "in focus" to an individual represents an estimate of the spatial structure of the visual environment, and is closely associated with the characteristic spatial statistics of natural images (Field, 1987, Field and Brady, 1997). To estimate these statistics, the visual system must compensate for the blur that optical and neural processes themselves introduce, a quantity that is unique not only to each individual but to each individual eye. We have shown that irrespective of these interocular differences, the physical stimulus that is perceived as best-focused is remarkably similar between eyes, and is tied to the magnitude of blur in the eye with better optical quality.

3.4.1 Perceptual constancy in spatial vision

The close correspondence between subjective focus and the magnitude of native optical blur emphasizes that the brain is adapted to its own aberrations as shown by previous studies (Artal et al., 2003, 2004, Sawides et al., 2011a, Sawides et al., 2011b, Sawides et al., 2013). This ideally ties the perception of focus to properties of the world rather than the observer, so that two observers will tend to agree which images are in focus even though their eyes filter the images in very different ways. Our finding supports the hypothesis that adaptation to spatial blur magnitude operate at subjective levels, especially that dictated by eye with better optical quality. This perceptual constancy for spatial vision is analogous to color constancy observed even in eyes with cataract development which results in similar color perception even in eyes with different wavelength filtering (Werner and Schefrin, 1993, Delahunt et al., 2004, Wuerger, 2013).

3.4.2 Sharpness dependence of perception

The dependence on sharper image for perception and adaptation is explained by findings that perceived blur is in fact dominated by the sharp component when a blurred and a sharpened image are physically combined (Georgeson et al., 2007, Radhakrishnan et al., 2014). In the present study we tested each eye separately, but the calibration for focus that we measured was based on long-term binocular viewing in which the images from both eyes were neurally combined, and in which the sharper image would again dominate. It is well known that in binocular viewing that eye with a sharper image dominates the eye with a blurrier image (Arnold et al., 2007, Georgeson et al., 2007). However, our findings are novel and important in showing that this sensory dominance persists to influence perceived focus even when the eyes are stimulated separately.

3.4.3 Cyclopean locus of blur adaptation

Differences in visual inputs from the two eyes have been studied extensively in the context of binocular vision and rivalry (Blake and Wilson, 2011). It has been shown, that during binocular viewing, the cyclopean percept is influenced by eye with the sharper image (Hoffman and Banks, 2010). But it remains unknown how the visual system calibrates and corrects for normal variability in image quality between the eyes, and whether this correction is applied to each eye separately or after their signals have converged. To test this, we used adaptive optics to control and manipulate the blur projected on each retina, and then compared judgments of image focus through either eye and how these judgments were biased by adapting to different levels of blur. Despite interocular differences in the magnitude of optical blur, the blur level that appeared best focused was the same through both eyes, and corresponded to the ocular blur of the less aberrated eye.

Moreover, for both eyes, blur aftereffects depended on whether the adapting blur was stronger or weaker than the native blur of the better eye, with no aftereffect when the blur equaled the aberrations of the better eye. Our results indicate that the neural calibration for the perception of image focus reflects a single “cyclopean” site that it is set monocularly by the eye with better optical quality. Many studies show (Ono and Barbeito, 1982, Erkelens, 2000, Ono et al., 2002, Hoffman and Banks, 2010), that people have conscious access to the cyclopean image, but not to the monocular images when viewing binocularly. These results establish that there is a single “cyclopean” locus of the neural compensation for the eye’s optical defects, calibrating the neural signals carried by either eye but set only by the better eye, and that the perception of focus corresponds to a unique null point in the sensitivity of the underlying neural code.

The spatial selectivity of blur adaptation while implicating a cortical site, could in theory, compensate separately for the two eyes. Spatial after-effects, unlike temporal coherence, show incomplete transfer between the eyes, and this has implicated adaptation in pools of both binocular and monocular neurons in early cortical areas (Blake et al., 1981). We found that, for spatial blur, the compensation is completely binocular, and perceptual adjustments are tied to the less aberrated eye in blur magnitude. This long-term binocular compensation driven by the sharper image is consistent with the short-term blur after-effects reported by Kompaniez et al. (2013).

3.4.4 Timescales of adaptation

There is increasing evidence that adaptation operates over multiple timescales (Kording et al., 2007, Vul et al., 2008, Wark et al., 2009, Bao and Engel, 2012). The subjective judgments of focus (Experiment 1) presumably reflect very long-term adjustments to the habitual blur, while the after-effects we found from introducing a sudden change in the ambient blur level (Experiment 2) represent very rapid but short-term adjustments. Even though the adaptation operates through different mechanisms during different timescales, our results reveal that these mechanisms are interrelated. In fact the blur level perceived neutral by the subject did not produce any after-effect, indicating that this is indeed a true calibration to native blur level and not just ‘learning’ by the observer to associate the presented blur level to the native blur level. These indicate subjective norm for focus also corresponds to an explicit norm in the visual code for blur (Webster and Leonard, 2008, Sawides et al., 2012) and aids understanding visual renormalization following cataract surgery (Fine et al., 2002).

3.4.5 Implications on refractive corrections

While we explored long-term adjustments to interocular differences that arise in the course of natural viewing, these differences are also increasingly introduced in long-term corrections for refractive errors, and both the form and dynamics of the neural adjustments are important for understanding the consequences of these corrections. One common example is monovision corrections for presbyopia. In these the dominant eye is corrected for far, while the contralateral eye is focused for near, so that only one eye is in focus. As noted above, it is argued that monovision works because the sharper image dominates the percept, although the degree of dominance depends on target size and contrast (Schor et al., 1987). Strategies to improve monovision corrections and improve binocular summation (Wright et al., 1999, Plainis et al., 2011, Tabernero et al., 2011) will likely benefit from a better understanding of how this compensations happens over long timescales for these induced interocular differences. The selectivity to the sharper image in sensory dominance, as suggested by our results, could be a key startegy for clinical treatment, and should be tested prior to providing a patient with a surgical monovision correction for presbyopia.

Amblyopia is another example where larger interocular differences exist between eyes (Levi, 2006). We demonstrate that the visual system is sensitive and selective even to smaller differences in blur such as that imposed by the higher order aberrations. This approach could probably be applied to analyze neural sources of interocular differences in spatial sensitivity, and how the visual system compensates for these differences to estimate the spatial structure of the world.

On the other hand, it is not uncommon to have mirror symmetric axes or orientation differences in axes of astigmatism between eyes. In addition, multifocal corrections with angular refractive designs might also introduce differences in blur orientation between eyes. It would be interesting to study the preference to orientation in eyes with different blur orientations.

3.5 Conclusion

Our results indicate that the neural calibration for the perception of image focus reflects a single ‘cyclopean’ site that is set monocularly by the eye with better optical quality. Consequently, what people regard as ‘best-focused’ matches the blur encountered through the eye with better optics, even when judging the world through the eye with poorer optics.

Chapter FOUR

Neural PSF in eyes with interocular differences in PSF orientation

In eyes with inherent differences in blur magnitude, we found a cyclopean locus of blur perception and adaptation. Orientation preference is also shown to be closely associated to retinal blur orientation. Differences in blur orientation could be commonly induced by surgical refractive corrections or present inherently in eyes with astigmatism or higher order aberrations. It would be interesting to study the preference to orientation in these eyes.

This chapter is based on the paper by Radhakrishnan, et al., "Single neural code for blur in subjects with different interocular optical blur orientation" Journal of Vision, 2015. The co-authors of the study are Lucie Sawides, Carlos Dorronsoro, Eli Peli and Susana Marcos.

The author of this thesis designed and performed the measurements on human eyes, and analyzed the data in collaboration with the co-authors. This work was presented in parts at the Association for Research in Vision and Ophthalmology (ARVO) annual meeting, May 2014 in Orlando, Florida, USA as an oral contribution.

4.1 Introduction

The human visual system is highly robust, constantly compensating for changes in the magnitude of blur in retinal images, and thus maintaining a relatively constant perception of the world despite changes in the environment (Webster et al., 2002, Webster et al., 2006) or in the subject's optics (Mon-Williams et al., 1998, Webster et al., 2002, Artal et al., 2004, Artal et al., 2006, Poulere et al., 2013). Experiments by Webster and colleagues showed that even brief exposures to altered blur can result in a measurable change in the neural adaptation states (shifts in perceived best-focus) of the visual system (Webster et al., 2002, Elliott et al., 2011, Webster, 2011). Another study (Sawides et al., 2011b) showed that the natural perceived best focus is highly correlated with the magnitude of optical blur at the retina and produced after-effects when adapting to images blurred by scaled versions of his/her own aberrations or to the aberrations of other subjects (Sawides et al., 2011a, Sawides et al., 2012).

Optical blur may be different across orientations, such as that produced by astigmatism. Strong after-effects in the perception of isotropic focus occur following short-term adaptation to images blurred with horizontal and vertical astigmatism (Sawides et al., 2010). Adaptation selectivity for the axis of astigmatism has been shown to occur for both real and simulated astigmatic images (Ohlendorf et al., 2011). Also uncorrected astigmats show a preference towards the orientation of their astigmatic axis, which shifts towards isotropy as early as two hours after wearing the astigmatic correction (Vinas et al., 2012).

Oriented blur also occurs in retinal images a result of asymmetric higher order aberrations such as coma. In a seminal work by Artal et al. (2004), visual quality was 40% better with images blurred with the subjects' actual Point Spread Function (PSF) than with rotated versions of the same PSF. Sawides et al. (2012) also showed a stronger bias to the images blurred with the subject's natural PSF, as opposed to a 90 degree rotated PSF even when the blur magnitude in the images were normnalized. In a later study, Sawides et al. (2013) introduced a pattern classification method

(Ahumada, 2002), to retrieve, in particular, the orientation of the internal code for blur of subjects. Positive and negative orientation classification maps were obtained from the weighted averages of the PSFs blurring the images subjectively selected as either better or worse perceived, respectively. Correspondingly, the positive classification maps were termed the positive neural PSF, and the negative classification map termed the negative neural PSF. They reported that, shape and orientation of the positive neural PSF was similar to that of the ocular PSF suggesting that not only is the internal code tuned to the overall amount of optical blur, but it is also tuned to a specific blur feature- the orientation of the high order PSF. All these prior studies were performed monocularly, and only the aberrations of the tested eyes were considered.

Even though the ocular aberrations are dynamic (Hofer et al., 2001), the shape of the PSF tends to remain similar across different pupil diameters and accommodation (Artal et al., 2003), enabling strong neural adaptation. Yet, it is not uncommon to find differences between both eyes of the same person in the pattern or magnitude of higher order aberrations (Marcos and Burns, 2000, Porter et al., 2001). Little is known about the way the visual system copes with such differences (as when each eye is separately exposed to different adapting image). A short-term adaptation experiment where right and left eyes were adapted to different images (either blurred, focused or gray, or astigmatic blur with orthogonal orientation) showed a significant interocular transfer in adaptation in both isotropic and astigmatic blur (Kompaniez et al., 2013). Also, various other studies suggest that a presence of sharp component influence largely the adaptation state in monocular or binocular viewing (Arnold et al., 2007, Radhakrishnan et al., 2014).

In our previous study, perceived best focus was measured monocularly in both eyes of subjects with similar or different blur magnitude between eyes. We reported that in subjects with different blur magnitude between eyes, the eye with a better optical quality dominates the perception of blur magnitude and the differences in the blur between eyes are addressed by the neural system, resulting in a single perceived best focus for both eyes (Radhakrishnan et al., 2015b). A question then arises on how the neural system deals with these inputs from eyes with different orientation in the optical blur of each eye.

In this study, we measured the internal code for blur in both eyes of subjects with similar and different PSF orientation between eyes and investigated the perceptual differences in the orientation bias of the internal code for blur between eyes.

4.2 Methods

The internal code for blur of the subjects was estimated using the pattern classification method described previously (Sawides et al., 2013). Subjects selected the better perceived image from a pair of presented images blurred with equal blur magnitude but different PSF orientations, and then scored their confidence in the selection, for a total of 500 pairs. Measurements were performed monocularly for each eye of the subject, covering the other eye with a patch. From the large number of responses, the “neural PSF” was estimated using a reverse correlation technique.

4.2.1 Apparatus

Ocular aberrations were measured in both eyes of all subjects with a Hartmann Shack wavefront sensor in the VioBio Adaptive Optics setup. The spherical refractive error was compensated using a Badal system. Psychophysical measurements were done under static closed-loop aberration correction using a membrane deformable mirror correcting residual defocus, astigmatism and high order aberrations. In the current study an average correction efficiency of 88.7% in RMS wavefront error was achieved. Visual stimuli were presented on a CRT monitor through the psychophysical ViSaGe platform (Cambridge Research Systems, UK). All measurements were done undilated with 5 mm artificial pupils.

4.2.2 Subjects

Both eyes of ten subjects (22 to 41 years old) were measured in this study. The subjects had no clinical astigmatism and their spherical refractive error ranged from +1.00 D to -5.50 D. All subjects had prior experience in performing psychophysical tasks. Two subjects with myopia >4 D performed the experiments wearing their habitual spherical soft contact lenses. Sighting dominance was established in subjects using the Miles test (Roth et al., 2002).

4.2.3 Measurement of the Neural PSF

The internal code for blur or the Neural PSF of the subjects was estimated using the pattern classification method (Fig. 4.1). Subjects selected the better perceived image from a pair of presented images blurred with equal blur magnitude but different PSF orientations. The "neural PSF" was estimated from these repetitive measurements for each eye using a reverse correlation technique.

Stimuli

A face image of 480 pixels that subtended 1.98 degrees at the retina was used. For each subject, test images were generated by convolving the face image with the higher order aberrations of 100 ocular PSFs that had different orientations of isotropic distribution orientations (Sawides et al., 2013). The blur magnitude was normalized, by optimizing the defocus component, for each subject (in terms of SR) to match the subject's better eye optical PSF or to that of the PBF (measured in Radhakrishnan et al., 2015a). All subjects, except S2, had PBF better than or equal to optical blur magnitude. The PBF blur magnitude was used for all subjects except for subject S2, for whom the better eye optical quality was used to generate the images. All convolutions were performed for a 5 mm pupil diameter. In total, 10 series of 100 test images were generated, one series for each subject. The same image series was used for both eyes of a subject.

Procedure

A gray field adaptation was provided for 30 s at the beginning of the measurements. The subject was then presented sequentially with a pair of images degraded with two different PSFs with different orientations but similar blur magnitude, interleaved with a gray field. Both the images and the gray field were presented for 500 ms. The subject performed a 2-AFC task and chose which of the two images of the pair was better perceived, and indicates confidence in the response on a 3 level scale. One session consisted of presentation of 50 random pairs taken from the 100 images of PSF patterns, ensuring that each image is presented at least once in a session. Each subject performed 10 such sessions (500 random image pairs per eye). A typical experiment involving measurements on both eyes lasted for approximately 5 hours, the subject was allowed to rest between sessions and the adaptive optics correction was re-measured during and after every session.

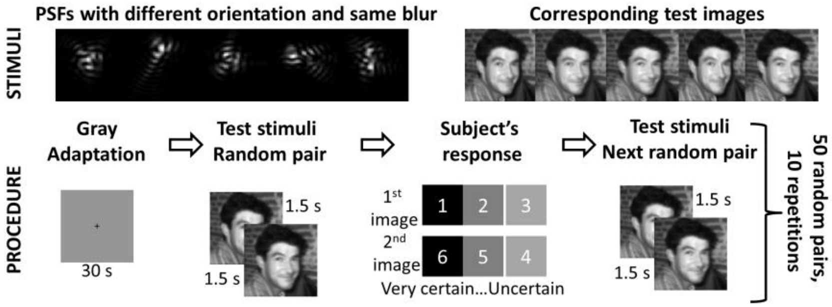

Figure 4.1: Pattern classification inspired method for estimation of preferred blur orientation

4.2.4 Data Analysis

Magnitude, Contour and Orientation of PSF

Using Fourier techniques (Goodman, 1996) the wavefront maps, PSFs, RMS wavefront error and the SR were calculated to the measured high order Zernike coefficients for a 5 mm pupil diameter. A difference of >6% in SR was considered significant (Radhakrishnan et al., 2015a).

The contour and orientation of the PSF was calculated by methods described in figure 4.2 (Sawides et al., 2013). The PSFs were centered at the center of mass and then sampled in 72 angular sectors of 5 degree each. The intensity of the PSF at mid-angle of each sector was obtained, was normalized to the maximum intensity and was plotted in a polar plot generating a contour diagram. The orientation axis of the PSF is given by the main axis of the best-fitting ellipse. The mean difference in ocular PSF orientation estimation for inter-session measurements in our study was 0.66 ± 0.34 degrees and a difference of > 20 degrees (mean orientation difference between optical and neural PSFs in Sawides et al., 2013) was considered as a meaningful difference in optical blur orientation between eyes.

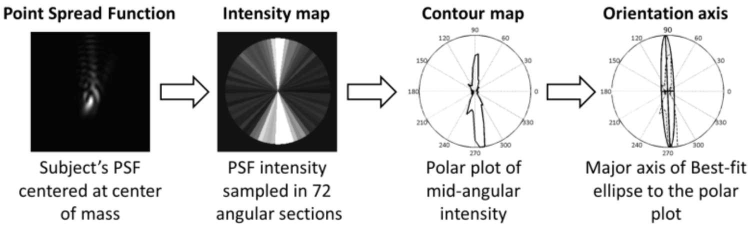

Figure 4.2: Estimation of PSF orientation (Adapted fromSawides et al., 2013)

The orientation of PSF thus estimated, was highly reproducible across sessions and different conditions. Typical fluctuations in accommodation (1 D, Charman, 2008) produced differences in the ocular PSF orientation of 0.24 ± 0.2 degrees. The orientation axis difference between the PSFs estimated for different wavelengths, based on wave aberration data across the visible spectrum (450-750 nm) was 3.02 ± 0.62 degrees. The orientation axis difference between the PSF with only high order aberrations and the PSF with the residual low order aberrations (including astigmatism) was 2.72 ± 0.95 degrees, indicating minimal influence of residual astigmatism.

Neural PSF estimation

Sawides et al. (2013) presented a method to estimate the internal code for blur, inspired by the classification images technique, and based on a reverse correlation (Ahumada, 2002, Eckstein and Ahumada, 2002). Calculation of the classification maps and extracting the contours of the positive and negative weights allowed estimation of shape of the neural PSF (Fig. 4.3).

PSFs corresponding to the images that were subjectively selected as better-perceived are given positive scores, and the other image in the pair is given negative scores. The PSF intensities are multiplied by a weight derived from the confidence of response: 10 for a very confident response, 5 to a less confidence response, and 1 for the lowest confidence response to each image of the pair selected as better focus.

Thus, a PSF in an image consistently selected as better focused and with high confidence will get a score of 100 (score 10x10 presentations). Alternatively, scores of -10, -5 and -1 are given to the images not selected as better focused. The noise effect by some random comparisons of two rather similar PSFs is countered by the high number of comparisons being made and by the weighted scoring system. All the weighted responses were then summed to obtain a pattern classification map. The contour of the positive weights of the classification map was termed as positive neural PSF and the contour of the negative weights of the classification map was termed the negative neural PSF. We calculated for each subject, the standard deviation in the scoring of a specific PSF pattern across different sessions. Pooled variance was calculated as the average of the standard deviations across subjects, the square root of which provides the repeatability parameter. The repeatability across subjects and between sessions, thus measured was 2.3 (15% of the full score range), indicating consistency in weighted score, across sessions by each subject.

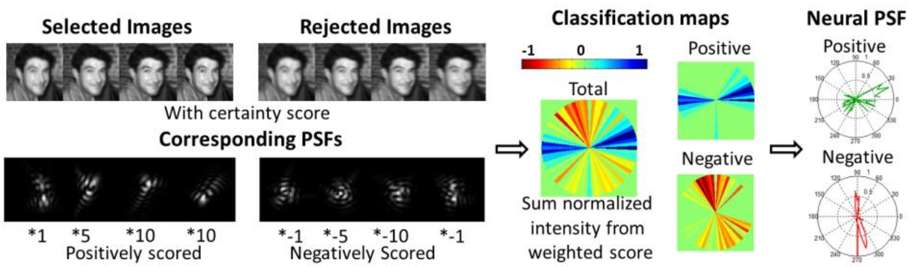

Figure 4.3: Estimation of neural PSF from using reverse correlation method from weighted pattern classification responses

Correlation and Orientation-difference analysis

The correlation between the energy distribution of the ocular PSFs (absolute intensities, not contours) and the sum weighted average of the PSFs perceived better and worse was calculated. The difference in orientation between any two PSF was calculated by rotating the PSF in 1 degree-steps and calculating the image correlation coefficient at each step. The relative rotation that resulted in maximum correlation coefficient was considered the orientation difference (in degrees) between the PSFs. For two PSFs to have similar orientation, the maximum correlation would be obtained for a rotation close to 0 degrees. In an alternative analysis, the correlation coefficients between the ocular PSF contours and the neural PSF contours was calculated using a circular correlation coefficient (Fisher and Lee, 1983). These analyses provided similar results (t-score = 0.7, df=71, p=0.27).

4.3 Results

4.3.1 Ocular aberration profile

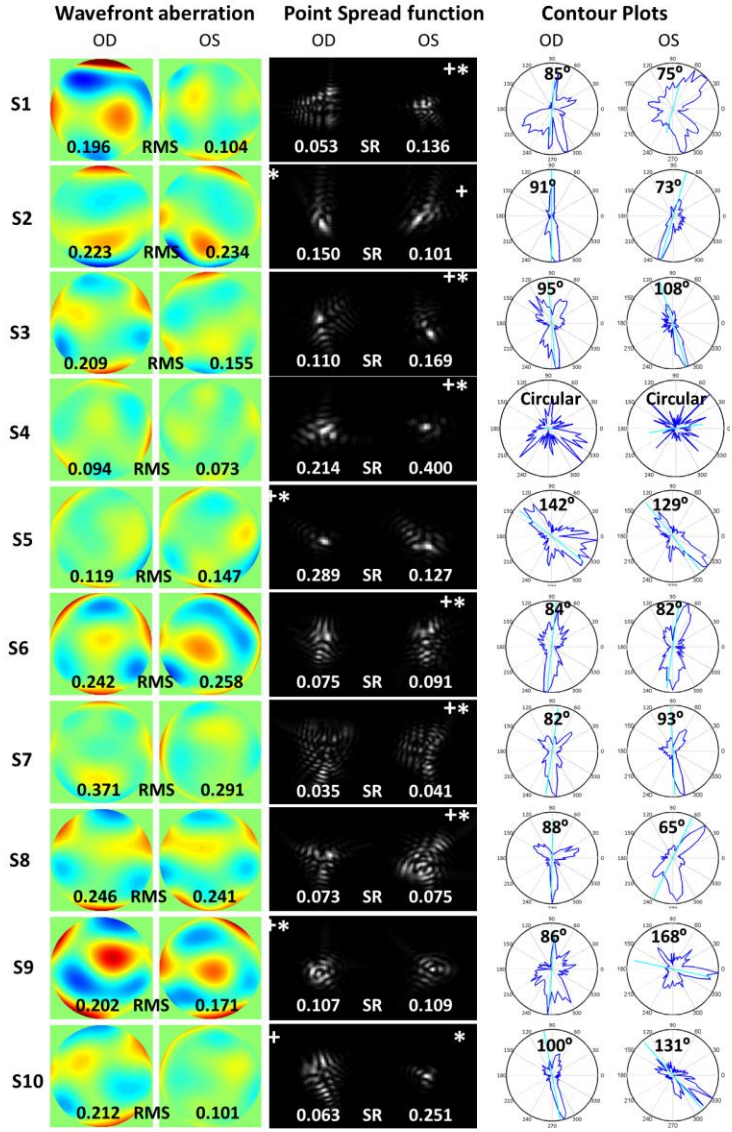

Figure 4.4: Wavefront aberration maps (left), PSFs (middle) and PSF contour plots (right) for both eyes of all subjects. Subjects S1-S7 had similar ocular PSF orientation between eyes, subjects S8-S10 had different (>20 degrees) ocular PSF orientations. Symbols + indicate the eye with sighting dominance and * indicate the eye with better optical quality.

Figure 4.4 shows the ocular higher-order aberration patterns, the corresponding PSFs, and the PSF contour plots in both eyes of the 10 subjects. The RMS for higher order aberration, the SRs and the orientation axes are shown in the insets. Under the criteria defined above for meaningful differences in blur magnitude and orientation between eyes S1-S5 had similar PSF orientation, but different blur magnitude between eyes; S6-S7 had similar PSF orientation and similar blur magnitude in both eyes; S8-S9 had similar blur magnitude but different PSF orientation; and subject S10 had both different PSF orientation and different blur magnitude between eyes.

4.3.2 Interocular similarity in neural PSF

Figure 4.5 shows the positive and negative neural PSF contours in comparison with their respective ocular PSF contours for each subject in each group. It could be seen that the orientation of the positive (green) and negative (red) neural PSFs are strikingly similar between the two eyes, despite inteorcular similarity or difference in blur magnitude and/or PSF orientation (blue). There was strong and significant interocular correlation in the orientations of the positive neural PSF ($r=0.95$, $p<0.001$) and negative neural PSF ($r=0.99$; $p<0.001$). Consequently, the neural PSFs were not statistically significantly different between eyes ($p=0.9$ and $p=0.36$, for positive and negative, respectively). Across all subjects, the average difference in orientation between the positive and the negative neural PSFs was 58 $\pm$ 18.73 deg and was statistically significant (t score=2.82, df=9, $p=0.022$).

The orientation differences between eyes in ocular PSF and the neural PSFs for each of the subjects are shown in figure 4.6. As seen, the high interocular difference in orientation of ocular PSF (27.1$\pm$ 30.4 deg, in blue) was found for neither the positive neural PSF (3.3 $\pm$ 1.95 deg, in green) nor the negative neural PSFs (1.1 $\pm$ 0.32 deg, in red).

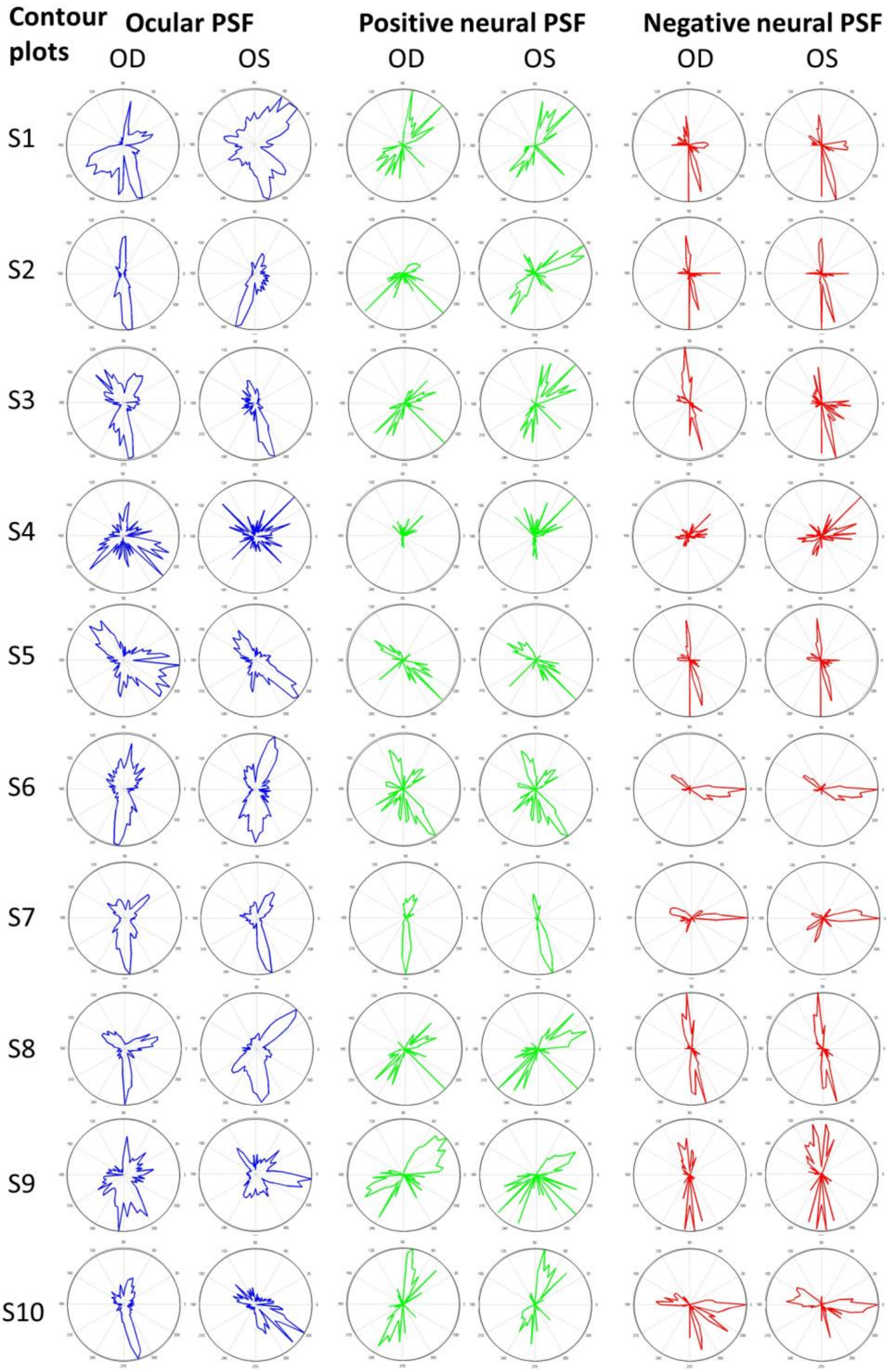

Figure 4.5: Ocular PSF contours (blue, left columns), positive neural PSF contour (green, middle columns), negative neural PSF contour (red, right columns) for both eyes of each subject.

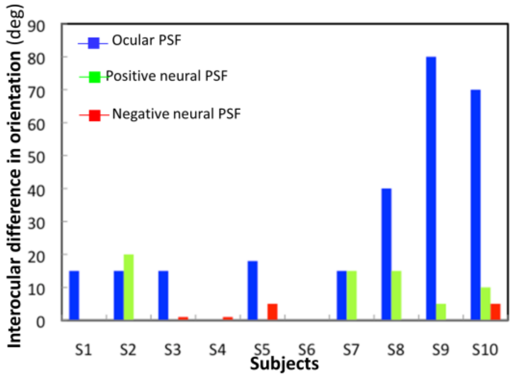

Figure 4.6: Interocular difference in orientation between eyes for Ocular PSF (blue), positive neural PSF (green), negative neural PSF (red) for the corresponding subjects and average across all subjects. In the ocular PSF contour panels, symbols + indicate the eye with sighting dominance and * indicate the eye with better optical quality

4.3.3 Interocular similarity: Intersubject differences

The interocular difference in orientation in different groups of subjects is shown in figure 4.7. Similar to the trend noted in average across subjects, the interocular difference in orientation (Fig. 4.7A) of the positive neural PSFs in subjects with similar (S1-S7) and different (S8-S10) ocular PSF orientations between eyes was 3.7 $\pm$ 2.03 deg and 2.33 $\pm$ 1.53 deg, respectively.

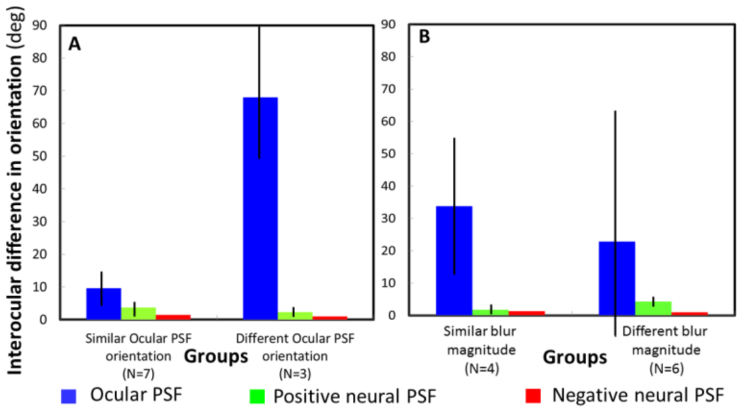

Figure 4.7: Interocular difference in orientation between of the ocular PSF (blue), positive neural PSF (green) and negative neural PSF (red). (A) Subjects with similar (S1-S7) and different (S8-S10) ocular PSF orientations (B) Subjects with similar (S6-S9) and different blur magnitudes (S1-S5, S10).

The difference was slightly higher (4.3 ± 1.68 deg), yet insignificant in subjects with different blur magnitude between eyes (Fig. 4.7B). The interocular difference in orientation of the negative neural PSF was close to 1 deg in all groups of subjects.

4.3.4 Neural PSF vs Ocular PSF

Figure 4.8 shows the average orientation differences between the ocular and neural PSFs. On average the largest differences in orientation occur between the negative neural PSF and the ocular PSF of the eye with better optics (51.8 ± 16.9 deg). The least difference in orientation was found between the positive neural PSF and PSF of the eye with better optical quality (10.5 ± 3.8 deg). Consequently, the positive neural PSF correlated more with the PSF of the eye with better optical quality (r=0.60, p=0.002) than the worse eye (r=0.53, p=0.008) and the PSFs perceived worse correlated significantly with the PSF of the worse eye PSF (r=0.63, p=0.002) than the PSF of the better eye (r=0.47, p=0.018).

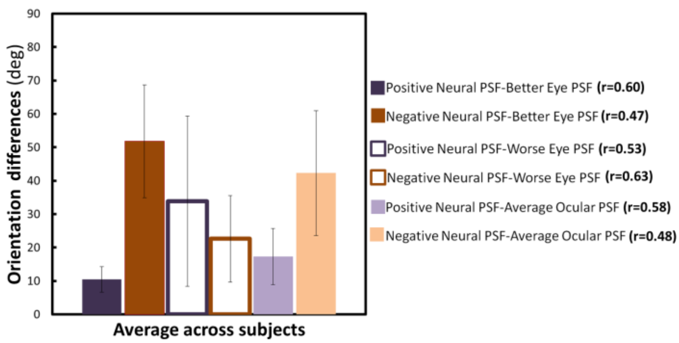

Figure 4.8: Difference in the orientation between positive and negative neural PSFs and the better eye PSF orientation (filled bars) and the worse eye PSF orientation (open bars). The corresponding correlation is given in parentheses. All correlations are significant (p<0.05).

4.3.5 Neural PSF: Intersubject differences

Figure 4.9A shows orientation differences between the ocular PSFs and the positive and the negative neural PSFs, in subjects with similar and different ocular PSF orientations between eyes. In subjects with similar ocular PSF orientation between eyes (S1-S7), as expected, the positive and negative neural PSF orientations differed similarly from either eye. In subjects with different orientations between eyes, the positive neural PSF differed least from the ocular PSF of eye with better optics (12.6 ± 7.2 deg), while the negative neural PSF differed the most from the ocular PSF of the eye with better optics (45.7 ± 17.3 deg).

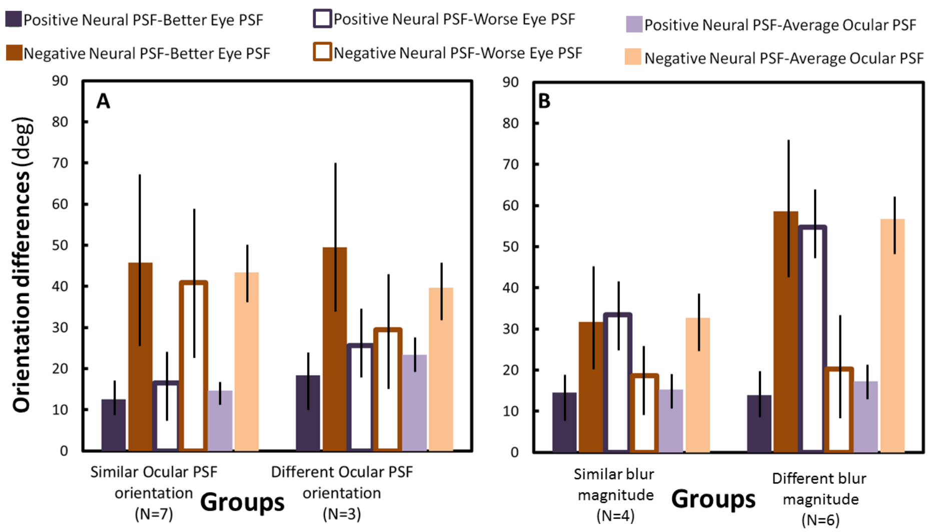

Figure 4.9: Difference in orientation between Ocular and Neural PSFs. (A) Subjects with similar (S1-S7) and different (S8-S10) blur orientation. (B) Subjects with similar (S6-S9) and different blur magnitudes (S1-S5, S10).

Figure 4.9B shows differences between the orientations of the ocular PSFs, and the orientation of the positive and the negative neural PSF, in eyes with similar and different ocular PSF magnitude. While in both groups of subjects the orientation difference was least for positive neural PSF and the ocular PSF of better eye (14.6 deg and 13.8 deg, for subjects with similar and dissimilar blur between eyes, respectively), and the negative PSF differed most from the ocular PSF of the better eye (31.6 ± 13.9 deg and 58.6 ± 29.6 deg, for subjects with similar and dissimilar blur between eyes, respectively), the actual differences were larger in subjects with different blur between eyes, indicating the role of blur magnitude in orientation preference.

4.4 Discussion

The physical retinal stimulus is affected by the eye's optical limitations, which are actively compensated for by the neural system, resulting in improved perceptual quality. Additionally, the visual system appears to be naturally adapted to the native level of blur, and be able to rapidly and continuously recalibrate to compensate for intrinsic or environmental changes in blur (Webster et al., 2002, Artal et al., 2004, Ohlendorf et al., 2011, Sawides et al., 2012, Haun and Peli, 2013, Sawides et al., 2013).

4.4.1 Sharpness dependence

A recent study reported short term adaptation to artificially induced interocular differences in blur, and demonstrated that the sharper images dominate perception irrespective of which eye was exposed to sharp adaptation (Kompaniez et al., 2013). Interocular differences in refractive error or ocular aberrations are not rare, and therefore the short-term adaptation recreated in the earlier experiment, can also occur naturally over long-term. We have recently reported that in eyes with different blur magnitude, the eye with a better optical quality dominates adaptation and perception with either eye (Radhakrishnan et al., 2015b).

In the current study, we further investigated the subjective bias to specific characteristics of high order blur (i.e. the main orientation of the PSF at the retina) and the relationship between the blur orientation of the perceived best image and the orientation of the PSF, when each eye is natively exposed to optical blur of different orientation. As previously found for the internal code for blur magnitude, there seems to be a single internal code for blur orientation for both eyes, with the preference given to the eye with better optical quality. This calibration appears to operate both at short-time scales (Kompaniez et al. 2013) and long-time scales, as found in this study (where subjects are chronically exposed to interocular differences in aberrations).

4.4.2 Cortical locus for internal blur code

The spatial selectivity of both blur magnitude and orientation does not compensate separately for the two eyes, unlike other effects such as the contingent aftereffects for color (Webster and Malkoc, 2000). Our finding supports the hypothesis that adaptation to blur orientation operates at a cortical locus and is controlled by the eye with better image. Many studies show that cyclopean percept is evidently influenced by the eye with sharper image under binocular viewing, and that people have conscious access to the cyclopean image, but not to the monocular images when viewing binocularly (Ono and Barbeito, 1982, Erkelens, 2000, Ono et al., 2002, Hoffman and Banks, 2010). We studied the internal code in each eye of the subjects, monocularly. We show that the orientation selectivity persists even when the eyes are stimulated separately, and match orientation that of the eye with least optical defects. The singleness in the internal code for blur suggests that the visual system adjusts for input from the eye with the less blurry image under binocular viewing conditions, as known from studies of rivalry (Arnold et al., 2007, Kim and Blake, 2007).

4.4.3 Ocular dominance

The orientation preference driven by the eye with the better optical quality appears to be an additional form of ocular dominance. The optimal method to measure ocular dominance is not clear, with gross inconsistencies between methods testing aiming dominance (hole-in-the-card) and sensory dominance such as binocular rivalry or asymmetry in visual acuity tests (Rice et al., 2008). In our subjects sighting dominance and better optical quality matched in most but not all the subjects. However, in eyes with different optical quality, the neural code was driven by the eye with better optical quality and not the sighting dominant eye. Few researchers aim in developing clinically-suited and reliable techniques for testing ocular (sensory) dominance based on polarizing glasses (Peli, 2002) or modified balancing techniques (Handa et al., 2012). Our results suggest that binocular measurement of the ocular aberrations (rapidly done using clinically available wavefront sensors) of the patient can help identifying the sensory dominant eye at least in eyes free of neural pathology.

4.4.4 *Implications on binocularity*

Our findings may also have implications for binocular blur perception, and may be related to recent observations of binocular summation. Binocular summation and disparity have been shown to decrease with increasing interocular differences in higher-order aberrations (Sabesan et al., 2012). While inducing asymmetric higher order aberrations (like coma) in orthogonal orientations between eyes decreased binocular summation, introducing coma with bilateral mirror symmetry, or matched orientation had significantly less impact in reducing binocular summation (Jimenez et al., 2008). The single code for blur imposed by the internal code of blur of one eye may impose limitations on the binocular sensitivity gain, in some subjects of our sample who had different PSF orientations between eyes.

4.4.5 *Implications on refractive corrections*

Interocular differences in optical quality could be inherent (Marcos and Burns, 2000, Porter et al., 2001) or surgically introduced following multifocal IOL implantations, decentration of monofocal IOLs or corneal refractive surgery. Why some subjects easily adapt to these changes while others do not may be explained by the selectivity of the visual system to the native pattern of higher order aberrations. It is likely that this selectivity to the orientation of the native aberrations of the eye with better optical quality, can explain to an extent these differences.

The current study focuses on patients without clinical astigmatism. In the presence of astigmatism, the orientation preference should be largely influenced by the magnitude and orientation of astigmatism (Sawides et al., 2010, Ohlendorf et al., 2011, Vinas et al., 2012). In fact correcting all the astigmatism, may in fact result in decreased visual performance (Villegas et al., 2014) and certain combinations of astigmatism and coma (two aberrations with marked oriented features) may in fact produce better visual quality than coma or astigmatism alone (de Gracia et al., 2010, de Gracia et al., 2011, Vinas et al., 2013). Interesting subsequent research may involve studying the factors influencing orientation preferences in eyes with residual astigmatism or orientation preferences.

4.5 Conclusion

In most subjects, the positive neural PSF closely correlated with the PSF of the eye with better optical quality. On an average, the negative neural PSF was oriented 58 degree apart from the positive neural PSF. Finally, we report that, the internal code for blur, in both magnitude and orientation, is the same for both eyes, suggesting a cyclopean locus for blur adaptation in the higher cortical regions.

Chapter FIVE

Short term adaptation to simulated pure Simultaneous Vision

Simultaneous vision is an increasingly used solution for the correction of presbyopia. These corrections, normally delivered in the form of contact or intraocular lenses, project on the patient's retina a focused image at one distance superimposed with degraded image other distances. It is expected that patients with these corrections are able to adapt to the complex retinal images, although the mechanisms or the extent to which this happens is not known. We studied the neural adaptation to simulated simultaneous vision by studying changes in the perceptual quality.

This chapter is based on the paper "Short tern neural adaptation to Simultaneous Bifocal Images" PLoS One, 2014 by Radhakrishnan A, Dorronsoro C, Sawides L and Marcos S.

The author of this thesis designed and performed the measurements in human eyes, and analyzed the data in collaboration with the co-authors. This work was presented in parts at the Association for Research in Vision and Ophthalmology (ARVO) annual meeting on May 2013, Seattle, USA and at the Young Researchers Vision Camp, June 2013, Leibertingen, Germany as an oral contribution.

5.1 Introduction

Presbyopia is the age-related physiological inability of crystalline lens to focus near objects (Glasser and Campbell, 1998). Multifocal optical corrections such as multifocal contact lenses or intraocular lenses have become an increasingly used solution to restore near vision (Kohnen, 2008, Lichtinger and Rootman, 2012), where certain pupillary regions are corrected for far vision, and other regions have a relative positive power, which allows correction for near. These multifocal solutions produce Simultaneous Vision (SV) wherein a distance correction is superimposed on a near correction creating an overlap of blurred and sharp images of the object at the retina at any viewing distance. Various studies report that the increase in visual performance at near comes at the expense of a degradation of the distance visual performance (Cillino et al., 2008, Cochener et al., 2011, Kim et al., 2011). On the other hand, it is also speculated that the optical degradation produced by the image overlap, is counteracted by the brain and the vision is improved by the suppression of either distance or near image, eventually adapting to the other (Charman, 2014a). However, how the visual system gets adapted to SV has never been tested.

Adaptation and recalibration of the visual system to lower and higher order aberrations have been reported by several studies. An improvement in visual performance after adaptation to defocus (Mon-Williams et al., 1998), particularly in myopic subjects (Poulere et al., 2013), has been reported. Also shifts in the isotropic point, have been found in subjects after adaptation to images artificially degraded with astigmatism (Sawides et al., 2010), and following astigmatic correction in previously non-corrected astigmats (Vinas et al., 2012). Studies have also shown that the subjects are adapted to the amount and orientation of blur introduced by the ocular higher order aberrations (Artal et al., 2004, Sawides et al., 2011b, Sawides et al., 2013). Perceived Best Focus (PBF), the amount of image blur producing perception of neither sharp nor blurred, is found to change after short-term exposure to images blurred with increased or decreased higher order aberrations (Sawides et al., 2011a), similar to those demonstrated by Webster and colleagues for artificially blurred or sharpened images (Webster et al., 2002, Webster, 2011). This change in the

PBF is considered as a recalibration response of the visual system to any form of blur. Many studies attribute this blur adaptation to a reduction in contrast associated with blur, and therefore, in fact, is a form of contrast adaptation (Pesudovs and Brennan, 1993, Webster and Miyahara, 1997, Webster, 2011).

Few clinical studies report comparison of visual function on patients implanted with multifocal intraocular lenses or fitted by contact lenses of various designs (Kaymak et al., 2008, Llorente-Guillemot et al., 2012). Despite the popularity of multifocal corrections, the impact of simultaneous images on visual performance, and to what extent patients can adapt to simultaneous vision corrections, have been hardly explored. In a recent study, de Gracia et al, (2013) using a newly developed Simultaneous Vision Simulator, found that the amount of near addition affected visual acuity differently, with additions around 2 D causing the largest degradation for far vision. However, if and how the brain adapts to the blur pattern produced by simultaneous bifocal vision corrections is still unknown. With bifocal corrections, the modulation transfer function decreases non-linearly for higher spatial frequencies, while preserving the contrast at lower spatial frequencies. These optical differences between Pure Defocus and bifocal corrections were somehow not seen in the contrast sensitivity measurements in subjects (Gambra et al., 2009).

The traditional assumption that visual performance with bifocal lenses surpasses the optical degradation imposed by the image superposition, owing to neural mechanisms that allow suppression of the defocused image (Charman, 2014a), is not supported by specific experimental outcomes. We question this interpretation and propose that a deeper understanding of the mechanisms of neural adaptation to multifocality is essential to optimize simultaneous vision designs for the correction of presbyopia.

We hypothesize that the visual system recalibrates to the form and strength of blur imposed by bifocality, following similar mechanisms to those of adaptation to Pure Defocus. In the current study we investigate the extent and amount of neural adaptation to the blur imposed by simultaneous vision, by measuring the visual after-effects produced following brief exposure to simultaneous bifocal images (with different near additions, and different proportions of far and near vision). The shift in perceived image quality (Perceived Best Focus and Perceptual Scores) was used as a measure of the neural adaptation and the image quality metrics were used to elucidate the possible mechanisms involved.

5.2 Methods

Simulated images, shown on a CRT monitor, were used to study perceived image quality of and short-term adaptation to simultaneous vision images. To ensure that all subjects had identically blurred images on the retina, the ocular aberrations of the subjects were corrected using the adaptive optics system. The simulation mimicked a subject viewing at far, wearing a full aperture simultaneous bifocal correction-a correction that utilizes the entire region of pupil for far and near corrections (eg: Tecnis® ZM900 multifocal IOL). Two experiments were designed to evaluate the perception and adaptation to PD and to SV images by measuring the changes in the Perceived Best Focus and in Perceptual Score. Overall, the experiments lasted for a total of 11 hours and were conducted on two consecutive days with regular breaks in between the sessions.

5.2.1 Apparatus

The experiments were performed using the AO system, which compensated the subject's lower and higher order aberrations during the psychophysical measurements. The refractive error of the subject is compensated using a Badal optometer. Subjects' aberrations were measured using a Hartmann-Shack wavefront sensor and are corrected using a membrane magnetic deformable mirror (Marcos et al., 2008). Test and adapting images were presented through an artificial pupil of 5 mm and via a psychophysical channel controlled by the ViSaGe psychophysical platform (Cambridge Research System, UK). In the current study an average correction efficiency of 86% in RMS wavefront error was achieved.

5.2.2 Subjects

The right eye of four subjects, aged 27 to 31 years, with spherical ametropia (<3 D) and astigmatism (<1 D) were measured in the experiment. Overall higher order RMS was 0.79±0.36 μm under natural conditions, and 0.11±0.04μm after AO-correction.

All except one subject were experienced in performing psychophysical experiments. All the participants provided written informed consent.

5.2.3 Stimuli

Image of a face (480 x 480 pixels) subtending 1.98° at the retina was blurred by convolution with a PSF corresponding to different magnitudes of defocus. For Pure Defocus image series (PD), the magnitude of defocus varied from 0 to 2 D in 0.01 D steps.

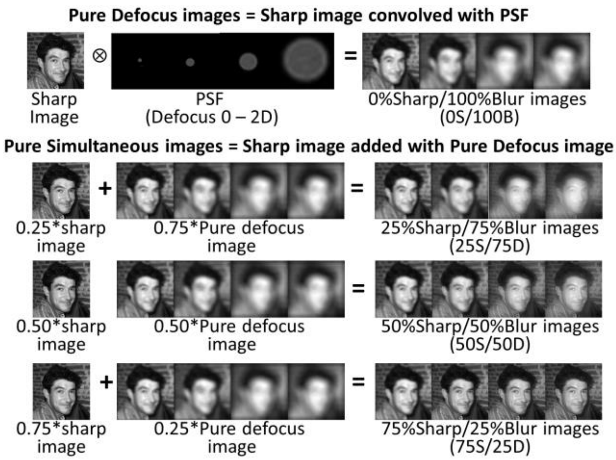

Figure 5.1: Numerical simulation of pure defocus and pure simultaneous vision image series

To generate the simultaneous vision (SV) images, a sharp image (0 D defocus) was added to a defocused image (0 to 3 D). Three simultaneous vision image series were generated by varying the proportion of the contribution of sharp and defocused images: 25% Sharp and 75% Defocus (25S/75D); 50% Sharp and 50% Defocus (50S/50D), 75% Sharp and 25% Defocus (75S/25D). For example, a 1 D defocus 75S/25D simultaneous image consists of a sharp image (weighted 75%) added to a 1 D defocused image (weighted 25%), and would be equivalent to a bifocal correction of 1 D addition with a 75% of the energy for far, and 25% for near. Figure 5.1 shows image generation process. All computations were performed for 5 mm pupil diameter.

5.2.4 Experiment 1: Perceived Best Focus measurement

Perceived Best Focus (PBF) is the just noticeable difference in blur that produces a perception of neutrality in blur/sharp vision. A change in the PBF after exposure to a new visual experience (also called after-effect) accounts for a renormalization of the visual response, so that the adapting stimulus itself appears more neutral, and represents a measure of the short-term adaptation to the new extrinsic factor (Webster et al., 2002, Webster, 2011). We studied changes in PBF after adaptation to PD and SV images. The test images were 201 PD images with defocus ranging from 0 to 2 D, in 0.01 D steps. The adapting images were PD images (6 different levels of defocus between 0.2 and 1.2 D), SV 25S/75D, 50S/50D and 75S/25D images (7 near additions between 0.2 and 1.5 D) as well as sharp adaptation condition (defocus=0) and neutral adaptation with a gray field. In total, 29 adapting conditions were tested.

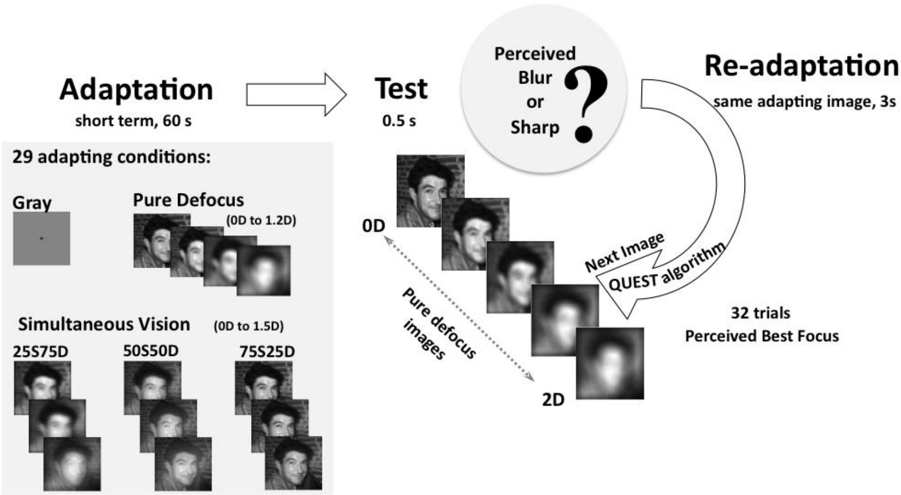

Figure 5.2: Estimation of Natural Perceived Focus and its change with adaptation. Subjects were adapted to random sequences of the 29 adapting conditions (gray field, sharp, Pure Defocus images of various magnitudes of defocus, and Simultaneous Vision images of different sharp/defocus proportions and magnitudes of defocus)

The task for the subject was based on a single stimulus blur detection with a criterion set by the observer (Ehrenstein and Ehrenstein, 1999) coupled with a QUEST paradigm of threshold estimation. This adaptive procedure calculates the sequence of stimulus based on initial probability of the threshold and response to actual trial (Pelli and Farell, 1995, Phipps et al., 2001) and was programmed using

Psychtoolbox (Brainard, 1997). The subject had to report whether the images presented were blurred or sharp. The QUEST routine usually converged in less than 32 trials, where the threshold criterion was set to 75%. The PBF was estimated as the average of the 10 last stimulus values, which oscillated around the threshold with standard deviation below 0.01 D. The results were analyzed in terms of PBF (in Diopters). It would be expected that the PBF increases when adapting to blur and decreases when adapting to sharper conditions. Figure 5.2 describes the experimental paradigm and adapting conditions.

The PBF shift was calculated as the difference in the PBF of the adapting image from the PBF after adaptation to a sharp image, equating a 0 D adaptation to a 0 D PBF thereby providing a common reference for all subjects and conditions. The PBF shift was then averaged across subjects. The trapezoidal rule was used to integrate the area under the PBF shift curve up to 1 D defocus in the adapting image for each adaptation condition (PD, 25S/75D, 50S/50D and 75S/25D). The change in area under the PBF shift curve corresponded the overall adaptation and was correlated with the proportion of defocus present in the adapting image series (1 for PD, 0.75 for 25S/75D, 0.5 for 50S/50D and 0.25 for 75S/25D).

5.2.5 Experiment 2: Perceptual Score measurement

Perceptual scoring experiment allowed testing perception of SV images (50% Sharp image and 50% Defocused image), that had non-monotonous optical quality, and how this is altered by adaptation. A control experiment using PD images was performed. Series of images with different magnitudes of defoci were presented in a random sequence to the subjects to assess their perceived image quality. The subject's task was to grade the quality of each test image in a 6-point scale, from very blurred (score of 0) to very sharp (score of 5). This procedure was repeated 5 times and the average Perceptual Score was obtained to quantify the perceived image quality for each image.

In the control experiment, a series of 18 PD test images (with defocus ranging from 0 to 1.2 D) were presented, and the scoring performed for 6 adapting conditions (sharp image, and 5 PD images with defocus ranging from 0.25 to 1.2 D) in addition to gray adaptation. To evaluate perceived image quality of SV images, subjects scored a series of 19 50S/50D SV test images (with magnitudes of defocus ranging from 0 to 3 D), following adaptation to 7 different conditions (sharp image, and 6 simultaneous vision images with 0.25 to 2.5 D. Figure 5.3 describes the experimental paradigm and adapting conditions. Smoothing cubic splines were used to fit the Perceptual Score responses. A smoothing parameter of 0.995 provided a good compromise between oscillation reduction (among contiguous points) and fidelity to the original raw curves. The goodness of the fitting was calculated as the mean difference (in Perceptual Score units) of the experimental data and the spline curves.

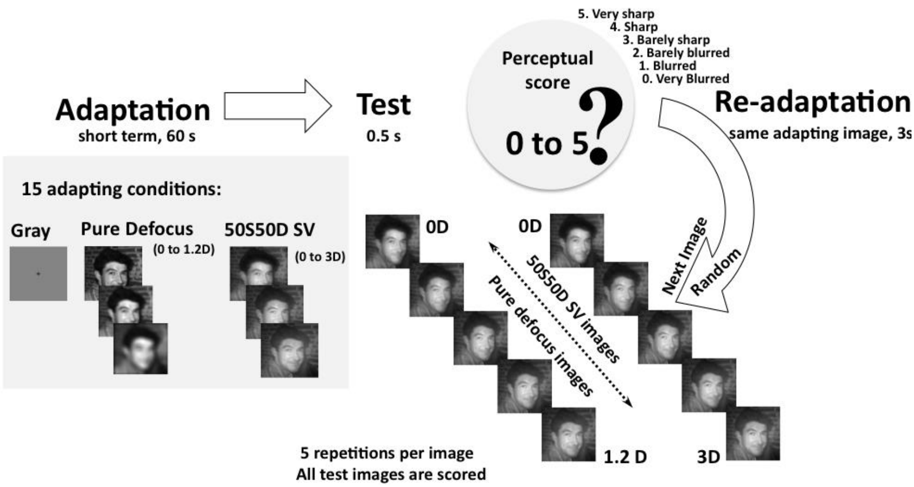

Figure 5.3: Perceptual Score experiment. Each test image (18 Pure Defocus and 19 50S/50B Simultaneous Vision) was presented in random sequence and were scored by subjects. Perceptual score was also measured after adaptation to 6 Pure Defocus (Sharp, 0.25 0.4, 0.6, 1 and 1.2 D) and 7 simultaneous vision (Sharp, 0.25, 0.5, 1, 1.5, 2 and 2.5 D) images.

For both PD and SV adaptations, the mean Perceptual Score, the Maximum Score Shift and the relative mean Perceptual Score was calculated. For each adapting image, the Mean perceptual score was calculated as the average score for the test images from 0 to 1.2 D. Perceptual Score shift is the difference in Perceptual Score for each adapting condition from sharp adaptation condition. The maximum value of each difference curve (maximum Perceptual Score shift) and the defocus in the test image that produced the largest shift under certain adapting condition were evaluated. Relative mean Perceptual Score was calculated as the ratio of the mean Perceptual Score of the adapting image to the mean Perceptual Score of the sharp image.

5.2.6 Image quality metrics

To understand what property of the image drives the perception and adaptation, image quality metrics were calculated. The RMS contrast for each test and adapting images used in Perceived Best Focus and Perceptual Score experiments were calculated as the standard deviation of the ratio of total luminance and mean luminance in the image, a method previously described by Peli (1990). Computations were performed using custom routines programmed in Matlab (Mathworks Inc).

Also, for the same images the Multi-Scale Structural Similarity Index-MSSSIM was calculated. This image quality metric described by Wang et al., (2004) considers changes in the structural, luminance and contrast components, for multiple scales. In the current study, the sharp image was considered as the reference image and the similarity of the defocused image is calculated from this reference. A Gaussian window of 11 with a standard deviation of 0.5 was used to mimic our experimental perceptual responses. Since the images were the same and differed only in the amount of blur, it can be assumed that the MSSSIM is indirectly related to the contrast degradation, at different scales. Higher values of MSSSIM indicate greater degradation of images. The quality metrics were obtained using ImageJ software (Wang et al., 2004).

5.3 Results

5.3.1 Changes in Perceived Best Focus with adaptation

Figure 5.5 (A-D, for each of the four subjects) shows the PBF as a function of the magnitude of defocus (expressed in diopters, D) in the adapting image. For PD images this corresponds to the amount of defocus, for SV it is equivalent to the power of addition for near vision in a bifocal correction in SV images. Adaptation to PD images produced the highest shift in the PBF. Adaptation to SV images also produced shifts in the PBF, which varied with the magnitude of defocus and with the proportion of defocus in the adapting image. For example, adapting to 75S/25D simultaneous images (i.e. a combination of 75% sharp image and 25% defocused image) produced little shift of the PBF, whereas adapting to 25S/75D images (25% sharp image and 75% defocused image) produced a shift approaching to that produced by PD images (0% sharp and 100% defocused image). Results are highly consistent across subjects, with slight variations in the magnitude of PBF shifts.

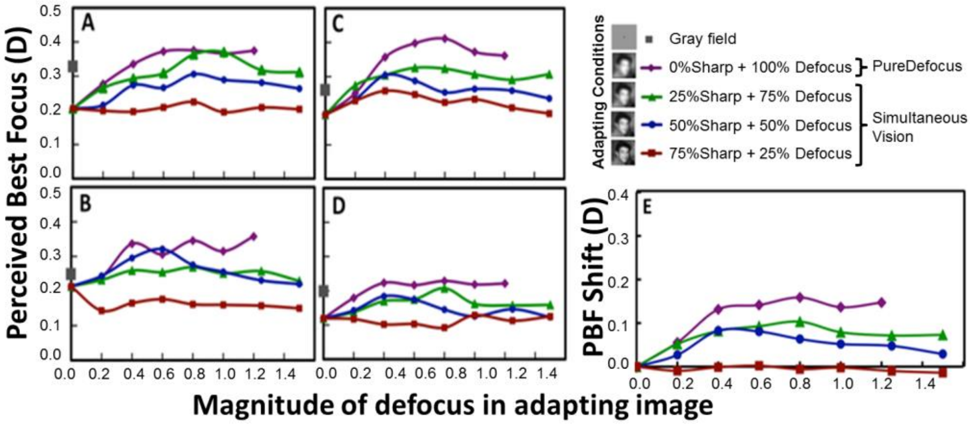

Figure 5.5: Shift in Perceived Best Focus after adaptation to Pure Defocus and Simultaneous Vision images. (A) – (D) show PBF for individual subjects for the different adapting conditions. (E) PBF shifts (differences with respect to the PBF after adaptation to a sharp image)

The PBF after adaptation to a gray field varied across subjects (shown as gray squares in figure 5.5). In addition, the PBF was not equal to zero after adaptation to a sharp (0 D, fully corrected) image, although it was generally lower than the PBF after gray field adaptation. Figure 5.5E shows the PBF shifts (difference in the PBF after blur image adaptation and the PBF after adaptation to a sharp image, expressed in diopters in PD images), averaged across subjects. The sharp image was used as a common reference to all subjects. For PD adapting images, PBF shift increased up to 0.18 for adaptation until 0.4 D, and then saturated. For SV adapting images the PBF shift increased up to 0.08 D with the magnitude of defocus in the adapting images reaching a maximum of 0.4 D for 50S/50D adaptation and up to 0.12 for adaptation until 0.8 D for 25S/75D, and then decreased significantly ($p<0.01$) for higher defocus values. The area under each average PBF shift curve was used to evaluate the amount neural adaptation for each adapting condition, larger is the area, greater will be the effect of adaptation. There was a highly significant correlation ($r=0.99$, $p<0.001$) between the area under the PBF shift curve and the proportion of defocus component in the adapting images (e.g.: 1 for PD and 0.50 for 50S/50D).

5.3.2 Perceptual Score and its shift with adaptation

Figure 5.6 shows the Perceptual Score of the images (cubic splines to the experimental data) as a function of the magnitude of defocus in the test images for PD images (A) or in the defocused component of SV images (B). Data are averaged across subjects for each adapting condition. The mean deviation between experimental measurements and fitted curves was 0.017 Perceptual Score. This deviation is much smaller than the intra/inter-subject variability (SD of 0.4 in the score). The superimposed crosses indicate the defocus values for which each curve deviates most from the sharp adaptation condition (red curve), i.e. the defocus for which neural adaptation produces maximum after-effects.

For PD, maximum shift was around 0.25 D of defocus (Fig. 5.6A). However, for SV, they are scattered across the different defocus component values (Fig. 5.6B). For PD images, increasing the magnitude of defocus in the test image progressively decreased the Perceptual Score. As shown in figure 5.5E, there was a very consistent shift of the curves towards higher scores following adaptation indicating that brief exposures to defocused images increase the perceived quality of defocused images.

For example, the same 0.4 D defocused image was scored on average close to 1 (blurred) after adaptation to a 0.25 D defocused stimulus, and close to 2.5 (less blurred), after adaptation to a 1 D defocused stimulus.

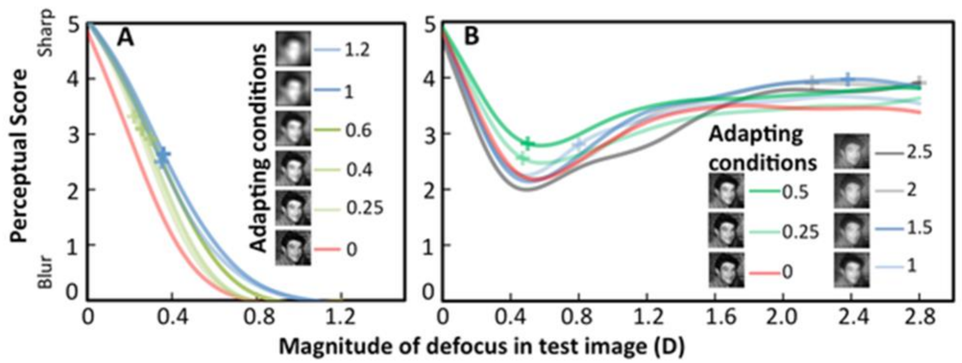

Figure 5.6: Perceptual Score and its change with adaptation to (A) Pure Defocus and (B) Simultaneous Vision 50S/50D image. The crosses indicate the images producing maximum after-effects. 0.5 D adapting image (red line) produces maximum blur adaptation

Unlike with PD images, scoring of the SV 50S/50D test images (Fig. 5.6B) did not decrease progressively with the magnitude of defocus (near addition). There was a progressive decrease in perceived quality for simultaneous images for near additions from 0 to 0.4-0.5 D and the perceived quality remained sharp (score >3) for higher amounts of addition (> 1.5 D) in the image. Lower additions in the simultaneous corrections tend to introduce small phase shifts in the blurred image which further degrades the perceptual image quality, while with higher additions the image become gray. Though, this compared to a sharp image has a poorer optical quality, the uniform grayness tends to diminish the impact on perceptual the image degradation.

5.3.3 Effect of adaptation on Mean Perceptual Score

The mean Perceptual Score was obtained for each adapting condition, by averaging the Perceptual Score of all test images with defocus up to 1.2 D. As shown in figure 5.7A, for PD (red solid circles), the mean Perceptual Score increased significantly and linearly with defocus in the adapting image (slope 0.57, r=0.99, p=0.001) until it reaches saturation at 1.2 D. The mean Perceptual Scores for SV images were higher than those for PD, but showed a similar trend. An initial linear increase occurred for lower amounts of defocus (small red open circles, slope=0.87, r=0.97, p=0.13), followed by a decrease for higher amounts of defocus (large red solid circles, slope=-0.3, r=0.94, p=0.02). These results are in good agreement with the PBF shift results, showing that as the adapting defocus increases, the test image with higher blur appears more focused.

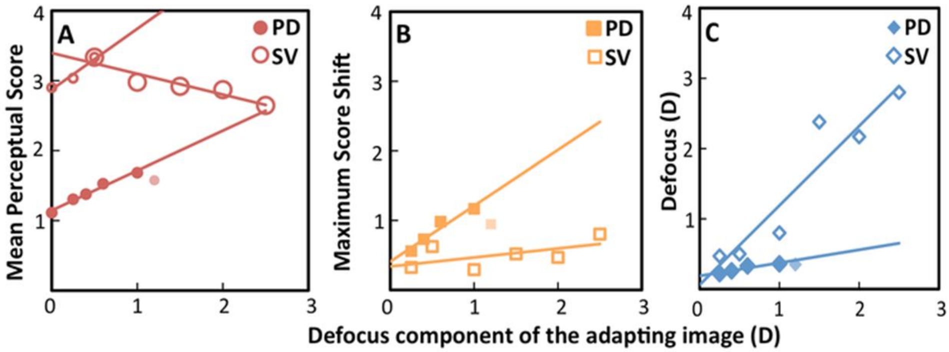

Figure 5.7: Effect of adaptation on the Perceptual Score. X-axis corresponds to the magnitude of defocus in the adapting images (A) Mean Perceptual Score: Pure Defocus shows a linear increase (slope 0.57, r=0.99, p<0.001); Simultaneous Vision shows an initial linear increase (small red open circles, slope=0.87, r=0.97, p=0.13) up to 0.5 D (double circle) and decrease for further defocus (large red open circles, slope=-0.3, r=0.94, p<0.02). (B) Maximum shifts in the Perceptual Score following adaptation to sharp for Pure Defocus (slope=0.80, r=0.97, p<0.03) and for Simultaneous Vision (slope= 0.13, r=0.59, p=0.2). (C) Defocus in test images with largest shift in Perceptual Score for Pure Defocus (slope=0.19, r=0.945, p<0.06) and for Simultaneous Vision (slope=1.13, r=0.94, p<0.005).

5.3.4 Effect of adaptation on the Maximum Score Shift

Figure 5.7B shows the maximum difference in Perceptual score for each adapting image from the sharp adaptation (Maximum Score Shift) which increase linearly with defocus in the adapting image (slope=0.80, r=0.97, p=0.03 for PD; slope=0.13, r=0.59, p=0.2 for SV). Maximum score shifts were all positive, indicating a recalibration, as blurred images are perceived as sharper after adaptation. If the blur component of the SV images were suppressed, the Maximum score shift would have been all negative, contrary to our results, indicating only sharp adaptation.

5.3.5 Defocus values producing Maximum Score Shift

Figure 5.7C represents the defocus values in the test image that produce the maximum shifts in the Perceptual Score under a certain level of adaptation. For both PD (blue solid diamonds) and SV (blue open diamonds) the test image producing maximum score shift increases linearly with increase in defocus in the adapting image (slope=0.19, r=0.945, p=0.06 for PD; slope=1.13, r=0.94, p<0.005 for SV), indicating a complete adaptation of an addition to its specific working distance.

5.3.6 Perceived Best Focus shift and Image quality

The PBF shift with adaptation correlated significantly with the overall image degradation of the PD adapting image represented as RMS contrast. PBF shift correlated strongly and significantly with RMS contrast and MSSSIM for PD adapting images (r_{rms}=-0.89, r_{MSSSIM}=-0.96, p<0.000 respectively). The coefficients of correlation between PBF shift and RMS contrast for 25S/75D, 50S/50D and 75S/25D adapting images were r=-0.80 (p<0.0001), r=-0.23 (p=0.12) and r=0.53 (p=0.002) respectively. Likewise, the correlation coefficients between PBF shift and MSSSIM of adapting images were r=-0.89 (p<0.0001), r=-0.57 (p=0.0007) and r=0.41 (p=0.02) for 25S/75D, 50S/50D and 75S/25D adapting images respectively.

Further analysis revealed that the process of SV adaptation is partly similar to adaptation to PD. Figure 5.8A shows that the MSSSIM of the image chosen as PBF was highly and significantly correlated with the MSSSIM of the adapting image regardless whether those were PD or SV images (r=0.95, p<0.0001). A 50% decrease in MSSSIM of PD adapting images produced an increase in PBF 150%. In other words reduction of image quality by half resulted in increase in PBF by 0.15 D for PD adapting images. Likewise, a reduction in MSSSIM from 1 to 0.9 in SV images resulted in the maximum increase in PBF of 0.1D.

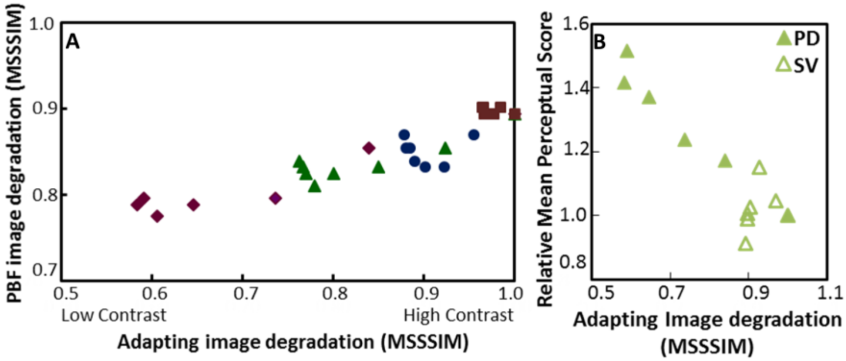

Figure 5.8: Image quality metrics (A) Change in PBF (MSSSIM) with change in MSSSIM of adapting images. (B) Relative mean Perceptual Score (mean Perceptual Score of adapting image/ mean Perceptual Score of sharp image) as a function of MSSSIM of Pure Defocus and Simultaneous Vision adapting images. There was an initial increase in relative mean Perceptual Score with decrease in the MSSSIM of adapting images.

5.3.6 Perceptual score and Image quality

The Perceptual Score of the images correlated strongly with image quality degradation when judging PD test images, for both the image quality metrics evaluated (RMS contrast: $r=0.94$, $p<0.001$; MSSSIM: $r=0.99$, $p<0.0001$). However, the Perceptual Scores for SV 50S/50D test images correlated significantly only with the MSSSIM ($r=0.67$, $p=0.001$) but not with RMS contrast ($r=0.21$; $p=0.28$), suggesting that local changes in contrast are better predictors of SV perception and adaptation than global contrast. Figure 5.8B shows the Mean Perceptual Score of the adapting image (relative to the Mean Perceptual Score of the sharp image) as a function of the MSSSIM of adapting images. For PD adapting images (solid green triangles), the relative mean Perceptual Score increased with a decrease in the image quality of adapting image ($r=-0.97$, $p<0.0001$). For SV adapting images (open green triangles), the relative mean Perceptual Score increased up to a point corresponding to the highest image degradations ($r=-0.99$, $p<0.0001$) and decreased for lower values of MSSSIM ($r=0.92$, $p<0.0001$).

5.4 Discussion

Multifocal optical corrections are becoming popular solutions for compensation of presbyopia, aiming at providing the patient with a range of focus for functional vision at near without compromising far vision (Cillino et al., 2008, Cochener et al., 2011). One of the hypotheses in adapting to these simultaneous images is that the brain suppresses the blurred component of the image, making the image look sharper to the subject than the actual physical degradation produced by superimposition of the images (Charman, 2014b). However, whether this really happens had never been tested.

5.5.1 Inter-subject differences in perception

In our study, the aberrations of the subjects were corrected to a large extent (86% on average) with adaptive optics and the subjects viewed the adapting and test images under similar viewing conditions. PBF after adaptation to a gray field, matching the natural viewing conditions, differed across subjects as reported in previous studies (Sawides et al., 2011a, Sawides et al., 2011b). This inter-subject difference in perceptual norm (internal code of blur) is likely to be driven by the amount of blur produced by the ocular aberrations (Sawides et al., 2011b). However, these individual differences were substantially reduced when subjects were instead adapted to a common stimulus in the experiment, with the shifts in the PBF and in the Perceptual Scores of the subjects following a similar trend upon adaptation (Fig. 5.5), which indicates that the recalibration of the internal code for blur follows similar patterns across individuals. In addition we found that the ability of the visual system to adapt blur was correlated with the magnitude of blur present in the subject's retina (RMS).

5.4.2 Simultaneous Vision vs Pure Defocus

Adaptation to Simultaneous Vision (SV) images produced a shift in the PBF similar to that produced by purely defocused images, although of lower magnitude, mostly influenced by the proportion and magnitude of the defocus present in the adapting image. For instance, adapting to a simultaneous image with 75% of defocus (and only 25% of sharp image content) produced somewhat similar after-effects to those produced by Pure Defocus (PD). The PBF and mean Perceptual score results were concurrent. There was a linear relation between the PBF shift (and Perceptual Score shift) with the magnitude of defocus in the adapting images, following adaptation to PD images. This effect of adaptation to PD was consistent across the two experiments (Fig. 5.5E, 5.6A), as well as with previous studies (Mon-Williams et al., 1998, Webster et al., 2002, Sawides et al., 2011b). The maximum PBF shift when adapting to SV images occurred for a magnitude of defocus in the defocus component of around 0.5 D, which was also, interestingly the SV image that was scored as more blurred in the Perceptual Score experiment, despite the test images being different in the experiments. The higher slope of the PD curve compared to the SV curve in the maximum score shift is indicative of the higher adapting effect of PD images.

5.4.3 Theories of adaptation to Simultaneous Vision

Traditionally, adaptation to SV images has been interpreted as a suppression of the blurred component of the SV image (Charman, 2014b). It would be expected that in case of suppression of blur, sharp adaptation would dominate, and therefore the PBF shift curves would remain mostly at the level of the PBF produced by sharp adaptation. Also, the maximum shift score (Fig. 5.7B) would have been negative. In case of dominance of the blur component alone, the PBF shift curves will be closer to those of Pure Defocus. PBF and mean Perceptual scores initially increased and then saturated, at 1.2 D for PD and at 0.5 D for SV. Also, our results show that the shift in PBF is highly correlated with the proportion of blur (Fig. 5.5E) and therefore thus does not support the suppression theory. It is possible that the adaptation effects are driven by partial suppression of either of the components or by contrast adaptation.

Changes in the contrast of the natural scenes have been suggested to strongly modulate the state of adaptation, more than differences in the amplitude spectrum frequency of the images (Webster and Miyahara, 1997). In fact, a proposed function of contrast adaptation is the adjustment of sensitivity to match the prevailing contrast gamut of the image (Webster and Miyahara, 1997). On the other hand, previous evidence shows that both perceptual judgments of focus and adaptation are controlled by the local blur of the image features, rather than by the global amplitude spectra of the images (Webster et al., 2002, Webster, 2011). Our perceptual results correlate better with MSSSIM metric than RMS contrast, supporting this theory. We have shown that the after-effects found in PBF and in the Perceptual Score of image quality correlate significantly with the MSSSIM. Peli and Lang (2001) showed that the high spatial frequency content is retained in a bifocal blur affecting the overall contrast. Thus a simultaneous vision defocus will have more global contrast compared to a monofocal blur of the same magnitude. In fact, our results (Fig. 5.8) show that both for PD and SV images, the adaptation correlates with image quality degradation, indicating similar underlying mechanisms for blur adaptation in both PD and SV images, driven by the effect of blur on local contrast changes in the images.

5.4.4 Timescales of adaptation to Simultaneous Vision

Our measurements investigate short-term adaptation (60 s) effects to different types of simultaneous blur. However, it is likely that long-term effects are induced by extending the duration of the adaptation period are similar to short term adaptation, as shown in various domains, such as color adaptation (Webster et al., 2006), adaptation to reduced contrast (Kwon et al., 2009), and adaptation to astigmatic lenses (Yehezkel et al., 2010). Whether short-term and long-term adaptations arise from a unique mechanism, or alternatively, different control mechanisms operate at different timescales, as shown for contrast adaptation (Bao and Engel, 2012), remains to be seen. However, the observed after-effects following the brief adaptation periods to SV images could persist long-term upon sustained correction, similar to the shift towards isotropy reported by Vinas et al. (2012) when subjects adapt to their astigmatic correction. Also, adjustments in the gain of the contrast response has been shown (Kwon et al., 2009) following adaptation to reduced contrast by contrast-discrimination measurements and functional Magnetic Resonance Imaging Blood-oxygen-level dependent (fmri BOLD) responses in the visual cortex (V1 and V2). It is likely that the compensatory perceptual and neural changes produced by a prolonged reduction in retinal image contrast produced in SV images, arise from a response gain mechanism to achieve a contrast gain.

5.4.5 Visual performance under Simultaneous Vision

Besides the well-known role of adaptation in perceptual constancy, it is also interesting to elucidate whether adaptation manifests in improvement of visual performance. A clinical study reported the effect of prior training on visual performance in patients implanted with different types of multifocal intraocular lenses (Kaymak et al., 2008). They reported that visual training to multifocality resulted in significantly better visual performance. Although those effects are likely related to perceptual learning, i.e. the subject acquiring cues allowing him/her a better response, a recalibration of the internal code for blur as demonstrated by our direct experiments of adaptation (Fig. 5.5A-D and 5.7A-B), could have played a role in the improvement.

The perceived image quality was worst for a range of near addition around 0.5 D and improved for higher additions. A similar trend in change of decimal visual acuity with SV was noted in a recent study, with worst acuity at around 2 D addition (de Gracia et al., 2013). While the actual addition range compromising visual quality/perception may vary with the spatial frequency content of the image and the actual task, this observation reinforces that not all near additions in a bifocal correction have equal impact on vision. Very interestingly, we found in this study that after adaptation to simultaneous images with selected near additions, subjects experienced an improvement in perceived image quality of SV images, for all adapting conditions. The adaptation is actually highest for any specific SV correction (defocus component) producing at that specific distance, indicating a full recalibration of the internal code for blur for the correction. Whether this increase in the perceived sharpness after adaptation is also followed by an improvement in visual performance remains to be explored.

5.4.5 Clinical Implications for Simultaneous Vision corrections

A presbyopic patient wearing a SV correction and viewing at near will experience much lower blur than that introduced by a single vision lens correcting only for far. In fact, for most subjects and conditions (near additions) images are perceived subjectively less degraded than images degraded by 0.25 D of pure defocus. In addition, we have shown that subjects are able to adapt to the blur produced by a SV correction almost instantly, and it is probable that this adaptation happens when switching between far and near vision. The close-to-1 slope for SV seen in figure 5.7C and the very high statistical significance of the increase indicate that the visual system recalibrates almost fully for each adapting SV image. In a clinical analogue, this will imply that a patient wearing a bifocal correction, fully recalibrates the internal code for blur to that specific correction (regardless of the near addition), thereby achieving maximum perceptual improvement for their conventional working distances. We have also shown that adaptation is selective to each addition and distance. It is also to be noted that different aberrations interact differently with the bifocal correction and this must be taken into account when providing simultaneous vision correction to presbyopic patients. Visual performance under natural viewing conditions could be tested non-invasively using the simultaneous vision system (de Gracia et al., 2013) introducing different pupil patterns in the bifocal correction or by actually fitting the bifocal contact lenses.

While we have demonstrated that subjects can indeed adapt to pure simultaneous vision as introduced by diffractive multifocal designs, a number of segmented refractive multifocal corrections, that provide simultaneous vision, are available. The performance of these corrections are likely to be influenced by the interaction of the optical design with the ocular optics. It would be interesting to study differences in the perceptual performance for different segmented bifocal designs, ideally in subjects without compensation of aberrations using adaptive optics.

5.5 Conclusion

Our results provide the first evidence of neural adaptation to bifocal images. A shift in the Perceived Best Focus, corresponding to the magnitude and proportion of defocus, occurs after adaptation to simulated Pure Defocus and Simultaneous Vision images. For simultaneous vision images, the perceptual quality varied non-monotonously. The largest perceptual degradation and adaptation was noted for a near addition of 0.5 D. The Perceived Best Focus and Perceptual Scores shifts correlate significantly with the image quality degradation of the adapting images. In addition, spatial calibration for simultaneous vision is found similar to that of pure defocus. These adaptation effects are important for understanding how vision changes with a bifocal correction, and may help to define strategies for multifocal lens design and the presbyopic patient management.

Chapter SIX

Subjective preferences to segmented bifocal patterns

Refractive multifocal corrections can be broadly classified as angular or radial segmented designs. In a diffraction limited system, any lens with equal energy between far and near will perform similarly. However, human eye is far from being diffraction limited and the visual system is known to show strong orientation preferences. In this chapter we measured subjective preferences to 14 designs of bifocal patterns that had equal energy distribution between far and near distances.

This chapter is based on the paper by Dorronsoro et al., titled "Perceived image quality with simulated segmented bifocal corrections" *(Submitted)*.

The coauthors of this study are Carlos Dorronsoro, Pablo de Gracia and Susana Marcos. The author of this thesis evolved the program for measurement, performed the measurements on human eyes, and analyzed the data in collaboration with the co-authors. A part of these results are presented in another thesis by Pablo de Gracia. This work was presented at the Association for Research in Vision and Ophthalmology (ARVO) annual meeting (May 2014) as a poster.

6.1 Introduction

Simultaneous vision corrections are increasingly used to treat presbyopia, the age-related loss of crystalline lens (Glasser and Campbell, 1998, Charman, 2014). These corrections aim at restoring the capability to see near and far objects by providing the eye with two or more superimposed foci, for near and far vision (Charman, 2014). Simultaneous vision is normally provided in the form of contact lenses, intraocular lenses or presbyopic LASIK (Alio and Pikkel, 2014, Charman, 2014). In some cases, extended depth of focus is achieved by increasing aberrations (Zlotnik et al., 2009, Benard et al., 2011). Multiple foci may be achieved through diffractive optics, where the design parameters primarily control the power of the lens (to correct for far refractive error), the dioptric distance between the far and near foci (near addition power), and the energy balance between foci (Glasser, 2008, Alio and Pikkel, 2014, Charman, 2014). Other lenses (intraocular and contact lenses) follow a refractive design, where some parts of the lenses are dedicated for far and others are dedicated for near, in some cases with a blending zone between both.

Despite the widespread use of simultaneous vision corrections, there is a lack of systematic studies investigating visual perception with those corrections. Most studies in the literature are limited to clinical studies investigating visual function with a certain lens, or a clinical comparison of visual performance in groups of patients implanted with different multifocal lenses (Bellucci, 2005, Cillino et al., 2008, Cochener et al., 2011). However, simultaneous vision is a radically new visual experience for the patient, and it is very likely that a particular solution can be optimized through a better understanding of the optical and neural aspects involved in simultaneous vision corrections.

We have recently developed a simultaneous vision simulator capable of providing the patient with a simultaneous vision experience (Dorronsoro and Marcos, 2009, de Gracia et al., 2013b). The system consists of two optical channels which project on the patient's retina, superimposed images of the same visual scene, one with far spherical correction and the other with the desired near addition. The system allows for evaluating directly the specific aspects of the bifocal correction, in the presence of the natural aberrations of the eye, by eliminating extrinsic factors such as such as flexure or conformity in contact lenses or tilt and decentration in intraocular lenses. The effect of near addition on visual acuity (high contrast and low contrast) was studied using the simultaneous vision simulator, and found that moderate additions (~2 D) produced the largest compromise of visual acuity (de Gracia et al., 2011). In a subsequent study, using a custom-developed adaptive optics simulator, we explored the effects of simultaneous vision with different near additions and near/far energy balances on visual perception, and the capability of the visual system to adapt to these corrections, indicating that neural aspects also play a role in vision with bifocal corrections (Radhakrishnan et al., 2014).

An unexplored aspect in refractive simultaneous vision lenses is the effect of far/near pupillary distribution on vision. In a recent computational study on diffraction-limited eyes we found that there are, in fact, differences in the optical performance and depth-of-focus produced by different multifocal segmented lenses with different zonal distributions, with angular patterns generally providing better performance (de Gracia et al., 2013a). The presence of the natural high order aberrations of the eye is likely to enhance these differences in performance across multifocal patterns and produce intersubject variability. While optical computer simulations neglect neural contributions, experimental visual simulations of bifocal designs on subjects incorporate both optical and neural factors, isolated from the sources of variability associated to particular implementations.

In this study, we simulated 14 different refractive bifocal designs with different far/near pupillary distributions using the simultaneous vision simulator with a transmissive spatial light modulator, and studied in subjects, perceptual preferences to these patterns. The patterns tested in this study include designs reminiscent of lenses existing in the market (i.e. bi-segmented angular patterns such as that found in the M-Plus IOL, Oculentis Inc (Alio et al., 2012b, Bonaque-Gonzalez et al., 2015) tested in different orientations, or concentric bifocal patterns such as those found in the ReZoom, AMO (Munoz et al., 2012). A psychophysical paradigm was implemented to answer the following questions: Do some bifocal patterns provide better perceived quality than others? If so, is performance similar across patients, or can bifocal vision be optimized by the choice of the best pattern for each individual? Psychophysical tests were performed on normal cyclopleged patients using a modified custom simultaneous vision instrument. We also assessed the influence of the optical aberrations on perceptual preference.

6.2 Methods

6.2.1 Subjects

Five normal subjects, aged between 29 and 42 years, with spherical refractive error ranging from +0.75 D to -5.50 D, participated in the study. None of the subjects had astigmatism > 1 D. All subjects had prior experience in participating in psychophysical experiments. The measurements were performed in one eye, with dilated pupils and paralyzed accommodation, induced with instillation of tropicamide 1%. All protocols met the tenets of the Declaration of Helsinki and had been approved by the ethics committee of CSIC. All subjects signed an informed consent.

6.2.2 Setup: Simultaneous vision instrument

The psychophysical measurements were performed with a modified version of the simultaneous vision simulator, described elsewhere (Dorronsoro and Marcos, 2009, de Gracia et al., 2013b). The instrument allows the simulation of ideal bifocal corrections, by projecting simultaneous bifocal images on the subject's retina. Figure 6.1 shows a schematic diagram of the system. The instrument consists of two visual channels capable of achieving different vergences by means of respective Badal optometers, with one channel focused for far vision, and the other for near vision, with a given addition. A CMOS camera (Thorlabs Inc, Germany) allows monitoring subject's centration, and a Pico-Projector (DLP, Texas Instruments) projects visual stimuli for performing psychophysical experiments with the instrument.

Previous versions of the instrument simulated pure simultaneous vision. For this study, the instrument was modified in order to simulate different pupil sampling patterns for different refractive powers at far and near, applied through different zones of the pupil. The system incorporates a transmission spatial light modulator (SLM) in a plane optically conjugate with the subject's pupil, a linear polarizer (LP) and a polarizing cube beam splitter (CBS). The SLM (LC2002 Holoeye, Germany) is based on a liquid crystal micro-display (1024 x 768 pixels in 36.9 x 27.6 mm), and is able to change the polarization angle of a linearly polarized incident light beam. In combination with the LP, the SLM is configured to produce a pupillary pattern such that light going through different areas will show perpendicular polarizations, according to an input binary image. The CBS, after the SLM, selectively reflects or transmits the incident light, depending on its polarization angle, and therefore directs the beam passing through different areas of the pupil through the far or near visual channels of the simultaneous vision instrument.

Visual stimuli are projected using a DLP pico projector onto a back-illuminated diffusing screen (Novix technologies, Australia). The projected stimulus is a gray-scale image of a face, with a maximum luminance of 32 cd/m^2. The screen target is focused on a retinal image plane inside the system, subtending a 0.75-deg retinal angle.

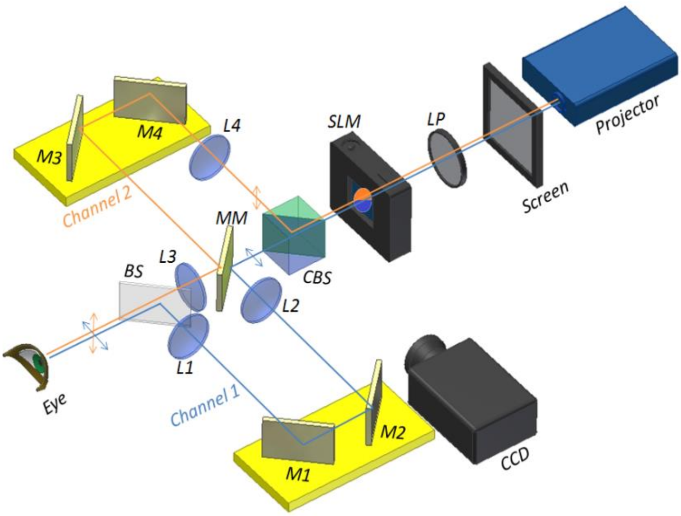

Figure 6.1: Simultaneous vision simulator with two Badal Channels (Channel 1: lenses L1 and L2 and mirrors M1 and M2. Channel 2: L3, L4, M3, M4) and a transmission liquid crystal spatial light modulator (SLM) optically conjugated with the pupil of the subject's eye. Both channels are split using a polarizing cube beam splitter (CBS) in combination with a linear polarizer (LP) and the SLM, and recombined using a double mirror (MM), and a Beam Splitter (BS).

Calibrations revealed that each channel transmits 44% of the light coming from the stimulus, when the maximum transmittance was programmed in the SLM for either channels. The light efficiency of each channel was equivalent, with less than 2% differences in the measured luminance of each channel, measured independently. The measured residual transmission was 1.36%, through the channels, when zero transmittance was programmed in the SLM, in good agreement with the SLM specifications (an intensity ratio of 1000:1 at 633 nm) and the nominal efficiency of the CBS (1000:1 for transmission and 100:1 for reflection). The SLM did not introduce significant chromatic shifts in the images projected through each channel.

6.2.3 Stimuli: Bifocal pupillary patterns

Fourteen different Bifocal Pupillary Patterns (BPP) were simulated in this study. A program written in Matlab controlled automatically the presentation of black-and-white images onto the SLM. Figure 6.2A shows the patterns programmed in the system, with regions for far vision represented in blue and regions of near vision represented in orange. The far and near vision pupillary zones are arranged in different angular (1-4; 9-10), radial (5-8; 11-12) or hybrid angular-radial (13-14) distributions, from 2 up to 8 zones. In all patterns, the energy distribution was 50/50 between far and near vision channels. The vergence of the far vision channel was set to correct for the subject's refractive error (simulating vision at far distance), while the vergence of the near vision channel was set to induce an additional refractive power of +3 D (simulating near distance). An artificial pupil of 6 mm was placed next to the SLM. A linear CCD image sensor (Retiga, QImaging, Canada), placed at the subject's pupil plane, was used to test the relative efficiency, and alignment of the channels (Fig. 6.2B) in this experimental implementation, and also the capability of the system to project the BPPs created in the SLM.

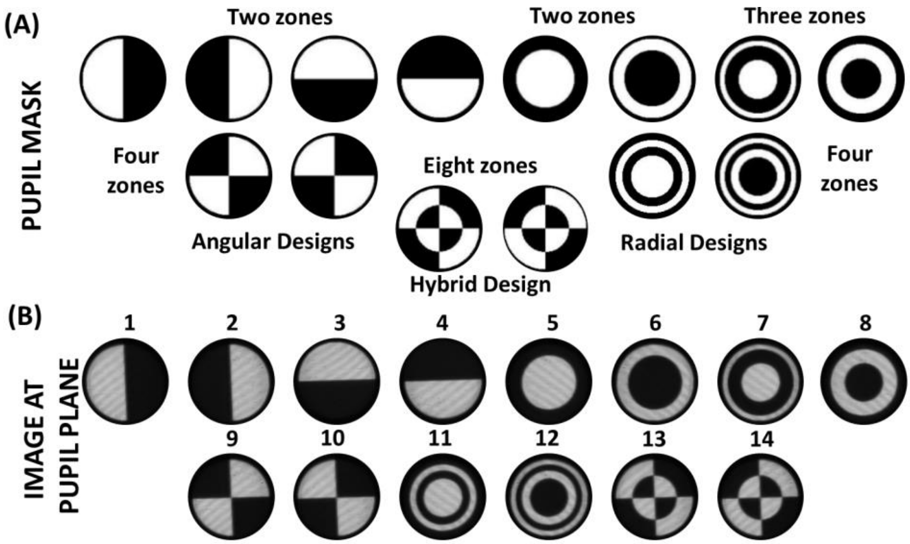

Figure 6.2. (A) Black and white segmented bifocal pupil masks. Black portions indicate area for near vision and white portion indicates area for distance vision. Far and near zones had equal energy. Six angular (4-two zones and 2-four zones), six radial (2-two, three and four zones) and one hybrid (eight zones) were evaluated (B) Image of the pupil mask captured by the CCD camera at pupil plane through far vision channel, blocking the near channel

6.2.4 Pattern preference measurements

The psychophysical experimental paradigm is described in Figure 6.3. Subjects viewed the face image through different BPPs, and their task was to score the quality of the perceived face image over pairs of successive BPPs, in a two alternative forced choice procedure with a weighted choice. The subjects responded whether the first or the second image (shown for 1.5 s each) was best perceived and the certainty of the response (very certain, quite certain, not certain), using a custom keyboard with six buttons. A Matlab function using PsychToolbox (Pelli and Farell, 1995, Brainard, 1997) was developed to synchronize the image presentation at the DLP and the pattern presentation at the SLM and for response acquisition. A total of 315 pairs of images were randomly presented to the subjects, representing all possible combinations of the 14 BPPs, repeated three times.

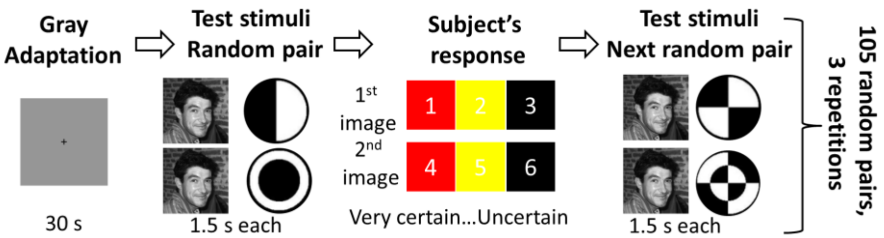

Figure 6.3: Classification image like method for assessing subjective preferences to segmented bifocal patterns

Thus, each segmented bifocal pattern was evaluated 39 times (excluding comparisons with itself) at any given distance. All subjects repeated the experiment in three different conditions representing far, near and intermediate observation distances (i.e. with the far vision channel set to 0 D, -3 D, and -1.5 D, respectively). On an average, the measurements lasted ~4 hours. The subject was given frequent breaks and cycloplegia was ensured by hourly instillation of 1% tropicamide.

6.2.5 Data analysis

Pattern selection & statistical significance

The statistical significance of the perceptual differences across patterns, was explored comparing the number of times that each pattern was selected with the expected values of a Bernoulli cumulative distribution function (Yates and Goodman, 2005). We tested the null hypothesis that if all the patterns were perceptually similar, the image comparisons and the corresponding scores would be driven just by chance (with probability 0.5). Thus a BPP is considered to produce a significant perceptual selection if the cumulative number of positive responses (when compared with other BPPs) represents a probability above 0.95 (indicating significant preference) or below 0.05 (indicating significant rejection). Alternatively, all responses with a probability between 0.05 and 0.95 are not significant, hence the hypothesis cannot be rejected and the BPP is considered neutral to the subject.

For a given subject and observation distance (far, intermediate or near), any BPP is presented 39 times paired with other BPPs. A BPP is significantly preferred if the cumulative score is 24 and rejected if it is less than 14. Pooling responses across subjects, at a specific distance (195 trials per BPP), a BPP is significantly rejected or preferred if the total cumulative response lie outside 86 and 108, respectively. Pooling responses across subjects and across observation distances (585 trials), statistically significant responses are outside 273 and 311.

Differences in perceived quality across subjects

To evaluate the differences and similarities across subjects in their responses, the perceptual strength of responses was considered (Sawides et al., 2013). A perceived quality score of a given BPP was obtained by adding the responses given to the each BPP across trials, assigning perceptual weights associated to subject's certainty of the response (10, 5 and 1 for the positive responses with increasing uncertainty, and likewise -10, -5 and -1 for the negative). The average perceived quality of a given BPP was obtained by averaging the score across subjects and observation distances.

A Multivariate ANOVA (3-way) was performed to test the influence of the factors: subjects, BPPs and observation distances on the mean of the perceptual quality. The analysis was performed for all distances and only far and near distances.

6.2.6 Ocular aberrations measurement

The ocular aberrations of the subjects were measured in order to investigate the potential optical coupling effects between a given BPP and a subject's eye's optics. Subjects' ocular aberrations were measured using a Hartmann-Shack wavefront sensor (HASO32, Imagine Eyes, France) integrated in a custom developed Adaptive Optics system, described in Marcos et al. (2008), while spherical error was corrected with a Badal optometer. The ocular aberrations up to 7th order Zernike polynomials were measured for a 6 mm pupil diameter under pupil dilation with 1%tropicamide.

6.2.7 Optical predictions

We used Strehl Ratio to evaluate the optical quality of the BPP design. The pupil function was calculated by adding the BPP phase map and the subject's wave aberration map, for 6 mm pupils and for different observation distances. For far vision the BPP was simulated with zero phase in the far vision zones and a spherical wave aberration (corresponding to the +3 D addition) in the near vision zones. The Strehl Ratio was calculated as the maximum of the corresponding Point Spread Functions (PSFs) using Fourier Optics (Goodman, 1996). A diffraction limited eye was also simulated, as a reference. The predicted BPP responses from optical computations were correlated with the subjective BPP responses, across subjects and conditions, and for each subject and condition individually.

6.3 Results

6.3.1 Pattern preferences and statistical significance

Figure 6.4 summarizes the pattern preference results and their statistical significance, for each subject and distance; and across subjects/distances. Green circles indicate significant preferences, red circles indicate significant rejections and gray circles indicate non-significant responses.

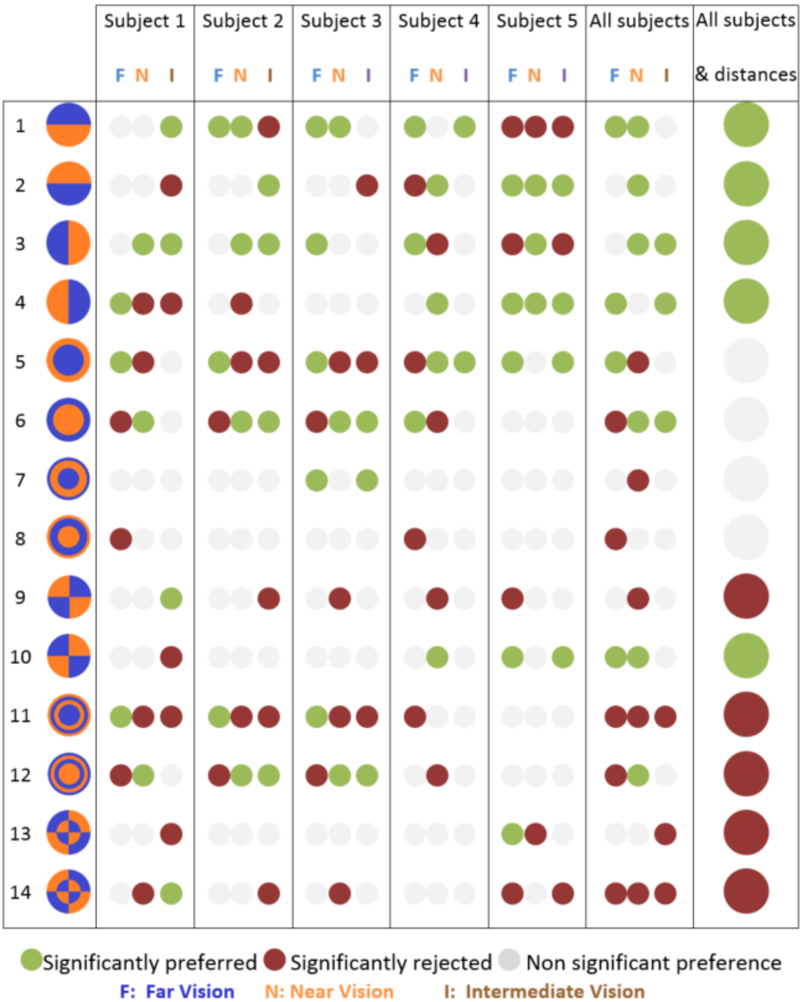

Figure 6.4: Preference maps for all subjects at far, intermediate and near distances. Last column shows pooled preferences across subjects and distances. Red dots indicate significant rejection, green dots indicate significant preference and gray dots indicate non-significant preferences at p<0.5.

As seen in figure 6.4, there was a relatively high number of significant selections (colored circles) of BPPs across subjects and distances. Across the 5 subjects, 3 distances (N=3) and 14 BPPs, 101 out of a total of 210 comparisons (48%) were significant. 25% BPPs were significantly preferred (green circles), and 23% BPPs were significantly rejected (red circles) when compared to all the other patterns under the same conditions. Despite intersubject variability, BPPs providing significant responses tended to be consistent across subjects. In fact, the pooled responses across subjects and across subjects and distances (last two columns in Fig. 6.4) revealed significant positive and negative responses in 10 out of the 14 BPPs.

6.3.2 Comparison of perceived quality across subjects

Figure 6.5 shows the perceived quality score for each of the 14 BPPs, for each subject (A to E) and on an average across subjects (Fig 6.5F), for far (blue), intermediate (brown) and near (orange) distances. Empty and solid columns represent statistically non-significant (gray dots in Fig. 6.4) and statistically significant (colored dots in Fig. 6.4) selections, respectively. The maximum possible perceived quality is 390 (13 comparisons with other patterns, 3 repetitions, scored with 10 perceptual points each). The average perceived quality (absolute value) of the patterns with significant selections was 71±92 (18±24 for patterns with non-significant selections). The strength of the score varied across subjects, ranging from 64±57 for S4 to 120±90 for S5 (averaging across BPPs and distances).

Subject-wise correlation analysis revealed that subjects S1, S2, S3 provided statistically similar perceived quality judgments ($R>0.6$; $p<0.0001$) to most BPPs, and different to those provided by S4 and S5. In fact, the scores of S4 showed a strong negative correlation ($R<-0.4$; $p<0.01$) with subjects S1 and S3. These correlations are likely driven by the responses to radial BBPs #5, #6, #11 and #12, which are strong and almost identical in subjects S1, S2 and S3, and almost opposed to that of S4. The strength of the scores to other radial BPPs (#7 and #8) is small (neutral) or non-significant in all subjects. Also, except for S5 who provided consistent scores at all distances (BPPs #2 and #4 were preferred for all distances and BPP #1 rejected, with high absolute values, >200), the scores for the same BPP at far and near correlated strongly and negatively (r=-0.54, p<0.00001) indicating a reversal of preference between far and near.

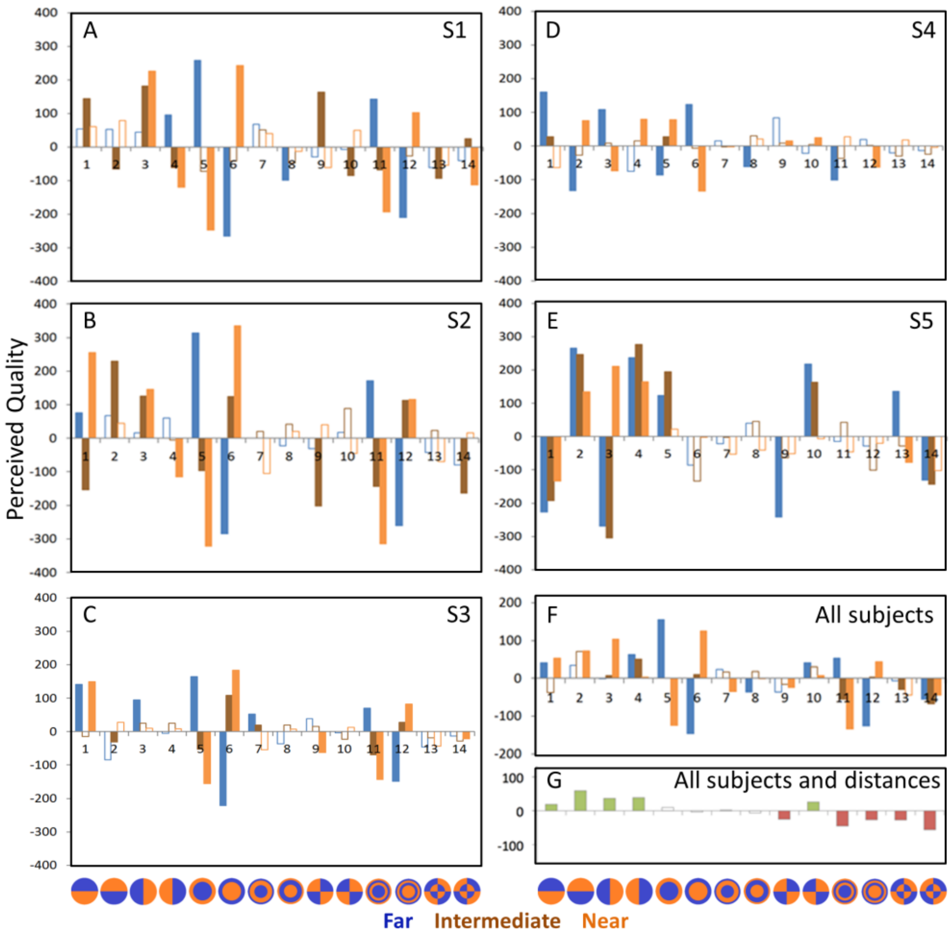

Figure 6.5: Perceived optical quality to BPP for far (blue), intermediate (brown) and near distances (orange). A-E shows data for individual subjects, F shows the average across subjects and G shows average across subjects and distances.

On average across subjects and distances (Figure 6.5G), BPPs #1-4 and #10 were significantly preferred (solid columns, corresponding to the red/green colored dots of the last column of Fig. 6.4), although with small average values of perceived quality, and #9 and #11-14 were significantly rejected.

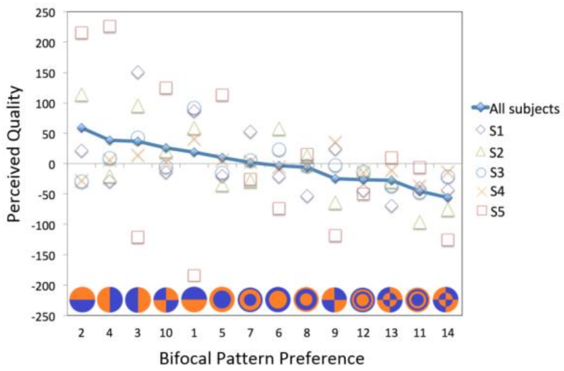

Figure 6.6: Perceived quality on an average across distances for each subject and for on an average across subjects (blue line)

Figure 6.6 shows the perceived quality averaged across distances for each subject, and averaged across distances and subjects (blue line). In this figure, the BPPs (x-axis) have been re-ordered according to the ranking of patterns in the average condition (all subjects, all distances). The scores from individual subjects (symbols) follow similar trends as the average, with most subjects (but not all) preferring or rejecting patterns as predicted by the average. On the other hand, while the best perceptual quality corresponds on average to BPP#2, this was not the best pattern for most subjects (which is BPP #3 for S1, BPP#9 for S3, BPP#1 for S4 and BPP#4 for S5). While the average score was low (mean of absolute values = 32, range +59 to -56), some subjects (S5, mean abs = 85) showed strong preferences (+226) and rejections (-184) and other subjects much weaker preferences (S3; mean abs = 18).

6.3.3 ANOVA

We studied the influence of subject, observation distance and BPP on the perceived quality score, using ANOVA. If all distances were considered, observation distance was, by far, the strongest statistical factor (p=0) on perceived quality. However, if the dataset from intermediate distance was removed from the analysis, the observation distance was not a significant factor (far and near vision are equivalent conditions, on average), and the patient factor was significant (p=0). In both cases (considering intermediate distance or not), BPP design and observation distance had a significant combined effect (p=0.01). Patient and observation distance also had a significant interaction (p=0) in all cases.

6.3.4 Ocular aberrations and optical predictions

Figure 6.7 shows the ocular high order aberration wavefront maps of the five subjects with their respective RMS values. Coma was the predominant aberration in S1, S2, S4 and S5, while trefoil was the predominant aberration in S3.

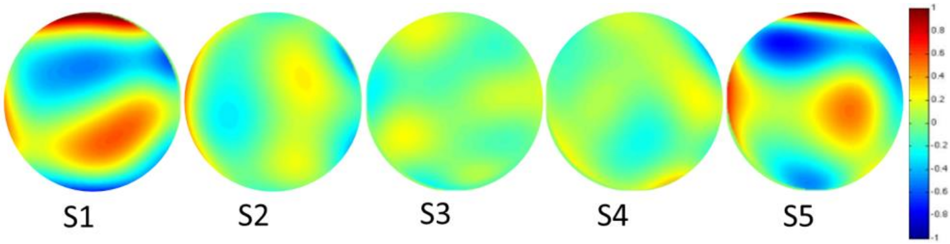

Figure 6.7: Ocular wave aberration maps, and corresponding RMS (in μ), for all subjects (6mm PD).

Simulating diffraction-limited optics (6 mm pupils, without aberrations), the differences in through-focus Strehl Ratio curves across BPPs were below 3%. However, there are large differences in performance across BPPs, in the same subject (for example by a factor as high as of 12 in SR, between BPP#5 and #3 in subject S5), and across subjects.

6.3.5 Perceived quality vs optical quality

Figure 6.8 shows correlation plots between the measured perceived quality and the simulated optical quality for all the BPPs, both at near and far distances. In 4 out of the 5 subjects (S1, S2, S3 and S5) the BPP producing the highest optical quality score (big symbols) matched the subjectively most preferred pattern. The correlation between perceived and image quality was highly statistically significant for subjects S1 and S2 (R>0.54 and p<0.005), and marginally significant for S3 and S5 (R<0.34 and p=0.07). However, subject 4 (Fig 6.8D), with high optical quality, showed a negative correlation (R=-0.47, p=0.01), and the optical simulation did not predict the preferred pattern.

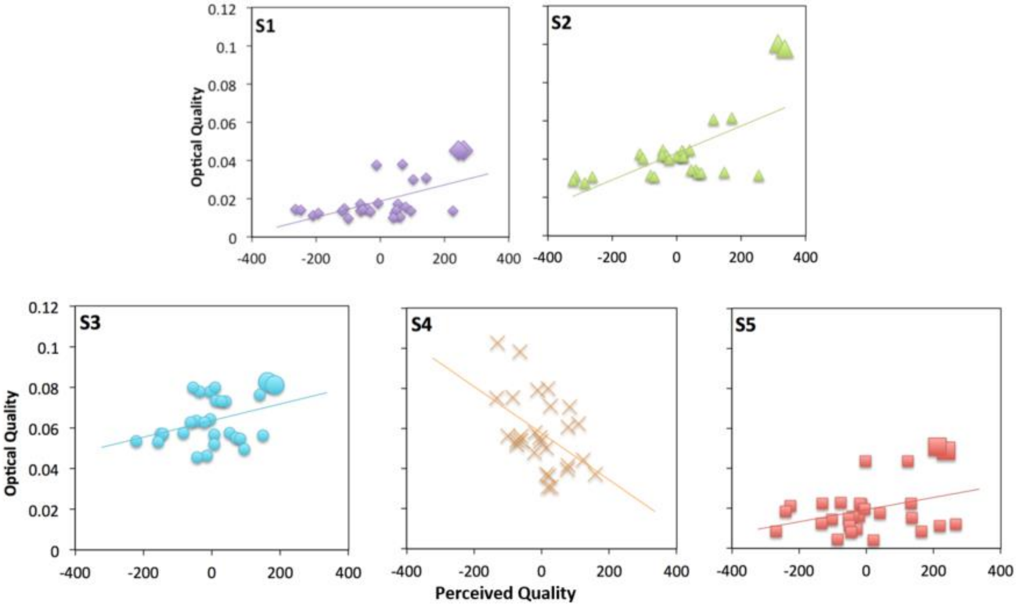

Figure 6.8: Perceived Quality vs Optical Quality for all subjects at far and near distances. Each symbol represents a different pattern.

6.4 Discussion

The Simultaneous Vision Simulator allows simulating non-invasively bifocal corrections in subjects before the implantation or fitting of the multifocal correction, or even before a particular correction is manufactured. In a previous study we simulated pure simultaneous vision (de Gracia et al., 2013b), an ideal situation in which the entire pupil is used for far vision and near vision at the same time, as it occurs in diffractive designs. On the other hand, computational studies have shown that the specific pupillary distribution for near and far produces differences in the thru-focus optical performance both in diffraction limited eyes with multizone radial and angular distributions (Legras et al., 2010, de Gracia et al., 2013a), and real eyes with angular bifocal patterns at different orientations (Alio et al., 2012a, Bonaque-Gonzalez et al., 2015).

The new simultaneous vision simulator presented in this study is capable of simulating any bifocal pupillary pattern, optically programmed by means of a Spatial Light Modulator, expanding the capability of simulating any refractive bifocal design. This capability of switching from one BPP to another allows direct psychophysical comparisons of pairs of corrections in the same subject and without the need of fitting or implanting corrections.

6.4.1 Angular vs Radial designs

We simulated 14 radial and angular segmented patterns (all of them with same addition and energy split between far and near vision) and found strong systematic perceptual differences across patterns, subjects, and observations distances. In general, patterns with semicircular far and near zones were preferred over other designs (BPPs #1-4, Fig. 6.4) and the preferences tended to change between far and near distances. However, we also found these preferences to be patient-specific (Fig. 6.5 and 6.6).

6.4.2 Simulations vs Preferences

Differences in pattern preferences across subjects seem, at least in part, to be driven by differences in the aberrations. The low, but significant correlation between optical and perceived visual acuity indicates some predictive power of Strehl Ratio as an estimator of pattern preference. The multifocal pattern producing the best perceived quality was well predicted by optical simulations in 4 out of 5 subjects. Optical predictions failed to predict the responses in one subject with very high optical quality, perhaps because the low amount of aberrations does not induce noticeable differences across patterns.

6.4.3 Inter-subject differences in preferences

Interestingly, high differences in performance were found with the same pattern at different orientations (i.e. BBP #1 - 4 in subjects S1, S2, S4 and S5, and BPPs #9-10 in subjects S1, S2 and S5), likely due to the differences arising from different optical interactions of the near and far zones with the asymmetric wavefront. Incidentally, the subject showing the strongest orientation preferences (S5, Fig. 6.5E), is the subject with the largest amounts of coma. The effect of pattern orientation, and the interaction with the ocular wavefront, is a matter of interest and will be further investigated using the simultaneous vision simulator developed here.

6.3.5 Implications

The two-channel nature of the simultaneous vision simulator used in this study limited the tested patterns to bifocal corrections. However, designs with more than two foci are penetrating the market, i.e. Trifocal e.g., FineVision (PhysIOL Inc), AT LISA (Zeiss Inc) (Vryghem and Heireman, 2013, Mojzis et al., 2014) and extended depth of focus contact lenses (Zlotnik et al., 2009) whose on eye performance is assessed by clinical studies. Studies based on optical simulations (de Gracia et al., 2013a) predict differences in performance when increasing the number of zones in multizonal patterns (i.e. 3- and 4- zone angular designs outperforming other configurations). Simulation of multifocal patterns needs to be addressed integrating alternative technology into these visual simulations, such as phase masks (Pujol et al., 2014, LaVilla et al., 2015), phase inducing SLMs (Canovas et al., 2014, Vinas et al., 2015) or temporal multiplexers (Dorronsoro et al., 2013, Dorronsoro et al., 2015).

6.5 Conclusion

Significant perceptual differences were found across the different far/near pupillary distributions of bifocal corrections, which varied across subjects and distances. The best perceived pattern can be predicted to a large extent from the ocular aberrations. A two-channel simultaneous vision simulator allows subjective validation of the bifocal patterns producing the best visual quality by including both optical aberrations and potential neural effects.

Chapter SEVEN

Subjective preference to orientation in angular bifocal IOL design

Multifocal IOLs can be diffractive or extended DoF or refractive designs. For these refractive segmented bifocal designs, we showed that the preferences vary between angular and radial designs. It is also well known that the visual system is tuned to specific orientation, mostly dictated by the orientation of blur in the retina. We studied this orientation tuning to a commercial angular bifocal IOL design by optically simulating the bifocal design using a simultaneous vision simulator and performing visual and perceptual performance measurements. These measurements were used to estimate the ideal IOL orientation for optimal performance.

This chapter is based on paper by Radhakrishnan et al., titled "Differences in visual quality with orientation of a rotationally asymmetric bifocal IOL design" *(Submitted)*.

The author of this thesis designed and performed the measurements on human eyes, and analyzed the data in collaboration with the co-authors. The results of this work has been accepted for presentation in the Annual Meeting of Association for Research in Vision and Ophthalmology, Seattle, 2016.

7.1 Introduction

Currently, a popular solution for the correction of presbyopia is the use of multifocal lenses in the form of contact or intraocular lenses (Charman, 2014b, a). These lenses are based on diffractive or refractive designs that produce a simultaneous image on the retina, i.e. superimposed images focused at near and at far. Refractive segmented designs render the entire pupil with zones focused at far or near. Clinical studies on visual functions in patients implanted with multifocal IOLs show that an increase near vision is generally observed at the expense of a degradation of the distance vision (Bellucci, 2005, Cillino et al., 2008, Cochener et al., 2011). However, systematic experimental studies are lacking on whether a particular IOL provides optimal through focus performance, and to what extent this is subject-dependent.

An earlier computational study showed that different distributions of near/far zones across the pupil resulted in different multifocal performance, even in diffraction-limited eyes. Simulations of angularly and radially segmented patterns of 2 to 50 zones showed that a lower number of zones (up to 3-4) were generally better than a higher number of zones, and that angular patterns tended to perform radial patterns (de Gracia et al., 2013a).

Performing comparative studies across lens designs in patients is challenging, and so far have been mostly restricted to contact lenses. For contact lenses, a same patient can perform a visual task with different lenses, although a side by side comparison is only possible using right and left eye. For intraocular lenses, Peli and Lang (2001) simulated the effect of bifocal lenses bypassing the optics of a pseudophakic patient implanted with a monofocal IOL in one eye. In general, it is only possible to test vision with one implanted IOL at a time, preventing the possibility of comparing visual quality across lens designs on the same patients. Visual simulators, based on adaptive optics or simultaneous vision, allow simulating different multifocal designs on the same patient, and therefore the possibility of conducting systematic studies.

Piers et al (Piers et al., 2004) simulated different amounts of spherical aberration in an adaptive optics instrument, and the effect of the spherical aberration magnitude on subjective depth-of-focus. Specific combinations of astigmatism and coma tested in an adaptive optics system can also improve visual performance thru-focus, at least in non-astigmatic patients (de Gracia et al., 2011).

Evaluations of the effect of the near addition on visual acuity with pure bifocal designs simulated using a simultaneous vision simulator revealed that not all additions are equally deleterious to vision (de Gracia et al., 2013b). In a subsequent study we found that perceived visual quality under simultaneous vision is affected by both the near addition magnitude and by the far/near energy ratio, and that the perceived visual quality of simultaneous vision images shifts after brief periods of adaptation to simultaneous vision images. (Radhakrishnan et al., 2014)

Adaptive Optics visual simulators with deformable mirrors and spatial light modulators as active elements have been used to demonstrate visual perception in real subjects with simulated multifocal designs with near/intermediate/far pupillary zones, both angular and radially segmented (Vinas et al., 2015), supporting optical predictions. Simultaneous vision simulators have probed specifically various bifocal designs with different pupillary distributions for near and far, and have shown that bifocal rotationally asymmetric designs outperform other bifocal designs in real subjects. However, the specific performance of a rotationally asymmetric design was highly patient-specific (Dorronsoro et al., 2014).

There is one angularly segmented, rotationally asymmetric intraocular lens in the market, the MPlus lens by Oculentis, (Wanders, 2013). The lens has been reported in numerous clinical studies targeting visual outcomes or visual quality questionnaires in implanted patients, in most cases with the near segment of the IOL placed inferiorly (Alio et al., 2012a, Alio et al., 2012b, Alio et al., 2012c, Thomas et al., 2013). There are some case reports that suggest that placing the lens in a different orientation could actually be beneficial (Bala and Meades, 2014), and suggestions that the aberrometric profile may play a role in the visual outcomes with this IOL (Ramon et al., 2012). A recent paper simulated optical performance in computer eye models with real corneal elevation maps and showed variations in the optical performance across orientations, which were associated to the angle of the corneal comatic axis in the tested eyes (Bonaque-Gonzalez et al., 2015). However, another study reported that, on average across group of patients, the orientation of the IOL does not influence visual performance (de Wit et al., 2015). Simultaneous Vision simulators are excellent tools to test the effect of orientation of rotationally asymmetric lenses on visual performance, allowing accounting for both optical and neural interactions of the optics/visual system with the multifocal pattern. As the system is fully programmable the different lens orientations can be automatically deployed, allowing comparing and rapid testing of vision across orientations.

In this study we used a custom-developed simultaneous vision simulator provided with a spatial light modulator to test the influence of lens orientation on perceived visual quality and visual acuity at different distances in patients with paralyzed accommodation.

7.2 Methods

7.2.1 Subjects

Twenty subjects (aged 21-62 years) participated in the study, with refractive errors ranging from +2.50 D to -5.50 D, astigmatism < 1 D. Eight of the subjects did not have prior experience in performing psychophysical experiments. All measurements were performed with paralyzed accommodation and therefore under simulated presbyopia. Cycloplegia was pharmacologically induced with 1% tropicamide (3 drops at 5 minutes interval 15 minutes prior to beginning of measurements and maintained by instilling one drop of every hour). The measurement protocols met the tenets of declaration of Helsinki and were approved by the review board of Consejo Superior de Investigaciones Cientificas. All subjects provided a written informed consent.

7.2.2 Setup

A custom simultaneous vision simulator (Fig. 7.1) was used to simulate angular bifocal corrections and to perform psychophysical evaluations at three distances.

The system has been described in detail in prior publications (Dorronsoro and Marcos, 2009, de Gracia et al., 2013b, Dorronsoro et al., 2014). In brief, two channels provided with two Badal systems separated by beam splitters recombine at a pupil plane, therefore allowing to change defocus independently. One channel is focused at far, while the other introduces a near addition that can be changed continuously. A Digital Light Projector (DLP; Optoma Inc; resolution of 800 x 600 pixels) projects visual stimuli that are viewed simultaneously through both channels. In a modified version of the instrument (Radhakrishnan et al., 2015) a transmission spatial light modulator (SLM) is placed in a pupil conjugate plane with a linear polarizer. Two orthogobnally oriented linear polarizers placed in the Badal channels projects near or far focused images, following the corresponding black and white pupillary masks displayed in the SLM. The current configuration of the system is showed in figure

7.1. The effective luminance of the test stimulus was 39 cd/m2. Test stimulus and pupillary mask presentation were synchronized in Matlab using the Psychtoolbox (Brainard, 1997).

In this study, the focus difference between the two channels was set to + 3 D. Far vision was simulated by placing the far channel (Badal 2) at best focus (BF) and the near channel (Badal 1) at BF+3 D. Near vision was simulated by placing Badal 2 at BF-3 D and Badal 1 at BF. Intermediate vision was simulated by placing Badal 2 at BF-1.5 D and Badal 1 at BF+1.50 D. All measurements were done for 4.5 mm pupil diameters (also addressed by the SLM).

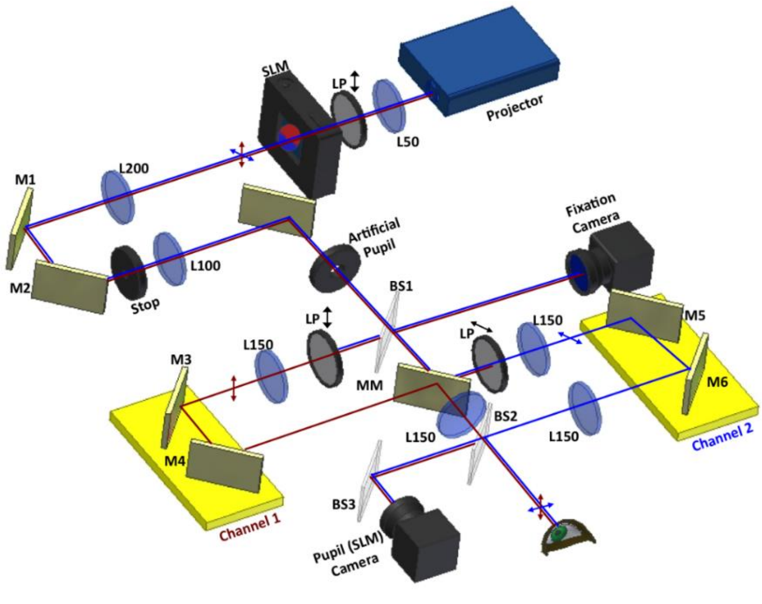

Figure 7.1: Schematic diagram of modified Simultaneous Vision Simulator

Simulation of the rotationally asymmetric IOL

We simulated the design of a commercial IOL, M Plus (Oculentis Inc). The lens has an angular profile with a small radial zone at the center for far vision. The far/near energy ratio was 60/40. Masks were created using Matlab and consisted of white and black portions of a circular image (4.5 mm diameter) representing far and near vision zones respectively (shown in Fig. 7.2). These patterns are programmed in the

SLM and presented at eight orientations. The angular notation (Fig. 7.2B) represents the orientation of the near zone. For convention, the right eye data are flipped horizontally (Marcos and Burns, 2000), so that 0 deg represents nasal orientation both in right and left eyes.

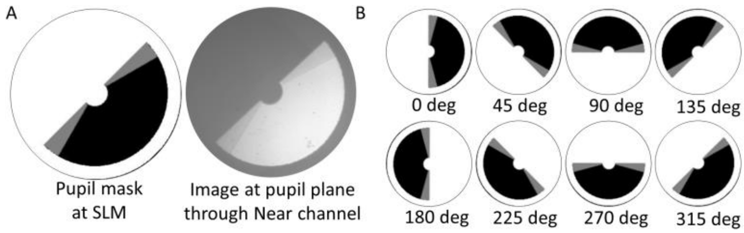

Figure 7.2: Gray-scale patterns programmed in the SLM, representing the Oculentis Mplus Lens. A. Programmed gray-scale image (left) and pupillary plane image captured on a CCD placed at the eye's pupil plane. B. Gray-scale patterns programmed at different orientations. White segments correspond to the far vision zone, black segment corresponds to near vision zones and the gray region corresponds to the transition zones.

7.2.3 *Perceptual Scoring*

Subjects viewed 2 deg visual field face images (Fig. 7.3, top) displayed by the DLP through one of the 8 orientations of the bifocal design(Fig 7.3, middle), presented in random order, interspersed with a gray field.

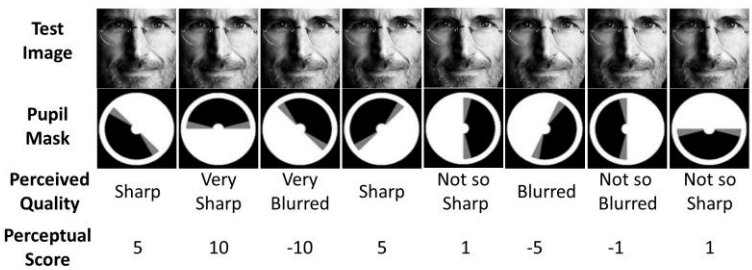

Figure 7.3: Illustration of a perceptual scoring setting for one subject on one face image (top) viewed through 8 different rotated patterns (middle). Scores ranged from -10 (very blurred) to + 10 (very sharp) (bottom)

For each presentation, the subject graded the image in a 6-point grading scale from very blurred (-10), blurred (-5), not so blurred (-1), not so sharp (1), sharp (5), and very sharp (10), using keyboard inputs. Figure 7.3 provides an example of the scoring given by one subject on a particular series of presentations. The measurement was repeated ten times and the average score for each orientation was calculated. Presentation of the test image and pupil mask, and acquisition of response were synchronized by custom routines written using Matlab.

7.2.4 Orientation preference

For testing the orientation preference (Fig. 7.4), subjects viewed subsequently, a face image (2 deg field) through two pairs of random orientation bifocal patterns. Each image was viewed for 1.5 s, with a gray screen presented in between each image pair presentation. The subject's task was to choose the better focused image (first or second) of the pair and indicate the confidence of choice on a 3 confidence level scale. Each session consisted of presentation of 36 random pairs and the measurements were repeated 10 times.

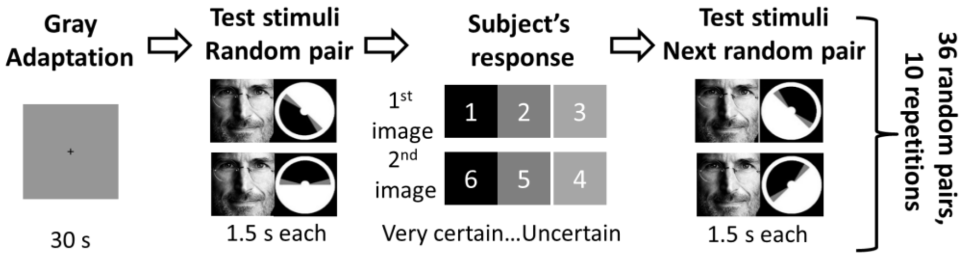

Figure 7.4: Illustration of the pattern preference psychophysical paradigm

7.2.5 Decimal Visual acuity measurements

Decimal visual acuity was measured using white E letters on a black background that was presented in eight random orientations of varying sizes (Fig. 7.5). At the beginning of the trial, an E target is presented of supra-threshold size and a random orientation. The task of the subject was to identify the orientation of the E-letter and respond using a keyboard (8-AFC). The size of E in the subsequent presentation is decreased or increased depending on the subject's response using a QUEST algorithm (Pelli and Farell, 1995, Ehrenstein and Ehrenstein, 1999, Phipps et al., 2001). The presentation orientation is randomized. A run consisted of 50 trials and 20 reversals and the visual acuity was measured as the average of last ten reversals. The measurements were repeated for all the eight orientations of the bifocal pattern and for far, intermediate and near distances. The measurements were repeated for all the eight orientations of the bifocal pupil pattern and for far, intermediate and near distances.

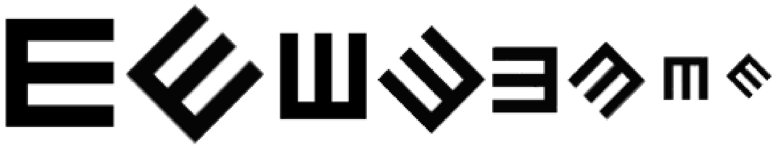

Figure 7.5: Decimal visual acuity measurement using E optotypes in 8 orientations

7.2.6 Aberrometric measurements

The ocular aberrations were measured using a Shack-Hartmann aberrometer (HASO32, Imagine Eyes), part of a custom-developed adaptive optics system (Marcos et al., 2008). Measurements were performed under cycloplegia. Defocus was corrected using a Badal optometer while the subject fixated a white Maltese-cross in a black background. Pupil diameter was limited to 4.5 mm using an artificial pupil placed at a pupil conjugate plane.

7.2.7 Optical Simulations

We simulated pattern orientation preference optically, using an "ideal observer model" whose responses to an orientation preference task (the same one performed by the subjects) are based on an optical metric (Viusal Strehl, VS, Iskander, 2006). For each subject, we computed the through-focus VS for each wavefront aberration resulting from the combination of the measured subject's ocular aberrations (astigmatism+HOA) and the bifocal patterns at each orientation. In all patients and for all distances (best focus, at +1.5 D and at +3 D) VS for each orientation was compared with that for all the other orientations. Scores of 10, 5 and 1 were assigned when the differences between the two orientations compared were above 75%, 50% and 25% thresholds respectively.

7.2.8 Data analysis

Both perceptual and optical preference measurements were analyzed similarly. Weights were assigned to the positive (images selected as better of the pair) and negative responses (other image in the pair) according to the confidence of the response (from +10 to +1 / -10 to -1). The scores assigned to each pattern orientation were summed and a sum weighted preference score was obtained. A polar plot was generated from the scores at each orientation and the centroid position for the corresponding polar plot was calculated for each distance. The orientation of the centroid indicates the preferred orientation and the radius indicates the strength of the preference. For identifying significant preferences, a Bernoulli statistics was used. A score greater than $\pm$15 for a given orientation is considered significant, indicating that that orientation produced significantly better optical or visual performance.

7.3 Results

7.3.1 Changes in Perceptual Score with pattern orientation

Figure 7.6 shows the Perceptual Score for different orientations across different distances as a polar plot. The center of the plot corresponds to a score of -10 and the outer line to +10 symmetrically in all orientations. Data for far are indicated in red, intermediate in green and near in blue. The average perceptual score across subjects did not vary across orientations or distances (Fig. 7.6A), although the curves tended to elongate for 0 and 180 deg. However, there were high intersubject variabilities in this performance. Fig. 7.6B-D show perceptual score plots for three individual subjects. For example, for S2, perceptual score is highest for 180 deg at far, and for 270 deg at intermediate and near. For the other two subjects shown (S11 and S18), the score is highest at 0 deg for both far and near, and 0 and 90 for far and near, respectively.

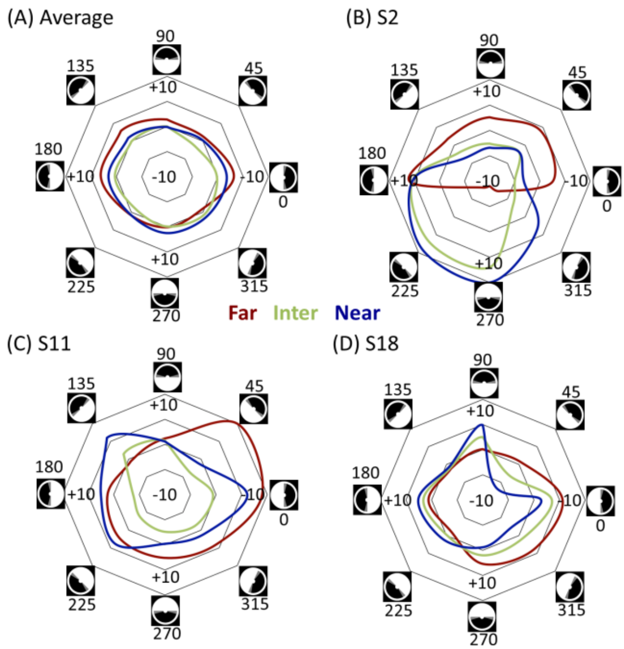

Figure 7.6: Perceptual score across orientations at far (in red), intermediate (in green) and near distances (in blue) (A) Average Perceptual Score (B)-(D) Examples on subjects

The overall perceived image quality across orientations at any distance was calculated as the area of the circle formed by the perceptual scores at the given distance. The mean score was 5.6 (SD: 1.2) at far, 2.1 (SD: 1.07) at intermediate, and 4.1 (SD: 1.05) at near. The mean difference in perceived image quality (score) between far and near was 2.5 (SD: 1.4) and was not significant (p=0.37).

7.3.2 Orientation preference

Figure 7.7 shows the weighted preference with the respective centroids for all subjects. The center of the plot corresponds to a preference score of -100 and extends symmetrically across all orientations to a score of +100. The arrows indicate the orientation of the centroid (preferred orientation) and the length of the vector indicates the strength of preference.

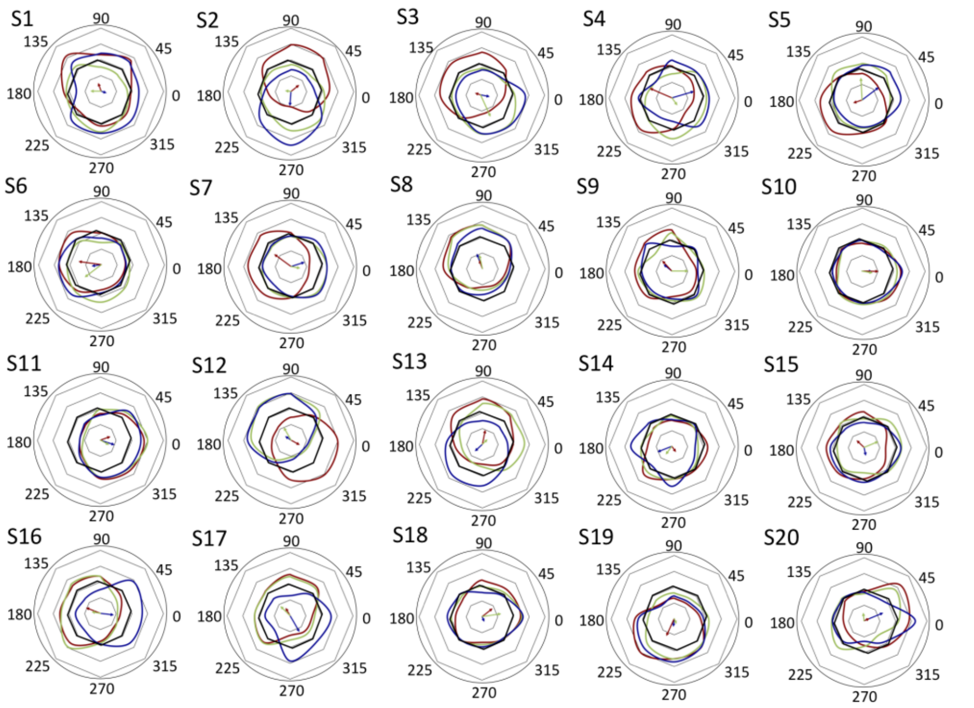

Figure 7.7: Weighted orientation preference for all subjects at far (red), intermediate (green) and near (blue) distances. At any orientation, the axes extend from +100 to -100 in the center with black line representing zero. Arrows indicate the preferred orientation at the respective distances with the length of the arrow indicating significant preferences.

The weighted perceptual preferences correlated significantly with the perceptual score across all subjects and distances (r=0.48, p=0.004). At far, 6 subjects preferred nasal quadrant orientations (0 + 44.5 deg), 4 subjects preferred superior quadrant orientations (90 + 44.5 deg), 8 subjects preferred temporal quadrant orientations (180 + 44.5 deg) and only 2 subjects preferred inferior quadrant orientations (270 + 44.5 deg). At near, 8 subjects preferred nasal quadrant, 5 temporal quadrant, 6 inferior quadrant and one the superior quadrant orientations.

Figure 7.8 shows the centroid locations for far (filled) and near (open). Values outside the inner circle (radius of 15) are significant. Eight subjects had strong orientation preference at far and 9 subjects had strong orientation preference at near. The mean angular difference in the centroid orientation between far and near was 27 + 22 degrees and correlated significantly (r=0.32, p<0.05), indicating that in most subjects the orientation preference was retained across distances.

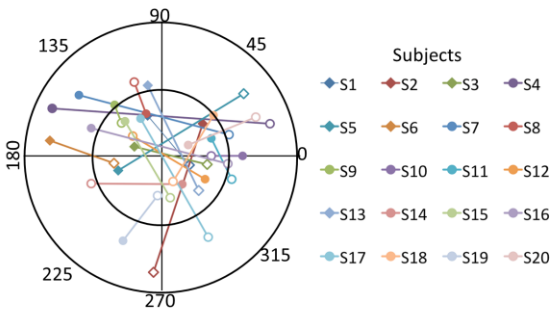

Figure 7.8: Centroid locations of the weighted orientation preference plots for all subjects. Filled symbols represent centroid locations for far and open symbols centroid locations for near. The inner circle represents the limit for statistical significance (i.e. values outside the circle are significant).

7.3.3 Changes in Decimal Visual acuity

Mean decimal visual acuity, across subjects and orientations was 0.63 at far (SD: 0.02) and 0.556 at near (SD: 0.021). This corresponds to one line difference in visual acuity with conventional charts (Grosvenor, 1996). As shown in figure 7.9, the visual acuity did not vary much across orientations at any distance. The maximum difference in average visual acuity across any two orientations at far, intermediate and near was 0.06, 0.11 and 0.05, respectively.

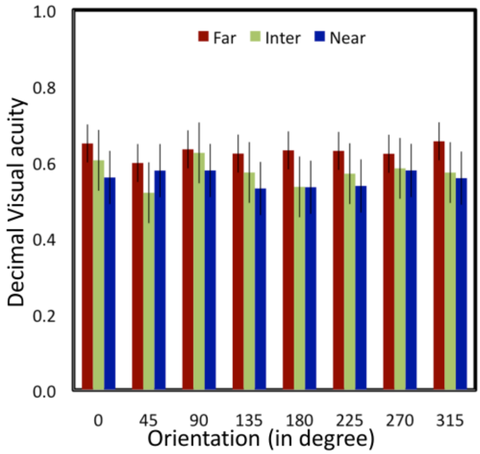

Figure 7.9: Average Decimal visual acuity at different orientations across subjects at far (red), intermediate (green) and near distances (blue)

7.3.4 Ideal observer model

Responses of an "ideal observer model" were based on the Visual Strehl values at the measured distances. In a diffraction-limited eye through-focus VS curves are the same for all orientations (Fig. 7.10 A). In real eyes, the amplitude and overall shape of the thru-focus curves may vary across orientations (an example for patient S2 is shown in Fig. 7.10B).

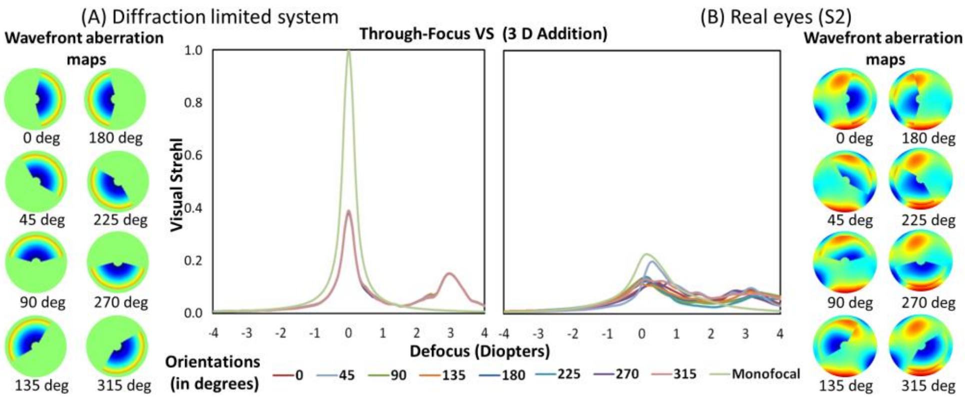

Figure 7.10: Wave aberrations and Through-focus VS for 8 orientations for (A) a diffraction-limited eye. (B) A subject's eye with real aberrations (S2)

Figure 7.11 shows the orientations preferences obtained for each subject using the ideal observer model, which responds based on VS values. As in the perceptual orientation preference plots (Fig. 7.7), the center of the plot corresponds to the optical preference score of -100 and extends symmetrically across all orientations to a score of +100. The arrows indicate the orientation of the centroid (preferred orientation) and the length of the vector indicates the strength of preference. The simulated optical preference plots and the measured perceptual preference plots correlated significantly at far and near distances (r_f=0.71, r_n=0.62, p<0.0001), although not for intermediate distances (r=-0.021, p=0.87). Bland-Altmann analysis revealed good agreement (better for far distance) between measurements and simulations at all distances (p_f=0.46, p_i= 0.19 and p_n=0.24).

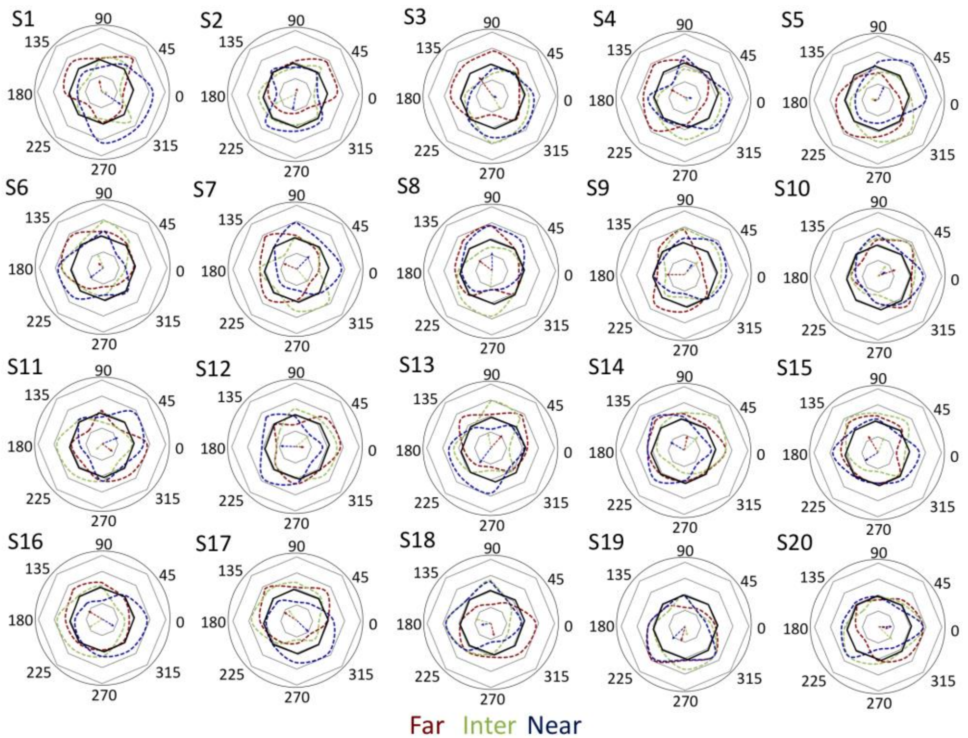

Figure 7.11: Simulated weighted orientation preference for far (red), intermediate (green) and near (blue) distances for all subjects. The axes extends from +100 to -100 in the center with black line representing the zero. Dashed arrows indicate the preferred orientation at the respective distances with the length of the arrow indicating significant preferences.

Figure 7.12 A-C shows the centroid locations of the perceptual preference (filled symbols) and optical simulated preference (open symbols) obtained from the polar plots for far, intermediate and near distances. There is, a high correspondence between perceptual and optical centroid locations for far (28 deg, SD: 29) and for near (36 deg, SD: 28) distances, both data falling in the same quadrant, but not for intermediate. Distances (80 deg, SD: 63). Correspondingly, there was a strong significant correlation (Fig. 7.13) between the perceptual and optical centroids at far and near distances (r_f=0.89, r_n=0.94, p<0.0001). Even at intermediate distance a weak correlation was observed (r_i=0.47, p<0.05).

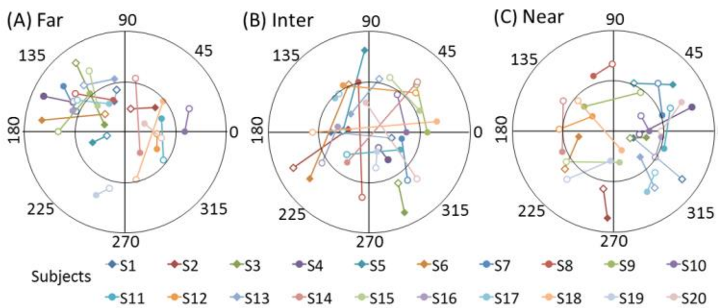

Figure 7.12: Centroid locations for measured (filled symbols) and simulated (open symbols) data at (A) far, (B) Intermediate and (C) Near distances for all subjects. Inner circle represents significant radius of centroids.

The radius of the centroid estimated from optical simulations was higher than from perceptual measurements in about 65% of the subjects across distances, probably resulting from discrepancies in perceptual weighting by the subject and the ideal observer. On an average, across distances and subjects, the difference in radius between simulations and measurements was 1.8 (SD: 7.8) and did not correlate significantly at any distance.

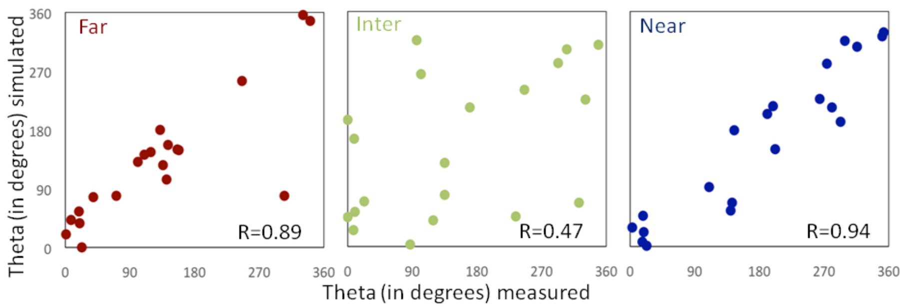

Figure 7.13: Correlations of the weighted orientation preference plot centroid angular coordinates (optimal orientation) from perceptual measurements and optical simulations for (A) far, (B), intermediate and (C) near distances.

7.4 Discussion

We evaluated systematically the perceptual and visual performance differences with orientation of an angularly segmented bifocal pattern simulated in a simultaneous vision simulator, mimicking the commercially available rotationally asymmetric IOL Mplus by Oculentis. While visual acuity did not change significantly with orientation, the perceptual score showed a clear bias towards specific orientations. Perceptual orientation preferences varied across subjects, and in some cases across distances. Interestingly, the orientation preference appears to be determined, to a large extent, by the eye's optical aberrations, which interact with the bifocal pattern differently for the different orientations, and those interactions are different across individuals. The results indicate that one may select the orientation of the lens to optimize perceived image quality. This optimization would be preferably made by measuring subjective preferences using a simultaneous vision simulator. Alternatively, simulations based on the patient's aberration pattern may be used to predict the optimal orientation of the lens, as the predicted best orientation has been show to highly correlate with the psychophysical measurement, with differences typically lying within a quadrant.

7.4.1 Visual performance

Multifocal IOL implantation is aimed at providing patients with good uncorrected visual acuity for both distance and near visual tasks. The bifocal design we tested provided high contrast visual acuity at far and near distances in the near normal visual acuity range. Concurrent to the distance dominant design of the tested bifocal, the visual acuity at near was >1 line lesser than the distance visual acuity. The visual acuity reported in our study was within the range of visual acuities reported in previous studies (Cillino et al., 2008, Cochener et al., 2011). Despite the absence of a correction at the intermediate region, the visual acuity was relatively well preserved at intermediate distance.

Decimal visual acuity measured at high contrast was unaffected by the orientation of the angular bifocal design. It is likely that the differences across orientations are not apparent with high contrast stimuli, although these differences may have been present in a low contrast visual acuity (Applegate et al., 2002, Vaz and Gundel, 2003, Chalita and Krueger, 2004, Rouger et al., 2010). In other words, conventional tests for visual acuity appear to be insensitive to changes introduced by blur orientation and might not be a useful indicator of preferred orientation of the IOL.

7.4.2 Perceptual difference across orientations

We performed two tests to assess perceived image quality at different orientations: perceptual scoring and perceptual preference. Results from both perceptual tests were similar in most subjects. Twelve of the 20 subjects had a significant correlation between perceptual scores and weighted perceptual scores for far distance across all orientations, and only in two subjects, these were uncorrelated or negatively correlated. Similar to visual acuity results, the overall perceptual quality was better at far than at near and was worse for intermediate distance. It is, however, to be taken into account that the intraocular lens design simulated was a bifocal (60F/40N) and had no energy dedicated at near. The residual optical quality at intermediate is likely to have resulted from the interaction between the ocular aberrations of each subject and the peak foci.

On an average, the orientation preferences showed a trend to the horizontal axis (Fig. 7.8A), although the orientation bias differed across subjects. The conventional orientation of IOL implantation in the clinic is with the near zone at 270 degrees, however only one subject showed consistent preferences at all distances to this orientation. While many subjects showed a horizontal preference at far, the vertical orientation was favoured more often at near distance. This bias could have an optical or neural origin. That the visual system may have an orientation tuning has been shown in several studies (Blakemore and Campbell, 1969, Appelle, 1972, Bosking et al., 1997, Dragoi et al., 2001). Several independent studies have shown that the human visual system is preferably tuned to horizontally oriented targets (Ohlendorf et al., 2011a, b) and that this is learned over time. Ohlendorf and colleagues showed that subjects could tolerate horizontally oriented astigmatism better than vertically oriented astigmatism. Also, Vinas et al. (2013) found lower visual degradation to induced horizontal astigmatism than to vertical or oblique astigmatism.

Whether the bias to particular orientation of the bifocal pattern has an optical or neural origin can be tested through different strategies, i.e. through the use of an adaptive optics simulator with two active elements, a deformable mirror capable of correcting the subject aberrations and an SLM introducing multifocal patterns, or through optical simulations based on the measured optical aberrations of the subject. In this particular strategy we opted the second approach. Adaptation to the native aberrations could still produce bias towards certain orientation, even if aberrations are totally corrected. Examples of long term bias to oriented blur, even after long term wear of corrective astigmatic lenses has been shown by several authors (Yehezkel et al., 2010, Vinas et al., 2012). Also, it has been shown that subjects are adapted to their own aberrations, and the images blurred with similar blur level but different orientation blur to the patient’s optics are perceived as more blurred than those degraded with the subject’s own blur orientation (Sawides et al., 2011, Sawides et al., 2012). That subjects can adapt to a new aberration pattern/blur orientation has been shown before (Sawides et al., 2010) and even to pure simultaneous vision blur (Radhakrishnan et al., 2014). Whether subjects can adapt to new oriented blur produced by a rotationally asymmetric lens remains to be investigated.

7.4.3 Perceptual differences across subjects

The perceptual preference to orientation showed distinct trends among groups of subjects. While some subjects showed consistent and strong orientation preference across distances, few subjects showed strong preferences that varied across distance and few subjects did not show any significant orientation preferences. On an average across all subjects, even though the preferred orientation was along the horizontal axis, the strength of preference was reduced, indicating that these preferences are highly subjective and should be treated on an individual-basis. This finding explains why a bias was not be apparent as a group trend by de Wit et al., (2015) in patients where the MPlus IOL had been implanted in different orientations.

7.4.4 Simulations vs Measurements

We simulated orientation preferences using an ideal observer model generated from the through focus VSOTF calculated from the ocular aberration measurements at best-focus. We found good agreement between optical simulations and the perceptual measurements. In fact at far, the preferred orientation estimated from perceptual measurements were within 45 degrees (smallest step of rotation measured in the study) of the preferred orientation obtained from simulations in 90% of the subjects. On the other hand, 40% of the subjects still had a difference of less than 20 degrees (clinically significant) between simulated and measured preferred orientation. These results suggest that the orientation bias is strongly influenced by the ocular optics. Most of the subjects had coma-like aberrations oriented along the oblique axis, which reflected in the orientation preferences (Bonaque-Gonzalez et al., 2015).

The optical simulations were performed using Visual Strehl as a metric, which represents exclusively optical contrast differences across orientations. It is conceivable that a metric that also considered the orientation of the retinal blur (produced by each combination of ocular aberration and bifocal pattern orientation) instead of overall contrast only may even improve the predictions. Given the good prediction of the orientation bias on optical grounds it is conceivable that the best selection of the lens orientation can be planned based on the optical aberrations. In any case, a full account of both the optics and neural aspects can be achieved by using a simultaneous vision simulator or adaptive optics visual simulators.

7.4.5 Implications

This study shows that choosing the optimal orientation of a rotationally asymmetric IOL may have an impact in improving the visual performance with these lenses. Several subjects showed clear preferences to a particular orientation which was the same at far, intermediate and near distances and few other subjects showed no typical tendencies with orientation at any distance. These are probably the most ideal subjects for the implantation of angularly segmented multifocal IOLs. On the other hand, over a third of the subjects showed a different preferred orientation for far and near distances. The orientation of implantation might, in these cases depend on the subject's visual needs or might be based on the preferences at far. Since some of these subjects have strong preferences to orientation, this further stresses the importance of orientation preference assessment prior to the surgical intervention.

We can only speculate on the rotation accuracy needed for this optimization, as our perceptual measurements were done in 45 deg increments, and the average difference between the predicted best orientation and that estimated from perceptual measurements (centroids from polar plots in each case) was around 20 deg. These accuracies can be easily achieved manually by surgeons. In brief, similarly to the selection of optimal orientations of toric IOLs (Ma and Tseng, 2008, Buckhurst et al., 2010), it is conceivable to develop algorithms based on the aberrations of the eyes that guide clinicians to choose the optimal orientation of the lens. These should preferably use the topography-based corneal aberrations, as the crystalline lens is removed in the procedure. Alternatively, adaptive optics or simultaneous vision systems can be used to base the decision on perceptual measurement in patients, provided that the lens is not fully opacified by cataract. These instruments can also be used to evaluate neural adaptation to multifocal corrections.

7.5 Conclusion

In this study, we measured visual and perceptual performance to different orientations of a commercial bifocal design at far, intermediate and near. The high contrast visual acuity did not differ much across orientations and distances. The perceptual performance and preferences were different across orientations and distances in most subjects. We show that these preferences are closely associated with the optical quality of the eye defined by the lower and higher order aberrations. In absence of modalities to customize the entire IOL design, small changes in the orientation of IOL implantation could result in improved perceptual quality. These preferences should be assessed prior to surgery, considering the visual needs of the patients and more importantly, taking into consideration, their own optical quality.

Chapter EIGHT

Neural adaptation to optically simulated pure simultaneous vision

We measured preferences to different bifocal designs and to different orientations of an angular design using a simultaneous vision simulator. It was demonstrated that the optics of the eye play an important role in these preferences. Previously we demonstrated, using adaptive optics, that the visual perception and neural adaptation are influenced by the multifocal design (far/near energy ratio). It would be interesting to study the impact of ocular aberrations on these adaptations. We studied the neural adaptation to optically induced simultaneous vision by studying changes in the Perceived Best Focus.

The author of this thesis developed instrumentation, designed and performed the measurements on human eyes, and analyzed the data in collaboration with the co-authors. This work was presented at the Association for Research in Vision and Ophthalmology (ARVO) annual meetings on May 2015 in Denver, Colorado, USA as a poster.

8.1 Introduction

The ability of the visual system to adapt to blur introduced by lower and higher order aberrations has been previously researched. Improvements in visual acuity after adaptation to myopic blur has been reported in independent studies by Pesudovs and Brennan (1993) and Mon-Williams et al. (1998). Similarly, Vinas and colleagues reported differences in visual acuity with the axis of induction of astigmatism and its changes over time after adaptation (Vinas et al., 2012, Vinas et al., 2013). The degradation in contrast sensitivity in myopes was found to be lesser than that in emmetropes with induction of myopic blur than with hyperopic blur, suggesting the role of preadaptation to blur (George and Rosenfield, 2004, Poulere et al., 2013). The neuronal explanations of the blur adaptation was further explored by Webster who demonstrated changes in the perceived best focus after short-term adaptation to blurred or sharp images (Webster et al., 2002, Webster, 2011). It was also reported that the visual system is adapted to its own aberrations in both magnitude and orientation (Artal et al., 2003, 2004, Sawides et al., 2011b, Sawides et al., 2013). In addition, Sawides and colleagues showed changes in what a subject perceives as “normal” changed after adaptation to astigmatism (Sawides et al., 2010), scaled versions of higher order aberrations (Sawides et al., 2012) or aberrations of other persons (Sawides et al., 2011a).

Simultaneous blur is a new visual experience, introduced by multifocal solutions that are often used to treat presbyopia, the age related loss of near vision (Glasser, 2008, Charman, 2014). These are usually provided in the form of multifocal contact lenses, intraocular lenses or as corneal refractive surgeries. Clinical studies show that these solutions augment near vision to the presbyopic patients at the expense of far visual performance (Bellucci, 2005, Cochener et al., 2011).

The degradation introduced in the visual and perceptual performance by this new visual experience has been studied in two independent research (de Gracia et al., 2013, Radhakrishnan et al., 2014), using different approaches. de Gracia et al. (2013) used a simultaneous vision simulator to optically simulate pure simultaneous vision.

In these measurements the ocular aberrations of the subjects were uncorrected. The visual performance, evaluated in terms of visual acuity, showed that degradation in far visual acuity varied non-linearly and non-monotonously with the amount of addition in the simultaneous vision corrections. The largest decrease in visual acuity was found for intermediate additions around 1.5 D. Radhakrishnan et al. (2014) later studied, perceptual quality with pure simultaneous vision by computationally simulating the blur. The convolved images were observed through an adaptive optics correcting the aberrations of the eye and perceptual quality was studied in terms of perceptual score. It was found that similar to visual acuity, the perceptual degradation varied with amount of near addition. However, in this case, the image producing the maximum degradation was the image containing a simultaneous blur of 0.5 D. It was also found that perceptual quality improved after adaptation to simultaneous blur, and that the adaptation (in terms of perceptual score) was maximum also at an addition of 0.5 D, corresponding to the images with maximum degradation. Concurrently, the change in perceived best focus (image blur producing neutral perception) following adaptation was maximum and saturated at 0.5 D. The origin of this discrepancy, in the near additions causing maximum perceptual degradation (1.5 D in de Gracia et al. (2013) and 0.5 D Radhakrishnan et al. (2014) is not clear.

Recent studies, using the simultaneous vision simulator (Dorronsoro et al., 2014, Radhakrishnan et al., 2016) or adaptive optics setup with spatial light modulator (Vinas et al., 2015) show that the ocular aberrations play an important role in perception to simultaneous vision patterns. While, the ocular aberrations were corrected during perceptual measurements (Radhakrishnan et al., 2014), they were present in de Gracia et al. (2013). This is a possible source for the differences in maximum degradation with simultaneous blur.

Also, the nature of the simulated blur (computationally simulated vs optically induced) has been shown to influence both visual and perceptual performances (Ohlendorf et al., 2011a, b). Ohlendorf and colleagues showed differences in amount of adaptation (change in visual acuity) when the astigmatic blur was induced optically or by convolution and suggested that the computational methods do not account for the neuronal processes.

Finally, the subjective tasks employed in both studies were different (visual acuity and blur judgments). The different range of spatial frequencies involved is another potential influencing factor (Vera-Diaz et al., 2010) to the above mentioned discrepancy.

This study was designed to explore which of these factors contribute to the discrepancy in simultaneous vision perception. We used a combined methodology, simulating simultaneous blur optically using a simultaneous vision simulator and not correcting the ocular aberrations as in de Gracia et al. (2013), and measuring the change in the perceived best focus following adaptation to simultaneous vision. While the previous study with simultaneous vision simulator (de Gracia et al., 2013) was limited to simulating only equal energy balance between far and near (50F/50N), we induce three different far/near energy levels (75F/25N, 5F/5N, 25F/75N) by equipping the simultaneous vision simulator by incorporating a spatial light modulator.

8.2 Methods

Pure simultaneous bifocal images of different far/near energy ratio were simulated optically using modified simultaneous vision simulator. Overall, the experiments lasted for a total of 2 hours with regular breaks during the measurement. The ocular higher order aberrations and residual astigmatism were not corrected in these measurements.

8.2.1 Subjects

Four subjects aged 28 to 42 years, with spherical ametropia (<6 D) and astigmatism (<1 D) participated in the measurements. In all subjects, cycloplegia was induced by instilling 1% tropicamide three times with 5 minutes interval prior to beginning the measurements and was maintained by instilling 1 drop at the end of an hour. Ocular aberrations (Fig. 8.1) in all subjects were measured for a 5 mm using custom developed adaptive optics system with a Shack Hartmann wavefront sensor (Marcos et al., 2008, Gambra et al., 2009). All the subjects had prior experience in performing psychophysical measurements and provided written informed consent.

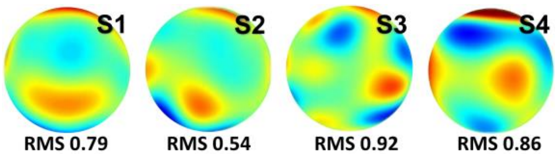

Figure 8.1: Ocular higher order aberrations and RMS for 5 mm PD

8.2.2 Apparatus

Figure 8.2 shows a schematic of the modified simultaneous vision simulator. Two Badal optometers (focused at far and near distances) and a spatial light modulator (SLM) was used to optically simulate simultaneous vision. The refractive error of the subject is compensated using the far channel Badal optometer and an addition of 3 D was induced with the near channel. To induce pure simultaneous vision, a checkerboard was displayed in the SLM. By varying the ratio between the black (near) and the white (far) boxes in the checkerboard, different far/near energy ratios for the pure simultaneous vision was achieved. Test and adapting images were presented using a DLP projector through an artificial pupil of 5 mm and via a psychophysical channel controlled using screen functions of the PsychToolbox (Matlab Inc).

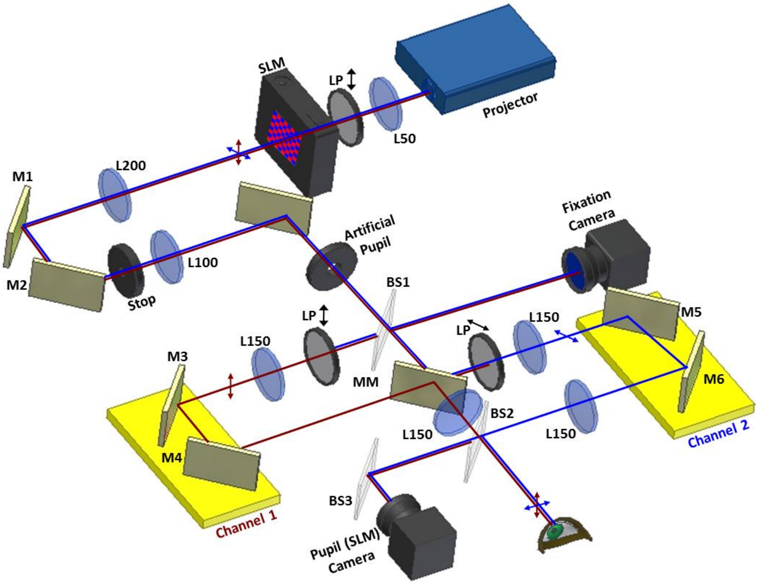

Figure 8.2: Schematic diagram of the modified Simultaneous Vision Simulator

8.2.3 Stimuli

Image of a face (100 x 100 pixels) subtending 2.06° at the retina was used in the measurements. Test images were a series of pure defocus images blurred by convolving a sharp image, to have a comparable scale for the Perceived Best Focus measured in Radhakrishnan et al. (2014). The magnitude of defocus varied from 0 to 3 D in 0.01 D steps (Fig. 8.3A). The test images were presented through the far Badal channel by displaying a white image on the SLM. Adapting images were generated by presenting a sharp image through different pupil masks in the SLM (Fig. 8.3B). During gray adaptation and sharp image adaptation, a white mask was projected at the SLM and the adapting image (gray field or sharp face) is viewed through the far Badal channel. For pure defocus and simultaneous vision adaptation, three defocus levels were tested (far channel at best focus and near addition 0.5 D, 1.5 D and 3D). For pure defocus adaptation, a black image is projected at the SLM and hence the adapting image is viewed only through the near (defocused) channel. A checker board of different white/black ratio was used to induce three different far/near ratios (25F/75N, 50F/50N, and 75F/25N). The far/near ratios correspond to the sharp/blur ratios simulated in the previous study in (Radhakrishnan et al., 2014).

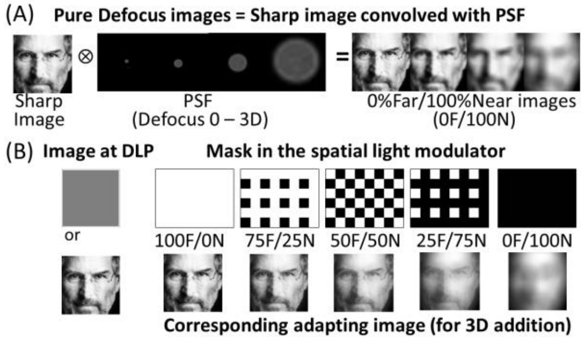

Figure 8.3: (A) Test image generation by convolution (B) Optical simulation of pure defocus and simultaneos vision images. The top panel represents the pupil mask presented through the spatial light modulator and the corresponding adaptingimages are represented in the lower panel.

8.2.4 Perceived Best Focus measurements

Perceived Best Focus was measured as described in the Radhakrishnan et al. (2014). The subject is adapted to the gray field or the adapting image for 30 s or 60 s respectively. The test images were 301 convolved PD images with defocus ranging from 0 to 3 D, in 0.01 D steps. The adapting images were a sharp image (100F/0N), PD (0F/100N) or Simultaneous Vision images (25F/75N, 50F/50N and 75F/25N) of 0.5 D, 1.5 D and 3 D near additions. In total, 13 adapting conditions were tested. The subject was presented with a gray screen (15 s) or an adapting image (60 s) was presented to the subject. The task for the subject was a single stimulus blur detection coupled with a QUEST (Quick Estimation by Sequential Testing) paradigm of threshold estimation. The subject had to report whether the images presented were blurred or sharp. The QUEST routine usually converged in less than 40 trials, where the threshold criterion was set to 75%. The 10 adapting images were presented in random order and gray adaptation measurements were repeated three times to assess consistency in measuremnets. The Perceived Best Focus was estimated as the average of the 10 last stimulus values, which oscillated around the threshold with standard deviation below 0.01 D. The results were analyzed in terms of Perceived Best Focus (expressed in Diopters). Overall the measurements lasted for 1.5 hours.

8.2.5 Data analysis

Mean comparisons (T-Test and Z-Test) were performed to study the differences in the Perceived Best Focus measurements between conditions and additions and correlations were calculated to evaluate the tendencies in perceived best focus shift.

8.3 Results

8.3.1 Perceived Best Focus following adaptation

Perceived Best Focus was measured using convolved test stimuli of Pure Defocus (similar to Radhakrishnan et al., 2014) after adaptation to optically induced Pure Defocus and Simultaneous Vision. As can be seen from figure 8.4A-D, the natural Perceived Best Focus (adaptation to gray image) varied across subjects, and correlated strongly and significantly with the RMS of residual ocular aberrations ($r=0.86, p<0.001$).

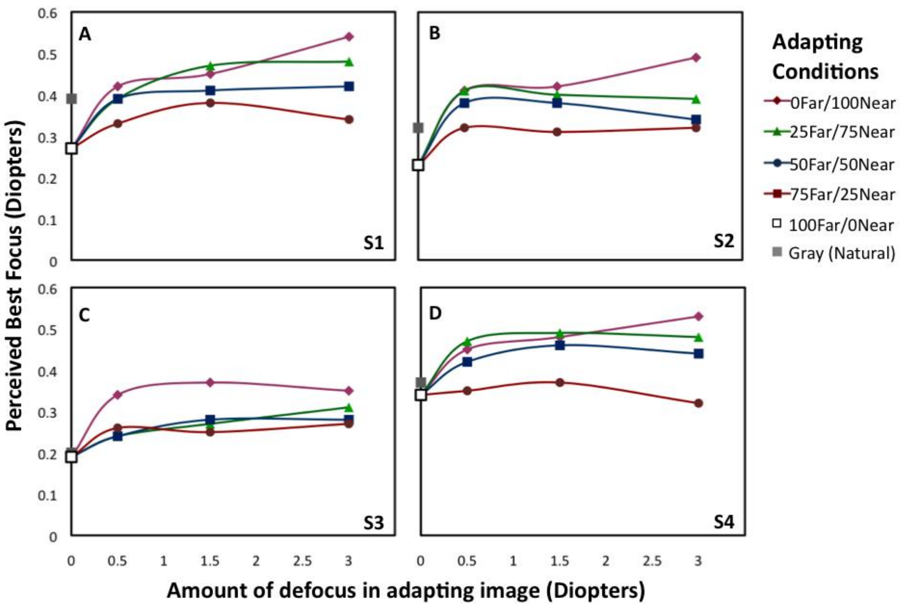

Figure 8.4: Perceived Best Focus after adaptation to optically simulated Pure Defocus and Simultaneous Vision for each subject.

The Perceived Best Focus changed after adaptation optically simulated sharp, pure defocus and pure simultaneous vision images. In subjects S3 and S4 (with high RMS), the perceived best focus after adaptation to gray image (gray squares) and a sharp image (white square) was similar in S3 and S4 ($p=0.29$). As could be seen from figure 8.4, despite intersubject differences, a similarity in trend was noted in adaptation. Largest change in Perceived Best Focus was produced by corrections focused at near (Pure Defocus images-0F/100N) and the correction with the more energy at far than near (75F/25N) produced the least changes. Subjects with higher RMS, in general showed smaller changes in Perceived Best Focus (r=-0.87, p<0.001).

8.3.2 Shift in Perceived Best Focus

Figure 8.5 shows the Perceived Best Focus Shift, calculated as the difference in Perceived Best Focus after adaptation to an adapting image and after adaptation to a sharp image. On an average across subjects, all adapting conditions produced a significant shift in the Perceived Best Focus (0.12 D±0.05, p=0.04). However, for S3, adapting to 75F/25N images produced little or no change in the Perceived Best Focus (0.006 D±0.03, p=0.83).

On an average, the shift in Perceived Best Focus increased linearly with an increase in the magnitude (near addition) and the proportion (energy ratio) of blur in the adapting image (r=0.83, p<0.001). Across subjects, a strong and significant correlation (r>0.76, p<0.005) was found between the energy distribution at near in the adapting image (percentage of near addition) and the Perceived Best Focus Shift, irrespective of the amount of near addition.

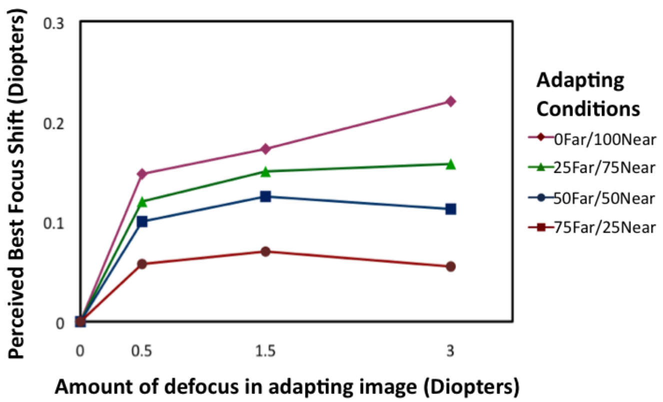

Figure 8.5: Average Perceived Best Focus shift

Pure defocus produced the largest shifts (0.18 D±0.04) in the Perceived Best Focus, on an average across subject and conditions. On an average, all the simultaneous vision conditions produced maximum shift in the Perceived Best Focus after adaptation to a near addition of 1.5 D (0.12 D±0.04) and this was significantly ($p=0.008$) higher than the shift produced by adapting to a 0.5 D (0.08±0.03).

Saturation of adaptation was defined as non-significant increase in the Perceived Best Focus shift from 1.5 D to 3 D. All simultaneous images produced a saturation of adaptation at 1.5 D addition. Unlike with convolved images, the optically simulated blur did not produce a saturation in adaptation with Pure Defocus except in one subject (S3). However, across subjects, this increase in Perceived Best Focus shift from 1.5 D to 3D (0.048 D±0.049) was barely significant ($p=0.06$).

8.4 Discussion

Previous studies on visual acuity (de Gracia et al., 2013) and perceptual performance (Radhakrishnan et al., 2014) with simultaneous vision showed a non-linear decrease in performance at intermediate and near additions respectively. This study explored the influence of several factors causing this discrepancy.

8.4.1 Optical induction vs Numerical simulation

As demonstrated with astigmatism adaptation by Ohlendorf and colleagues (2011a), we found that the visual system can tolerate better the simultaneous blur when induced optically, as shown by the maximum adaptation to 1.5 D as opposed to 0.5 D in (Radhakrishnan et al., 2014). While the previous technique ensures uniformity in the physical properties of the stimuli at the retina, current methodology is probably better in representing real-life situations with simulating multifocal corrections.

8.4.2 Ocular aberrations

In presence of ocular aberrations, larger intersubject differences were present (Fig 8.4). However, the general trend of adaptation to simultaneous vision and pure defocus was comparable to the previous study (2014). The change in perceived best focus was correlated with the level of blur-far/near energy ratio and the amount of addition (Fig 8.5) with pure defocus inducing largest adaptation.

8.4.3 Subjective task

Computer simulations by Dorronsoro et al. (2013) had shown that the optical degradation with simultaneous vision (and with pure defocus) is frequency dependent. It was assumed that the difference in the simultaneous blur causing maximum degradation has rooted from the differences in task-visual acuity in (de Gracia et al., 2013) and blur judgement in (Radhakrishnan et al., 2014)). The current experiment used subjective tasks and adapting conditions (3 far/near energy ratios) similar to Radhakrishnan et al. (2014) and optically inducing simultaneous vision similar to de Gracia et al. (2013). Yet we found the maximum degradation occurred at 1.5 D (0.13 D in Perceived Best Focus shift). It is very unlikely, that the differences in perceptual degradation is caused by subjective tasks and has likely resulted from different techniques used to simulate simultaneous blur.

8.4.4 Implications

In this study, we found that pure defocus produced almost twice as much shift in the Perceived Best Focus compared to simultaneous vision (Fig 8.5). In other words, the blur introduced by the multifocal corrections were better tolerated than blur introduced by monofocal corrections. This probably implies that patients already adapted to blur (presbyopes or eyes with cataract), can adapt to the simultaneous vision better. Also, we found maximum blur perception (shift in the Perceived Best Focus) for intermediate additions (1.5 D). While this is not the conventional near addition in the commercial IOLs, it should be taken into consideration while customizing the multifocal prescription to a lower addition ranges.

Finally, we have presented a methodology that allows for studying neural adaptation by optically inducing different levels of simultaneous blur (or pure defocus). While in this study, we have studied only adaptation to pure simultaneous vision, this instrument has been demonstrated to be capable of generating any bifocal design (Dorronsoro et al., 2015) and has a greater scope for evaluating not only visual performance, but also neural adaptation to segmented bifocal corrections. This instrument, could in fact be considered the rudimentary version of much evolved multifocal visual simulators, combining phase masks and adaptive optics (Vinas et al., 2015) or portable, open-field simulators simulating pure bifocal or multifocal corrections using temporal multiplexing (Dorronsoro et al., 2015).

8.5 Conclusion

We have demonstrated for the first time, adaptation to optically induced simultaneous vision of different far/near energy, in same subjects, using a modified simultaneous vision simulator. Our results suggest that a simultaneous vision optically simulated is tolerated better and the general trend in adaptation to simultaneous vision is unaffected by methodological differences between the current study and previous studies.

Chapter NINE

Visual and perceptual performance with see-through, portable Simultaneous Vision Simulator

The predominant choice for treatment of presbyopia still revolves around conventional techniques like bifocal or progressive spectacle lenses providing an alternating vision. Simultaneous vision corrections are increasingly becoming the preferred correction, inspired by the availability of various designs of bifocal or multifocal contact lenses and intraocular lenses. A clinical tool to demonstrate simultaneous vision to subjects will provide realistic expectations following surgery. We developed a see-through, hand-held, miniaturized simultaneous vision simulator and assessed visual and perceptual performance in subjects with simulated presbyopia.

This chapter is based on the paper by Dorronsoro et al., titled "Portable simultaneous vision device to simulate multifocal corrections" *(Submitted)*.

The co-authors of the chapter Carlos Dorronsoro, Jose-Ramon Alonso designed the miniaturized system. The author of this thesis was involved in design, calibration and validation of the tunable lens. The programming of the tunable lens was done by

Daniel Pascual. The author of this thesis designed and performed the measurements on human eyes, and analyzed the data in collaboration with the co-authors.

This work was presented at the Association for Research in Vision and Ophthalmology (ARVO) annual meeting (May 2015) in Denver, Colorado, USA as poster, at the International Society of Presbyopia Conference, (September 2015) in Barcelona, Spain, and at the International OSA Network of student meeting (September 2015) in Valencia, Spain as oral contributions.

9.1 Introduction

There is an increasing proportion of presbyopes in the population demanding treatments that provides a comfortable vision at all distances. An increasingly used solution for presbyopia is multifocal optics, using diffractive or refractive profiles, resulting in bifocal, trifocal and extended-depth-of-focus designs. These corrections, generally delivered in the form of contact lenses, intraocular lenses or corneal laser ablation patterns, produce a retinal image that has superimposed blurred and sharp images at all distances. Most clinical studies are limited to reports of visual acuity or contrast sensitivity in patients with multifocal corrections measured at different distances, or patient satisfaction questionnaires, generally aiming at finding to what extent near vision is improved without compromising distance vision, when compared to a monofocal lens (Bellucci, 2005, Cillino et al., 2008, Cochener et al., 2011, Kim et al., 2011, Llorente-Guillemot et al., 2012).

Visual simulators of multifocal corrections allow undertaking systematic studies of visual performance with multiple lens designs, which can be directly compared by the patient. These simulators work by projecting the equivalent phase maps of a multifocal lens non-invasively onto the patient's pupil plane. Most visual simulators are based on adaptive optics elements, for example deformable mirrors or spatial light modulators (Fernandez et al., 2009, Schwarz et al., 2011, Canovas et al., 2014, Vinas et al., 2015). The systems can operate in a closed loop i.e., a wavefront sensor continuously monitors the aimed combined wave aberration of the eye and correction, and the actuators of a deformable mirror respond to maintain this correction) or statically i.e. a given correction is programmed in a pixelated reflective phase-only spatial light modulator (Vinas et al., 2015). Visual stimuli are generally projected in a display in the system, allowing the subject to perform psychophysical tasks under the programmed corrections (Sawides et al., 2011a, Sawides et al., 2011b, Sawides et al., 2012).

We have recently presented two-channel visual simulators for simulation of bifocal corrections. These systems use two channels, one focused at far and the other one focused at near are combined at the pupil plane, for simulating a pure simultaneous vision correction (de Gracia et al., 2013b) or in combination with a transmission spatial light modulator and polarizers, simulate refractive corrections of different pupillary pattern distributions for near and far. A study investigating systematically the effect of the magnitude of the near addition on visual acuity revealed that intermediate additions (around 2 D) deteriorated far vision more than lower or higher additions (de Gracia et al., 2013b). Corrections with different distributions of near and far regions across the pupil resulted in different visual performance in the same patient, indicating that not all corrections (even with the same addition and energy ratio for far are near) are perceptually similar (Dorronsoro et al., 2015). Furthermore, best perceived quality with an angularly segmented bifocal design is biased by the actual orientation in which the lens is placed, likely affected by the actual combination of the correction and the patient's optics (Radhakrishnan et al., 2016). Using visual simulators, we also found that subjects can adapt to bifocal corrections (Radhakrishnan et al., 2014).

While current visual simulators allow rapid simulation of several multifocal corrections, allowing the same patient to compare across designs, the use of current devices is mostly limited to experimental environments, given their relatively high dimensions. In addition, they are not designed to allow one experience the real world through the simulated multifocal correction, but rather small (typically <2 deg) visual field projections. Visual simulators have proved efficient tools for understanding multifocal vision and to help in the design of new multifocal profiles. However, they hold great promise as a clinical tool in the daily cataract surgery or contactology practice where clinicians and patients face the decision of opting for a multifocal correction. These systems offer the possibility of testing a lens design before it is implanted, or narrowing down the contact lens of choice in a generally lengthy trial and error procedure.

In this study, we developed a hand-held, see-through, portable simultaneous vision simulator, based on a novel temporal multiplexing approach, using electronically tunable lenses, and validated the use of this device in simulation of different multifocal lens profiles. The device was tested on subjects, who performed visual acuity, perceptual scoring and perceptual performance tasks under simulated monofocal, bifocal and trifocal simultaneous vision corrections.

9.2 Methods

9.2.1 Portable Simultaneous Vision Simulator

A hand-held simultaneous vision simulator was developed, whose active component is an optomechanically tunable lens (EL-10-30, Optotune Inc, Switzerland), working in temporal multiplexing. Figure 9.1A shows a schematic diagram of the system. The image formed by the tunable lens (TL) is conjugated with the subjects' pupil using a pair of achromatic doublets (75 mm EFL). Two pairs of mirrors (M3-M6, Fig. 9.1A) emulate two porro prisms to project upright images on the subjects' retina in a 14 degree visual field and M1, M2 are used to place the image in the line of sight of the viewer. Figure 9.1B shows the photo of the working prototype and the same being used by a patient (Fig. 9.1C). The tunable lens was controlled by a custom-developed electronic driver programmed in C++ that varied the voltage between 0 and 5 at 45 KHz, and induced an optical power shift in a range of -1.50 D to +6 D. The temporal pattern of the variation defined the through-focus energy profile of the lens. Multifocality is simulated by rapidly varying the optical states of the lens, controlling the state of the lens (focus position) and the amount of time the lens remains in any given state (energy dedicated to a particular focus). For example, a 70%Far and 30%Near bifocal lens is simulated by inducing two optical states in a 20 ms time period, with the far state induced for 14 ms and the near state for 6 ms in a pattern, and is repeated over time.

9.2.2 Calibrations

The voltage-diopter reciprocity of the tunable lens was characterized by imaging a standard ETDRS visual acuity chart (Early Treatment Diabetic Retinopathy Study chart) placed at distance of 3 m, through the tunable lens and a Badal system, by a CCD camera with a high numerical aperture objective focused at infinity. Defocus introduced by the Badal system (each 0.25 D) were compensated by changing the voltage of the tunable lens.

The optical aberrations induced by the tunable lens in different focus positions was measured using a Hartmann-Shack wavefront sensor incorporated in VioBio adaptive optics system (Marcos et al., 2008, Gambra et al., 2009). The tunable lens was placed (vertically) at a conjugate pupil plane of the system and the change in the Zernike coefficients with change in defocus was documented.

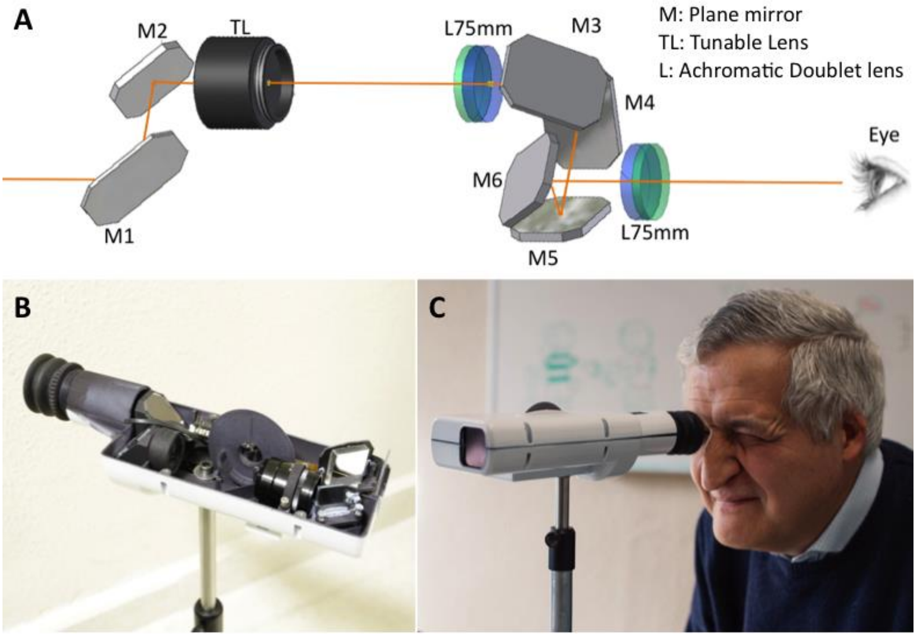

Figure 9.1: (A) Schematic of miniaturized simultaneous vision simulator. The image formed by the tunable lens (TL) is projected on to the eye using a pair of achromatic doublets of 75 mm EFL. M1, M2 are used to align the optical axis of the device with line of sight. Mirrors M3-M6 function as two porro prisms for image re-erection. (B) SimVis Mini prototype showing principal components (C) Subject viewing through SimVis Mini.

The ability of the tunable lens to represent bifocal and trifocal optical designs was tested using a custom-developed high-speed focimeter, based on laser ray tracing (Birkenfeld et al., 2014). A ring-shaped beam of 8 rays, generated by a 2 mirror galvanometer deflecting a laser beam (one ray traced every 1.25 ms) was imaged through monofocal, bifocal and trifocal states of the tunable lens, using a CCD camera with adjustable exposure time. All optical calibrations were performed with a fixed pupil diameter of 6 mm, obtained with a diaphragm placed next to the tunable lens.

9.2.3 Simulated lenses

Three monofocal, two bifocal and two trifocal corrections were simulated using the simultaneous vision simulator. The monofocal corrections were 100%Far (100F), 100%Intermediate (100I) and 100%Near (100N); the bifocal corrections were 50%Far/50%Near (50F/50N) and 70%Far/30%Near (70F/30N); and the trifocal corrections assessed were 33%Far/33%Intermediate/33%Near (33F/33I/33N) and 50%Far/20%Intermediate/30%Near (50F/20I/30N). For all subjects, the far distance focus was set to their best subjective focus (which corrected their spherical refractive error) determined by a bracketing technique. The intermediate focus was set to +1.5 D, and the near focus was set to +3 D.

9.2.4 Visual scenes

For visual acuity measurements, a visual acuity chart displayed using an iPAD (Figure 9.2A) with retina display (maximum luminance 119 cd/m^2, 264 ppi, 9.7") was placed at the different distances. A real visual scene was simulated in a laboratory environment, with targets at far (4 m), intermediate (66 cm) and near (33cm) distances for perceptual measurements. The visual scene consisted of a poster of a landscape (subtending 4 degrees at the retina) and a high contrast letter (logMAR 1) at far, covering the upper right quarter of the visual field, a laptop with high contrast text (retinal subtense of 4 degrees) at intermediate distance (maximum luminance 117cd/m^2, 116 ppi, 13.3") covering the upper left quadrant and a mobile phone with the same high contrast text (maximum luminance 128 cd/m^2, 342 ppi, 4.3") covering the inferior zone (6 degrees retinal subtense) at near distances. For near and intermediate distance the same continuous text of non-serif letters was used and the size of the letters at near was 14pt and at intermediate distance it was 18pt. In total, 30% of the visual scene was dedicated for far vision, 30% for intermediate vision and 40% near vision (Fig. 9.2B).

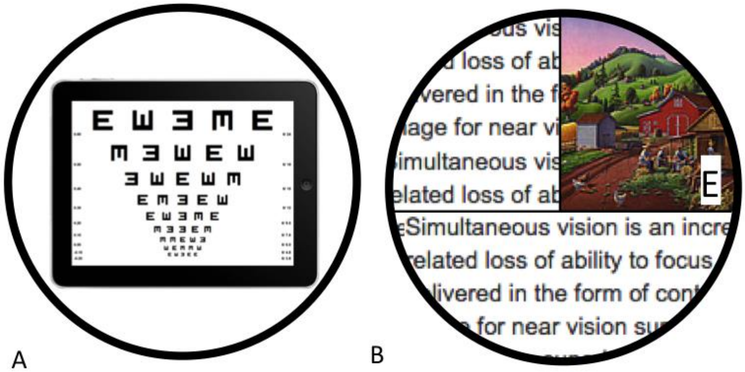

Figure 9.2: (A) Visual acuity measurements using commercial software application displayed in a HD display tablet (B) Perceptual preference measurements using visual scene with landscape for far and a high contrast text for intermediate and near distances.

9.2.5 *Subjects*

Measurements were performed on 9 subjects, with age range 20 to 62 years. In all subjects (except one presbyope), presbyopia was pharmacologically simulated by instilling one drop of 1% tropicamide 3 times, from 15 minutes prior to measurements and maintained by hourly instillation. The experimental session lasted 2 hours. Mean spherical refractive error ranged from -5.50 D to +2.75 D. None of the subjects had astigmatism > 1 D. The experiments conformed to the tenets of the Declaration of Helsinki, with protocols approved by the Consejo Superior de Investigaciones Científicas Ethics Committee. All participants provided written informed consent.

9.2.6 *Visual acuity measurements*

LogMAR visual acuity was evaluated at all distances under the simulated corrections using a commercial software application (Fast acuity XL, Kybervision Inc) controlled using and displayed in the portable HD display device described above. Tumbling E letters at four orientations were displayed (Fig. 9.2A) and the visual acuity was measured as the smallest size of letters that could be resolved by the subjects. Visual acuity was assessed at the three distances in random order. The geometric mean was used to calculate averages of visual acuities across subjects (Holladay, 1997).

9.2.7 Perceptual scoring measurements

The perceived image quality of the global visual scene (overall score) and at far, intermediate, near distances was judged by the subject using a perceptual scoring technique (Radhakrishnan et al., 2014). The subject viewed the visual scene (Fig. 9.2B) through each optical correction presented in random order. For each presentation, the subject scored the visual scene from very blurred (score 0) to very sharp (score 5). The measurements were repeated three times and the average score was calculated for each refractive option induced at a given distance.

9.2.8 Preference measurements

The preference to a specific simultaneous vision correction was tested using a 2-AFC (Pelli and Farell, 1995, Ehrenstein and Ehrenstein, 1999) in pairwise comparisons between corrections. Subjects viewed the visual scene for 5 seconds through a correction and subsequently viewed the same scene through another correction for 5 seconds. The six combinations of the two bifocal and two trifocal corrections (50F/50N, 70F/30N, 33F/33I/33N and 50F/20I/30N) were tested in random order. The chosen correction of the pair was given a score of +1 and the other correction in the pair was given a score of -1. The measurements were repeated 10 times and the sum score was calculated for each correction. For testing the significance of the preference of a given correction, a Bernoulli cumulative distribution function statistics was used (assuming random choices), with a significance level of 0.05 (Yates and Goodman, 2005). Any score greater than +10 (out of +30 possible) indicates significant preference and -10 indicates (out of -30) significant rejection.

9.3 Results

9.3.1 Optical measurements in the portable Simultaneous Vision device

As shown in figure 9.3A, the voltage and defocus induced show an almost linear relationship (within the 0.25 diopter step used in the induction). A voltage increment around 0.5 V is needed in the tunable lens, to compensate for each diopter of defocus induced with the Badal channel.

As expected, aberrations of the tunable lens increased with an increase in the power, as shown in figure 9.3B. Solid symbols stand for horizontal aberrations while empty symbols stand for vertical aberrations. Vertical aberrations could be accounted for by the asymmetric effect of gravity on the membrane in vertical position of the lens and therefore on the wavefront. The change in root mean square of astigmatism and other higher order terms were clinically irrelevant within a range of 5 D induced defocus (<0.05 microns for 6 mm pupils, equivalent to the repeatability of wavefront measurements on real eyes). The subsequent measurements on real eyes were performed with 5 mm pupils, and 3 D additions.

Figure 9.3C shows laser spots at the CCD camera of the high speed focimeter, corresponding to the rays traced through the tunable lens. The simulated monofocal corrections for far vision (top-left quadrant) and for near vision (top-right quadrant) direct the rays to different positions (outer and inner dotted circles, respectively). The power of the lens is proportional to the ring diameter. Bifocal (bottom-right) and trifocal (bottom-left) corrections produce the same diameters (dotted circles), indicating a similar optical power induced in static and dynamic regimes. Moreover, when the bifocal correction is observed at long exposure times, two clearly separated spots are seen (with no light in between them) indicating that the transition between one foci and the other is quick enough, and no energy loss is captured by the camera. At very short exposure times (and high power in the laser) the camera captures either one spot (corresponding to one foci) or the other, with a transition time limited to less than 1 ms.

A visual inspection through the portable simultaneous vision simulator confirmed that the temporal multiplexing was fast enough to produce temporal fusion, and that all the simulated lenses produced images of the visual scene with a static appearance in the retina, without flicker or oscillations.

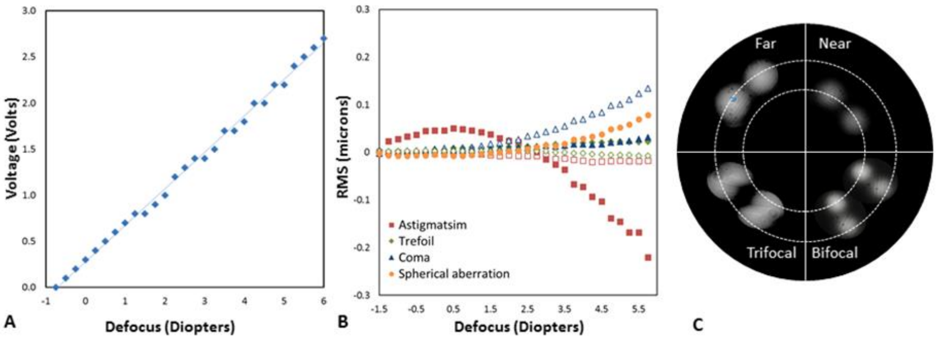

Figure 9.3: (A) Voltage vs induced defocus. (B) Measured lower and higher order aberrations (RMS in microns) with induced defocus. Solid symbols stand for horizontal aberrations while empty symbols stand for vertical aberrations. (C) Laser spots at the CCD camera of the high speed focimeter, corresponding to monofocal and multifocal corrections. Outer circle stand for far vision optical power. Inner circle stand for near vision optical power. See text for details.

9.3.2 Visual acuity with simulated multifocal corrections

Figure 9.4A shows the logMAR visual acuity at far vs at near, averaged across subjects (N=9). The size of the bubbles represents the intermediate visual acuity. Each color represents a different simulated correction. There is a linear change in visual acuity for far and near across the designs. As the percentage of energy at far increased for a given design (the extreme being a monofocal design focused at far, 100F), visual acuity increased at far ($r=-0.96$, $p<0.0001$) and decreased at near ($r=0.76$, $p<0.0001$) linearly. Figure 9.4B represents the range of visual acuity for far-to-near, for each design, with the green square representing visual acuity at intermediate distance. Monofocal corrections (100F and 100N) provide good visual acuity when in focus (mean logMAR 0.015±0.03) with compromised visual acuity at the non-focused distance (mean logMAR VA 0.51±0.23). On the other hand, the monofocal intermediate correction (100I) and the simultaneous vision corrections provided moderate visual acuity at all distances. Among these corrections, the multifocal benefit calculated as the average of visual acuity at the three distances was highest for 100I (logMAR VA 0.12±0.04). The multifocal corrections 50F/50N, 70F/30N, 33F/33I/33N and 50F/20I/30N had an average multifocal benefit of logMAR 0.27±0.05, 0.3±0.09, 0.27±0.08 and 0.25±0.05 respectively.

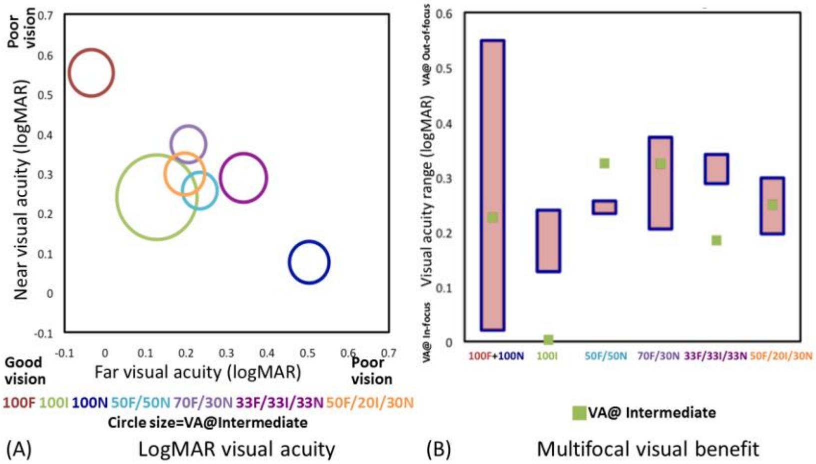

Figure 9.4: (A) LogMAR visual acuity at far vs near with different monofocal and multifocal corrections, averaged across 9 subjects. Each color represents a different correction. The size of the bubble represents VA at intermediate distance; (B) Range of visual acuity for far and near with different monofocal and multifocal corrections, averaged across 9 subjects. Green squares represent Visual Acuity at Intermediate distance.

9.3.3 Perceptual Score of multifocal corrections

The average perceptual score varied systematically across designs (Fig. 9.5A). The perceived quality at far or near correlated significantly and strongly with the percentage of energy devoted to far or near in each correction ($r=0.92$, $p<0.0001$). The overall perceptual score correlated significantly with the intermediate ($r=0.65$, $p<0.0001$) and far ($r=0.51$, $p<0.001$) perceptual scores, but not with the near perceptual score ($r=-0.07$, $p=0.57$). On average, the overall perceptual score was maximum for the 100I correction (score 3.5±0.6) among the monofocal corrections, and was maximum for 50F/20I/30N (score 2.7±0.6) among the multifocal corrections. Figure 9.5B shows the perceptual scores for individual subjects for the monofocal corrections (red, green and blue bubbles represent far, intermediate and near corrections). For 100F, the perceptual score was 5 in all subjects at far, but for the same correction at near it ranged from 0 to 3. Similarly, perceptual score for 100N ranged from 4 to 5 at near and at far it ranged from 0 to 3. Monofocal intermediate correction showed the largest range of perceptual scores across subjects at far (1.7 to 3.3) and near (1.3 to 5) distances, indicating large intersubject variability in the responses. On the other hand, the multifocal corrections (Fig. 9.5C) had similar range of perceptual score at far and near distances. Specifically, the 50F/20I/30N showed the narrowest range at far (2 to 4) and 33F/33I/33N had the smallest range at near (2.1 to 4.3).

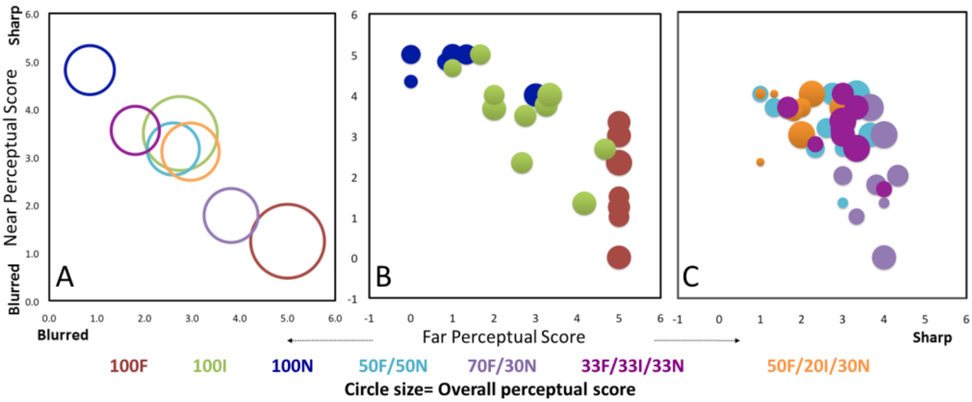

Figure 9.5: Perceptual score at far and near distances. Bubble size indicates overall score. (A) Average across subjects for all corrections. (B) For monofocal corrections in all subjects. (C) For simultaneous vision corrections in all subjects.

9.3.4 *Preference results*

Preference maps (Fig. 9.6) were generated to identify significant preferences in each pairwise comparison, for simultaneous vision corrections. Assuming Bernoulli's distribution, green dots indicate that the design indicated in the right label (vertical axis) was preferred significantly over the one in the lower label (HORIZONTAL AXIS) and a red dot indicates that the design indicated in the right label was significantly rejected compared to the one in the lower label. Gray dots indicate non-significant preferences. When the pooled responses from all subjects are considered simultaneously (marked as 'Average' preference map in figure 9.6), 50F/20I/30N was preferred significantly over other designs. However, as shown in figure 9.6, preference maps from individual subjects clearly shows high inter-subject variability and are different to the average trend.

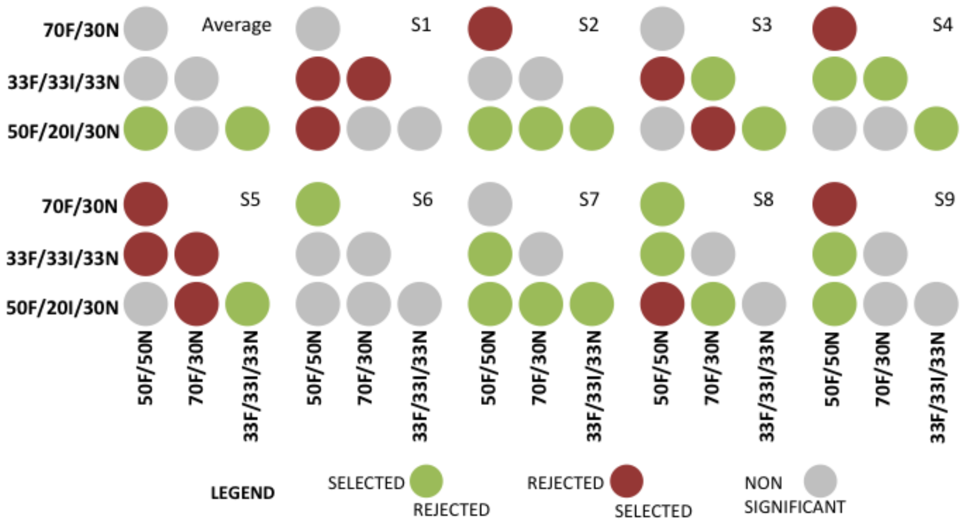

Figure 9.6: Preference maps for simultaneous vision corrections. Green dot indicates that the design indicated in vertical axis (right label) was preferred significantly over the one in the horizontal axis (lower label) and a red dot indicates that the design indicated in the right label was significantly rejected compared to the one in the lower label. Gray dots indicate non-significant preferences.

9.4 Discussion

The frequency of choosing a multifocal correction as a treatment of presbyopia, as well as the number of designs commercially available, is rapidly increasing. However, how the world looks like through a multifocal correction is not easy to imagine. Clinicians often fail at offering a multifocal solution to a patient if they subjectively believe that the patient may not be satisfied post-operatively, or from prior experience of unsatisfied patients following multifocal IOL implantations. Contact lens specialists often rely on a trial and error approach, trying multiple contact lens designs until the optimal solution is identified. We have presented a novel portable through-focus simultaneous vision simulator that allows experiencing the real world through realistic optical simulations of multifocal corrections. The system holds promise as a tool to help selecting the optimal treatment for the patient.

9.4.1 Visual and perceptual quality with Monofocal corrections

In our study, we evaluated visual acuity and perceived visual quality with monofocal designs at far, intermediate and near distances. Both metrics varied similarly across conditions. As expected, the monofocal corrections at far and at near provided the maximum quality for the corresponding distance in focus and reduced drastically the visual acuity at the other distance. The monofocal intermediate correction decreased far and near visual acuity, though to a lesser extent, and provided an acceptable intermediate vision. This result agrees with reports in eyes implanted with monofocal and multifocal IOLs (Cillino et al., 2008, Cochener et al., 2011, Llorente-Guillemot et al., 2012). In fact, monofocal lenses outperformed multifocal designs both at far and intermediate, although not at near. However the higher intersubject variability performance with monofocal designs focused at intermediate distance suggests that, while this may be a possible approach to treat presbyopia in some subjects, this is not by any means optimal for all subjects.

9.4.2 Visual and perceptual quality with simultaneous vision corrections

We evaluated visual acuity and perceived visual quality with two bifocal and two trifocal designs that had equal energy distribution across distances or had larger energy dedicated for far. The multifocal visual benefit was, on an average, 1.1 times higher with the multifocal corrections than monofocal corrections at far or near. Trifocal corrections provided, as expected, higher visual acuity at the intermediate distance compared to bifocal corrections. On average, the bifocal correction with equal energy between far and near and the far dominant trifocal correction provided better overall performance than the other lenses. Thus both visual acuity and perceptual score vary across subjects as expected from the optical principles of each design. However, the overall perceptual scores for both monofocal and multifocal corrections varied over a wide range (from 4.8–1) across subjects. These perceptual differences in responses found across subjects (Fig. 9.5B,C) are likely due to intersubject differences in the optics, neural processing or due to differences in visual needs.

9.4.3 Pattern preferences to simultaneous vision corrections

Direct comparisons of each multifocal design against others revealed general trends, as well as statistically significant differences across subjects. As a general trend, the trifocal design that was far dominant (50F/20I/30N) was preferred over other simultaneous designs. On the other hand a trifocal design that provided very low energy at far (33F/33I/33N) compared to the other designs was systematically rejected by the subjects. A bifocal 50F/50N design produced in general better visual response than other configurations, although specific preferences/rejections were highly subject-dependent. While the visual scene was constructed to represent a realistic environment at different distances, it is true that the frequency content and the distribution of targets at each distance may have somewhat influenced the results, and responses may have differed with a different visual scene. Those changes may reflect different visual needs across subjects depending on their activity and the related near/intermediate/far content (Bellucci, 2005).

9.4.4 Inter-subject differences in preference

We found large inter-subject variability in the preferences across lens designs, with each subject revealing a different preference pattern (Fig. 9.6). While the overall energy in the corrections was the same across the designs, the perceptual blur reported was undeniably different across subjects, due to the different through focus energy distribution profile of each design, interactions between the native aberrations and the lens design, and likely, due to different blur tolerances across individuals. Besides modifying the near add (de Gracia et al., 2013a) or the balance distribution for near/intermediate/far, it is conceivable to customize the lens design to the patient preference, or at least consider the patient's preference when selecting the optimal lens.

9.4.5 Implications

Most studies in the literature report (Bellucci, 2005, Llorente-Guillemot et al., 2012) visual function measurements in eyes already implanted with a given lens design. Visual simulators allow testing multiple designs on the same eye, and identifying the optimal selection. A number of bench prototypes and commercial visual simulators are available based on various optical principles. To our knowledge, this is the only simulator that is based on temporal multiplexing, and that providing a programmable through-focus open-field simulation. Most adaptive optics instruments reported in the literature are either on-bench (Yoon and Williams, 2002, Guo et al., 2008, Dorronsoro and Marcos, 2009, de Gracia et al., 2013b) or are limited to simulating only one design at a time or visual tests are displayed in a small-field display (not open view) (Schwarz et al., 2011, Canovas et al., 2014, Pujol et al., 2014).

The opportunity of simulating commercially available lens designs using a portable see-through device opens the possibility of easily transferring this tool to the clinic to help identifying the optimal correction.

9.4.6 Limitations and future prospects

The miniaturized simultaneous vision simulator described here simulates a multifocal correction by temporal multiplexing. This rapidly and effectively reproduces any through-focus energy profile and the measurements are found to be repeatable. These can also reproduce haloes associated with multifocal corrections. However, this technique fails to simulate diffractive effects caused by the concentric rings in the diffractive IOLs or the spatial distribution of the refractive designs. Yet, our results demonstrate that the visual and perceptual outcomes are primarily affected by the far/near energy distribution, hence making the system useful as a screening tool. Some of these disadvantages can be addressed to some extent by using phase plates or incorporating light modulators used in on-bench prototypes (Dorronsoro et al., 2015, Vinas et al., 2015), to simulate specific effects. In addition, the system can be expanded to a binocular device by replicating a second channel for the contralateral eye. Such a system could simulate not only monocular multifocal corrections, but also other presbyopia correction alternatives such as monovision and modified monovision, which involve different corrections in each eye.

9.5 Conclusion

The visual and perceptual performances are affected to a great extent by the far/near energy ratio. Our results show clear inter-subject differences in perceptual preference of simultaneous vision correction. The hand-held Simultaneous Vision Simulator based on temporal multiplexing is an effective tool to optically simulate multifocal corrections. Clinical implementation of this technique can make practice of multifocal prescription evidence-based by assessing subjective needs and preferences prior to invasive intervention.

Chapter TEN

Perception of presbyopic corrections simulated using miniaturized, binocular, open-field vision simulator

Simultaneous vision, monovision and modified monovision corrections are replacing more conventional alternating vision corrections as the treatment option for presbyopia. While multifocal corrections induce complex retinal image blur, monovision corrections induces differences in blur between eyes. The choice of treatment is more clinician dependent and less evidence based. We developed a prototype of portable, see-through, binocular vision simulator and assessed perceptual performance with different combinations of presbyopia corrections, based on temporal multiplexing, including monovision and modified monovision.

The coauthors of this chapter are Carlos Dorronoso, Daniel Pascual and Susana Marcos, The programming of the tunable lens was done by Daniel Pascual. The author of this thesis designed, calibrated and validated the instrument, and performed measurements in human eyes and analyzed the data in collaboration with the co-authors.

This work has been accepted for presentation at the Association for Research in Vision and Ophthalmology (ARVO) annual meeting (May 2016) in Seattle, Washington, USA as an oral presentation.

10.1 Introduction

Presbyopia is the inability to accommodate in the aging eye, resulting in blurred near vision (Glasser and Campbell, 1998). It is estimated that around 1.04 billion people are affected globally (Holden et al., 2008). Alternating vision solutions are the most common treatments for presbyopia, where an additional correction at near (near addition) is provided over far vision correction (Charman, 2014a). Gaze-dependent alternating vision solutions are being replaced by multitude of newer options such as monovision, modified monovision and simultaneous vision corrections (Charman, 2014a, b), aimed at providing clear vision at all distances.

Simultaneous vision corrections are spectacle independent, multifocal optical solutions delivered in the form of contact lenses and IOLs, which result in superimposition of blurred and sharp images at the retina at all distances (Charman, 2014b). Several clinical studies report that these lenses provide a reasonable visual quality at all distances and cause hardly any binocular disparities (Glasser, 2008, Lichtinger and Rootman, 2012, Llorente-Guillemot et al., 2012). Visual acuity and contrast sensitivity at far distance with a multifocal lens, is moderately degraded compared to a monofocal correction, but is better at near distance (Bellucci, 2005, Cillino et al., 2008, Cochener et al., 2011, Kim et al., 2011, de Gracia et al., 2013). Even though few studies show that subjects adapt to these simultaneous vision corrections (Kaymak et al., 2008, Radhakrishnan et al., 2014), functional vision and subjective tolerance is reduced due to haloes (Yamauchi et al., 2013) and may even result in lens explantation (Kamiya et al., 2014, van der Mooren et al., 2015). The subjective symptoms can be addressed to a large extent by demonstrating to patients, preoperatively, vision with multifocal corrections.

Few of the visual simulators that are available for simulating multifocal vision are on-bench prototypes (Dorronsoro and Marcos, 2009, de Gracia et al., 2013, Vinas et al., 2015), have limited field of view (Schwarz et al., 2011, Canovas et al., 2014) or are monocular (Dorronsoro et al., 2013, Dorronsoro et al., 2015). It has been demonstrated that the visual performance with simultaneous vision is dependent both on the optical properties of the lens - amount of near addition (de Gracia et al., 2013), pupillary distribution (Dorronsoro et al., 2014, Vinas et al., 2015) and energy at far (Dorronsoro et al., 2015).

On the other hand, monovision and modified monovision corrections are popular treatment options that needs binocular consideration. In these correction techniques the dominant eye is corrected for far vision and the non-dominant eye is corrected for near vision (Garland, 1987, Johannsdottir and Stelmach, 2001, Evans, 2007). The main disadvantage of this type of correction is the large disparity in visual quality introduced between eyes. In an attempt to reduce the binocular consequences, modified monovision treatments are attempted making the dominant eye slightly myopic and the non-dominant eye is made slightly hyperopic, suggesting that the depth of focus compensates for the induced visual deficits (Schor et al., 1987, Collins and Goode, 1994, Wright et al., 1999). In modified monovision corrections, one of the eyes is corrected for far (usually the dominant eye) and the contralateral eye is provided with a non-monofocal options (Fisher, 1997). Contrast sensitivity, high contrast visual acuity and binocular functions were found to normal in presbyopic subjects with monovision given in spectacles and modified monovision with multifocal contact lenses (Fisher, 1997). Some studies also reported that pre-presbyopes adapted easily to monovision corrections than presbyopes (Johannsdottir and Stelmach, 2001). However, monovision corrections have several disadvantages, despite the professed visual advantages, including decreased binocular visual acuity in high illumination, decrease in stereo acuity from 36-62 arc seconds depending on subjects' ability to adapt and decrease in binocular contrast sensitivity, especially at high spatial frequency range (Kohnen, 2008).

In this study we present a new prototype of binocular, open-field vision simulator suitable for clinical applications, based on temporal multiplexing, that can be used to simulate different binocular presbyopic corrections. The prototype was used to study the perceptual performance in subjects through binocular combinations monofocal, bifocal, trifocal, monovision and modified monovision corrections.

10.2 Methods

10.2.1 Setup: Binocular simulator for Presbyopic corrections

The prototype of binocular vision simulator (Fig. 10.1A) was developed as two identical optical channels similar to the monocular prototype (Dorronsoro et al., 2013, Dorronsoro et al., 2015). The optical channels are rectilinear, with a tunable lens (EL-10-30-C, Optotune Inc, Switzerland), projection lenses and an erecting prism, mounted using adjustable tube mounts, which made the system more compact than the monocular prototype. Both the tunable lenses (of each channel) were controlled by a single driver and synchronized with a custom developed software in Visual C. The image formed by the tunable lens is conjugated with the subjects' pupil using a pair of achromatic doublets of 50 mm EFL providing a visual field of 20 degrees. A Schmidt-Pechan prism (combination of roof prism and half penta-prism with an air interface) rendered the image erect (horizontally and vertically) and aligned with the visual axis. The use of this prism limited the effective visual field to 12 degrees, however, did not affect the overall contrast. A diaphragm placed next to the tunable lens acted as artificial pupil.

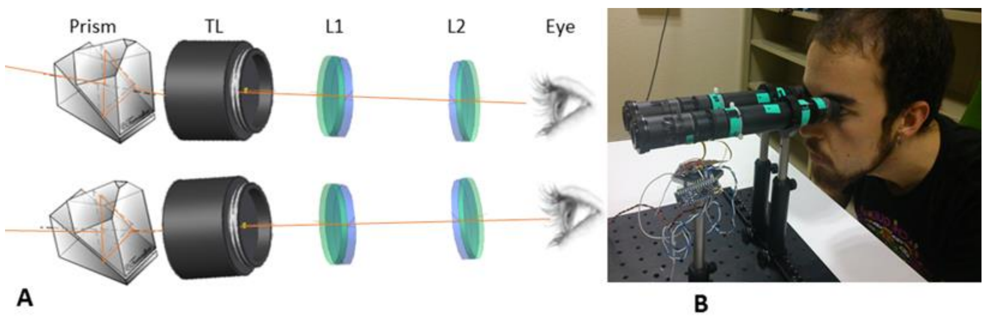

Figure 10.1: (A) Schematic diagram of the binocular vision simulator. L1 and L2 are 50mm EFL used for placing the eye at the conjugate foci of the tunable lens (TL). A Schmidt-Pechan prism is used for image re-inversion (B) Image of a subject viewing through the system

The calibration of the tunable lens was performed as described in Dorronsoro et al. (2015). The optical positions were fine-tuned and equal magnification through each channel were verified using a CCD camera placed at the focal length of a collimator and imaging objects at infinity (>1 km) through the system. The two channels are mounted on a graduated rail that helped in measuring the inter-pupillary distance and could be moved about y-axis. Figure 10.1B shows a subject viewing through the binocular system.

10.2.2 Presbyopic corrections simulated

Psychophysical measurements were performed under simulated binocular presbyopic corrections. Binocularly symmetric corrections included monofocal correction in both channels at far, intermediate and near distances (F+F, I+I, N+N respectively). For monofocal corrections, tunable lens was placed at a static focus of 0 D (for far), +1.5 D (for intermediate) and +3 D (for near). Binocular simultaneous vision correction were induced by multiplexing both the tunable lens at different focus states. It included, bifocal correction with 50%Far/50%Near (2SV+2SV), trifocal correction with 50%Far/20%Intermediate/30%Near (3SV+3SV) energy distributions in both channels, and combinations of bifocal and trifocal (2SV+3SV, 3SV+2SV) in either of the channels.

Monovision was simulated by focusing one channel at far and the other at near (F+N). Modified monovision corrections were induced by setting a monofocal focus at far or near in one channel and setting a simultaneous vision correction in the other channel (F+2SV, F+3SV, 2SV+N and 3SV+N). For psychophysical measurements a visual scene was created with a poster and a high contrast target at far (4m), a laptop at intermediate (66 cm) and a smartphone at near (33cm) distances as in the previous study (Dorronsoro et al., 2015).

10.2.3 Subjects

Eight subjects, with age range 23 to 45 years, participated in the measurements. Presbyopia was induced in both eyes by instilling 1% tropicamide 3 times, 15 minutes prior to measurements. The pupil diameter was set to 5 mm to limit the aberrations of the tunable lens and to provide uniform pupil size across subjects.

None of the subjects had astigmatism > 1 D and the spherical refractive error ranged from 0 D to -6 D. Two subjects performed measurements wearing contact lenses and all subjects except one (S#5) had prior experience in performing psychophysical measurements. The measurements were approved by the Institutional review board of CSIC and met the tenets of Declaration of Helsinki. All subjects provided a written informed consent

Ocular dominance was assessed using Miles test (Roth et al., 2002). Binocular fusion, through two channels, was tested and adjusted for each subject, for the three distances by placing a reticule in each channel, prior to and after cycloplegia. Overall the measurements lasted for about 2 hours. For each subject, the refractive corrections at far, intermediate and near distances were assessed for each eye.

10.2.4 Perceptual scoring measurements

Image quality of the global visual scene and at far, intermediate, near distances was assessed using a perceptual scoring technique. The subject viewed the visual scene through each optical correction presented in random order. For each presentation, the subject scored the visual scene from very blurred (score 0) to very sharp (score 5). The measurements were repeated three times and the average score was calculated for each simulated presbyopic correction. Perceptual score was assessed for seventeen combinations of presbyopia corrections: Three binocular monofocal correction (F+F, I+I, N+N); 4 binocular simultaneous vision correction (2SV+2SV, 3SV+3SV, 2SV+3SV, 3SV+2SV); Five monovision and modified monovision corrections with dominant eye corrected for far (F+N, F+2SV, F+3SV, 2SV+N, 3SV+N); and five correction with dominant eye corrected for near (N+F, N+2SV, N+3SV, 2SV+F, 3SV+F) were evaluated. For each combination of presbyopia correction, perceptual score (from very sharp to very blurred) was obtained at far, intermediate, near distances and for overall scene. Six repetitions were made for each distance and the average was calculated for each combination.

10.2.5 Perceptual preference measurements

The preference to a specific simultaneous vision correction was tested using a two alternative forced choice (Pelli and Farell, 1995, Ehrenstein and Ehrenstein, 1999). Subjects viewed the visual scene for 5 seconds through a presbyopic correction followed subsequent viewing of the same scene through another presbyopic correction for 5 seconds. For pattern preference measurements, the dominant eye was always corrected for far and 36 pairs of the following 9 combinations were assessed: 3SV+3SV, 2SV+2SV, 2SV+3SV, 3SV+2SV, F+N, F+2SV, F+3SV, 2SV+N and 3SV+N. Subjects performed a 2-AFC task and selected one of the two combinations presented successively while viewing the same scene. The correction that was preferred among the pair was given a score of +1 and the other correction in the pair was given a score of -1. The measurements were repeated six times and the sum score was calculated for each correction. For testing the significant preference, a Bernoulli CDF (Yates and Goodman, 2005) was assumed at 0.05 significance level.

10.3 Results

10.3.1 Perceptual scoring of binocular presbyopia corrections

The average binocular perceptual score varied systematically (Fig 10.2a) similar to monocular perceptual scores. Perceptual score at a specific distance correlated significantly ($p<0.0001$) and strongly with the average energy dedicated to the specific distance in both eyes ($r=0.65$), or the energy at better focus for that distance in either eye ($r=0.66$) or the energy for that distance in the dominant eye ($r=0.59$). The overall perceptual score correlated significantly ($p<0.0001$) with the intermediate ($r=0.62$) and far ($r=0.40$) perceptual scores and less strongly with the near perceptual score ($r=0.21$, $p=0.01$). Across repetitions, the perceptual score was very consistent for all subjects, conditions and distances (average variation in score 0.45 ± 0.27).

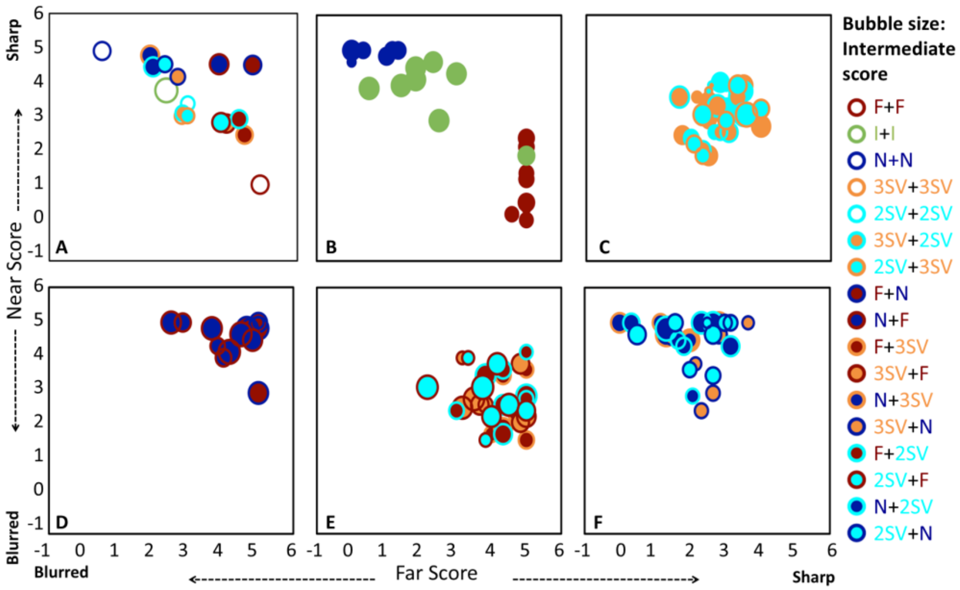

Figure 10.2: Binocular perceptual score for far (x axis), near (y axis) and intermediate distance (bubble size) (A) Average across subjects for all corrections (B) Binocular monofocal corrections in all subjects (C) Binocular simultaneous vision corrections in all subjects (D) Monovision corrections (E) Far dominant modified monovision corrections (F) Near dominant modified monovision corrections

As seen from figure 10.2B-E binocular monofocal corrections had largest variation across distances (mean F-N score 3.5 ± 0.78); binocular simultaneous vision and monovision corrections had the most consistent performance across distance (mean F-N score 0.64±0.48, 0.60±0.83 respectively). Perceptual score for far and near dominant modified monovision corrections varied less but similar to their monofocal counterparts (mean F-N score 1.92±0.96).

Despite intersubject differences in the scoring (Fig. 10.3), the perceptual score was maximum at far and near for the monovision and modified monovision corrections in all subjects. On an average across conditions and subjects, the perceptual score was significantly lower for intermediate distance (2.64±1.04), than for far (3.11±1.36) or near (3.61±1.17) distances (df=2, p<0.0001). In addition the scores varied significantly across subjects (df=7, p<0.01). The overall score was significantly higher (p<0.0001) for the monovision and modified monovision corrections (3.8±1.2) than binocular simultaneous vision corrections (2.5±0.5). Among the modified monovision conditions, there was no significant difference (p=0.92) in overall perceptual score when correcting the dominant eye for far or near.

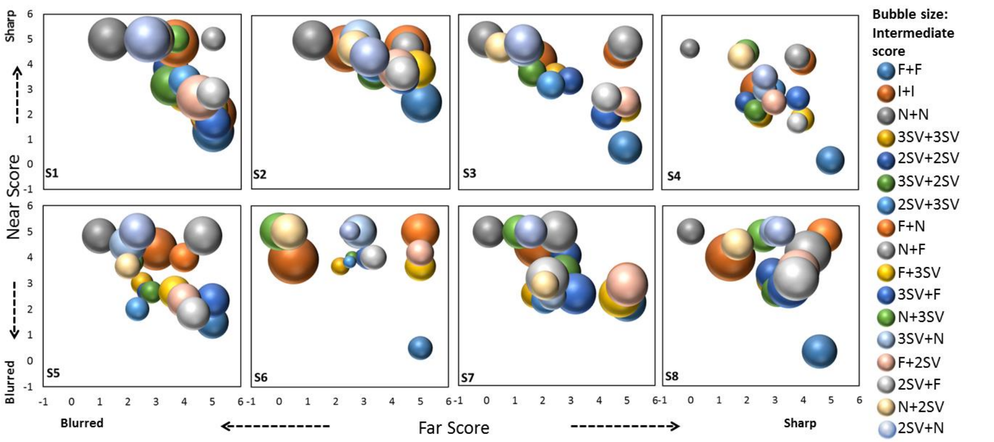

Figure 10.3: Binocular perceptual score for far (x axis), near (y axis) and intermediate distance (bubble size) for individual subjects

10.3.2 Preferences to binocular presbyopic solutions

Among the designs tested, the monovision corrections were preferred 97% of the times and a far dominant modified monovision (F+3SV or F+2SV) were preferred about 63% of the times presented. The preference maps showing pair-wise comparisons across the corrections is shown in figure 10.4, for each subject and on an average across subjects. Assuming a Bernoulli's distribution of $p<0.05$, green dots indicate that the design on the vertical axis was preferred significantly over the one in horizontal axis and a red dot indicates that the design on the vertical axis was significantly rejected compared to the one in horizontal axis, while a gray dot indicates non-significant preferences. As reflected in the percentage preferences, monovision and modified monovision (far or near dominant) corrections were preferred in general by all subjects.

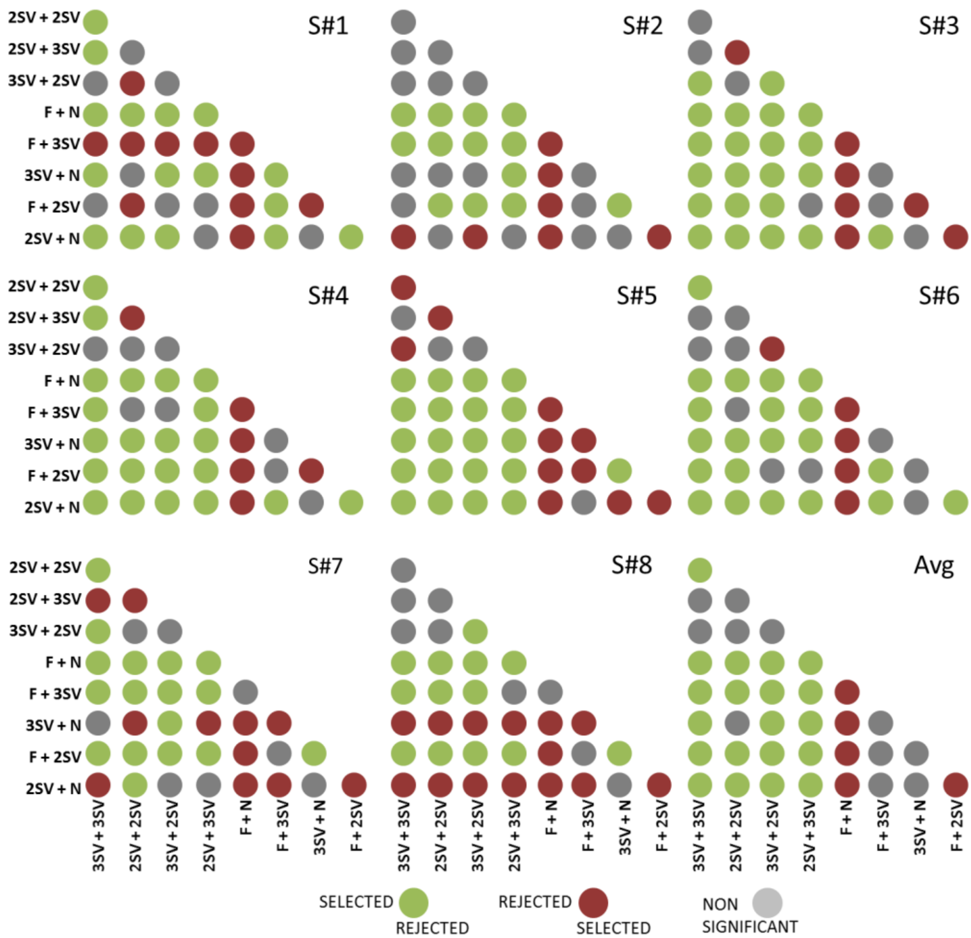

Figure 10.4: Preference maps for pair-wise comparison of binocular simultaneous vision, monovision and modified monovision corrections for all subjects and on an average across subjects

The binocular pattern preference varied for the different presbyopic combinations across subjects: subject S#1 prefers near dominant modified monovision correction and binocular bifocal simultaneous vision correction; while subjects S#2, S#7, S#8 prefer far dominant designs and subjects S#3-S#6 prefer at least one monofocal correction compared to binocular simultaneous vision corrections. Interestingly, on an average across subjects, the binocular bifocal (2SV+2SV) pattern was significantly preferred over any other binocular simultaneous vision corrections and the other simultaneous vision corrections were neither preferred nor rejected significantly (except binocular trifocal corrections).

10.4 Discussion

Owing to increasing availability of newer designs and with obvious advantages over conventional presbyopia correction options (Charman, 2014a), combinations of simultaneous vision and monovision corrections are becoming more and more popular (Kohnen, 2008, Lichtinger and Rootman, 2012, Charman, 2014b). Unless presbyopia solutions that are as similar to the physiological lens as possible are available, these will be the predominant correction technique. These lenses provide fairly good visual quality regardless the viewing direction or distance, yet introduce a complex retinal blur (Simpson, 1992, Kim et al., 2011) or binocular adaptation issues. The ability of the subject to cope up with the new visual experience forms a key factor in success of these treatments. Tools that enable patients to experience this complex blur prior to surgery or contact lens fitting can contribute to a large extent towards the success of these corrections. We developed a binocular, portable, open-field instrument that could optically simulate various presbyopia corrections.

10.4.1 Perceptual quality with Monofocal corrections

In our study, we binocularly evaluated three monofocal corrections at far, intermediate and near distances. The trends in the monofocal perceptual scores were similar to those reported in the previous study (Dorronsoro et al., 2015). Monofocal corrections showed distance-dependent perceptual performance with large intersubject variability. These findings suggest that monofocal corrections, even though provides superior visual quality, cannot be optimized either across distances or across subjects. Several studies comparing eyes implanted with monofocal and multifocal IOLs report similar findings (Cillino et al., 2008, Cochener et al., 2011, Llorente-Guillemot et al., 2012). In fact, few studies show that the visual performance of the monofocal lens outperformed the multifocal lens in both far and intermediate distances and were worse only at closer distances. In addition, the monofocal IOLs was free of haloes and glare providing a much superior visual quality at night compared to their multifocal counterparts.

10.4.2 Perceptual quality with simultaneous vision corrections

The simultaneous vision corrections chosen for this study are the bifocal and trifocal solutions that were significantly preferred on an average in the previous study (Dorronsoro et al., 2015). Binocularly, the perceptual score was similar at far and near distances and was similar across subjects. In addition, the perceptual quality was not as greatly degraded in the as with monofocal corrections at non-focal distances. In fact, as seen from the perceptual score measurements, these corrections were not perceived as too blurred by any of the subjects, at any distance. Binocular vision is an important and meaningful aspect of visual function. Multifocal IOLs provide a broad range of vision from far to near foci. Thus a binocular multifocal correction can be better adapted as it provides a stable visual quality across all distances (Koch and Wang, 2007, Blaylock et al., 2009, Benard et al., 2011), and also provide better binocular functions compared to unilateral implantations as suggested by clinical outcomes (Haring et al., 1999, Mesci et al., 2010).

10.4.3 Perceptual quality with monovision and modified monovision

In this study we measured binocular perceptual quality with monovision, far- and near- dominant modified monovision corrections. The monovision corrections provided excellent vision at far and near distances and fairly good quality of vision at intermediate distances. In a study by Schor and colleagues, it was reported that both perceptual and binocular functions with monovision corrections were better in pre-presbyopes than presbyopes (Johannsdottir and Stelmach, 2001). In our cohort, most were young subjects or pre-presbyopes with induced presbyopia. These tendencies could have influenced the perceptual outcomes. In addition, there were no differences perceptual performances when the dominant eye or non-dominant eye is corrected for far vision with a monofocal correction or simultaneous vision correction, suggesting sharpness dependence of perception. Our previous studies on simulated simultaneous vision (Radhakrishnan et al., 2014), or interocular differences in visual quality (Radhakrishnan et al., 2015a, Radhakrishnan et al., 2015b) and those studies on induced interocular blur differences also report the sharpness dependence of visual perception (Arnold et al., 2007, Kompaniez et al., 2013) and adaptation (Haun and Peli, 2013, Radhakrishnan et al., 2014, Radhakrishnan et al., 2015a). Similarly, irrespective of whether the design was far or near dominant, the perceptual quality was better than binocular simultaneous options, even though most subjects preferred a far-dominant monovision correction. Some studies show that the modified monovision corrections provide better binocular contrast sensitivity and visual acuity compared to monovision correction in addition, to providing better binocularity, greater comfort and lesser glare (Schor et al., 1987, Kohnen, 2008). In this study, while the perceptual quality for modified monovision was somewhat lower than that for monovision, it is recommendable to evaluate binocular visual functions prior to monovision prescription.

10.4.4 Pattern preferences to binocular presbyopic corrections

Forced choice method was implemented to study preferences to different presbyopic corrections. Under binocular simulation of presbyopic corrections the monovision and modified monovision corrections were preferred over simultaneous vision. The presence of a sharp component in the monovision and modified monovision corrections could have influenced the preferences. Among the simultaneous vision corrections, contrary to monocular measurements, on an average the binocular bifocal correction was preferred as opposed to the trifocal correction. As could be seen from figure 10.4 the preferences among simultaneous vision corrections are similar and the average change could be attributed to the difference among population. In addition, among the simultaneous vision corrections, it could be observed that most patterns were neither significantly rejected or selected emphasizing the uniformity in performance. Most subjects preferred far-dominant monovision corrections; one subject (an uncorrected low myope) preferred near dominant corrections indicating that subjects prefer corrections that are represent their conventional visual experience. Many previous studies suggest that the perceptual quality is closely associated with the retinal image quality in both blur orientation (Sawides et al., 2013, Radhakrishnan et al., 2015b) and magnitude (Sawides et al., 2011, Radhakrishnan et al., 2015a).

10.4.5 Inter-subject differences

Large inter-subject variability is found in the perceptual scoring measurements, especially for monofocal and modified monovision corrections. While all subjects seem to favor monovision and modified monovision corrections, it could be hypothesized that these responses were primarily driven by the sharp component in one of the eyes. This is supported by the outcomes of our previous studies on adaptation interocular blur differences (Radhakrishnan et al., 2015a, Radhakrishnan et al., 2015b) and is supported by several studies on binocular rivalry and summation (Schor et al., 1987, Arnold et al., 2007). However, preferences among modified monovision and simultaneous vision corrections, show intersubject differences with some subjects preferring modified monovisions that are near-dominant and some preferring far dominant designs. These results further emphasize the dependence on the visual needs for a successful presbyopic correction and need for clinical instruments to simulate the same.

10.4.6 Implications

Following the previous hand-held monocular vision simulator, we have developed a binocular vision simulator that provides an open field binocular simulation of presbyopic corrections. We demonstrate in this study a non-invasive method that optically simulates a simultaneous multifocal vision or monovision and modified monovision corrections. While we have measured primarily binocular perceptual outcomes, the instrument is well suited to study functions of binocularity like stereopsis, fusion etc. Furthermore, using mirrors for image re-inversion, the field of view can be almost doubled and the size of the instrument can be further reduced. A head mounted model could be evolved and this would make the system an ideal one for clinical evaluations for all possible presbyopic correction techniques.

10.5 Conclusion

In our subjects, monovision and modified monovision corrections were perceptually preferred compared to other corrections. The developed binocular portable vision simulator can simulate different combinations of presbyopic corrections in an open-field setup and is a clinically useful tool for systematic evaluation of presbyopia corrections.

Chapter ELEVEN

Conclusions

In this thesis, we improved the simultaneous vision simulator, implementing the spatial light modulator to induce pupil patterns. A psychophysical channel was incorporated and synchronized with the pupil channel and two Badal channels. We also developed a portable, hand-held, vision simulator based on temporal multiplexing technology. We performed a series of psychophysical measurements and clinically viable measurements towards understanding optical, perceptual and adaptational implications of various presbyopia correction techniques. Our results help in understanding how the visual system deals with current multifocal and presbyopic corrections. These are key in designing newer optical designs for presbyopia that can provide an optimal visual solution.

Achievements

The main accomplishments of this thesis are:

- We studied the adaptation to long-term differences in interocular blur, in specific the role of blur magnitude and orientation in neural adaptation.
- We developed methods to numerically simulate pure simultaneous vision correction and implemented psychophysical paradigms to evaluate blur judgment of a simultaneous vision blur.
- We constructed the modified simultaneous vision simulator that combined spatial light modulator with a psychophysical channel to induce multifocality. The utility of the system to test visual and perceptual performance and study the adaptation to optically induced simultaneous vision has been validated.
- We implemented methods to assess significant preferences to blur introduced by patterns having similar physical characteristics.
- We built and validated a hand-held, see-through tool to optically induce simultaneous vision. We performed measurements in subjects to assess performance with and preference to different designs of simultaneous vision correction.
- We developed a binocular vision simulator for simulation of premium presbyopic solutions like monovision and modified monovision corrections. We demonstrated the utility of the system in subjective perceptual assessments.

Specific conclusions

1 In subjects with different blur magnitude between eyes, what people perceive as 'best-focused' matches the blur encountered in the eye with better optics, even when judging the world through the eye with poorer optics.

2 In subjects with different blur magnitude and orientation, the orientation of the blur perceived as better focused correlated with the orientation of blur in the eye with better optical quality.

3 The orientation of positive neural PSF was about 60 degrees apart from the orientation of negative neural PSF.

4 The internal code for blur is the same for both eyes, in both magnitude and orientation, even under binocular dissociation, suggesting a cyclopean locus for blur adaptation in the higher cortical regions.

5 The Perceived Best Focus shifts after adaptation to both pure defocus and pure simultaneous vision. The change in Perceived Best Focus correlated strongly to the magnitude (amount of near addition) and the proportion (far/near ratio) of blur in the image.

6 Maximum perception of blur and maximum adaptation to simultaneous vision was noted for low near additions (0.50 D).

7 Mechanism of perception of/adaptation to simultaneous vision is found to be similar to that of monofocal blur driven by contrast adaptation.

8 Subjects preferred strongly the blur introduced by an angular, two segmented bifocal design. Radial designs were neither significantly preferred nor rejected. Hybrid designs were strongly rejected by the subjects. Preferences changed across distances and across subjects.

9 For an angular bifocal design, preferences changed with change in orientation of the bifocal design and across distances. Most subjects preferred horizontal orientation of the near segment. High contrast visual acuity did not change significantly across orientations.

10 Subjective orientation preference to a bifocal angular design was predicted by optical metrics, combining the bifocal design and ocular aberrations.

11 Trends in Perceived Best Focus shift following adaptation was similar when blur was either induced optically or simulated by convolution. Optically induced simultaneous blur was, in general, better tolerated.

12 The hand-held SimVis (monocular and binocular) based on temporal multiplexing is an effective tool to optically simulate multifocal correction enabling multifocal prescription evidence-based and by providing subjects with firsthand information on multifocality.

13 We found that visual and perceptual performances are affected to a great extent by the far/near energy ratio and by visual needs of the subject. Simultaneous vision corrections provided uniform and acceptable visual performances at all distances.

14 Binocularly, subjects preferred monovision and modified monovision corrections (monofocal + simultaneous vision combinations) compared to binocular simultaneous vision corrections.

Future work

The results of the current work opens avenue for a number of studies on multifocal vision. It would be interesting to evaluate in eyes implanted with multifocal IOLs, using the second generation adaptive optics system (AO2), the effect of optically simulating different multifocal solutions on visual, perceptual and neural performance, by compensating the existing multifocality using the combination of deformable mirror and spatial light modulator. This would provide direct data on how well the visual system can adapt to newer multifocal designs.

A more direct follow up would be to induce the same multifocal design by optical simulations and also by fitting a contact lens, in the same subjects, to study effects of lens decentration and tear interaction on perceptual performance. These results could be included in the ideal observer model and a nomogram could be evolved and tested in study patients, pre- and post- contact lens/intraocular lens implantation. In addition to presbyopia, multifocal solutions are also used increasingly for myopia and post cataract surgery. While in myopia there is an impairment of far vision, in presbyopia it is near vision and a patient with cataract has constant blur at all distances. The three groups probably differ in the processing of the visual information and this could be evaluated using methods developed and implemented in this thesis.

Finally, it would be ideal to develop and validate a simultaneous vision simulator, for clinical use, that not only simulates the blur magnitude corresponding to multifocal vision, but also include other optical properties such as the effect of diffraction rings in a diffractive optics multifocal solution, the segments and its orientations of a refractive design and in general the chromatic effects associated with multifocal designs.

Disseminations

Publications resulting from this thesis

Peer reviewed

1. **Radhakrishnan A,** Dorronsoro C, Sawides L, Peli E, Marcos S: Single neural code for blur in subjects with different interocular optical blur orientation. J Vis. 2015; 9(3): e93089.
2. **Radhakrishnan A,** Dorronsoro C, Sawides L, Webster M, Marcos S: A cyclopean neural mechanism compensating for optical differences between the eyes. Curr Biol. 2015; 25(5): R188-189.
3. **Radhakrishnan A,** Dorronsoro C, Sawides L, Marcos S: Short term neural adaptation to simultaneous bifocal vision. PLoS One. 2014; 9(3): e93089.

In review

1. Dorronsoro C, **Radhakrishnan A,** de Gracia P, Sawides L, Marcos S: Perceived image quality with simulated segmented bifocal corrections. *Submitted*.
2. **Radhakrishnan A,** Dorronsoro C, Marcos S: Subjective preference to orientation in angular bifocal IOL design. *Submitted*.
3. Dorronsoro C, **Radhakrishnan A,** Alonso-Sanz JR, Pascual D, Velasco-Ocana M, Perez-Merino P, Marcos S: Portable simultaneous vision device to simulate multifocal corrections. *Submitted*.

Citable conference abstracts

1. **Radhakrishnan A,** Dorronsoro C, Marcos S: Adaptation to optically induced simultaneous bifocal vision, Invest Ophthalmol Vis Sci, 2015, 56: E-Abstract 2905
2. Dorronsoro C, Alonso-Sanz JR, Daniel Pascual, **Radhakrishnan A,** Ocana MV, Pere-Merino P, Marcos S, Visual performance and perception with bifocal and trifocal presbyopia corrections simulated using a hand-held simultaneous vision device, Invest Ophthalmol Vis Sci, 2015, 56: E-Abstract 4306
3. **Radhakrishnan A,** Dorronsoro C, Sawides L, Webster M, Peli E, Marcos S: Internal code for blur: Interocular effects, Invest Ophthalmol Vis Sci, 2014, 55: E-Abstract 5970
4. Dorronsoro C, **Radhakrishnan A,** de Gracia P, Sawides L, Alonso-Sanz JR, Cortes D, Marcos S: Visual testing of segmented bifocal corrections with a compact simultaneous vision simulator, Invest Ophthalmol Vis Sci, 2014, 55: E-Abstract 781
5. Dorronsoro C, **Radhakrishnan A,** Sawides L, Marcos S: Optical quality and subjective judgments of blur under pure simultaneous vision, Invest Ophthalmol Vis Sci, 2013, 54: E-Abstract 4608

Other Publications

1. Vinas M, Doorronsoro C, Gonzalez V, Cortes D, **Radhakrishnan A,** Marcos S: Testing vision with angular and radial multifocal designs using adaptive optics. *Submitted*.

2. Dorronsoro C, Radhakrishnan A, Marcos S: Percepción ciclópea para compensar las diferencias visuales entre los ojos. Menta y Cerebro. 2015; 6: 48-49.

3. Vinas M, Dorronsoro C, Sawides L, Pascual D, Cortes D, **Radhakrishnan A**, Marcos S: Longitudinal chromatic aberration of the human eyes in the

visible and near infrared from Hartmann-Shack wavefront sensing, double-pass and psychophysics, Invest Ophthalmol Vis Sci, 2014, 55: E-Abstract 5974

4. Sawides L, Dorronsoro C, **Radhakrishnan A**, Peli E, Webster M, Marcos S: Perceived blur and higher-order aberrations, J Vis, 2013, 13: T3.

Invited talks

"Visual perception and adaptation to Presbyopia correction", Young Researchers' Vision Camp, 2015, Leibertingen, Germany.

Other conference presentations

1. "Hand held vision simulator for evaluating visual and perceptual performance of Presbyopia corrections", International OSA Network of Students Conference, 2015, Valencia, Spain.
2. "Effect of object size on blur perception", 2nd IOSA Scientific Seminar series, 2015, Madrid, Spain
3. "Perception and Neural adaptation to multifocal optical patterns", 4th Optical and Adaptational Limits of Vision Annual meeting, 2015, Murcia, Spain
4. "Adaptation to contralateral diffrences in blur", Visual and Physiological Optics conference, 2014, Wroclaw, Poland
5. "Neural Adaptation to multifocal optics", 3rd Optical and Adaptational Limits of Vision Annual meeting, 2014, Stockholm, Sweden
6. "Adaptation to blur caused by Higher Order Aberrations", 2nd Optical and Adaptational Limits of Vision Annual meeting, 2013, Santorini, Greece

7. "Adaptation to Simultaneous Vision", Young Researcher's Vision Camp, 2013, Leibertingen, Germany

8. "Neural adaptation to Simultaneous Bifocal Vision", 1st Optical and Adaptational Limits of Vision Annual meeting, 2012, Madrid, Spain

Bibliography

Ahumada AJ, Jr. (2002) Classification image weights and internal noise level estimation. J Vis 2:121-131.

Alio JL, Pikkel J (2014) Multifocal Intraocular Lenses: The art and the practice. E-book: Springer International Publishing.

Aller TA, Wildsoet C (2008) Bifocal soft contact lenses as a possible myopia control treatment: a case report involving identical twins. Clin Exp Optom 91:394-399.

Almeder LM, Peck LB, Howland HC (1990) Prevalence of anisometropia in volunteer laboratory and school screening populations. Investigative ophthalmology & visual science 31:2448-2455.

Anderson RS, McDowell DR, Ennis FA (2001) Effect of localized defocus on detection thresholds for different sized targets in the fovea and periphery. Acta Ophthalmol Scand 79:60-63.

Anderson SJ, Mullen KT, Hess RF (1991) Human peripheral spatial resolution for achromatic and chromatic stimuli: limits imposed by optical and retinal factors. The Journal of physiology 442:47-64.

Appelle S (1972) Perception and discrimination as a function of stimulus orientation: the "oblique effect" in man and animals. Psychol Bull 78:266-278.

Applegate RA, Marsack JD, Ramos R, Sarver EJ (2003) Interaction between aberrations to improve or reduce visual performance. J Cataract Refract Surg 29:1487-1495.

Applegate RA, Sarver EJ, Khemsara V (2002) Are all aberrations equal? J Refract Surg 18:S556-562.

Arnold DH, Grove PM, Wallis TS (2007) Staying focused: a functional account of perceptual suppression during binocular rivalry. J Vis 7:7 1-8.

Arnulf A, Dupuy O, Flamant F (1951) [Distribution of light in the image of a luminous point on the retina]. Comptes rendus hebdomadaires des seances de l'Academie des sciences 233:974-976.

Artal P (1990) Calculations of two-dimensional foveal retinal images in real eyes. J Opt Soc Am A 7:1374-1381.

Artal P (2014) Optics fo the eye and its impact in vision: a tutorial. Advances in Optics and Photonics 6:28.

Artal P, Chen L, Fernandez EJ, Singer B, Manzanera S, Williams DR (2003) Adaptive optics for vision: the eye's adaptation to point spread function. J Refract Surg 19:S585-587.

Artal P, Chen L, Fernandez EJ, Singer B, Manzanera S, Williams DR (2004) Neural compensation for the eye's optical aberrations. J Vis 4:281-287.

Artal P, Guirao A, Berrio E, Williams DR (2001) Compensation of corneal aberrations by the internal optics in the human eye. J Vis 1:1-8.

Artal P, Navarro R (1994) Monochromatic modulation transfer function of the human eye for different pupil diameters: an analytical expression. J Opt Soc Am A Opt Image Sci Vis 11:246-249.

Atchison DA, Guo H (2010) Subjective blur limits for higher order aberrations. Optom Vis Sci 87:E890-898.

Atchison DA, Smith G (2000) Optics of the Human Eye. Oxford: Butterworth-Heinemann.

Banks MS, Sekuler AB, Anderson SJ (1991) Peripheral spatial vision: limits imposed by optics, photoreceptors, and receptor pooling. J Opt Soc Am A 8:1775-1787.

Banyal RK, Prasad BR (2005) Pixel size and pitch measurements of liquid crystal spatial light modulator by optical diffraction. Pramana J Phys 65:7.

Bao M, Engel SA (2012) Distinct mechanism for long-term contrast adaptation. Proc Natl Acad Sci U S A 109:5898-5903.

Barbero S (2006) Refractive power of a multilayer rotationally symmetric model of the human cornea and tear film. J Opt Soc Am A Opt Image Sci Vis 23:1578-1585.

Barbero S, Marcos S, Jimenez-Alfaro I (2003) Optical aberrations of intraocular lenses measured in vivo and in vitro. J Opt Soc Am A Opt Image Sci Vis 20:1841-1851.

Bass M, DeCusatis CM, Enoch JM, Lakshminarayanan V, Li G, MacDonald C, Mahajan VN, Stryland EV (2010) Handbook of Optics, Volume 1: Geometrical and Physical Optics, Polarized Light, Components and Instruemnts.

Bellucci R (2005) Multifocal intraocular lenses. Curr Opin Ophthalmol 16:33-37.

Benard Y, Lopez-Gil N, Legras R (2011) Optimizing the subjective depth-of-focus with combinations of fourth- and sixth-order spherical aberration. Vision Res 51:2471-2477.

Benavente-Perez A, Nour A, Troilo D (2014) Axial eye growth and refractive error development can be modified by exposing the peripheral retina to relative myopic or hyperopic defocus. Investigative ophthalmology & visual science 55:6765-6773.

Birkenfeld J, de Castro A, Marcos S (2014) Contribution of shape and gradient refractive index to the spherical aberration of isolated human lenses. Invest Ophthalmol Vis Sci 55:2599-2607.

Blake R, Overton R, Lema-Stern S (1981) Interocular transfer of visual aftereffects. J Exp Psychol Hum Percept Perform 7:367-381.

Blakemore C, Campbell FW (1969a) Adaptation to spatial stimuli. The Journal of physiology 200:11P-13P.

Blakemore C, Campbell FW (1969b) On the existence of neurones in the human visual system selectively sensitive to the orientation and size of retinal images. The Journal of physiology 203:237-260.

Blakemore C, Nachmias J, Sutton P (1970) The perceived spatial frequency shift: evidence for frequency-selective neurones in the human brain. The Journal of physiology 210:727-750.

Blaylock JF, Si Z, Prescott C, Aitchison S (2009) Intermediate optimization of vision with bilateral nonaspheric multifocal intraocular lens implantation. J Cataract Refract Surg 35:303-311.

Born M, Wolf E (1999) Principles of Optics. London: Cambridge University Press.

Bosking WH, Zhang Y, Schofield B, Fitzpatrick D (1997) Orientation selectivity and the arrangement of horizontal connections in tree shrew striate cortex. J Neurosci 17:2112-2127.

Brainard DH (1997) The Psychophysics Toolbox. Spatial vision 10:433-436.

Buckhurst PJ, Wolffsohn JS, Davies LN, Naroo SA (2010) Surgical correction of astigmatism during cataract surgery. Clin Exp Optom 93:409-418.

Burns SA, Tumbar R, Elsner AE, Ferguson D, Hammer DX (2007) Large-field-of-view, modular, stabilized, adaptive-optics-based scanning laser ophthalmoscope. J Opt Soc Am A Opt Image Sci Vis 24:1313-1326.

Campbell FW, Green DG (1965) Optical and retinal factors affecting visual resolution. The Journal of physiology 181:576-593.

Campbell MC (1984) Measurement of refractive index in an intact crystalline lens. Vision Res 24:409-415.

Carrasco M, Frieder KS (1997) Cortical magnification neutralizes the eccentricity effect in visual search. Vision Res 37:63-82.

Chalita MR, Krueger RR (2004) Correlation of aberrations with visual acuity and symptoms. Ophthalmol Clin North Am 17:135-142, v-vi.

Charman WN (2008) The eye in focus: accommodation and presbyopia. Clin Exp Optom 91:207-225.

Charman WN (2014a) Developments in the correction of presbyopia I: spectacle and contact lenses. Ophthalmic Physiol Opt 34:8-29.

Charman WN (2014b) Developments in the correction of presbyopia II: surgical approaches. Ophthalmic Physiol Opt 34:397-426.

Charman WN, Jennings JA (1976) The optical quality of the monochromatic retinal image as a function of focus. The British journal of physiological optics 31:119-134.

Charman WN, Radhakrishnan H (2010) Peripheral refraction and the development of refractive error: a review. Ophthalmic Physiol Opt 30:321-338.

Cheng X, Bradley A, Thibos LN (2004) Predicting subjective judgment of best focus with objective image quality metrics. J Vis 4:310-321.

Chung ST (2004) Reading speed benefits from increased vertical word spacing in normal peripheral vision. Optom Vis Sci 81:525-535.

Chung ST (2013) The Glenn A. Fry Award Lecture 2012: Plasticity of the visual system following central vision loss. Optom Vis Sci 90:520-529.

Chung ST, Jarvis SH, Woo SY, Hanson K, Jose RT (2008) Reading speed does not benefit from increased line spacing in AMD patients. Optom Vis Sci 85:827-833.

Chung ST, Legge GE, Tjan BS (2002) Spatial-frequency characteristics of letter identification in central and peripheral vision. Vision Res 42:2137-2152.

Cillino S, Casuccio A, Di Pace F, Morreale R, Pillitteri F, Cillino G, Lodato G (2008) One-year outcomes with new-generation multifocal intraocular lenses. Ophthalmology 115:1508-1516.

Clifford CW, Webster MA, Stanley GB, Stocker AA, Kohn A, Sharpee TO, Schwartz O (2007) Visual adaptation: neural, psychological and computational aspects. Vision Res 47:3125-3131.

Cochener B, Lafuma A, Khoshnood B, Courouve L, Berdeaux G (2011) Comparison of outcomes with multifocal intraocular lenses: a meta-analysis. Clin Ophthalmol 5:45-56.

Collins MJ, Goode A (1994) Interocular blur suppression and monovision. Acta ophthalmologica 72:376-380.

Cornsweet TN (1970) Visual perception. London: Acadeic Press.

Crescitelli F (1960) Physiology of vision. Annu Rev Physiol 22:525-578.

Cufflin MP, Mankowska A, Mallen EA (2007) Effect of blur adaptation on blur sensitivity and discrimination in emmetropes and myopes. Investigative ophthalmology & visual science 48:2932-2939.

Davis JA, McNamara DE, Cottrell DM, Sonehara T (2000) Two-dimensional polarization encoding with a phase-only liquid-crystal spatial light modulator. Applied optics 39:1549-1554.

de Castro A, Ortiz S, Gambra E, Siedlecki D, Marcos S (2010) Three-dimensional reconstruction of the crystalline lens gradient index distribution from OCT imaging. Opt Express 18:21905-21917.

de Gracia P, Dorronsoro C, Gambra E, Marin G, Hernandez M, Marcos S (2010) Combining coma with astigmatism can improve retinal image over astigmatism alone. Vision Res 50:2008-2014.

de Gracia P, Dorronsoro C, Marcos S (2013a) Multiple zone multifocal phase designs. Optics letters 38:3526-3529.

de Gracia P, Dorronsoro C, Marin G, Hernandez M, Marcos S (2011) Visual acuity under combined astigmatism and coma: optical and neural adaptation effects. J Vis 11.

de Gracia P, Dorronsoro C, Sanchez-Gonzalez A, Sawides L, Marcos S (2013b) Experimental simulation of simultaneous vision. Investigative ophthalmology & visual science 54:415-422.

De Valois R, De Valois K (1988) Spatial Vision. New York: Oxford University Press.

De Valois RL, Yund EW, Hepler N (1982) The orientation and direction selectivity of cells in macaque visual cortex. Vision Res 22:531-544.

Delahunt PB, Webster MA, Ma L, Werner JS (2004) Long-term renormalization of chromatic mechanisms following cataract surgery. Visual neuroscience 21:301-307.

Delori FC, Webb RH, Sliney DH, American National Standards I (2007) Maximum permissible exposures for ocular safety (ANSI 2000), with emphasis on ophthalmic devices. J Opt Soc Am A Opt Image Sci Vis 24:1250-1265.

de Wit DW, Diaz J, Moore TC, Moutari S, Moore JE (2015) Effect of position of near addition in an asymmetric refractive multifocal intraocular lens on quality of vision. J Cataract Refract Surg 41: 945-955.

Diedrich E, Schaeffel F (2009) Spatial resolution, contrast sensitivity, and sensitivity to defocus of chicken retinal ganglion cells in vitro. Visual neuroscience 26:467-476.

Diether S, Schaeffel F (1999) Long-term changes in retinal contrast sensitivity in chicks from frosted occluders and drugs: relations to myopia? Vision Res 39:2499-2510.

Dorronsoro C, Alonso JR, Marcos S (2013) Miniaturized simultaneous vision simulator. vol. PCT/2014ES/070725 (Network, E. E., ed).

Dorronsoro C, Marcos S (2009) Instrument for the simulation of multifocal ophthalmic corrections. vol. WO/2010/116019 US.

Dorronsoro C, Radhakrishnan A, de Gracia P, Sawides L, Alonso-Sanz JR, Cortes D, Marcos S (2014) Visual testing of segmented bifocal corrections with a compact simultaneous vision simulator. Investigative ophthalmology & visual science 55.

Dragoi V, Rivadulla C, Sur M (2001) Foci of orientation plasticity in visual cortex. Nature 411:80-86.

Dragoi V, Sharma J, Sur M (2000) Adaptation-induced plasticity of orientation tuning in adult visual cortex. Neuron 28:287-298.

Dreher AW, Bille JF, Weinreb RN (1989) Active optical depth resolution improvement of the laser tomographic scanner. Applied optics 28:804-808.

Eckstein MP, Ahumada AJ, Jr. (2002) Classification images: a tool to analyze visual strategies. J Vis 2:1x.

Efron U (1995) Spatial Light Modulator technology: Materials, devices and applications. New York: Marcel Dekker.

Ehrenstein WH, Ehrenstein A (1999) Psychophysical methods: In modern techniques in neuroscience research. Berlin: Springer.

Elliott SL, Georgeson MA, Webster MA (2011) Response normalization and blur adaptation: data and multi-scale model. J Vis 11.

Elliott SL, Hardy JL, Webster MA, Werner JS (2007) Aging and blur adaptation. J Vis 7:8.

Engel SA, Rumelhart DE, Wandell BA, Lee AT, Glover GH, Chichilnisky EJ, Shadlen MN (1994) fMRI of human visual cortex. Nature 369:525.

Erkelens CJ (2000) Perceived direction during monocular viewing is based on signals of the viewing eye only. Vision Res 40:2411-2419.

Evans BJ (2007) Monovision: a review. Ophthalmic Physiol Opt 27:417-439.

Fernandez EJ, Vabre L, Hermann B, Unterhuber A, Povazay B, Drexler W (2006) Adaptive optics with a magnetic deformable mirror: applications in the human eye. Opt Express 14:8900-8917.

Field DJ (1987) Relations between the statistics of natural images and the response properties of cortical cells. J Opt Soc Am A 4:2379-2394.

Field DJ, Brady N (1997) Visual sensitivity, blur and the sources of variability in the amplitude spectra of natural scenes. Vision Res 37:3367-3383.

Fine I, Smallman HS, Doyle P, MacLeod DI (2002) Visual function before and after the removal of bilateral congenital cataracts in adulthood. Vision Res 42:191-210.

Finger S (1994) Origins of Neuroscience: A history of explorations into brain function. New York: Oxford University Press.

Fiorentini A, Berardi N (1980) Perceptual learning specific for orientation and spatial frequency. Nature 287:43-44.

Fisher NI, Lee AJ (1983) A correlation coefficient for circular data. Bimetrika 70:1.

Gambra E, Sawides L, Dorronsoro C, Marcos S (2009) Accommodative lag and fluctuations when optical aberrations are manipulated. J Vis 9:4 1-15.

Gambra E, Wang Y, Yuan J, Kruger PB, Marcos S (2010) Dynamic accommodation with simulated targets blurred with high order aberrations. Vision Res 50:1922-1927.

Garland MA (1987) Monovision and related techniques in the management of presbyopia. CLAO J 13:179-181.

Geischeider GA (1997) Psychophysics: The fundamentals. New Jersey: Lawrence Erlbaum Publishers.

Georgeson MA, May KA, Freeman TC, Hesse GS (2007) From filters to features: scale-space analysis of edge and blur coding in human vision. J Vis 7:7 1-21.

Georgeson MA, Sullivan GD (1975) Contrast constancy: deblurring in human vision by spatial frequency channels. The Journal of physiology 252:627-656.

Gibson EJ (1963) Perceptual learning. Annual review of psychology 14:29-56.

Glasser A (2008) Restoration of accommodation: surgical options for correction of presbyopia. Clin Exp Optom 91:279-295.

Glasser A, Campbell MC (1998) Presbyopia and the optical changes in the human crystalline lens with age. Vision Res 38:209-229.

Goodman J (1996) Introduction to Fourier Optics. New York: McGraw-Hill Companies Inc.

Greenlee MW, Tse PU (2008) Functional neuroanatomy of the human visual system: A review of functional MRI studies. Berlin: Springer Berlin Heidelberg.

Gregory LR (1997) Eye and Brain. New Jersey: Princeton University Press.

Grill-Spector K, Malach R (2004) The human visual cortex. Annual review of neuroscience 27:649-677.

Handa T, Shimizu K, Mukuno K, Kawamorita T, Uozato H (2005) Effects of ocular dominance on binocular summation after monocular reading adds. J Cataract Refract Surg 31:1588-1592.

Handa T, Shimizu K, Uozato H, Shoji N, Ishikawa H (2012) A new method for quantifying ocular dominance using the balancing technique. The American orthoptic journal 62:77-86.

Hartridge H (1925) Helmholtz's Theory of Accommodation. Br J Ophthalmol 9:521-523.

Harvey BM, Dumoulin SO (2011) The relationship between cortical magnification factor and population receptive field size in human visual cortex: constancies in cortical architecture. J Neurosci 31:13604-13612.

Haun AM, Peli E (2013) Adaptation to blurred and sharpened video. J Vis 13.

Hofer H, Artal P, Singer B, Aragon JL, Williams DR (2001) Dynamics of the eye's wave aberration. J Opt Soc Am A Opt Image Sci Vis 18:497-506.

Hoffman DM, Banks MS (2010) Focus information is used to interpret binocular images. J Vis 10:13.

Hofmeister EM, Kaupp SE, Schallhorn SC (2005) Comparison of tropicamide and cyclopentolate for cycloplegic refractions in myopic adult refractive surgery patients. J Cataract Refract Surg 31:694-700.

Howland B, Howland HC (1976) Subjective measurement of high-order aberrations of the eye. Science 193:580-582.

Howland HC, Howland B (1977) A subjective method for the measurement of monochromatic aberrations of the eye. Journal of the Optical Society of America 67:1508-1518.

Hubel DH (1988) Eye, Brain and Vision. New York: Scientific American Library.

Iskander DR (2006) Computational aspects of the visual Strehl ratio. Optom Vis Sci 83:57-59.

Johannsdottir KR, Stelmach LB (2001) Monovision: a review of the scientific literature. Optom Vis Sci 78:646-651.

Kamiya K, Hayashi K, Shimizu K, Negishi K, Sato M, Bissen-Miyajima H, Survey Working Group of the Japanese Society of C, Refractive S (2014) Multifocal intraocular lens explantation: a case series of 50 eyes. Am J Ophthalmol 158:215-220 e211.

Kaymak H, Fahle M, Ott G, Mester U (2008) Intraindividual comparison of effect of training on viusal performance with ReSTOR and Tecnis diffractive multifocal IOLs. J Refract Surg 24:7.

Kim MJ, Zheleznyak L, Macrae S, Tchah H, Yoon G (2011) Objective evaluation of through-focus optical performance of presbyopia-correcting intraocular lenses using an optical bench system. J Cataract Refract Surg 37:1305-1312.

Koch DD, Wang L (2007) Custom optimization of intraocular lens asphericity. Trans Am Ophthalmol Soc 105:36-41; discussion 41-32.

Kohnen T (2008) Multifocal IOL technology: a successful step on the journey toward presbyopia treatment. J Cataract Refract Surg 34:2005.

Kompaniez E, Sawides L, Marcos S, Webster MA (2013) Adaptation to interocular differences in blur. J Vis 13:19.

Kording KP, Tenenbaum JB, Shadmehr R (2007) The dynamics of memory as a consequence of optimal adaptation to a changing body. Nature neuroscience 10:779-786.

Kwon M, Legge GE, Fang F, Cheong AM, He S (2009) Adaptive changes in visual cortex following prolonged contrast reduction. J Vis 9:20 21-16.

Levi DM (2006) Visual processing in amblyopia: human studies. Strabismus 14:11-19.

Lewis P, Baskaran K, Rosen R, Lundstrom L, Unsbo P, Gustafsson J (2014) Objectively determined refraction improves peripheral vision. Optom Vis Sci 91:740-746.

Leyland M, Zinicola E (2003) Multifocal versus monofocal intraocular lenses in cataract surgery: a systematic review. Ophthalmology 110:1789-1798.

Liang J, Grimm B, Goelz S, Bille JF (1994) Objective measurement of wave aberrations of the human eye with the use of a Hartmann-Shack wave-front sensor. J Opt Soc Am A Opt Image Sci Vis 11:1949-1957.

Liang J, Williams DR, Miller DT (1997) Supernormal vision and high-resolution retinal imaging through adaptive optics. J Opt Soc Am A Opt Image Sci Vis 14:2884-2892.

Lichtinger A, Rootman DS (2012) Intraocular lenses for presbyopia correction: past, present, and future. Curr Opin Ophthalmol 23:40-46.

Llorente-Guillemot A, Garcia-Lazaro S, Ferrer-Blasco T, Perez-Cambrodi RJ, Cervino A (2012) Visual performance with simultaneous vision multifocal contact lenses. Clin Exp Optom 95:54-59.

Logean E, Dalimier E, Dainty C (2008) Measured double-pass intensity point-spread function after adaptive optics correction of ocular aberrations. Opt Express 16:17348-17357.

Lopes-Ferreira D, Neves H, Queiros A, Faria-Ribeiro M, Peixoto-de-Matos SC, Gonzalez-Meijome JM (2013) Ocular dominance and visual function testing. BioMed research international 2013:238943.

Lundstrom L, Gustafsson J, Unsbo P (2007a) Vision evaluation of eccentric refractive correction. Optom Vis Sci 84:1046-1052.

Lundstrom L, Gustafsson J, Unsbo P (2009) Population distribution of wavefront aberrations in the peripheral human eye. J Opt Soc Am A Opt Image Sci Vis 26:2192-2198.

Lundstrom L, Manzanera S, Prieto PM, Ayala DB, Gorceix N, Gustafsson J, Unsbo P, Artal P (2007b) Effect of optical correction and remaining aberrations on peripheral resolution acuity in the human eye. Opt Express 15:12654-12661.

Ma JJ, Tseng SS (2008) Simple method for accurate alignment in toric phakic and aphakic intraocular lens implantation. J Cataract Refract Surg 34:1631-1636.

Maghzi AH, Minagar A, Waubant E (2013) Neuroprotection in multiple sclerosis: a therapeutic approach. CNS Drugs 27:799-815.

Mankowska A, Aziz K, Cufflin MP, Whitaker D, Mallen EA (2012) Effect of blur adaptation on human parafoveal vision. Investigative ophthalmology & visual science 53:1145-1150.

Marcos S (2003) Image quality of the human eye. Int Ophthalmol Clin 43:43-62.

Marcos S (2005) Calidad óptica del ojo. Investigacion y Ciencia 34:9.

Marcos S, Burns SA (2000) On the symmetry between eyes of wavefront aberration and cone directionality. Vision Res 40:2437-2447.

Marcos S, Sawides L, Gambra E, Dorronsoro C (2008) Influence of adaptive-optics ocular aberration correction on visual acuity at different luminances and contrast polarities. J Vis 8:1 1-12.

Marsack JD, Thibos LN, Applegate RA (2004) Metrics of optical quality derived from wave aberrations predict visual performance. J Vis 4:322-328.

McCollough C, Webster M (2011) McCollough effect. Scholarpedia 6:1.

McGovern DP, Webb BS, Peirce JW (2012) Transfer of perceptual learning between different visual tasks. J Vis 12:4.

McLellan JS, Prieto PM, Marcos S, Burns SA (2006) Effects of interactions among wave aberrations on optical image quality. Vision Res 46:3009-3016.

Miller DT, Kocaoglu OP, Wang Q, Lee S (2011) Adaptive optics and the eye (super resolution OCT). Eye 25:321-330.

Mon-Williams M, Tresilian JR, Strang NC, Kochhar P, Wann JP (1998) Improving vision: neural compensation for optical defocus. Proceedings Biological sciences / The Royal Society 265:71-77.

Montes-Mico R, Alio JL (2003) Distance and near contrast sensitivity function after multifocal intraocular lens implantation. J Cataract Refract Surg 29:703-711.

Mutti DO, Sinnott LT, Mitchell GL, Jones-Jordan LA, Moeschberger ML, Cotter SA, Kleinstein RN, Manny RE, Twelker JD, Zadnik K, Group CS (2011) Relative peripheral refractive error and the risk of onset and progression of myopia in children. Investigative ophthalmology & visual science 52:199-205.

Myers GA, Stark L (1990) Topology of the near response triad. Ophthalmic Physiol Opt 10:175-181.

Navarro R (2009) The Optical Design of the Human Eye: a Critical Review. J Optom 2:16.

Navarro R, Ferro M, Artal P, Miranda I (1993) Modulation transfer functions of eyes implanted with intraocular lenses. Applied optics 32:6359-6367.

Nishida S, Ashida H, Sato T (1994) Complete interocular transfer of motion aftereffect with flickering test. Vision Res 34:2707-2716.

Ohlendorf A, Schaeffel F (2009) Contrast adaptation induced by defocus - a possible error signal for emmetropization? Vision Res 49:249-256.

Ohlendorf A, Tabernero J, Schaeffel F (2011a) Neuronal adaptation to simulated and optically-induced astigmatic defocus. Vision Res 51:529-534.

Ohlendorf A, Tabernero J, Schaeffel F (2011b) Visual acuity with simulated and real astigmatic defocus. Optom Vis Sci 88:562-569.

Ono H, Barbeito R (1982) The cyclopean eye vs. the sighting-dominant eye as the center of visual direction. Perception & psychophysics 32:201-210.

Ono H, Mapp AP, Howard IP (2002) The cyclopean eye in vision: the new and old data continue to hit you right between the eyes. Vision Res 42:1307-1324.

Oyster C (1999) The human eye. New York: Sinauer.

Paune J, Queiros A, Quevedo L, Neves H, Lopes-Ferreira D, Gonzalez-Meijome JM (2014) Peripheral myopization and visual performance with experimental rigid gas permeable and soft contact lens design. Cont Lens Anterior Eye 37:455-460.

Pausus A, Gzibovska S, Stolcere A, Jurasevska K, Cikmacs P, Krumina G (2014) The effect of object size on blur perception. In: VII European meeting in Visual and Physiological Optics (Iskander, D. R. and Kasprzak, H. T., eds) Wroclaw, Poland.

Peli E (1990) Contrast in complex images. J Opt Soc Am A 7:2032-2040.

Peli E (2002) The optical functional advantages of an intraocular low-vision telescope. Optom Vis Sci 79:225-233.

Peli E, Lang A (2001) Appearance of images through a multifocal intraocular lens. J Opt Soc Am A Opt Image Sci Vis 18:302-309.

Pelli DG, Farell B (1995) Psychophysical methods: In Handbook of Optics. New York: Mc Graw Hill Publishers.

Pesudovs K (2005) Involvement of neural adaptation in the recovery of vision after laser refractive surgery. J Refract Surg 21:144-147.

Pesudovs K, Brennan NA (1993) Decreased uncorrected vision after a period of distance fixation with spectacle wear. Optom Vis Sci 70:528-531.

Petelczyc K, Bara S, Lopez AC, Jaroszewicz Z, Kakarenko K, Kolodziejczyk A, Sypek M (2011) Imaging properties of the light sword optical element used as a contact lens in a presbyopic eye model. Opt Express 19:25602-25616.

Phipps JA, Zele AJ, Dang T, Vingrys AJ (2001) Fast psychophysical procedures for clinical testing. Clin Exp Optom 84:264-269.

Plainis S, Petratou D, Giannakopoulou T, Atchison DA, Tsilimbaris MK (2011) Binocular summation improves performance to defocus-induced blur. Investigative ophthalmology & visual science 52:2784-2789.

Poggio T, Fahle M, Edelman S (1992) Fast perceptual learning in visual hyperacuity. Science 256:1018-1021.

Polat U, Schor C, Tong JL, Zomet A, Lev M, Yehezkel O, Sterkin A, Levi DM (2012) Training the brain to overcome the effect of aging on the human eye. Scientific reports 2:278.

Porter J, Guirao A, Cox IG, Williams DR (2001) Monochromatic aberrations of the human eye in a large population. J Opt Soc Am A Opt Image Sci Vis 18:1793-1803.

Porter J, Queener H, Lin J, Thorn K, Awwal AA (2005) Adaptive optics for vision science: Principles, practices, design and applications. E-Book: Wiley Publications.

Poulere E, Moschandreas J, Kontadakis GA, Pallikaris IG, Plainis S (2013) Effect of blur and subsequent adaptation on visual acuity using letter and Landolt C charts: differences between emmetropes and myopes. Ophthalmic Physiol Opt 33:130-137.

Pujol J, Aldaba M, Giner A, Arasa J, Luque S (2014) Visual performance evaluation of new multifocal intraocular design before surgery. Investigative ophthalmology & visual science 55:E-Abstract: 3752.

Radhakrishnan A, Dorronsoro C, Sawides L, Marcos S (2014) Short-term neural adaptation to simultaneous bifocal images. PloS one 9:e93089.

Radhakrishnan A, Dorronsoro C, Sawides L, Webster MA, Marcos S (2015a) A cyclopean neural mechanism compensating for optical differences between the eyes. Curr Biol 25:R188-189.

Radhakrishnan A, Sawides L, Dorronsoro C, Peli E, Marcos S (2015b) Single neural code for blur in subjects with different interocular optical blur orientation. J Vis 15:15.

Radhakrishnan A, Dorronsoro C, Marcos S (2016) Subjective preference to orientation in angular bifocal IOL design. In preparation.

Radhakrishnan H, Pardhan S, Calver RI, O'Leary DJ (2004) Effect of positive and negative defocus on contrast sensitivity in myopes and non-myopes. Vision Res 44:1869-1878.

Raymond JE (1993) Complete interocular transfer of motion adaptation effects on motion coherence thresholds. Vision Res 33:1865-1870.

Rea MS, Figueiro MG, Bullough JD, Bierman A (2005) A model of phototransduction by the human circadian system. Brain Res Brain Res Rev 50:213-228.

Rice ML, Leske DA, Smestad CE, Holmes JM (2008) Results of ocular dominance testing depend on assessment method. J AAPOS 12:365-369.

Rieke F, Rudd ME (2009) The challenges natural images pose for visual adaptation. Neuron 64:605-616.

Ringach DL, Hawken MJ, Shapley R (1997) Dynamics of orientation tuning in macaque primary visual cortex. Nature 387:281-284.

Roorda A (2010) Applications of adaptive optics scanning laser ophthalmoscopy. Optom Vis Sci 87:260-268.

Roorda A (2011) Adaptive optics for studying visual function: a comprehensive review. J Vis 11.

Roorda A, Williams DR (2002) Optical fiber properties of individual human cones. J Vis 2:404-412.

Roth HL, Lora AN, Heilman KM (2002) Effects of monocular viewing and eye dominance on spatial attention. Brain 125:2023-2035.

Rouger H, Benard Y, Legras R (2010) Effect of monochromatic induced aberrations on visual performance measured by adaptive optics technology. J Refract Surg 26:578-587.

Rynders MC, Navarro R, Losada MA (1998) Objective measurement of the off-axis longitudinal chromatic aberration in the human eye. Vision Res 38:513-522.

Sabesan R, Zheleznyak L, Yoon G (2012) Binocular visual performance and summation after correcting higher order aberrations. Biomedical optics express 3:3176-3189.

Sawides L (2013) Correction and control of Ocular aberrations with Adaptive Optics. In: Institute of Applied Ophthalmology, vol. Doctorate, p 293 Valladolid: Universidad de Valladolid.

Sawides L, de Gracia P, Dorronsoro C, Webster M, Marcos S (2011a) Adapting to blur produced by ocular high-order aberrations. J Vis 11.

Sawides L, de Gracia P, Dorronsoro C, Webster MA, Marcos S (2011b) Vision is adapted to the natural level of blur present in the retinal image. PloS one 6:e27031.

Sawides L, Dorronsoro C, de Gracia P, Vinas M, Webster M, Marcos S (2012) Dependence of subjective image focus on the magnitude and pattern of high order aberrations. J Vis 12:4.

Sawides L, Dorronsoro C, Haun AM, Peli E, Marcos S (2013) Using pattern classification to measure adaptation to the orientation of high order aberrations. PloS one 8:e70856.

Sawides L, Marcos S, Ravikumar S, Thibos L, Bradley A, Webster M (2010) Adaptation to astigmatic blur. J Vis 10:22.

Schaeffel F, Howland HC (1991) Properties of the feedback loops controlling eye growth and refractive state in the chicken. Vision Res 31:717-734.

Schor C, Landsman L, Erickson P (1987) Ocular dominance and the interocular suppression of blur in monovision. Am J Optom Physiol Opt 64:723-730.

Schwartz SH (2004) Visual perception. New York: McGraw Hill Publishers.

Schwiegerling J (2002) Scaling Zernike expansion coefficients to different pupil sizes. J Opt Soc Am A Opt Image Sci Vis 19:1937-1945.

Seidemann A, Schaeffel F, Guirao A, Lopez-Gil N, Artal P (2002) Peripheral refractive errors in myopic, emmetropic, and hyperopic young subjects. J Opt Soc Am A Opt Image Sci Vis 19:2363-2373.

Shen J, Thibos LN (2011) Peripheral aberrations and image quality for contact lens correction. Optom Vis Sci 88:1196-1205.

Simpson MJ (1992) Diffractive multifocal intraocular lens image quality. Applied optics 31:3621-3626.

Smith G, Atchison DA (1997) The eye and viusal optical instruments. New York: Cambridge University Press.

Smith G, Cox MJ, Calver R, Garner LF (2001) The spherical aberration of the crystalline lens of the human eye. Vision Res 41:235-243.

Tabernero J, Schwarz C, Fernandez EJ, Artal P (2011) Binocular visual simulation of a corneal inlay to increase depth of focus. Investigative ophthalmology & visual science 52:5273-5277.

Tarrant J, Severson H, Wildsoet CF (2008) Accommodation in emmetropic and myopic young adults wearing bifocal soft contact lenses. Ophthalmic Physiol Opt 28:62-72.

Thibos L (2012) Sampling theory of visual resolution and its clinical applications. E-book: Springer-Science+Business Media.

Thibos L, Bradley A (1995) Modeling off axis vision: Effect of spatial filtering and sampling by retinal neurons. Singapore: World Scientific Press.

Thibos LN (1998) Acuity perimetry and the sampling theory of visual resolution. Optom Vis Sci 75:399-406.

Thibos LN, Applegate RA, Schwiegerling JT, Webb R, science VSTMV, its a (2002a) Standards for reporting the optical aberrations of eyes. J Refract Surg 18:S652-660.

Thibos LN, Bradley A, Zhang XX (1991) Effect of ocular chromatic aberration on monocular visual performance. Optom Vis Sci 68:599-607.

Thibos LN, Hong X, Bradley A, Cheng X (2002b) Statistical variation of aberration structure and image quality in a normal population of healthy eyes. J Opt Soc Am A Opt Image Sci Vis 19:2329-2348.

van der Mooren M, Steinert R, Tyson F, Langeslag MJ, Piers PA (2015) Explanted multifocal intraocular lenses. J Cataract Refract Surg 41:873-877.

Vaz TC, Gundel RE (2003) High- and low-contrast visual acuity measurements in spherical and aspheric soft contact lens wearers. Cont Lens Anterior Eye 26:147-151.

Villegas EA, Alcon E, Rubio E, Marin JM, Artal P (2014) Refractive accuracy with light-adjustable intraocular lenses. J Cataract Refract Surg 40:1075-1084 e1072.

Vinas M, de Gracia P, Dorronsoro C, Sawides L, Marin G, Hernandez M, Marcos S (2013) Astigmatism impact on visual performance: meridional and adaptational effects. Optom Vis Sci 90:1430-1442.

Vinas M, Dorronsoro C, Gonzalez V, Cortes D, Marcos S (2015) Testing vision with radial and angulary segmented multifocal patterns using adaptive optics. Investigative ophthalmology & visual science 56:E-Abstract: 1358.

Vinas M, Sawides L, de Gracia P, Marcos S (2012) Perceptual adaptation to the correction of natural astigmatism. PloS one 7:e46361.

von Helmholtz H (1881) Treatise on Physiological Optics. Electronic edition (2001): University of Pennsylvania.

Vul E, Krizay E, MacLeod DI (2008) The McCollough effect reflects permanent and transient adaptation in early visual cortex. J Vis 8:4 1-12.

Wang B, Ciuffreda KJ (2005) Blur discrimination of the human eye in the near retinal periphery. Optom Vis Sci 82:52-58.

Wang YZ, Thibos LN, Bradley A (1997) Effects of refractive error on detection acuity and resolution acuity in peripheral vision. Investigative ophthalmology & visual science 38:2134-2143.

Wang Z, Bovik AC, Sheikh HR, Simoncelli EP (2004) Image quality assessment: from error visibility to structural similarity. IEEE transactions on image processing : a publication of the IEEE Signal Processing Society 13:600-612.

Wark B, Fairhall A, Rieke F (2009) Timescales of inference in visual adaptation. Neuron 61:750-761.

Watson AB, Ahumada AJ (2011) Blur clarified: a review and synthesis of blur discrimination. J Vis 11.

Watson AB, Pelli DG (1983) QUEST: a Bayesian adaptive psychometric method. Perception & psychophysics 33:113-120.

Webster MA (2011) Adaptation and visual coding. J Vis 11.

Webster MA, De Valois RL (1985) Relationship between spatial-frequency and orientation tuning of striate-cortex cells. J Opt Soc Am A 2:1124-1132.

Webster MA, Georgeson MA, Webster SM (2002) Neural adjustments to image blur. Nature neuroscience 5:839-840.

Webster MA, Leonard D (2008) Adaptation and perceptual norms in color vision. J Opt Soc Am A Opt Image Sci Vis 25:2817-2825.

Webster MA, Miyahara E (1997) Contrast adaptation and the spatial structure of natural images. J Opt Soc Am A Opt Image Sci Vis 14:2355-2366.

Webster MA, Mizokami Y, Svec LA, Elliott SL (2006) Neural adjustments to chromatic blur. Spatial vision 19:111-132.

Webster MS, Webster MA, Taylor J (2001) Simultaneous blur contrast. SPEI Proceedings 4299-45:414.

Werner JS, Schefrin BE (1993) Loci of achromatic points throughout the life span. J Opt Soc Am A 10:1509-1516.

Westheimer G, Campbell FW (1962) Light distribution in the image formed by the living human eye. Journal of the Optical Society of America 52:1040-1045.

Wright KW, Guemes A, Kapadia MS, Wilson SE (1999) Binocular function and patient satisfaction after monovision induced by myopic photorefractive keratectomy. J Cataract Refract Surg 25:177-182.

Wuerger S (2013) Colour constancy across the life span: evidence for compensatory mechanisms. PloS one 8:e63921.

Yates RD, Goodman DJ (2005) Probability and stochastic processes: A friendly introduction for Elctrical and Computer engineers. New Jersey: John Wiley & Sons Inc.

Yehezkel O, Sagi D, Sterkin A, Belkin M, Polat U (2010) Learning to adapt: Dynamics of readaptation to geometrical distortions. Vision Res 50:1550-1558.

Yoon GY, Williams DR (2002) Visual performance after correcting the monochromatic and chromatic aberrations of the eye. J Opt Soc Am A Opt Image Sci Vis 19:266-275.

Zaidi Q, Ennis R, Cao D, Lee B (2012) Neural locus of color afterimages. Curr Biol 22:220-224.

Zlotnik A, Ben Yaish S, Yehezkel O, Lahav-Yacouel K, Belkin M, Zalevsky Z (2009) Extended depth of focus contact lenses for presbyopia. Optics letters 34:2219-2221.

Instituto de Optica “Daza de Valdés”. Consejo Superior de Investigaciones Científicas
Serrano 121, 28006 Madrid. Tel. 91 5616800. Fax: 91 5645557.
http://www.io.cfmac.csic.es

HOJA DE INFORMACION AL POSIBLE PARTICIPANTE

(Según normativa RD 223/2004)

Medida de la calidad del sistema óptico del ojo. Aberraciones

1. El objetivo de este experimento es la medida de las propiedades ópticas y geométricas de calidad los componentes oculares (córnea y cristalino). Los resultados aportarán información a la comunidad científica y clínica sobre el funcionamiento óptico del ojo, tanto normal como tras una intervención o tratamiento.

2. Se realizarán medidas con prototipos experimentales (aberrometría de Hartmann-Shack; corecciones bifocales con sistema vision simultanea) y/o con sistemas comerciales (topografía corneal de anillos de Placido; autorefractómetro; sistema de imagen de Scheimpflug). En general, las medidas requieren la fijación a un estímulo visual y la captura de imágenes. Normalmente las medidas se repiten 1 a 5 veces para asegurar la validez de los resultados.

3. En determinados casos las medidas se realizan tras la administración de un midriático o un ciclopégico (gotas que dilatan la pupila) por parte de su oftalmólogo.

4. Para algunas pruebas se podrá realizar una impronta dental (similar a la que realizan los dentistas), que se empleará para facilitar su estabilidad durante el experimento. Dicha impronta no plantea ningún problema; es necesario que nos advierta en caso de llevar algún tipo de implante dental.

5. La intensidad del haz de los prototipos experimentales utilizado se encuentra en niveles **absolutamente seguros**, siendo menor que la utilizada en la mayor parte de aparatos oftálmicos.

6. Las medidas no suponen tratamiento adicional ni alteración con respecto a la prescripción (en caso de haberla) que haya sido administrada por su oftalmólogo.

7. Dada la inocuidad de las medidas no se tiene constancia ni se contempla la posibilidad de ningún acontecimiento adverso

8. El carácter de este experimento es absolutamente voluntario. Podrá ser interrumpido en cualquier momento sin perjuicio por parte del sujeto.

9. Los datos y resultados del experimento son confidenciales, sólo teniendo acceso a ellos los científicos involucrados en el proyecto. Los datos se publicarán de forma anónima. Tras la publicación los datos se conservarán de forma anónima.

10. No dude en indicarnos cualquier duda que tenga sobre el experimento. Persona de contacto: Prof. Susana Marcos. Instituto de Óptica, Consejo Superior de Investigaciones Científicas. Serrano 121, 28006 Madrid. Tel: +34 915616800 x 942314. Fax: +34 915645557

Instituto de Optica "Daza de Valdés". Consejo Superior de Investigaciones Científicas
Serrano 121, 28006 Madrid. Tel. 91 5616800. Fax: 91 5645557.
http://www.io.cfmac.csic.es

FORMULARIO DE CONSENTIMIENTO INFORMADO

(según normativa BPC-CPMP/ICH/135/95)

Medida de la calidad del sistema óptico del ojo. Aberraciones oculares

Dº -- DNI ---
Domicilio en --
Tlf.__________________________

Manifiesta que ha sido informado sobre la naturaleza de las pruebas a las que se somete y ha entendido lo referente a su participación en la medida de la calidad del sistema óptico del ojo, estando advertido de los siguientes aspectos:

1. Estas medidas forman parte de una investigación

2. El propósito de las pruebas es la medida precisa de la calidad del sistema óptico del ojo, tanto en condiciones normales, como tras una intervención o tratamiento, mediante sistemas experimentales.

3. La participación en estas medidas experimentales no altera la intervención o los tratamientos de los que el sujeto pudiera estar siendo objeto. La posible intervención o tratamiento se llevará a cabo (y de manera idéntica) independientemente de la participación o no en las medidas.

4. Si bien el sujeto participante no debe esperar ningún beneficio clínico, los resultados de este experimento ofrecen una descripción de la calidad óptica del ojo no alcanzada por ningún otro instrumento convencional en la práctica clínica. Con ello, se contribuirá al conocimiento del ojo normal, y la repercusión en la calidad óptica de los tratamientos y las cirugías del segmento anterior, y por tanto a la mejora de estas intervenciones en el futuro.

5. Dada la inocuidad de las medidas no se tiene constancia ni se contempla la posibilidad de ningún acontecimiento adverso. Las medidas generalmente requerirán una única visita y no suponen tratamiento adicional ni alteración (en caso de haberla) con respecto a la prescripción que haya sido administrada por su oftalmólogo.

6. Las pruebas a realizar podrán incluir medidas con uno o varios de los siguientes instrumentos: topógrafo corneal de anillos de Placido (instrumento comercial), biometría óptica ocular (instrumento comercial), autorefractómetro (instrumento comercial); imagen de Scheimpflug de segmento anterior (instrumento comercial); aberrometría de trazado de rayos; aberrometría de Hartmann-Shack; sistema vision simultanea; y tomografía de coherencia óptica de segmento anterior.

7. En algunos casos las medidas se realizan generalmente tras la administración de un midriático o un ciclopléjico (gotas que dilatan la pupila).

8. En algunos casos se realizará una impronta dental (similar a la que realizan los dentistas), que se empleará para facilitar su estabilidad durante el experimento. Dicha impronta no plantea ningún problema; es necesario que nos advierta en caso de llevar algún tipo implante dental.

9. La intensidad del haz utilizado en los prototipos experimentales se encuentra en niveles **absolutamente seguros**, siendo menor que la utilizada en la mayor parte de aparatos oftálmicos.

10. La realización de la prueba no supone gasto alguno al sujeto participante

11. El carácter de este experimento es absolutamente voluntario. Podrá ser interrumpido por parte del sujeto sin perjuicio y en cualquier momento.

11. Los datos y resultados del experimento son confidenciales, sólo teniendo acceso a ello los científicos involucrados en el proyecto. Los datos se publicarán de forma anónima. Tras la publicación los datos se conservarán de forma anónima.

12. El monitor (es), auditor(es), el Comité Bioético de Investigación y las autoridades reguladoras tendrán garantizado el acceso a los datos del sujeto para verificar los procedimientos y datos sin violar la confidencialidad. Firmando el formulario del consentimiento informado, el sujeto o representante legalmente aceptable autorizan tal acceso.

12. No dude en indicarnos cualquier duda que tenga sobre el experimento, o cualquier duda o incomodidad que quiera hacernos notar durante la prueba. Persona de contacto: Prof. Susana Marcos. Instituto de Óptica, Consejo Superior de Investigaciones Científicas. Serrano 121, 28006 Madrid. Tel: +34 915616800 x 942314. Fax: +34 915645557

13. La persona se compromete a guardar de una forma absolutamente confidencial todos los elementos del estudio, incluidos el objetivo y el procedimiento del estudio. La persona no debe divulgar de manera parcial o total, ni por escrito ni oralmente, las informaciones concernientes a este estudio a ninguna otra persona o estamento. La persona se compromete igualmente a no hacer ninguna copia o reproducción de las informaciones relativas a este estudio y tampoco a utilizarlas. Si la persona incumple su responsabilidad podrá ser sujeto de sanciones administrativas.

Presto libremente mi conformidad para participar en el estudio

En Madrid, a __ de ______________ de 2015

Firma del sujeto (o representante legalmente aceptable)	Firma del investigador responsable